UNIVERSITAT DE BARCELONA

Development of a Safer and More Standardized Cell Therapy for Huntington's Disease using Isolated Stem Cell-Derived Striatal Neuroblast Subpopulations

Francisco Jose Molina Ruiz

Development of a Safer and More Standardized Cell Therapy for Huntington's Disease using Isolated Stem Cell-Derived Striatal Neuroblast Subpopulations

Francisco J Molina Ruiz

Barcelona, May 2024

UNIVERSITAT DE BARCELONA
Creatio
Production and validation center of advanced therapies
UNIVERSITAT DE BARCELONA
ASCTN TRAINING

Development of a Safer and More Standardized Cell Therapy for Huntington's Disease using Isolated Stem Cell-Derived Striatal Neuroblast Subpopulations

Doctoral degree by the

University of Barcelona.

Doctoral Programme in Biomedicine

UNIVERSITAT DE BARCELONA

Dissertation submitted by:

Francisco Jose Molina Ruiz

This thesis has been supervised by Dr. Josep M- Canals Coll in the Department of Biomedicine from the Faculty of Medicine and Health Science, University of Barcelona.

Josep M. Canals Coll

BARCELONA, MAY 2024

*"Ad **astra** per aspera"*

…

*"Through hardship, to the **stars**"*

…

*"Hacia las **estrellas**, por el camino más duro"*

…

-Virgil-

A mis héroes, **Papá y Mamá**.

La culpa de ser quien soy hoy, para bien o para mal, es **vuestra**.

ABSTRACT

Abstract

Neurodegenerative diseases (NDs) are characterized by a selective and irreversible loss of neurons in a specific brain area. NDs are incurable and debilitating, becoming the greatest unmet clinical need of our time. Huntington's Disease (HD) constitutes an example of a devastating ND, characterized by degeneration of striatal projection neurons (SPNs) leading to motor, cognitive and behavioral symptoms. Cell replacement therapies (CRTs) are distinguished by their potential to replace cells lost during the degenerative process and have shown a great potential to replace degenerated neurons in animal models and in clinical trials in Parkinson's Disease (PD) and HD patients. In fact, CRT is the only approach currently focused on the structural and functional restoration of atrophied striatal tissue in HD, by replenishing the degenerating SPN population. In recent years, human pluripotent stem cells (hPSCs) have become a key cell source for CRTs given the scarcity and heterogeneity of previously used fetal-derived neural progenitors. However, hPSCs are prone to acquire genomic alterations *in vitro*, mainly due to suboptimal culture conditions and inappropriate routines to monitor genome integrity, which poses a challenge to both the safety of clinical applications and the reliability of basic and translational hPSC research. Furthermore, directing hPSCs into specific neuronal types *in vitro* is complex and the clinical translation of hPSC-derived neural progenitors is limited by the heterogeneity of cell products obtained using existing differentiation protocols. Therefore, clinical translation of CRTs for NDs requires standardization of production procedures for reproducible generation of defined functional cell products, by ensuring the presence of correctly specified target SPN progenitors and the absence of unwanted overly proliferative cell types

In this thesis, we have investigated if standardization of cell culture conditions and genomic screening strategies could decrease the prevalence of genomic alterations affecting hPSCs used as starting material in CRTs. We demonstrated that application of a Quality Management System (QMS) such as ISO9001:2015 to standardize cell culture conditions and genomic monitoring routines leads to a striking improvement of genomic stability in hPSCs cultured *in vitro*, as evidenced by a reduced probability of potentially pathogenic chromosomal aberrations and subchromosomal genomic alterations. We also described that CD200 is a cell surface marker suitable for the enrichment of hPSC-derived striatal neuroblasts (NBs). We set up and optimized an immunomagnetic sorting pipeline which allows for high-yield enrichment of striatal NBs in heterogenous cell populations

resulting from *in vitro* differentiation. Our data demonstrate that implementation of this approach leads to a reduction of the heterogeneity and batch-to-batch variation of the final cell population. Furthermore, we showed that sorted cell populations are composed of correctly specified, SPN-committed progenitors with the potential to generate different SPN subtypes, which result in a higher yield of neurons with an SPN phenotype upon terminal *in vitro* differentiation. We also provided evidence thar the use of CD200- based selection at different timepoints of *in vitro* differentiation results in obtention of cell compositions enriched in different subtypes of postmitotic striatal NBs. Finally, we demonstrate that transplanted selected NBs survive upon intra-striatal transplantation in adult mice with no evidence of graft overgrowth *in vivo*.

In conclusion, our findings underscore the critical need for implementing QMS in academic laboratories engaged in hPSC research to enhance the consistency and safety of applications of hPSC-derived cell products. Additionally, our results highlight the potential of the dual approach of combining standardization of hPSC culture conditions and CD200-based cell sorting of postmitotic striatal NBs before transplantation as a promising strategy to optimize the outcomes of hPSC-derived CRT products after transplantation. These strategies collectively advance the development and translation of safer, effective, and reproducible cell products to be used for clinical CRT applications in HD and potentially other NDs.

RESUMEN

Resumen

Las enfermedades neurodegenerativas (NDs) se caracterizan por una pérdida selectiva e irreversible de neuronas en áreas específicas del cerebro. Las NDs son incurables y debilitantes, representando la mayor necesidad clínica no satisfecha de nuestro tiempo. La enfermedad o corea de Huntington (HD) es un ejemplo de una devastadora ND, marcada por la degeneración de las neuronas de proyección estriatales (SPNs), que da lugar a síntomas motores, cognitivos y conductuales. Las terapias de reemplazo celular (CRTs) han mostrado un gran potencial para reemplazar neuronas degeneradas en modelos animales y ensayos clínicos para pacientes con enfermedad de Parkinson (PD) y HD. Las CRTs son el único enfoque actualmente dirigido a la restauración estructural y funcional del tejido estriatal atrofiado en HD, mediante la sustitución de la población de SPNs degenerados. En los últimos años, las células madre pluripotentes humanas (hPSCs) se han convertido en una fuente celular clave para las CRTs debido a la escasez y heterogeneidad de los progenitores neuronales derivados de tejido fetal utilizados previamente. Sin embargo, las hPSCs son propensas a adquirir alteraciones genómicas *in vitro*, principalmente debido a condiciones de cultivo subóptimas y rutinas inapropiadas para monitorear la integridad del genoma, lo que representa un desafío para la seguridad de las aplicaciones clínicas de las hPSCs y la fiabilidad de la investigación con este tipo celular. Además, la diferenciación de hPSCs hacia tipos neuronales específicos *in vitro* es un proceso complejo, y la translación clínica de los progenitores neuronales derivados de hPSCs está limitada por la heterogeneidad de los productos celulares obtenidos utilizando los protocolos de diferenciación existentes. Por lo tanto, el desarrollo de CRTs para NDs también requiere la estandarización de los procedimientos de producción para la generación de productos celulares funcionales definidos de manera reproducible, asegurando la presencia de progenitores correctamente especificados hacia el tipo neuronal de interés y la ausencia de tipos celulares no deseados y con fenotipo excesivamente proliferativo.

En esta tesis, hemos investigado si la estandarización de las condiciones de cultivo celular y las estrategias de detección genómica podrían disminuir la prevalencia de alteraciones genómicas que afectan a las hPSCs utilizadas como material de partida en estrategias de CRT. Nuestros resultados demuestran que la aplicación de un Sistema de Gestión de Calidad (QMS) como ISO9001:2015 para estandarizar las condiciones de cultivo celular y las rutinas de monitoreo genómico conduce a una notable mejora de la

estabilidad genómica en las hPSCs cultivadas *in vitro*, evidenciado por una probabilidad reducida de adquisición de aberraciones cromosómicas potencialmente patogénicas y alteraciones genómicas subcromosómicas. También hemos descrito que CD200 es un marcador de superficie celular adecuado para el enriquecimiento de neuroblastos (NBs) estriatales derivados de hPSCs. Hemos desarrollado y optimizado un proceso de selección celular inmunomagnético que permite un enriquecimiento altamente eficiente de NBs estriatales en poblaciones celulares heterogéneas resultantes de la diferenciación *in vitro*. Nuestros datos demuestran que la implementación de este enfoque lleva a una reducción de la heterogeneidad y de la variabilidad inter-lote de la población celular final. Además, mostramos que las poblaciones celulares aisladas mediante este proceso están compuestas por progenitores especificados correctamente hacia la generación de diferentes subtipos de SPNs, lo que resulta en un mayor rendimiento de neuronas con fenotipo de SPN tras la diferenciación terminal *in vitro*. También proporcionamos evidencia de que el uso de la selección basada en CD200 en diferentes puntos temporales de la diferenciación *in vitro* permite la obtención de composiciones celulares enriquecidas en diferentes subtipos de NB estriatales postmitóticos. Finalmente, demostramos que los NBs seleccionados y trasplantados sobreviven tras el transplante intra-estriatal en ratones adultos sin evidencia de sobrecrecimiento del transplante *in vivo*.

En conclusión, nuestros hallazgos enfatizan la necesidad de implementar un QMS en los laboratorios académicos dedicados a la investigación de hPSCs para mejorar la consistencia y seguridad de las aplicaciones de productos celulares derivados hPSCs. Además, nuestros resultados destacan el potencial del enfoque dual de combinar la estandarización de las condiciones de cultivo de hPSCs y la selección celular de NBs estriatales postmitóticos basada en el uso del marcador de superficie CD200 antes del trasplante como una estrategia prometedora para optimizar los resultados de los productos derivados de hPSCs después del trasplante.Colectivamente, estas estrategias podrían acelerar el avance del el desarrollo y la translación de productos celulares más seguros, efectivos y reproducibles para ser utilizados en aplicaciones clínicas de CRT en HD y potencialmente en otras NDs.

INDEX

Index

ABBREVIATIONS

Abbreviations

AC	Anterior commissure
aCGH	Comparative genome hybridization array
AD	Alzheimer's disease
ADORA2A	Adenosine A2A receptors
aIP	Apical intermediate progenitors
ALS	Amyotrophic lateral sclerosis
ANOVA	Analysis of variance
ANT	Anterior
APC	Allophycocyanin
ARPP-21	Cyclic AMP-regulated phosphoprotein, 21 kD
ASCL1	Achaete-scute family bHLH 1
ASO	Antisense oligonucleotide
ATMP	Advanced therapy medicinal product
BCL11B	B-cell lymphoma/leukemia 11B
BCL2L1	B-cell lymphoma/leukemia 2L1
BDNF	Brain-derived neurotrophic factor
bFGF	Basic fibroblast growth factor
bIP	Basal intermediate progenitors
BSA	Bovine serum albumin
c-MYC	Cellular myelocytomatosis oncogene
CAG	Cytosine-adenine-guanine
CB	Calbindin-D28k
CC3	Cleaved caspase 3
CDx	Cluster of differentiation x
cDNA	Complementary deoxyribonucleic acid
CGH	Comparative genome hybridization
ChAT	Choline acetyltransferase
CHDI	Cure Huntington's Disease Initiative Foundation
CINS	Cholinergic interneurons
CK4/6i	Cyclin kinase 4/6 inhibitor
CLL	Chronic lymphocytic leukemia

CNA	Copy number alterations
CNV	Copy number variations
CO_2	Carbon dioxide
CR	Calretinin
CRISPR	Clustered regularly interspaced short palindromic repeats
CRT	Cell replacement therapy
CSRMI	Cedars-Sinai Regenerative Medicine Institute
CTIP2	COUP-TF-interacting protein 2
CY3	Cyanine 3
DA	Dopamine
DAPI	4′,6-diamidino-2-phenylindole
DARPP-32	cAMP-regulated phosphoprotein of 32kDa
DCX	Doublecortin
DEG	Differentially expressed gene
DIV	Days *in vitro*
DLB	Dementia with Lewy bodies
DLX1-6	Distal-less homeobox 1-6
DMC	Data monitoring committee
DMEM/F12	Dulbecco's Modified Eagle Medium F12
DNA	Deoxyribonucleic acid
dNB	Direct pathway neuroblast
DPBS	Dulbecco’s phosphate-buffered saline
DPS	Days post-sorting
DRD1	Dopamine receptor D1
DRD2	Dopamine receptor D2
dSPN	Direct pathway striatal projection neurons
E x	Embryonic day x
EBF1	Early B-cell factor 1
EDTA	Ethylenediamine tetraacetic acid
eGP	External globus pallidus
EMA	European Medicines Agency
ENK	Enkephalin
ESC	Embryonic stem cell

FABP7	Fatty acid binding protein 7
FACS	Fluorescence-activated cell sorting
FBS	Fetal bovine serum
FC	Flow cytometry
FDA	Food and Drug Administration
FITC	Fluorescein isothiocyanate
FOXP1/2	Forkhead box P1/2
FPA	Frequent polymorphic alteration
FTD	Frontotemporal dementia
GABA	Gamma-aminobutyric acid
GAD2	Glutamate decarboxylase 2
GAP43	Growth-associated protein 43
GDNF	Glial cell line-derived neurotrophic factor
GE	Ganglionic eminence
GENEA	Genea Biocells
GIVIMP	Guidance Document on Good *In Vitro* Method Practices
GLI3	GLI family zinc finger 3
GLU	Glutamate
GO	Gene ontology
GO:BP	Gene ontology biological processes
GP	Globus pallidus
GPM6A	Glycoprotein M6A
GSX1/2	GS homeobox 1/2
HD	Huntington's disease
hESCs	Human embryonic stem cells
HEPES	2-[4-(2-hydroxyethyl)piperazin-1-yl]ethanesulfonic acid
HES5	HES family basic/helix-loop-helix transcription factor 5
hiPSC	Human induced pluripotent stem cells
HMGB2	High-mobility group box 2
hMSC	Human mesenchymal stem cell
HNA	Human nuclear antigen
hNFT	Human neural fetal tissue
hPSC	Human pluripotent stem cell

HTT	Huntingtin
I.P.	Intraperitoneal
ICC	Immunocytochemistry
ICM	Inner cell mass
ID4	Inhibitor of differentiation 4
IFITM3	Interferon-induced transmembrane protein 3
iGP	Internal globus pallidus
Ig	Immunoglobulin
IHC	Immunohistochemistry
INA	Internexin neuronal intermediate filament protein alpha
iNB	Indirect pathway neuroblast
IP	Intermediate progenitor
iPSC	Induced pluripotent stem cell
ISCCR	International Society for Stem Cell Research
ISCI	International stem cell initiative
ISH	In situ hybridization
ISL-1	Insulin gene enhancer protein Islet 1
ISO	International organization for standardization
iSPN	Indirect pathway striatal projection neuron
IT15	Interesting transcript 15
KCl	Potassium chloride
KDa	Kilodalton
Ki-67	Marker of proliferation Kiel 67
KLF4	Krüppel-Like Factor 4
LGE	Lateral ganglionic eminence
LHX6	LIM/homeobox protein 6
MACS	Magnetic-associated cell sorting
MAP2B	Microtubule-associated protein 2b
MARS-Seq	Massively parallel single-cell ribonucleic acid sequencing
MB	Magnetic-associated cell sorting buffer
MDK	Midkine
MEIS2	Meis homeobox 2
MGE	Medial ganglionic eminence

mHTT	Mutant huntingtin
MLLT11	Mixed-lineage leukemia translocated to 11
mRNA	Messenger ribonucleic acid
MSA	Multiple system atrophy
MSC	Mesenchymal stem cell
MZ	Mantle zone
NAc	Nucleus accumbens
NADPH	Nicotinamide adenine dinucleotide phosphate
NANOG	Nanog homeobox
NB	Neuroblast
NCAM1	Neural cell adhesion molecule 1
NCx	Neocortex
ND	Neurodegenerative disease
NE	Neuroepithelial
NEJM	New England Journal of Medicine
NEP	Neuroepithelial progenitors
NES	Nestin
NFT	Neural fetal tissue
NIH	National Institutes of Health
NGFR	Nerve growth factor receptor
NKX2.1	NK2 Homeobox 1
NOS	Nitric oxide synthase
NPC	Neural progenitor cell
NPY	Neuropeptide Y
OCT	Optimal cutting temperature
OCT4	Octamer-binding transcription factor 4
OECD	Organization for Economic Co-operation and Development
OR	Odds ratio
OT	Olfactory tubercle
P	Phase
p-MSA	Parkinsonian subtype, Multiple System Atrophy
PC	Principal component
PCA	Principal component analysis

PD	Parkinson’s disease
PDYN	Prodynorphin
PE	Phycoerythrin
PENK	Proenkephalin A 119-159
PLP1	Proteolipid protein 1
POA	Preoptic area
PoA	Post-adaptation conditions
PolyQ	Poly glutamine repeats
PrA	Preadaptation conditions
PSA-NCAM	Polysialylated neuronal cell adhesion molecule
PSC	Pluripotent stem cell
PSP	Progressive supranuclear palsy
PST	Post-transplant
PV	Parvalbumin
QA	Quinolinic acid
QMS	Quality management system
RBP1	Retinol binding protein 1
rcf	Relative centrifugal force
RG	Radial glia
RNA	Ribonucleic acid
RNAi	Interference ribonucleic acid
RNA-seq	Ribonucleic acid sequencing
ROCK	Rho-associated protein kinase
ROS	Reactive oxygen species
RU	Rockefeller University
RT	Reverse transcription
S1PR1	Sphingosine-1-phosphate receptor 1
SCA	Spinocerebral ataxia
SEM	Standard error of the mean
SFRP1	Secreted frizzled related protein 1
SIX3	SIX homeobox 3
SN	Substantia nigra
SNc	SN pars compacta

SNr	SN pars reticulata
SNP	Single nucleotide polymorphism
SOP	Standard Operating Procedure
SOX2/8	SRY-Box transcription factor 2/8
SP8/9	Specificity protein 8/9
SPARC	Secreted protein acidic and cysteine rich
SPN	Spiny projection neuron
SRY	Sex-determining region Y
SST	Somatostatin
STMN2	Human stathmin 2
STN	Subthalamic nucleus
STR	Striatum
SVZ	Subventricular zone
TAC1	Tachykinin 1
TF	Transcriptional factor
TGFβ	Transforming growth factor beta
TH	Tyrosine hydroxylase
TIS21	Tetradecanoyl phorbol acetate-inducible sequence 21
TLGM	Translational Laboratory in Genetic Medicine
TTYH1	Tweety family member 1
TUBB-3	β III tubulin
UMAP	Uniform manifold approximation and projection
VIM	Vimentin
VIP	Vasoactive internal polypeptide
VTA	Ventral tegmental area
VZ	Ventricular zone
WGE	Whole ganglionic eminence
WCRI	WiCell Research Institute
wtHTT	Wild type huntingtin
ZFPx	Zinc finger protein x
ZFP36L1	

LIST OF FIGURES

List of Figures

LIST OF TABLES

List of Tables

INTRODUCTION

Introduction

1. Neurodegenerative Diseases (NDs)

The term 'neurodegenerative diseases' (NDs) covers a wide spectrum of neurological disorders, which can manifest with many different symptoms depending on the affected region, including cognitive impairment, speech difficulties, and motor dysfunction. The underlying pathological hallmark shared by this heterogeneous group of disorders is the loss of neuronal and/or glial populations in the central (brain) and/or the peripheral (spinal cord) nervous system (Yacoubian, 2017). The areas of the brain and spinal cord in which neuronal loss occurs dictate the clinical features of a given ND. NDs are characterized by an initial dysfunction of specific neuronal or glial cell types (initially restricted to a defined area) followed by the progressive worsening over time, with eventual extension to involve additional cell types in more widespread brain areas (Hussain et al., 2018; Williams, 2002).

Genetic alterations and environmental risks constitute the main causes behind these conditions, although the etiology of some of these disorders is still unknown. All in all, aging remains the primary risk factor for most neurodegenerative diseases, which poses a significant challenge for the current fast-growing aging society. According to a report released by the United Nations, 1 in 11 world population was over 65 in 2019 and by 2050 the ratio will be almost doubled to 1 in 6. As the global population ages, the prevalence of NDs including Alzheimer's Disease (AD), Parkinson's Disease (PD) and Huntington's Disease (HD), is fast increasing. Notably, the number of cases of dementia in the developed world is projected to rise from 13.5 million in 2000 to 21.2 million in 2025, and to 36.7 million in 2050. The number of deaths caused by AD (the most common ND) is now on par with the number of deaths caused by stroke, which is the third most common leading cause of death in the world (Zheng & Chen, 2022).

Despite significant research efforts, there are currently no cures for NDs. While there are some treatments available that can help to manage the symptoms of these conditions, they do not address the underlying causes of neurodegeneration and are not able to halt or reverse the progression of the disease. There are several reasons why it has been difficult to develop effective treatments for NDs. One of the main challenges is the complexity of the brain and the lack of understanding about the underlying biological

processes that lead to neurodegeneration. Another challenge is that NDs often develop over many years and are often not diagnosed until the later stages of the disease when significant damage has already occurred. This makes it generally difficult to intervene early in the disease process when it may be more effective to treat.

In addition to their high prevalence, NDs are associated with a significant impact on both individuals and society. In fact, these conditions are linked to severe short- and long-term disabilities and significantly reduce the quality of life for those affected by them. They also often lead to an increased reliance on caregivers and can place a significant burden on families and the healthcare system. A report from the European Brain Council (Gustavsson et al., 2011) calculated that 7.5 million people were affected by PD, AD, and other NDs. Besides the personal and social costs of NDs, there is also a gigantic economic cost. The direct and indirect costs of caring for individuals with NDS, such as lost productivity, medical expenses, and long-term care costs, are estimated to be billions of dollars annually. More specifically, in Europe alone this financial burden was calculated to be more than 130 billion € per year (Olesen et al., 2012). As such, there is a pressing need for cures to treat these incurable conditions, since it would not only improve the lives of those affected by these conditions, but it would also have a significant impact on society by reducing the economic and social burden of these diseases.

A wide range of common and uncommon NDs have been recognized, including AD, PD, HD, amyotrophic lateral sclerosis (ALS), dementia with Lewy bodies (DLB), progressive supranuclear palsy (PSP), multiple system atrophy (MSA), corticobasal degeneration (CBD), frontotemporal dementia (FTD), spinocerebellar ataxia (SCA) disorders, and spinal muscular atrophy, among others. NDs are classified either by their clinical symptoms (mainly motor, cognitive and psychiatric), by the proteins involved in the disorder (and their misfolding and aberrant aggregation) (Agbas, 2018; C. A. Ross & Poirier, 2004; Soto & Pritzkow, 2018); or by the affected cell type, usually neurons or glial cells (Kovacs, 2014; Williams, 2002). Here, we will focus on HD and will cover the most relevant aspects of this disease (including the striatum as the main affected brain area in HD patients) and its potential therapeutic options.

2. The Striatum and Motor Control

2.1. Overview of the basal ganglia and the striatum

The basal ganglia and related nuclei consist of a variety of highly-interconnected subcortical cell groups (that is, groups of neurons that lie below the cerebral cortex) engaged primarily in motor control, together with a wider variety of roles such as motor learning, executive functions and behavior, and emotions. The term *basal ganglia* in the strictest sense refers to nuclei embedded deep in the brain hemispheres (striatum or caudate-putamen and globus pallidus or GP), whereas *related nuclei* consist of structures located in the diencephalon (subthalamic nucleus, or STN), mesencephalon (substantia nigra pars compacta, or SNc; and substantia nigra pars reticulata, or SNr), and pons (pedunculopontine nucleus; Fig.1; Lanciego et al., 2012).

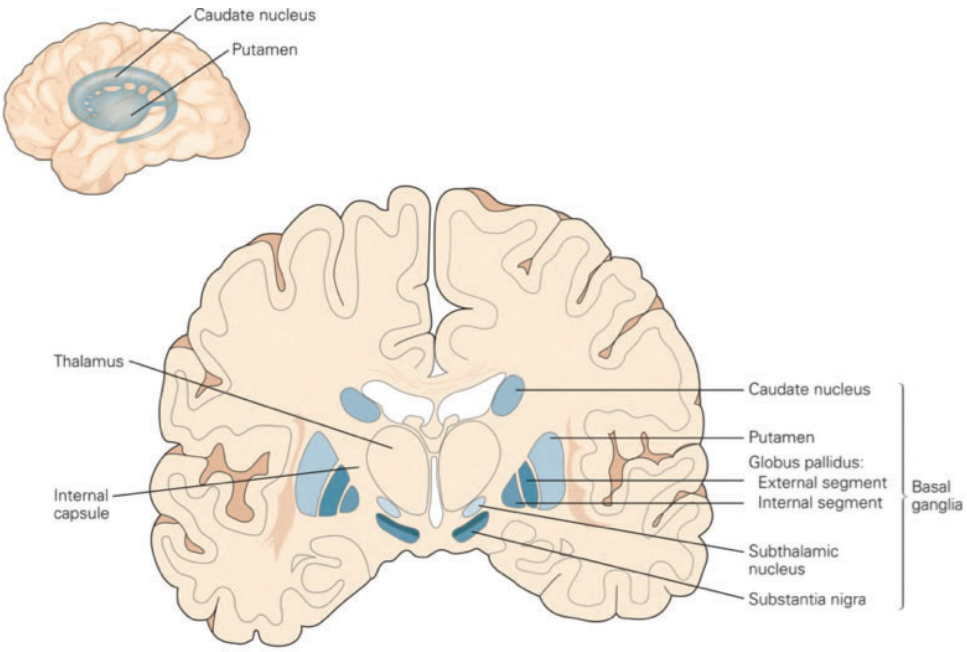

Figure 1. The basal ganglia and surrounding structures. Basal ganglia nuclei are colored in this coronal section. Adapted from (Nieuwenhuys et al., 1981)

The basal ganglia connect the cerebral cortex with neuronal systems which convert cortical activity into directed behavior. Historically, given the obvious motor symptoms of two major diseases of the basal ganglia (PD and HD), the basal ganglia have been exclusively associated with the control of movement for most of the history of neuroscience, and their motor function has been most extensively studied. However, in the past few decades it has become increasingly clear that beyond their undisputed role

in the control of movement, the structures of the basal ganglia are crucial to cognitive functions such as learning and memory.

2.2. Striatal anatomical organization and basal ganglia afferences

The corpus striatum is the largest subcortical brain structure from the basal ganglia. It is a heterogeneous structure that receives afferents from several cortical and subcortical structures and projects to various basal ganglia nuclei (Lanciego et al., 2012), playing an important role in the control of motor, cognitive and limbic functions. This broad range of striatal functions stems from the fact that parallel pathways from the motor, sensory, associative, and limbic cortices run through different regions of the striatum (Alexander et al., 2003; Haber, 2022; Hunnicutt et al., 2016; Middleton & Strick, 2000). Along these lines, the striatum has a complex organization that divides it along several, overlapping parameters, despite lacking clear internal demarcations. From an anatomical perspective, the corpus striatum is commonly divided into two cytoarchitecturally similar but functionally distinct dorsal and ventral striata. The dorsal striatum (also known as neostriatum, or striatum from this point on) consists of the caudate nucleus and putamen (separated by the internal capsule in humans and primates) and is associated to control of motor and cognitive functions (Parent & Hazrati, 1995). In turn, the ventral striatum consists of the nucleus accumbens (NAc) and olfactory tubercle (OT), and regulates the limbic function of motivation, affect, and reward (Fig.2; Chen et al., 2020; Grueter et al., 2012; Russo et al., 2010).

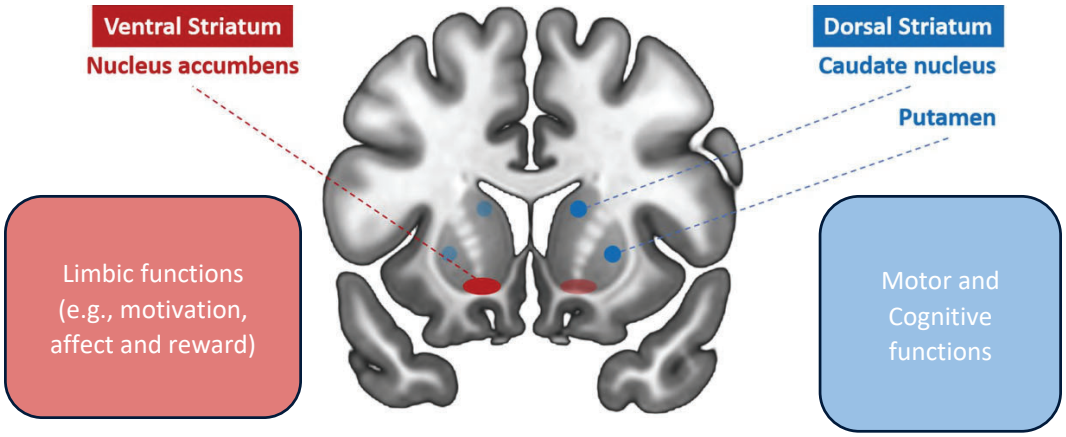

Figure 2. Overview of the striatal anatomical organization of the corpus striatum into two main structures: dorsal striatum (or neostriatum) and ventral striatum. The main brain functions associated to each of these compartments are also indicated. Adapted from (Ponsi et al., 2021)

To control motor and cognitive functions, the striatum processes and integrates all the incoming information that is received from excitatory glutamatergic inputs from the cortex and the thalamus and dopaminergic afferences from the SNc (Alexander et al., 2003; Middleton & Strick, 2000). This is achieved via the coordinated activation of two different output pathways, the so-called direct (or striatonigral) and indirect (or striatopallidal) pathways (Albin et al., 1989; M. R. DeLong, 1990), whose activation results in an opposite effect on basal ganglia function (activation and inhibition respectively; Fig.3).

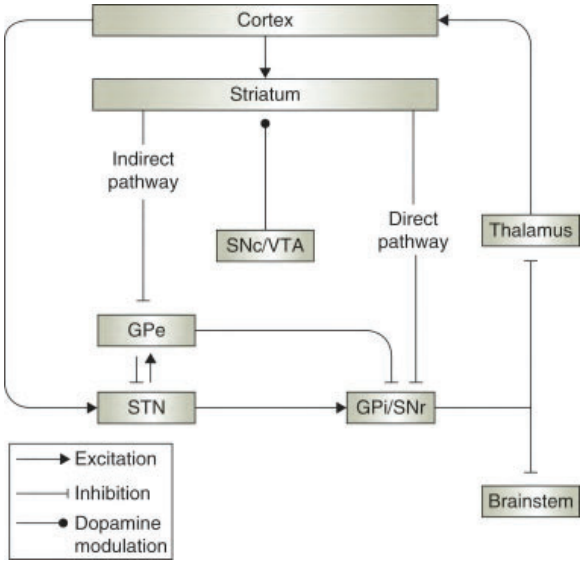

Figure 3. Schematic of the main connections of the basal ganglia.Adapted from (Yin & Knowlton, 2006). GPe, external part of the globus pallidus; GPi, internal part of the globus pallidus; SNc, substantia nigra pars compacta; SNr, substantia nigra pars reticulata; STN, subthalamic nucleus; VTA, ventral tegmental area

The activation of the direct pathway sends inhibitory signals to the basal ganglia's GABAergic output nuclei (internal GP or iGP and SNr) which in turn project to thalamocortical and brainstem motor circuits) (Bolam et al., 2000; Gerfen, 1984). The reduction in inhibitory signals leaving the basal ganglia results in disinhibition of these circuits, facilitating the initiation and execution of voluntary movement (Chevalier et al., 1985). Conversely, activation of the indirect pathway sends excitatory signals to the external GP (eGP) and STN which projects glutamatergic axons to stimulate the iGP/SNr (Silberberg & Bolam, 2015; Smith et al., 1998), increasing the activity of the basal ganglia's output nuclei. This increase in activity results in suppression of the thalamocortical circuitry, ultimately inhibiting movement (Kravitz et al., 2010; Kreitzer & Malenka, 2008; Smith et al., 1998). The balance between both pathways is essential for the correct function of the basal ganglia (M. DeLong & Wichmann, 2010; Leisman et al., 2013). Both pathways converge in the iGP/SNr GABAergic nuclei which send axons

to the thalamus to return the information to the cortex (striato– thalamo–cortical circuit). The maintenance of balance in the excitability and function of these two pathways, which is critical in the execution of controlled movements in time and space, is mainly ensured by dopamine released from SNc neurons. Dopamine helps to increase the excitability of the direct pathway (Lahiri & Bevan, 2020) and decrease that of the indirect pathway to facilitate proper voluntary motor skills.

2.3. Striatal cell populations and histochemical compartments

In many areas of the brain, signal processing is facilitated by a highly ordered arrangement of inputs, outputs, and interneurons, for example, into layers (Grossberg, 2003; Sur & Rubenstein, 2005). However, the striatum is a nonlaminar, highly heterogeneous structure with projection neurons interspersed among a diverse range of interneurons . Most of the striatal neurons are GABAergic spiny projection neurons (SPNs) along with aspiny local interneurons (approximately 90-95% and 5-10 % respectively; Figure 4). Striatal SPNs are responsible to process the afferent information and to send it to the surrounding nuclei of the basal ganglia via inhibitory projections (Schuurmans & Guillemot, 2002).

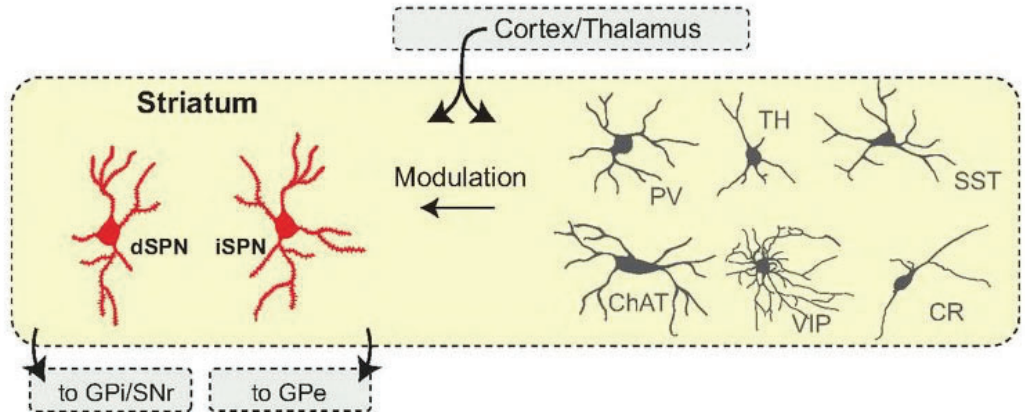

Figure 4. **Main striatal inputs and outputs.** The main excitatory inputs to striatum come from cortex and thalamus, which innervate both the SPNs (left) and interneurons (right). SPNs include both the dSPNs (in red) and the iSPNs (in red), which send axonal projections to downstream basal ganglia nuclei including, respectively, the SNr/GPi and GPe. The local populations of diverse interneurons are integrated within the striatum and can modulate the activity of SPNs. Adapted from (Knowles et al., 2021). ChAT, choline acetyltransferase; CR, calretinin; dSPN, direct pathway SPN; GPe, external part of the globus pallidus; GPi, internal part of the globus pallidus; iSNP, indirect pathway SPN; PV, parvalbumin; SNr, substantia nigra pars reticulata; SST, somatostatin; SPN, striatal projection neuron; TH, tyrosine hydroxylase; VIP, vasoactive internal polypeptide.

Striatal SPNs follow two distinct, yet complementary, basic organizational plans that define the intrinsic architecture of the striatal network. In terms of the network's functional organization, SPNs are subdivided into two neuronal subtypes according to the output nuclei of the basal ganglia to which they project and the molecular markers they express. As such, there are two different subtypes of striatal SPNs: direct pathway SPNs (dSPNs) and indirect pathway SPNs (iSPNs), each displaying different neurochemical composition. Both direct and indirect SPNs express the dopamine and cAMP-regulated phosphoprotein of 32kDa (DARPP-32) and the calcium-binding protein calbindin-D28k (CB) (Ouimet et al., 1984; Parent et al., 1996). Nevertheless, direct pathway SPNs (dSPNs) express the dopamine D1 receptors (DRD1) and the muscarinic M4 receptors, as well as the neuropeptides dynorphin and SP. Conversely, indirect pathway SPNs (iSPNs) show high expression of the dopamine D2 receptors (DRD2) and adenosine A2A receptors (ADORA2A), as well as the neuropeptide ENK (Cicchetti et al., 2000; Lanciego et al., 2012). In terms of axonal projections, differences are also found between different SPN subtypes: dSPNs preferentially project to the SN, while iSPNs send axons to the eGP (Fig.4). Functionally, it is proposed that dSPN activation promotes action selection and positive reinforcement, whereas iSPN are important to suppress unwanted motor sequences (Cui et al., 2013; Freeze et al., 2013; Kravitz et al., 2012; Vicente et al., 2016). However, direct and indirect pathway SPNs have opposite effects on movement while being completely intermixed within the striatum forming a relatively uniform mosaic in a precise three-dimensional organization which ensures the balanced activation of direct and indirect pathways (Gangarossa et al., 2013; Tinterri et al., 2018; Yung & Bolam, 2000).

Concerning the other striatal neuronal cell types, the firing of SPNs is affected by interneurons; these are classified into four groups based on their neurochemical and morphological characteristics: (1) large aspiny ChAT-positive cholinergic interneurons (CINs) and a diverse group of aspiny medium-size GABAergic interneurons which can be further classified into (2) large parvalbumin (PV)-positive interneurons, (3) calretinin (CR)-positive medium-sized interneurons and (4) somatostatin (SST)-, NPY- and nitric oxide synthase (NOS)- positive medium-sized interneurons (Cicchetti et al., 2000; Deng et al., 2007; Figueredo-Cardenas et al., 1996; Kawaguchi et al., 1995). The roles of the SST+ and CR+ GABAergic interneurons remain uncertain; however, CINs and PV+

interneurons are known to modulate striatal projection neurons (Deng et al., 2007). While GABAergic interneurons exert a powerful inhibitory influence on SPNs (Koós & Tepper, 1999; Tepper et al., 2004), the function of CINs is primarily modulatory and cannot be simply characterized as excitatory or inhibitory (Fig.4). CINs are critical regulators of striatal activity despite constituting a small percentage (1–3%) of striatal cells and their scattered distribution throughout the striatum. This is because of their highly ramified morphology that enables a single neuron to release acetylcholine across a large volume (Tanimura et al., 2018). As such, CINs project to both SPN subtypes, helping to regulate the duration, strength, and spatial pattern of striatal SPN output (Oldenburg & Ding, 2011)

The second organizational scheme of mature striatal architecture, which is superimposed upon the first relatively simple cellular organization, corresponds to the striatum's division into two major neurochemically distinct compartments: small cellular islands known as striosomes (which appear to be an extension of the ventral striatum) and a surrounding matrix (Fig.5). Although both striosomes and matrix contain both dSPNs and iSPNs which are fully intermingled (giving rise to a cellular mosaic that is essential for maintaining a functional balance of striatal activity) these compartments form immunohistologically and functionally distinct modules differing by their input and output patterns of connectivity (Crittenden et al., 2016; Gangarossa et al., 2013; Kelly et al., 2018; Miyamoto et al., 2018; Tinterri et al., 2018). Striosomes occupy 10–15% of the volume and are dispersed in a continuum throughout the 80–85% occupied by the matrix (Brimblecombe & Cragg, 2017).

2.4. Embryonic striatal SPN development

All neural progenitors descend from the neuroepithelial (NE) progenitor cells that form the neural tube in the developing embryo. After the closure of the neural tube, distinct rostral, medial, and caudal regions develop to ultimately give rise to the frontal, middle, and hindbrain regions of the brain (Stiles & Jernigan, 2010). In mammals, the striatum is derived from the embryonic ventral telencephalon (developing forebrain), which contains the lateral ganglionic eminence (LGE) which mainly gives rise to SPNs (Deacon et al., 1994; Nery et al., 2002; Olsson et al., 1998; Wichterle et al., 2001); and the medial ganglionic eminence (MGE) that gives rise to the interneurons of the striatum,

GP, and cortex, among others (Fig.6A; Marin et al., 2000). Embryonic striatal development involves a critical period during which the shaping of striatal circuitry takes place. This developmental window brings into play a host of specification, migration, and interaction processes as well as numerous transcriptomic programs, all tightly regulated in time and space (Lebouc et al., 2020).

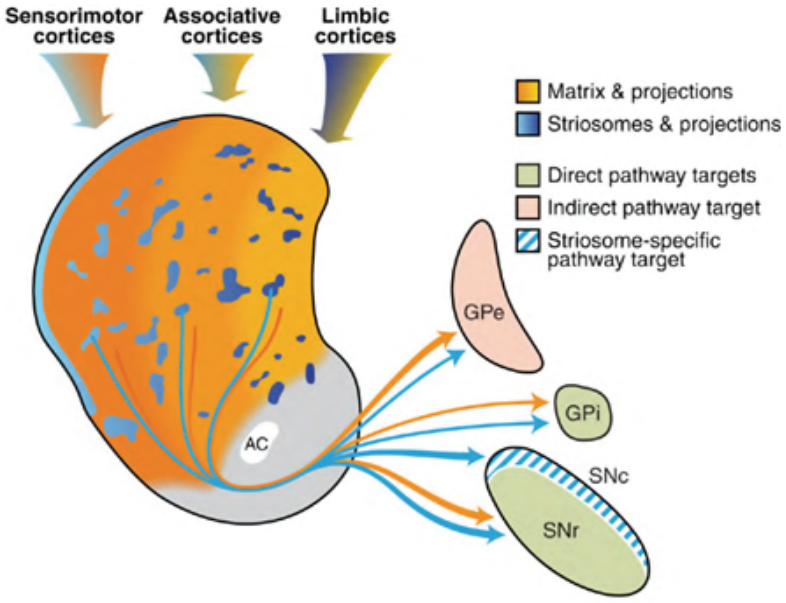

Figure 5. Neuroanatomical connections of the basal ganglia model of the direct, indirect, and striosome-specific striatal projection pathways from the dorsal striatum. Striosomes are shown in blue, and the extra-striosomal matrix in orange. Shading of the striatum from medial (right) to lateral (left) schematically indicates limbic, associative, and sensorimotor striatal domains. Arrows flowing into the striatum are colored to represent the relative abundance of inputs from limbic cortical regions to striosomes and from sensorimotor and associative regions to the matrix. Arrows exiting the striatum represent GABAergic efferent connections from the spiny projection neurons (SPNs) in the striosome and matrix compartments to their respective downstream target nuclei. The nucleus accumbens is shown in gray. Adapted from (Crittenden & Graybiel, 2011). GPe, external segment of the globus pallidus; GPi, internal segment of the globus pallidus (entopeduncular nucleus, in rodents); SNr, substantia nigra pars reticulata; SNc, dopamine-containing substantia nigra, pars compacta; AC, anterior commissure; STN, subthalamic nucleus.

The LGE, which forms in rodents at embryonic day 9.5 (E9.5), is an intense neurogenic zone containing a pool of NE progenitor cells in the ventricular region. These NE cells first give birth to cells which send projections into the subventricular region of the LGE and thus shape radial glia (RG). The latter are the RG cells from which all SPNs originate (Sousa & Fishell, 2010). The same pool of RG cells then differentiates sequentially into two distinct subpopulations of intermediate progenitors (IP) during striatal neurogenesis, first into apical (aIP) then into basal IP (bIP) cells, although the link

between these two types of neuronal progenitors and the two SPN subpopulations has not yet been established (Fig.6B; Pilz et al., 2013; Turrero García & Harwell, 2017).

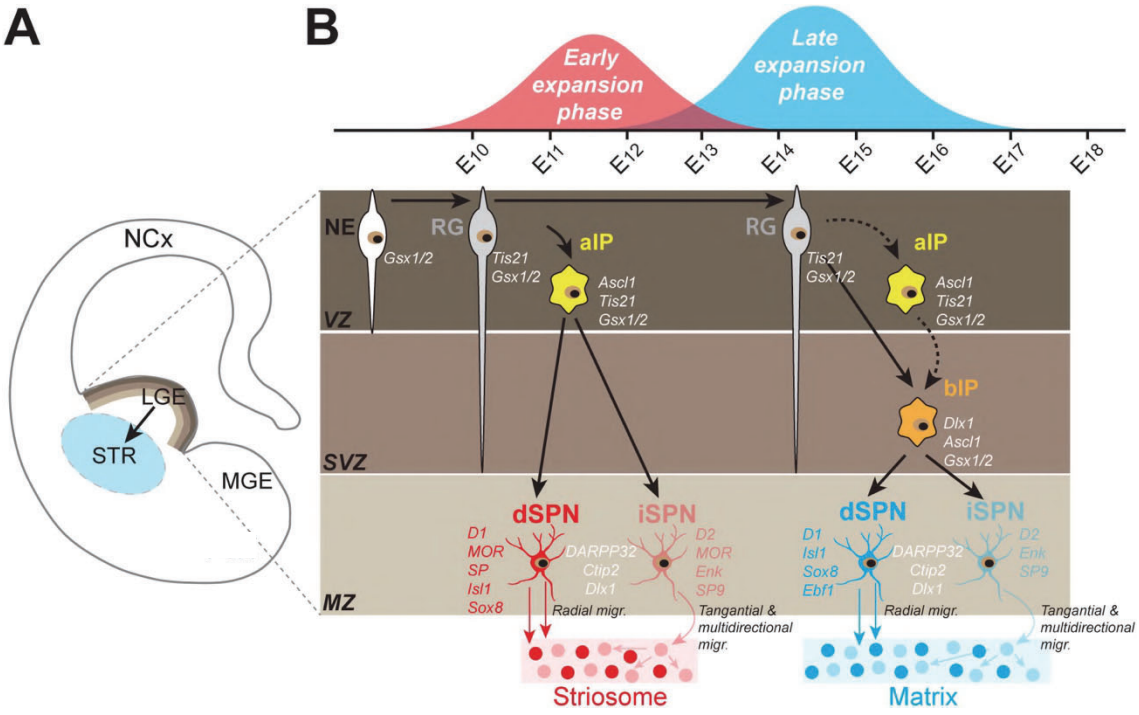

Figure 6. Current model of embryonic mechanisms underlying striatal architecture and the ontogenesis of SPNs. **(A)** Schematic representation of a coronal hemisection of the developing brain in which are represented the neocortex (NCx), striatum (STR), lateral ganglionic eminence (LGE), medial ganglionic eminence (MGE) and the preoptic area. **(B)** Enlargement of the LGE region indicating the different expansion phases of neuroepithelial (NE) cells leading to the formation of striosomal and matrix striatal compartments. In the early (E10-E13.5 in mice) expansion phase, NE cells give rise to radial glial (RG) cells that generate apical intermediate precursors (aIP), which in turn give rise to striosomal dSPNs and iSPNs. A second wave of expansion takes place between E12.5 and E17 (in mice), during which RG cells give rise directly or indirectly through aIP (dashed arrows) to basal intermediate precursors (bIP) which will produce matrix dSPNs and iSPNs. While striosomal and matrix dSPNs eventually reach their final destination in the developing striatum following radial migration, iSPNs reach their targets through a tangential and multidirectional migration process. The molecular identity of the different neuronal progenitors is indicated by the expression of transcription factors (Gsx1/2; Tis21; Ascl1; Dlx1), whereas the molecular identity of mature striosomal and matrix SPNs appears in red and blue, respectively. Adapted from (Lebouc et al., 2020) . dSPN, direct pathway SPN; En, embryonic day n in mice; iSPN, indirect pathway SPN; MZ, mantle zone; SPN, striatal projection neuron; SVZ, subventricular zone; VZ, ventricular zone

Kelly et al. showed the existence of a developmental program integrated within mice LGE RG cells, which runs sequentially in time and space in two phases with a partial temporal overlap. During an early phase extending from ~E10 to ~E13.5, the pool of RG cells is restricted to the production of aIPs that in turn give rise almost exclusively to striosomal SPNs. Then, almost all matrix SPNs are generated at a later and longer phase

beginning at ~E12.5 and ending at ~E17, from the same pool of RG cells after an intermediate differentiation step into bIPs (Fig.6B; Kelly et al., 2018a). Moreover, a differential gene expression profile is associated with each cell type. NE cells express the transcriptional factor (TF) GS homeobox 1/2 (Gsx1/2), while RG cells express Gsx1/2 and the TF Tis21 ($Gsx1/2^{+}/Tis21^{+}$). In turn, in IP cells, two neurogenic factors appearing sequentially during striatal neurogenesis allows aIPs from bIPs to be distinguished. Specifically, aIPs express the TF achaete-scute family bHLH 1 (Ascl1) but not the TF distal-less homeobox 1 (Dlx1), whereas bIPs express both (Ascl1+/Dlx1+; Fig.6B). This sequential gene expression is proposed to be involved in the chronological production of the two SPN subtypes, where Dlx1 would act downstream from Ascl1 within the bIPs to give rise to matrix SPNs (Kelly et al., 2018; Martín-Ibáñez et al., 2012). Along these lines, Dlx TFs have been proposed to drive forebrain GABAergic neuronal differentiation, with Dlx2 and Dlx1 (co-expressed in most SVZ progenitors) promote activation of Dlx5 and Dlx6 thereby generating cells with four degrees of Dlx redundancy, creating an evolutionarily buffered foundation for ensuring the generation of forebrain GABAergic SPNs (Anderson et al., 1997). The progenitors within the LGE can be further distinguished through differential transcription factor expression from those found in neighboring eminences. For example, the MGE expresses the transcription factors NK2 Homeobox 1 (Nkx2.1) and LIM/homeobox protein 6 (Lhx6), whereas the LGE does not (Chen et al., 2017; Mayer et al., 2018)

From this transcriptional and morphologically diverse population of embryonic progenitors in the LGE, the vast majority of postmitotic neurons become GABAergic striatal SPNs (Corbin et al., 2001; Stenman et al., 2003; Wichterle et al., 1999, 2001). In parallel with, but independently from, the developmental program defining striosome/matrix compartmentalization, many other transcriptomic programs are activated in these same IPs, downstream from Ascl1 and Dlx1, to induce SPN neurogenic specification into dSPNs and iSPNs. The identity of dSPNs is specified by three main TFs, namely Insulin gene enhancer protein Islet-1, Early B-Cell Factor (Ebf1) and SRY-Box Transcription Factor 8 (Sox8), which are expressed as early as E11 in mice and required for the proper development and survival of these neurons (Fig.6B). More broadly, these factors ensure the normal development of the direct projection pathway by promoting the development of embryonic and early postnatal functional direct pathway

connectivity (Lobo et al., 2006, 2008). Regarding Ebf1 specifically, this TF has been shown to be involved in the proper differentiation of matrix compartment dSPNs (Lobo et al., 2006, 2008). For the generation and survival of iSPNs, it has been shown that the TFs Ikaros and Helios are important and also regulate the expression of the iSPN marker ENK (Martín-Ibáñez et al., 2010, 2012). In addition, the TF Sp8 and Sp9 (and their downstream TF Six3) are instrumental for the normal development of iSPNs by driving the striatopallidal progenitor differentiation into iSPNs and also by participating in ensuring the survival of these postmitotic differentiated neurons (Fig.6B) (Long et al., 2009; D. D. Song & Harlan, 1994; Xu et al., 2018; Zhang et al., 2016). While dSPNs and iSPNs are derived from both aIPs and bIPs, which produce striosomal and matrix SPNs, respectively, the relationship between the developmental origins of these two organizational schemes remains to be understood (Lebouc et al., 2020).

After dSPNs and iSPNs are specified in the LGE subventricular zone (SVZ), they migrate alongside the radial glia towards the mantle zone (MZ) to integrate the different compartments under formation (early migration towards the striosomes and later migration towards the surrounding matrix). Once in the MZ, dSPNs and iSPNs actively intermix to shape the mosaic cell architecture that is key for the striatum's function. While it is commonly accepted that SPNs migrate radially to colonize the entire striatum (Halliday & Cepko, 1992; Hamasaki et al., 2003; Song & Harlan, 1994), this assumption has recently been questioned. In fact, it has been showed that after the early specification of dSPNs/iSPNs, iSPNs gradually invade the striatal mantle, laterally and then medially, by a dSPN-dependent tangential and multidirectional migration (Fig.6B; Tinterri et al., 2018). Thus, tangential migration is thought to actively participate in the intermixing of dSPNs and iSPNs within both compartments, in association with the classical radial migration profile of dSPNs (Hagimoto et al., 2017; Tinterri et al., 2018). The mechanisms governing this iSPN migration pattern are still unknown, although Ebf1 seems to play an important role in this process as its inactivation leads to an altered dSPN/iSPN intermixing (Tinterri et al., 2018). The underlying implication is that although dSPN/iSPN specification is largely independent, their intermixing within the different compartments is conditioned by the proper development of both subpopulations, which cooperate and interact together to shape a mature and functional striatal network. Along these lines, the TF Forkhead box P1 (FoxP1), which is expressed in both dSPNs and

iSPNs, could also be involved in this migration process since it has recently been shown to be necessary for the correct migration of iSPNs generated during the early phase of striatogenesis (Anderson et al., 2020).

3. Huntington's disease (HD): the "most curable" of incurable NDs

3.1. History

Back in 1872, Dr. George Huntington wrote a vivid, comprehensive description of hereditary chorea (Huntington, n.d.), in which he reported features such as its hereditary nature, associated psychiatric and cognitive symptoms, and the disease onset in adult life between 30 and 40 years of age. Most importantly, he also outlined the progressive nature of the disease stating. Even though the hereditary nature of chorea had been already described in the 19th century (Elliotson, 1832; Harper, 2002; Watt, 1990), the level of detail of Huntington's description of this condition is what ultimately led to the eponymous designation of this monogenetic, autosomal dominant neurodegenerative disorder as HD (Huntington, n.d.).

However, it took more than a century since this account for the first major advance in this disorder to take place, when in 1983 the location of the gene whose mutation causes HD was reported to be linked to a polymorphic DNA marker that maps to human chromosome 4 (Gusella et al., 1983). In fact, this milestone made HD the first disease gene to be mapped using DNA polymorphisms. It was not until ten years later in 1993 that the single gene responsible for HD (huntingtin, or HTT) was identified by the HD Collaborative Research Group (MacDonald et al., 1993), allowing for the discovery of the causative mutation.

3.2. Etiology and genetics

HD is a genetically inherited autosomal dominant ND (Ross & Tabrizi, 2011). Its causative mutation is almost fully penetrant and truly dominant, which makes genetic testing a bleakly reliable method to diagnose HD, or to predict its future onset (Wild, 2016). Consequently, the presence of this mutation has become the accepted molecular standard to confirm HD status. It is located in exon 1 of the HTT gene (also called Interesting Transcript 15 or IT15), located at chromosome 4p16.3, and which encodes the corresponding HTT protein. The normal function of this protein is not completely

understood yet, although it appears to be related to the modulation of several cell processes including apoptosis, energy metabolism, and neurogenesis (Cattaneo et al., 2005; Reiner et al., 2003). The 348 KD protein contains a polyQ tract in the N-terminal domain, encoded by the repetition of the cytosine-adenine-guanine (CAG) trinucleotide (MacDonald et al., 1993). The mutated HTT (mHTT) protein presents an excessive number of CAG repeats which translates into an expansion of the polyQ tract which affects protein folding and consequently its activity and is believed to be necessary to elicit its toxic effects (Goldberg et al., 1996; Trottier et al., 1995).

Following the autosomal-dominant pattern of inheritance, there is a 50% chance of transmission of the condition to offspring, following an unbroken line of affected relatives, being only able to pass the mutation to the next generation if the individual inherits the mutation himself (Kay et al., 2017). Individuals with HD can become symptomatic at any point between early childhood to old age (ages of 1 to 80 years), but it tends to develop in middle age (the average age of onset is 45 years) being clinically asymptomatic until then (Myers, 2004). However, every individual bearing the CAG expansion mutation in HTT will, at some point, slowly succumb to the progressive, cognitive, motor, and psychiatric impairment that characterize HD, being this mutation the common denominator of all HD patients.

Healthy, unaffected individuals bear CAG repeats in the range of 6-35; mutations in which repeat number is increased to 36-39 repeats show reduced penetrance (some subjects develop HD, while others live without showing any clinical sign). Furthermore, 40 or more repeats will result in full penetrance which inevitably leads to the onset of motor symptoms. CAG repeats of 40-50 will typically cause adult-onset symptoms, and those above ~60 cause juvenile-onset HD (Tartaglione et al., 2017). Along these lines, the length of the CAG repeat is inversely correlated with the onset of clinical symptoms (Duyao et al., 1993). Thus, the age of clinical onset is primarily predicted by the extent of the CAG repeat expansion (although the most common is around the age of 40) and considered to result from cumulative toxic insults, together with environmental and other genetic factors (Wexler, 2004).

3.3. Clinical course

HD has a mean age at onset of 40 (Ross & Tabrizi, 2011). It is a rare disorder with a prevalence of 5–10 individuals per 100,000 in the Caucasian population. Some juvenile forms exist but are rare, accounting for 5% of the cases. The symptoms vary between individuals but are usually characterized by a triad of motor, cognitive, and psychiatric symptoms:

i. Motor symptoms can be divided into the choreiform movements with gait disturbances that tend to appear early in the course of the disease (which constitute one of the most striking signs of the disease); and motor impairments such as bradykinesia (slow movements), akinesia (loss of ability to perform voluntary movements), rigidity and impaired postural reflexesthat are observed in later stage patients (Ghosh & Tabrizi, 2018).

ii. Cognitive symptoms (universal in HD) can be detected up to a decade before diagnosis as subtle cognitive impairments (Paulsen et al., 2008), progressing to subcortical and frontal dementia in advanced-stage HD. Examples of these symptoms include early deficits in visual attention, psychomotor speed and visuomotor and spatial integration (Tabrizi et al., 2013), executive dysfunction, general cognitive slowing, impaired short-term memory, or dementia (Ghosh & Tabrizi, 2018).

iii. Psychiatric symptoms and/or emotional deficits among which depression and anxiety are the most common features, affect a large proportion of patients. Whether these two conditions correlate to disease stage or not is yet to be determined, being possible to observe them even in premanifest HD (Paulsen et al., 2001). On the other hand, some other symptoms such as apathy worsen over time as HD progresses, being significant predictors of functional decline (Tabrizi et al., 2013). Other psychiatric symptoms include irritability, aggression, obsessive-compulsive thoughts and behaviours, psychosis and hyposexuality (later stages) and hypersexuality (early HD; Novak & Tabrizi, 2010). Sadly, suicide is the second most common cause of death in HD, mostly taking place when premanifest patients enter manifest stages and again when loss of independence starts to occur in advanced HD (Lanska et al., 1988).

In terms of clinical course, HD is a slowly progressive condition in which there is relentless deterioration of these cognitive, motor and psychiatric faculties over a 20-to-30-year period (G. P. Bates et al., 2015). Once motor and cognitive impairments begin, progression inexorably continues over the course of the illness, which is uniformly fatal (Ross et al., 2014). Two distinct periods can be distinguished in the course of HD, namely the 'premanifest' and 'manifest' periods. In fact, the former can be even further subdivided. Initially, there is a period during which individuals are indistinguishable from healthy controls ('presymptomatic'), which usually lasts up to 10-15 years before disease onset. This is followed by the 'prodromal' period, characterized by subtle motor, cognitive and behavioural changes, before the 'manifest' period (Ghosh & Tabrizi, 2018). Manifest HD displays slow progression of motor and cognitive symptoms, with irregular progression of chorea (often prominent early but plateauing later) and a steadier progress of fine motor impairments. Once motor and cognitive impairments begin, progression inexorably continues over the course of the illness, which is uniformly fatal (Ross et al., 2014). Notably, HD displays much clinical heterogeneity regarding the balance of motor, cognitive and psychiatric symptoms that predominate, even within families.

3.4. Neuropathology

As mentioned above HD is caused by a single mutation in the HTT gene that results in generation of a toxic mHTT protein (Fig.7A). The neurotoxic (gain-of-function) properties of mHTT are probably accompanied by some loss of wtHTT properties (loss-of-function disease); both contributing to the pathogenesis of HD (Salado-Manzano et al., 2020). Both wtHTT and mHTT are ubiquitously expressed in the body, although they concentrate in the brain and testes (MacDonald et al., 1993). HTT normally interacts with vesicular structures at the synapse, such as clathrin-coated vesicles, endosomal compartments and microtubules (DiFiglia et al., 1995; Hoffner et al., 2002; Velier et al., 1998). The polyQ expansion of mHTT triggers a pathogenic cascade, with both cell autonomous and non-cell autonomous mechanisms involved (Zuccato et al., 2010).

Shortly, the spectrum of cellular aberrations (G. P. Bates et al., 2015), and the resulting neuropathology caused by mHTT involves neuronal cell loss mainly in the striatum (Fig.7A). In fact, one of the earliest and most striking changes in the brain in HD is the atrophy of the striatum, predominantly implicating the degeneration of striatal GABAergic SPNs (up to 95% of SPNs projecting to the GP and SN are lost), and atrophy

of the cortex, subcortical white matter, thalamus and hypothalamic nuclei (although hippocamps and hypothalamus are only affected in later stages) Vonsattel & Difiglia, 1998; Vonsattel et al., 1985). Of note, while SPNs are the main targets of HD, striatal interneurons have been shown to cope with the neurodegenerative processes that are at play in this condition with relative ease. In fact, virtually all the major types of striatal interneurons are believed to be relatively spared in HD (Cicchetti et al., 2000; Deng et al., 2007).

The loss or damage of SPNs is not only associated to HD, but also extends to a spectrum of pathologies that include PD or obsessive-compulsive disorders. In HD, iSPNs are believed to be the most vulnerable and are preferentially lost in brains of presymptomatic and fully symptomatic patients. In contrast, dSPNs are believed to be relatively spared early in the progression of the disorder (Albin et al., 1989; Vonsattel et al., 1985), . The earlier vulnerability of iSPNs in HD could induce imbalances in striatal output to other basal ganglia nuclei, which affects the final outflow to the thalamus and contribute to the motor disturbances in the disease. Interestingly, data from a study by the HD iPSC Consortium shows that mutant mHTT impairs neurodevelopmental pathways that could disrupt synaptic homeostasis and increase vulnerability to the pathologic consequence of expanded polyQ repeats over time and suggests that alterations in an integrated epigenetic network affect neuronal development and could impair adult neurogenesis (HD iPSC Consortium, 2017).

Although a comprehensive understanding of the downstream pathogenic cellular processes is still being sought, two processes that appear to play a key role in HD are altered protein homeostasis and disturbances in mitochondrial function (Fig.7B; Salado-Manzano et al., 2020). Imbalances in the proteasome lead to the activation of proteases that cleave mHTT, generating more toxic species. In parallel, mitochondrial dysfunction is enhanced by defects in calcium homeostasis, aberrant ROS production and oxidative damages (Fig.7B; Saudou & Humbert, 2016). Brain-derived neurotrophic factor (BDNF) may also play a crucial role (Baydyuk & Xu, 2012; Zuccato & Cattaneo, 2007). BDNF is a potent neuroprotector with special affinity for striatal neurons and is decreased in HD due to the imbalances in transcriptional dysregulation and vesicular transport that also occur during the disease (Gauthier et al., 2004; Moumné et al., 2013). As previously described by our group, the decrease of BDNF induces dysfunction of enkephalinergic

neurons which aggravates the symptomatology of HD (Canals et al., 2004). In fact, one of the most studied therapies preclinically has been the exogenous administration of BDNF, as it has demonstrated an ability to improve several motor and cognitive symptoms (Canals et al., 2004). In conclusion, in HD, striatal SPNs receive a combination of pro-apoptotic signals in cell-autonomous and non-cell-autonomous ways that contribute to their vulnerability, leading to dysfunction or even death (Ehrlich, 2012; Morigaki & Goto, 2017).

3.5. Unmet clinical need, current therapeutics, and areas of research

HD is a relatively rare condition with considerably lower prevalence than many other neurodegenerative diseases (such as AD or PD), although it is the most common monogenic neurological disorder. Epidemiological studies of HD report a wide variety (more than ten-fold) in the prevalence rates of the disease worldwide(Rawlins et al., 2016). Approximately, 2 to 10 people per 100,000 worldwide are affected by the disease de (Pringsheim et al., 2012; Ross & Tabrizi, 2011). In Western populations, the figure is higher with 10.6 to 16.7 affected individuals per 100,000 (Evans et al., 2013; Fisher & Hayden, 2014). This is a direct consequence of the fact that the original HD mutation is considered to be originated in Western Europe, having spread around the world largely through emigration (Barboza & Ghisi, 2018). In fact, various populations such as the Chinese, Japanese, African Blacks and Finnish populations are expected to show a lower frequency of HD. In Japan, for instance, HD prevalence is estimated to be from 0.11–0.45 per 100,000 individuals (Squitieri et al., 1994). Approximately 30,000 people in the USA and 38,000 people in Europe suffer from this condition, and a further 250,000 people worldwide are at risk of having inherited the mutated gene (Leegwater-Kim & Cha, 2004). Importantly, these numbers are apparently increasing as showed by Evans and colleagues, who found that in 2010 almost twice as many people as in 1990 had clinical features of HD in the UK, which directly results in an increase in its already substantial associated economic burden (Evans et al., 2013). The direct medical costs of a patient with early and late-stage HD, according to estimates, is $3,257-$4,947 and $22,582-$37,495 per year respectively in the USA, much of which can be attributed to nursing home care costs (Divino et al., 2013). Another study estimated the annual costs of HD in the UK in between £2,250 in the earliest stage of HD and £89,760 per person in the later stages (Jones et al., 2016).

Even more relevant, from a clinical perspective, is the societal burden of HD. The lack of real treatment options stands in stark contrast to the impact that those symptoms have on the lives of not only patients but also their families and caregivers. As the course of the condition progresses, patients suffer from increasing physical and mental deficits, which in turn results in decreasing personal autonomy. The consequences of this progressive decline negatively impact the quality of life of HD patients, leads to suicide motivated by depression and originates physical dependence caused by the impact of symptoms on daily activities (Di Maio et al., 1993; Helder et al., 2001). Furthermore, impairment of the mental health of HD patients constitutes another source of suffering and emotional stress among family members throughout the course of the disease.

As most neurodegenerative conditions, HD is currently untreatable and treatments with the potential to positively influence the underlying pathogenesis are likely to be a long way from becoming a reality (Bartus & Johnson, 2017; Gribkoff & Kaczmarek, 2017; Wild & Tabrizi, 2014). However, despite being rare, HD receives a great deal of research attention since it possesses certain features that make it more likely to be a curable problem than other neurodegenerative conditions. First, its diagnosis is almost definitive and can be made before death given the autosomal dominant nature of the condition. This opens the door to accurately model and study the disease *in vitro* and *in vivo*. More importantly, HD is a reasonably homogeneous condition. Second, early diagnosis can be made before symptom onset. This is a crucial advantage, as it means that therapy can begin before major neuronal loss, when it may be more difficult to slow progression and impossible to correct existing deficits. Finally, the HD community has a history of cooperation, which has made large-scale clinical trials possible, as well as long-term longitudinal studies of disease progression that have provided rich data sources to inform the design of future trials, particularly regarding appropriate trial end points (Tabrizi et al., 2013).

Even though many therapies have been tested at clinical trials for HD, none has been shown to alter the natural history of this condition (Mason & Barker, 2016). Hence, there are no known disease-modifying drugs currently available, as only symptomatic treatments such as movement-suppressing drugs, antidepressants, and physical therapy exist (Fig.8; Reidling et al., 2018). Although these treatment (largely anecdotal rather than evidence based) partially treat a subset of symptoms to improve the quality of life of

patients, they unfortunately do not halt the progression of the disease. In fact, currently there are only two medications approved by the Food and Drug Administration (FDA)for the treatment of HD, both treating chorea symptoms: tetrabenazine (TBZ; Xenazine™, approved in 2008) and its more recently approved deuterated version, deutetrabenazine (AUSTEDO™) (Potkin & Potkin, 2018). Psychiatric symptoms, which are often the most troubling for patients, are often treated with standard drug treatments used in non-HD patients, and the current care of HD patients involves many paramedical disciplines, including speech and language therapy, physiotherapy, nursing, and social care. In turn, pharmacological relief of motor symptoms, such as chorea and dystonia, attempt to restore the balance of neurotransmitters including GABA, dopamine (DA) and glutamate (Glu), but in general their efficacy is very limited (Pidgeon & Rickards, 2013; Van Vugt & Roos, 2012).

To address the toxic gain-of-function of mHTT in HD, there is an extended field working on the development of huntingtin lowering therapies, with the most advanced currently being the lowering of mHTT levels by targeting its mRNA transcripts. Huntingtin-lowering strategies that target RNA or DNA (Fig.8) are reviewed elsewhere (Carroll et al., 2011; Tabrizi et al., 2019; Wild & Tabrizi, 2017). RNA it is easily accessible in both nucleus and cytoplasm and is unprotected by repair machinery (Wild & Tabrizi, 2017). Among these, therapies targeting RNA, such as antisense oligonucleotides (ASOs), aim to reduce the translation of HTT mRNA transcripts, which

should theoretically inhibit all downstream toxic effects and slow, halt or reverse the progression of HD pathology and symptoms (Lane et al., 2018).

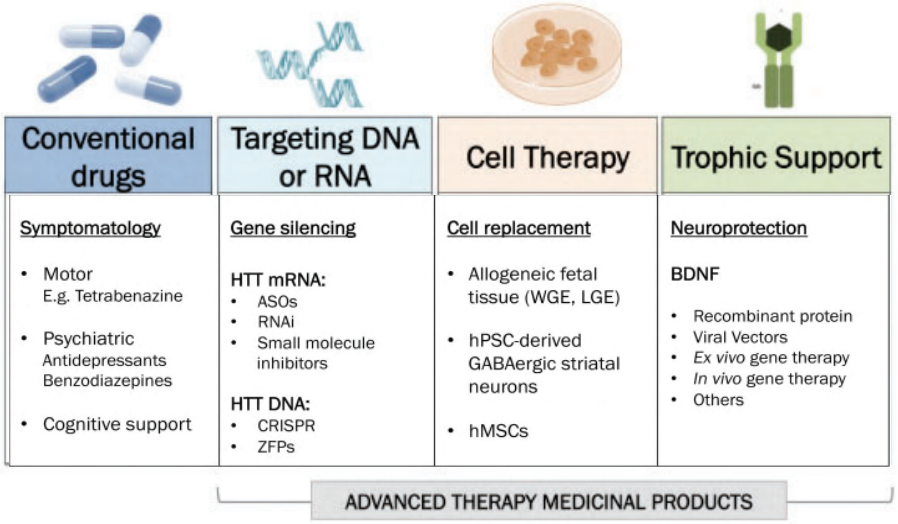

Figure 7. Treatment approaches for Huntington's Disease (HD). Conventional drugs are either targeting motor (e.g., tetrabenazine) or psychiatric symptoms (e.g., antidepressants or benzodiazepines). Therapies targeting DNA or RNA such as ASOs can be applied to silence HTT mRNA. Cell therapy possesses disease-modifying potential through cell replacement. Trophic support is mainly seeking for a neuroprotective effect. Adapted from (Salado-Manzano et al., 2020). ASOs, antisense-oligos; BDNF, brain-derived neurotrophic factor; CRISPR, clustered regularly interspaced short palindromic repeats; hMSCs, human mesenchymal stem cells; hPSCs, human pluripotent stem cells; LGE, lateral ganglionic eminence; HTT, huntingtin; RNAi, RNA interference. WGE, whole ganglionic eminence; ZFPs, zinc-finger proteins

Within RNA-targeting strategies, ASOs are the most advanced in the clinical pipeline, having already reached phase III (P3) clinical trials in HD patients under the name of tominersen (previously known as RO7234292 and IONIS-HTT Rx; F. Hoffmann-La Roche AG and Ionis Pharmaceuticals, Inc.). However, in March 2021 Roche announced that the pivotal clinical trial (P3 GENERATION HD1 or NCT03761849, which completed enrollment of 800 patients in April 2020; Leavitt & Tabrizi, 2020) had stopped after 17 months of the originally planned 25-month trial period, following an unblinded review of an independent Data Monitoring Committee (DMC). Preliminary results demonstrated that patients who received tominersen every 16 weeks performed comparably to their peers on placebo, while those who took tominersen every eight weeks fared worse than the placebo cohort. Despite a lack of clinical efficacy, both regimens achieved a reduction in mHTT levels compared to placebo. However, post-hoc analyses of data from P3 GENERATION HD1 suggested that younger patients with a low disease

burden may have benefited from treatment with tominersen. Consequently, Roche initiated the P2 GENERATION HD2 study (NCT05686551) in February 2023, that aims to recruit 300 participants aged between 25 and 50 with prodromal or early manifest HD. As part of this trial, safety, and efficacy of different doses of tominersen (60 or 100 mg) administered every 16 weeks compared with placebo will be evaluated, with primary results expected by 2026.

Hence, although HTT-lowering therapies are promising, several questions remain open, such as the administration route, the potential toxicity due to lowering endogenous wild type, as well as mHTT by some ASOs, and the need to develop biomarkers that can report on the central lowering of mHTT and early reversal of neuronal dysfunction (Leavitt & Tabrizi, 2020; Lu & Yang, 2012). Furthermore, failures of P3 GENERATION HD1 as well as similar clinical trials such as the P1b/2 PRECISION HD (NCT03225833) and P2 VIBRANT HD (NCT05111249) have thrown into question the clinical efficacy of HTT lowering approaches.

All in all, lack of curative solutions for HD patients, combined with an increasing societal and economic burden associated with the disease, creates a significant unmet medical need, and emphasizes the need to urgently develop new therapeutic options.

4. Cell therapy strategies in HD

4.1. Rationale and mechanism of action

Advanced therapy medicinal products (ATMPs) comprise three different types of medicinal products: gene therapy, cell therapy and tissue engineered products. In addition, they can be combined with medical devices (so called combined ATMPs), for example, a biomaterial used to encapsulate a cell line that releases a neuronal pro-survival molecule (Lindvall & Wahlberg, 2008). ATMPs hold great potential in addressing unmet medical needs for those pathologies that currently cannot be cured with conventional treatments. There are extensive efforts in developing these innovative drugs, which are associated with high levels of complexity in their design, manufacture, distribution, regulation, and application. Despite their complexity, ATMPs such as gene and cell therapy have already demonstrated their safety and efficacy in treating diseases, including

cancer and hematological malignancies. For these reasons, several groups have explored the possibilities of applying cell, gene and tissue engineered therapies to treat NDs.

The ultimate goal of cell therapy in neurodegenerative diseases is to restore the basal ganlia circuitry and hence the lost function due to a neural circuit damage that occurs during neurodegeneration. This restorative goal can be achieved through three main approaches: (i) functional replacement of lost neural cells; (ii) enhancement of endogenous regeneration (which is a significant process in some regions of the adult brain in animal models, but its significance still widely discussed in human patients); and (iii) supply of pro-survival factors that are decreased because of the pathogenesis of the disease. In this context, cell therapy is a potential medical intervention for HD, currently being the only approach focused on structural and functional restoration of atrophied tissue in HD by replenishing the degenerating SPN population (Bachoud-Lévi et al., 2021). In fact, cell therapy has the potential to have an important place in the treatment of HD for individuals with existing cell loss, considering that experimental therapies for HD cannot recover cells already lost, and striatal cell loss can be measurable even decades before disease onset (Klöppel et al., 2009; Tabrizi et al., 2012). This is especially true in the absence of therapies that can be delivered in the presymptomatic stage of the natural history (to which could prevent cell loss), and also in the event that future disease-modifiers may only slow (rather than halt) disease progression. Although it is anticipated that cell therapy may be a stand-alone treatment for some patients with HD, graft-induced improvement could eventually be overtaken by the underlying disease process, therefore, it is important to note that cell therapy is likely to be fully compatible with other potential therapies on the horizon, thus addressing both existing and ongoing cell loss and potentially making it widely applicable. It is also possible that implanted cells could be engineered pre-transplantation to deliver disease-modifying molecules (Rosser et al., 2022).

HD is a potential indication for regenerative medicine and represents a ND paradigm in which to establish principles for its safe and efficient clinical translation. As such, HD possesses biological features that makes it a particularly good cell therapy target. There is a focal area of degeneration and a single cell type loss (at least in the early to moderate stages of manifest disease) which starts well before symptom onset, correlates best with clinical evolution, and is the best marker of disease progression (Tabrizi et al., 2012).

Moreover, the degeneration of extra striatal regions in HD may be partly caused by the earlier disappearance of their striatal targets, in accordance with the hierarchy of neuronal network disturbance in HD (McColgan et al., 2018); hence, restoration of lost striatal cells could even reduce this retrograde degeneration (Dunnett & Rosser, 2011a). Furthermore, HD presents a valuable model of neurodegeneration more generally in which to investigate how to succeed in cell therapy in a wide range of neurodegenerative conditions, based on three main features. First, it can be diagnosed with certainty in life and indeed, prior to symptom manifestation. Secondly, the underlying pathophysiology and the clinical phenotype of the disease are well understood, which allows for optimization of clinical outcome measures and the development of a platform for clinical trials. Thirdly, there are multiple animal models available (rodent, primate, and model organisms), which provide an excellent laboratory platform for discovery and preclinical research of novel therapeutics for HD (Dunnett & Rosser, 2011a).

Cell therapy approaches present many advantages over conventional treatments. Cell grafts can provide continuous replenishment of neurotransmitters and hold the potential to integrate in the brain network and to produce long-term neuromodulation of the lost functionality in the basal ganglia (Dunnett & Björklund, 2017; Piquet et al., 2012). Either engineered to overexpress trophic factors or unmodified, stem cells release trophic factors such as BDNF and glial cell line-derived neurotrophic factor (GDNF) among others, as well as other growth factors and cytokines. The cocktail of small molecules continuously secreted by the cells has the potential to modulate neuroplasticity and induce neurogenesis (Drago et al., 2013; Reza-Zaldivar et al., 2019; Salgado et al., 2015; Vogel et al., 2018).

4.2. Allogeneic fetal neural tissue transplantation strategies

4.2.1. Preclinical studies

The first cell replacement therapy approach to be explored, which started to be considered more than 30 years ago, is based on transplantation of human neural fetal tissue (hNFT) issued from human fetal cells after abortion. These allografts were initially derived from the whole ganglionic eminence (WGE), an area of the fetal brain that largely gives rise to striatal areas in adults and which contains the LGE (Deacon et al., 1994; Döbrössy & Dunnett, 2003; A. E. Evans et al., 2012; Graybiel et al., 1989; Marin et al., 2000; Mazzocchi-Jones et al., 2009; Olsson et al., 1995, 1998; Pauly et al., 2012; Straccia

et al., 2016). Noteworthy, a short time after the first early-study WGE transplants, the strategy was modified to enrich the population of striatal precursor cells, by dissecting only the LGE, rich in SPNs. While some studies revealed some behavioral improvement in rodents using both strategies, survival and striatal graft volume were greater in WGE grafts (Kordower et al., 1995). Hence, cells from the WGE are considered the "gold standard" for cell replacement in HD as the donor cells have the capacity to differentiate into the target cell type (Precious, 2017).

Using this approach, minced tissue pieces or cell suspension preparations derived from the fetal neural tissue were first transplanted via stereotaxic surgery to animal models. There has been a substantial amount of preclinical work that has demonstrated that SPNs precursors procured directly from the developing striatum can survive, continue differentiating, make neural connections (host-to-graft innervation) and improve motor deficits when transplanted into animal models of HD, including rat and non-human primates (Bachoud-Levi et al., 2000; Capetian et al., 2009; Kendall et al., 1998; McLeod et al., 2013; Paganini et al., 2014; Pundt et al., 1996; Schackel et al., 2013; Yhnell et al., 2016). These studies have demonstrated that implanted cells can create functional synaptic connections and integrate into the neural circuitry, provided they meet the following conditions: (i) they are obtained during the appropriate developmental window; and (ii) they are directed to a GABAergic SPN fate (Dunnett & Rosser, 2014). Along these lines, it is important to bear in mind that optimal grafts are those derived from fetal WGE collected during the peak period of SPN neurogenesis (around 8-10 weeks of gestation in humans) (Dunnett & Rosser, 2011b).

4.2.2. Human pilot studies

The preclinical evidence provided the rationale for exploring cell replacement in HD patients and promoted subsequent fetal neural transplantation studies into the damaged striatum of mid-stage HD patients in several locations worldwide, in order to explore whether this strategy could repair the damaged circuitry and thus restore motor and cognitive functions. These studies have provided evidence of safety and feasibility of intra-striatal transplantation of hNFT in HD.

All in all, since the first-in-human trial in 1990, there have been a limited number of small pilot trials conducted worldwide (Table 1; Bachoud-Lévi, 2017). Most of these

open-label studies had single-figure sample sizes (from 1 to 16 patients depending on the study), in part due to the constraints associated with the use of human fetal tissue. A total of nine groups were involved in the initial trials of hNFT transplantation in HD using either cell suspensions or small blocks of dissected tissue from the ganglionic eminence, with clinical data available for 46 of patients. Out of these, only four showed dramatic and long-lasting improvements over more than six years following transplantation (Bachoud-Lévi, 2017).

Of note, in the Créteil pilot trial, transplantation showed benefit in three out of five patients, with results clearly more robust than those of previous studies; this was confirmed by different blinded evaluations, including clinical outcomes, positron emission tomography, electrophysiology, digitalized movement analysis or video records of the total motor score (Bachoud-Levi et al., 2000; Bachoud-Lévi et al., 2000, 2006; Gaura et al., 2004). Reasons for the lack of effectiveness of transplantation of the other two patients were postulated to be advanced disease stage which did not allow for efficient graft vascularization, as shown by post-mortem analyses (Bachoud-Lévi et al., 2002; Cisbani et al., 2013) and graft rejection (Krystkowiak et al., 2007). In a separate study in London, graft survival was confirmed in two patients by increased raclopride positron emission tomography signal (Reuter et al., 2008). While one of these patients remained relatively stable, the second one showed motor improvement and was able to return to normal life and cope with daily-life activities after five years.

In summary, these promising and pioneering studies, which assessed different parameters including feasibility, safety, and tolerability of this procedure in patients with HD, did not present major complications associated with the surgery. However, they yielded mixed results, and did not generate enough data supporting its long-term beneficial effects. Despite the benefit showed in the Créteil and London studies and improvements observed up to 1.5 years following transplantation in other studies, they failed in halting disease progression. This failure has been linked to the lack of effective donor sources (heterogeneity and shortage of fetal tissue of suitable quality), trial design heterogeneity (different patient characteristics, cell sources, surgical procedure or immunosuppression regimens) and transplantation of poorly defined cell populations.

Furthermore, the use hNFT is hindered by the ethical concerns associated with the use of aborted human fetal tissue (Bachoud-Lévi, 2017).

Table 1. List of Huntington's disease (HD) cell transplantation pilot open-label trials using human neural fetal tissue (hNFT) performed worldwide. Adapted from (Bachoud-Lévi, 2017) . Ant, anterior; Aziat, azathioprine; C, caudate; Cyclo, cyclosporine; GE, ganglionic eminence; LGE, lateral ganglionic eminence; LVE, lateral ventricular eminence; mid, median; P, putamen; post, posterior; Pred, prednisolone; W, weeks; WGE, whole ganglionic eminence.

	Los Angeles	Créteil	Tampa	Nest, UK	London	Florence
References	(Keene et al., 2007, 2009; Kopyov et al., 1998; Philpott et al., 1997; B. D. Ross et al., 1999)	(Bachoud-Levi et al., 2000; Bachoud-Lévi et al., 2000, 2002, 2006; Douaud et al., 2006; Gaura et al., 2004)	(Cicchetti et al., 2000; Cisbani et al., 2017.; Furtado et al., 2005; Hauser et al., 2002)	(Barker et al., 2013; Maxan et al., 2018; Rosser et al., 2002)	(Reuter et al., 2008)	(Gallina et al., 2008, 2010, 2014; Mascalchi et al., 2014; Paganini et al., 2014; Porfirio et al., 2015)
Injectate	Micropieces	Micropieces	Micropieces	Suspension	Suspension	Suspension
GE part	LGE; 1 sural nerve	WGE	LVE	WGE	WGE	WGE
N fetuses / age	5-8/~9-10 W	1-2/7-9 W	1-8/8-9 W	1/8.5-12 W	2-3/9-10 W	1/9-12.4 W
N and tracts location	1-2 C; 3-4 P	2 C; 2 ant-P; 1 post-P	0-2 C; 3-6 P (max post)	4-6:2 C; 2 ant-P; 2 post-P	1 C; 3 P ant, mid, post	Mean 6.6 (3-9 C and P)
Volume/tract	80-120 µL	40 µL	16-20 µL	12 µL	NA	50 µL
Immunosuppression	Cyclo M18-35	Cyclo, Pred, Aziat M18	Cyclo M6	Cyclo, Pred, Aziat>M6	Pred, Cyclo1 Y	Cyclo, Pred, Aziat 1Y
Grafted patients (N)	14	5	7	5	2	16
Autopsied cases (N)	3	n/a	4	1	n/a	1
HLA antibodies	n/a	n/a	n/a	n/a	n/a	9/16

4.3. Human pluripotent stem cells (hPSCs)

More readily available and renewable alternative sources of SPNs are required to circumvent the significant constraints associated with the use of fetal-derived cells. Along these lines, human pluripotent stem cells (hPSCs) represent a potentially unlimited alternative source of tissue to enable the clinical translation of cell therapies for HD, and thus have been investigated as donor cell sources mainly in preclinical studies in animal models. hPSCs are a unique class of undifferentiated cells characterized by an unlimited self-renewal capacity and their ability to differentiate into all specialized cells of the adult body by developing into cell types that represent the three embryonic germ layers—mesoderm, ectoderm and endoderm. hPSCs can be classified into two main types with different origin: human embryonic stem cells (hESCs) and human induced pluripotent

stem cells (hiPSCs). These two cell types hold unprecedented promise for a wide range of uses, including mechanisms of embryonic development (Zhu & Huangfu, 2013), disease modelling, drug discovery (Avior et al., 2016), and regenerative medicine (Yamanaka, 2020).

hESCs are derived from the inner cell mass (ICM) of preimplantation embryos in the blastocyst stage (five to eight days after fertilization; Evans & Kaufman, 1981; Thomson et al., 1998), with the first hESC line being generated in 1998 (Thomson et al., 1998). In turn, hiPSCs are produced by inducing dedifferentiation of adult somatic cells to a pluripotent state via cell reprogramming (Takahashi et al., 2007; Takahashi & Yamanaka, 2006). Reprogramming is usually done by administering four transcription factors: Oct4, Klf4, Sox2 and c-Myc to adult somatic cells. The first hiPSCs were generated by Yamanaka et al. in 2006 (Takahashi et al., 2007). Of note, these cells would maintain any genetic modification derived from its origin, which is especially relevant for a genetic disease such as HD. While hESCs are arguably the closest to clinical trial at the current time (largely because they have been the subject of research for the longest time and are thus underpinned by a large body of knowledge), the ethical concerns associated with their use are a major issue limiting their clinical application. The main advantage of hiPSCs over hESCs for regenerative medicine applications is that hiPSCs have less ethical concerns than previous approaches and are expected to generate less immune reaction than previous approaches (especially given the possibility to use them as an autologous therapy), although further investigation is warranted (Aron Badin et al., 2019; Mehler et al., 2020; Scheiner et al., 2014).

Specifically for cell replacement applications in the context of HD, hPSCs have to be differentiated *in vitro* towards the cell type of interest (SPN progenitors). Consequently, endogenous *in vivo* striatal development has been mimicked by an increasing number of published protocols for differentiating hPSCs towards committed SPN progenitors (Adil et al., 2018; Arber et al., 2012; Aubry et al., 2008; Besusso et al., 2020; Choompoo et al., 2021; Comella-Bolla et al., 2020; Delli Carri et al., 2013; Jeon et al., 2012, 2014; Ma et al., 2012; Nicoleau et al., 2011; Wu et al., 2018).The first protocol to differentiate hESCs to striatal precursors *in vitro* was described in 2008 (Aubry et al., 2008). Over the years, several groups have succeeded in generating hPSC-derived

GABAergic SPNs (as demonstrated by immunostaining for SPN markers, electrophysiology, gene expression profile-based analyses and functional integration *in vivo)* with very promising results, as summarized elsewhere (Reddington et al., 2014) including efforts by our group (Comella-Bolla et al., 2020; Straccia et al., 2016; Telezhkin et al., 2015).

5. Roadblocks for clinical translation of hPSC-derived therapies

5.1. hPSC in vitro genomic instability

Although it has only been 24 years since human hESCs were first derived (Thomson et al., 1998), and around 15 years since human hiPSCs were originally described (Takahashi et al., 2007), the use of human hPSCs has gained momentum and become increasingly widespread. hPSC-based therapies for the treatment of degenerative diseases including heart disease, diabetes or neurodegenerative disease have been developed by the differentiation of hPSCs to the affected cell type for subsequent transplantation into patients. In fact, clinical trials for regenerative medicine using derivatives of these cells are already underway or on the horizon and have, up to now, shown the cells to be generally safe (Barker et al., 2017; da Cruz et al., 2018; Mandai et al., 2017; Schwartz et al., 2012, 2015; Schweitzer et al., 2020; W. K. Song et al., 2015).

However, despite the progress and the investment made towards research and development aimed at harnessing the curative potential of hPSCs, their clinical translation has been hampered by the presence of mutations in these cells. Although hPSCs are mostly diploid when first derived, it is now recognized that they can acquire different types of genetic alterations on prolonged cell culture passages (Halliwell et al., 2020). Indeed, one potential clinical trial of retinal pigment cells from an autologous iPSC line for age-related macular degeneration was halted once it was discovered that the cells carried a point mutation even though the significance of this particular mutation was unknown (Garber, 2015; Mandai et al., 2017). This case highlighted the fact that genetic changes in hPSCs could jeopardize not only the safety of hPSC-based cell products for regenerative medicine (Sato et al., 2019; Yasuda et al., 2018), but also lead to heterogeneous differentiation propensity of the starting material, altered gene expression profiles and inefficiency of the final cell product (Halliwell et al., 2020).

Around twenty years ago, genomic instability in hPSCs was first recognized when karyotypic abnormalities in hESCs were detected by G-banding karyotypes as non-random gains of particular chromosomes or fragments of chromosomes, notably chromosomes 12 and 17 (Baker et al., 2007; Draper et al., 2004). Later, a large collaborative study published in 2011 by the International Stem Cell Initiative (ISCI) showed that these aberrations were present across the entire genome in cell lines analyzed worldwide (Amps et al., 2011). As of today, many different genomic abnormalities have been discovered in both hESC and hiPSC lines (Lund et al., 2012; Martins-Taylor & Xu, 2012; Ronen & Benvenisty, 2012), ranging from whole chromosome aneuploidies to subchromosomal aberrations (such as gene duplications and deletions and single base pair changes) (Amps et al., 2011; Laurent et al., 2010; Peterson et al., 2011; Taapken et al., 2011). Interestingly, many of these genetic abnormalities are often recurrent and while aberrations are found across the entire genome, there are some chromosome regions more prone to gains or loses. Interestingly, some of these recurrent abnormalities are particularly subtle and difficult to detect by most widely-used standard cytogenetic procedures (G-banding) and may therefore go unnoticed even when present in a substantial proportion of the cells (Halliwell et al., 2020).

The repetitive, non-random nature of many of these recurrent mutations observed in hPSCs, as well as their high prevalence and its propensity to rapidly out-compete normal cells in culture within few passages, has been directly linked the selective growth advantage that these aberrations confer to the cells in culture (Ben-David et al., 2010; Fathi et al., 2018). Furthermore, genetic instability may not only provide a selective advantage in the form of a faster cell cycle time, an altered pattern of differentiation, or an increased rate of survival, but also change hPSC functional characteristics, including decreased differentiation potential, increased capacity to self-renew and a shift towards malignant properties. In fact, many of the recurrent chromosomal aberrations seen in hPSC are also associated with known human cancers, which raises concerns over using these cells for therapeutic applications (Keller & Spits, 2021).

Overall, due to their frequency and functional consequences which can affect the outcome of both research and clinical, applications recurrent genetic alterations found in cultured hPSCs are not acceptable. Even if the underlying mechanisms that cause the observed genetic variations are unclear, it has become evident that suboptimal *in vitro*

culture conditions (Thompson et al., 2020) and the high levels of DNA damage compared to somatic cells are the two main drivers of genomic alterations which compromise the maintenance of genetically normal hPSCs. Consequently, and even if some of the abnormalities detected in hPSCs are likely to have been already present in the embryos or somatic cells from which the cell line was derived or have been induced during such derivation (Amps et al., 2011; Rouhani et al., 2016), an increasing number of reports link the occurrence of acquired genomic abnormalities to suboptimal cell culture techniques, prolonged passage or changing the culture conditions (Baker et al., 2007; Forsyth et al., 2006; Garitaonandia et al., 2015; Jacobs et al., 2016).

To ensure the genomic integrity of hPSCs, it is of foremost importance to develop culture conditions that minimize change in hPSC cultures. As important as minimizing genomic variability in hPSC cultures is to implement appropriate screening methods which can reliably detect not only chromosomal aneuploidies, but also more insidious subchromosomal aberrations. However, and mainly due to the cost and labor involved, current screening practices are infrequent and unsatisfactory, which could lead to the use of hPSCs harboring undetected mutations which could affect their clinical application. Along these lines, the genetic instability showed by hPSCs in culture makes the frequent reassessment of genomic integrity an essential requirement when planning to use them for experiments, as an increasing number of reports is recommending (Schweitzer et al., 2020; Yamanaka, 2020).

As clinical trials using hPSC-derived cells are underway, it is crucial that the implications of genomic alterations in hPSCs are understood, as well as how to detect and minimize their occurrence in hPSC cultures. To accomplish this goal, reproducible conditions of maintenance and genomic screening need to be established. Thus, the implementation of a quality management system (QMS) which defines standards for hPSC culture, controls, detects, and tracks errors affecting the quality of the cultured cells, and ensures the accuracy, reliability, and traceability of results is indispensable not only to minimize genomic variability in hPSC *in vitro*, but also to avoid misdetection of genomic alterations of the cell lines. Under a QMS, changes in cell culture conditions are minimized, cell culture practices are optimized, and the quality of the used reagents is ensured, which provides a fertile ground to explore its effects on the genetic stability of hPSCs. In fact, the Organization for Economic Co-operation and Development (OECD)

has recently published the Guidance Document on Good *In Vitro* Method Practices (GIVIMP; OECD, 2018) to foster confidence in *in vitro* alternatives to animal testing.

5.2. Heterogeneity of hPSC-derived grafts

Even though striatal differentiation protocols have improved in terms of quality and reproducibility over the years, current methods have not been able to synchronize the birth and development of cell populations to the extent seen in normal striatal development; consequently, the resulting neural compositions exhibit broad cellular heterogeneity concerning developmental stage and lineage specification. This lack of purity leads to an inefficient production of the target SPN phenotype with only 40–50% efficiency in hPSC differentiation towards a SPN phenotype being reported at best (Li & Rosser, 2017). Furthermore, resulting neural compositions are variable depending on individual experiments and cell lines (Osafune et al., 2008), which results in high batch-to-batch variation impeding their clinical and experimental utility.

From a safety perspective, the issue of teratoma formation and graft overgrowth due to the presence of residual undifferentiated cells in the graft must also be overcome. who also demonstrated *in vivo* integration of these hESC-derived progenitors following intra-striatal transplantation into a QA rat model (Aubry et al., 2008). However, despite succeeding in differentiating hESCs into SPNs, this protocol was also associated to some risk of teratoma formation, due to the possible presence of unwanted undifferentiated cells in the graft (Grabel et al., 2012; Hentze et al., 2009). One of the first studies reporting transplantation of hPSC-derived striatal progenitors into rodent striatum demonstrated *in vivo* integration of the graft, but also found evidence of substantial graft overgrowth and limited integration, with presence of immature, highly proliferative cells in the grafts (Aubry et al., 2008). Later works from our group and others have optimized neural differentiation methods to minimize the possibility that a cell product contains overly proliferative populations, and showed graft survival, further *in vivo* differentiation into functional DARPP-32^{+} SPNs, and partial improvement of striatal function others (Adil et al., 2018; Arber et al., 2012; Besusso et al., 2020; Comella-Bolla et al., 2020; Delli Carri et al., 2013; Jeon et al., 2012, 2014; Ma et al., 2012; Wu et al., 2018); however, the data demonstrating lack of uncontrolled growth will need to be robust for clinical applications (Garcia Jareño et al., 2022).

In summary, clinical translation of striatal differentiation protocols requires standardization of production procedures for reproducible generation of defined functional cell products, by ensuring the presence of correctly specified target SPN progenitors and the absence of unwanted overly proliferative cell types.

OBJECTIVES

Objectives

I. To analyze the consequences of standardizing routine *in vitro* culture conditions in the genomic stability of hPSCs.

II. To identify and validate cell surface marker signatures of striatal progenitor subtypes derived from hPSCs.

III. To investigate whether hPSC-derived postmitotic striatal progenitors can be isolated using previously identified cell surface signatures.

IV. To analyze if isolated hPSC-derived postmitotic striatal progenitors can survive *in vivo* following intra-striatal transplantation in adult mice.

V. To study whether different subpopulations of hPSC-derived postmitotic striatal progenitors can be isolated at different timepoints of *in vitro* differentiation.

MATERIALS AND METHODS

Materials and Methods

1. Literature search

We used NIH's PubMed.gov (https://pubmed.ncbi.nlm.nih.gov/; accessed on 24 February 2022) to perform several literature searches of published studies of interest. For all of them, we excluded from the search all studies which were published before 1990 or after 2021. We filtered publications of interest using the following search queries: (i) hPSCs, hPSC, human pluripotent stem cell or human pluripotent stem cells; (ii) hESCs, hESC, human embryonic stem cell or human embryonic stem cells; (iii) hiPSCs, hiPSC, human induced pluripotent stem cell or human induced pluripotent stem cells; (iv) (hPSCs, hPSC, human pluripotent stem cell or human pluripotent stem cells) and (karyotype, G-band or aCGH); (v) (hESCs, hESC, human embryonic stem cell or human embryonic stem cells) and (karyotype, G-band or aCGH); and (vi) (hiPSCs, hiPSC, human induced pluripotent stem cell or human induced pluripotent stem cells) and (karyotype, G-band or aCGH)

2. Human Pluripotent Stem Cell lines

We analyzed a total of 11 control and 8 disease-affected female hPSC lines, which are listed in Table 2. All the disease-affected hPSC lines carry an *HTT* gene CAG expansion of different length, but indicative of Huntington's disease in all cases. The use of hPSC lines of the present study is under the ethical permission 0336/2939/2019 (Generalitat de Catalunya, Barcelona, Spain). All cells were regularly tested for mycoplasma contamination and karyotype normality and grown in a 37 ºC incubator with a humidified atmosphere and 5% CO_2.

3. Animals

Adult male C57BL/6J mice (Charles River Laboratories, Wilmington, MA, USA) were housed with access to food and water *ad libitum* in a climate-controlled room under a 12-hour light/dark cycle. All procedures involving the use of animals were approved by the Animal Experimentation Ethics Committee of the Universitat de Barcelona (183/20; Barcelona, Spain) in compliance with the Spanish (RD 53/2013) and European (2010/63/EU) regulations for the care and use of experimental animals.

4. Human Pluripotent Stem Cell culture

4.1. Initial expansion of hPSC lines with original protocols

We received the hPSC lines from several centers, and the cells were initially expanded using the original protocols [Pre-adaptation (PrA) condition]. We tested up to 5 different protocols which have been previously described in the literature (Bradley et al., 2011; HD iPSC Consortium, 2012; Meiser et al., 2021; Ooi et al., 2019; Warmflash et al., 2014). For each cell line, a vial of the initial PrA cell bank was thawed and adapted to the standard cell culture conditions used in our laboratory [Post-adaptation (PoA) condition], which refer to the hPSC maintenance in mTeSR1 media with ROCK inhibitor protocol.

4.2. Human PSC Thawing in mTeSR1 media with ROCK inhibitor

Frozen hPSC vials were removed from liquid nitrogen storage tanks and transferred to dry ice. Vials were thawed in 37 ºC bath by gently swirling in the water for about 15 seconds. Prior to the complete thawing, cells were transferred to a 10 ml conical tube and 9 ml of warmed serum-free defined mTeSR1 medium, which contains recombinant human bFGF and recombinant human TGFβ (complete mTeSR1: mTeSR1 basal medium (85850) and mTeSR1 supplemented 5 × 8 (85852); StemCell Technologies Inc., Cambridge, MA, USA) were added dropwise. While adding the medium, the tube was gently moved to mix the cells. This was followed by centrifugation at 1000 rpms (revolutions per minute) for 3 minutes. Supernatant was removed, and cells were resuspended in 2 ml / well of pre-warmed complete-mTeSR1 medium with 10 μM of ROCK inhibitor (Y-27632; Abcam Inc; MA, USA) with a P1000 pipette. Then, the cell suspension was added to Matrigel (354230; Corning Inc., New York, NY, USA) feeder-free coated 6-well plates.

4.3. Human PSC maintenance in mTeSR1 media with ROCK inhibitor

Following thawing, all hPSCs were cultured on Matrigel feeder-free coated 6-well plates in 2 mL of complete mTeSR1 medium. The medium was changed every day (every 24 h ± 2).

Table 2. List of human pluripotent stem cell (hPSC) lines used for this study

Cell Line	hPSCreg® / NIH ID	Disease Status	hESC / hiPSC	Institution*
GENEA-019	**GENEAe020-A**	Unaffected	hESC	GENEA
H9	**WAe009-A**	Unaffected	hESC	WCRI
RUES2	**RUESe002-A**	Unaffected	hESC	RU
RUES2 2123	**RUESe002-A-1**	Unaffected	hESC	RU
CTR2161	**CHDIi013-A**	Unaffected	hiPSC	CHDI
CTR2162	**CHDIi014-A**	Unaffected	hiPSC	CHDI
CTR2164	**CHDIi016-A**	Unaffected	hiPSC	CHDI
CTR2175	**CHDIi027-A**	Unaffected	hiPSC	CHDI
CTR2190	**CHDIi042-A**	Unaffected	hiPSC	CHDI
CTR33n1	**CS83iCTR33n1**	Unaffected	hiPSC	CSRMI
GENEA-018	**NIHhESC-12-0169**	Affected HD	hESC	GENEA
GENEA-020	**GENEAe015-A**	Affected HD	hESC	GENEA
HD65Q	**NA**	Affected HD	hESC	TLGM
RUES2 1811	**RUESe002-A-2**	Affected HD	hESC	RU
HD60n5	**CS21iHD60n5**	Affected HD	hiPSC	CSRMI
HD2158	**CHDIi010-A**	Affected HD	hiPSC	CHDI
HD2170	**CHDIi022-A**	Affected HD	hiPSC	CHDI
HD2174	**CHDIi026-A**	Affected HD	hiPSC	CHDI
HD2197	**CHDIi049-A**	Affected HD	hiPSC	CHDI

** GENEA: Genea Biocells, Australia; WCRI: WiCell Research Institute, USA; RU: The Rockefeller University, USA; CHDI: Cure Huntington's Disease Initiative Foundation Inc., USA; CSRMI: Cedars-Sinai Regenerative Medicine Institute, USA; TLGM: Translational Laboratory in Genetic medicine, Singapore.*

The hPSC cultures were passaged when cell confluence reached 70–80% (twice per week). Cells were gently washed twice with 2 mL of Dulbecco's (D)-phosphate-buffered saline (PBS) without calcium and magnesium (DPBS (-/-), 14190–250; Thermo Fisher Scientific Inc., Waltham, MA, USA) and incubated for 20–25 min with dispase in DMEM/F12 (07923; StemCell Technologies Inc., Cambridge, MA, USA) with 10 µM of ROCK inhibitor at 37 °C. Then, dispase was removed, and cells were harvested in DMEM/F12 (36254; StemCell Technologies Inc., Cambridge, MA, USA) media by pipetting up and down using a 5-mL pipette to avoid single-cell desegregation. Cells were centrifuged at 1250 rcf for 3 min and resuspended with warm and fresh Complete-mTeSR1 medium with 10 µM of ROCK inhibitor at the desired dilution. Then, cell suspension was seeded on tempered Matrigel coated 6-well plates. Differentiated colonies were removed manually using a stereotypic microscope and a 10-mL sterile tip prior passaging.

5. Routine testing of hPSCs genomic stability

5.1. Sample fixation for karyotyping (G-banding)

The hPSCs were karyotyped regularly upon thawing and after every 10 passages, as well as before and after experimental use of hPSCs (as to ensure genomic integrity of the starting material) at Ambar Lab (L'Hospitalet de Llobregat, Barcelona, Spain) by G-banding test. Nevertheless, samples were prefixed to preserver the samples until their analysis. Three wells of six-well plates at 60% confluent were raised as follows. Cultures were incubated for 1 h with Complete mTeSR1 with 0.2 µg/mL of Karyomax Colcemid (15212-012; Life Technologies, Vancouver, Canada) at 37 °C. Then, cultures were washed thrice with 2 mL of DPBS (-/-) and incubated for three minutes with StemPro Accutase (A1110501; Thermo Fisher Scientific Inc., Watham, MA, USA) at 37 °C. Then, cells were desegregated as a single-cell, and 4 mL of Complete mTeSR1 were added per well to dilute and inactivate the enzyme. Cell suspension was transferred to a 15 mL conical tube and centrifuged for 3 min at 1250 rcf. Then, supernatant was aspirated carefully to not aspirate the pellet of cells which were washed with 5 mL of DPBS (-/-) and centrifuged again for 3 min at 1250 rcf. The pellet was gently resuspended in 10 mL of hypotonic solution composed of 0.075 M of KCl (10575-090; VWR International Eurolab, Barcelona, Spain). The hypotonic solution was added gently drop-to-drop while the tube was agitated. Cell suspension was kept for 10 min at 37 °C water bath to rest and then pre-fixed with 1 mL of cold (−20 °C) Carnoy fixative solution composed of (1:3) methanol (20847; VWR International Eurolab, Barcelona, Spain) and acetic acid (1310081612; PANREAC Quimica SLU, Barcelona, Spain). Carnoy was gently dropped while vortexing the tube. After 10 min of centrifugation at room temperature and 2220 rcf, pellet was resuspended in 10 mL of cold (−20 °C) Carnoy fixative solution while vortexing. The tube was sealed and stored at −20 °C until picked up for its analysis.

5.2. Sample preparation for microarray-based Comparative Genome Hybridization (aCGH)

The aCGH assay was performed regularly before and after adaptation to standardized cell culture conditions detailed in appropriate Standard Operating Procedures (SOPs), by Ambar Lab. A cell suspension is harvested in the laboratory before sending the sample to the company. The hPSC cultures were harvested when cell confluence reached 80%. Cells were gently washed twice with 2 mL of DPBS (-/-) and incubated for 5 min with StemPro

Accutase at 37 °C. Then, single-cell suspension was harvested in 2 mL of complete mTeSR1. Cells were centrifuged at 1250 rcf for 3 min and resuspended with 2 mL of DPBS (-/-) and set at 4 °C before the immediate shipping to Ambar Lab.

6. *In vitro* ventral differentiation protocol

Performed using the *in vitro* ventral forebrain differentiation protocol previously described by our group to the harvesting and cell counting stage at 16 DIV or 17 DIV (Comella-Bolla et al., 2020). Following cell sorting at 16 DIV, the cells were centrifuged and resuspended in Advanced DMEM/F-12 (12634010, Thermo Fisher Scientific Inc., Waltham, MA, USA) supplemented with GlutaMax supplement 100X (35050061, Thermo Fisher Scientific Inc., Waltham, MA, USA), 100 U/ml Penicillin-Streptomycin (15140122, Thermo Fisher Scientific Inc., Waltham, MA, USA) and serum-free B-27 supplement 50X (17504044, Thermo Fisher Scientific Inc., Waltham, MA, USA) to a concentration of 1 x 10^6 live cells/ml. Subsequent cell plating and further differentiation of the cultures to 37 DIV was performed as previously described (Comella-Bolla et al., 2020).

For the MARS-Seq experiments, four consecutive passages of each hESC line were differentiated to 8DIV according to the *in vitro* ventral forebrain differentiation protocol (Comella-Bolla et al., 2020), and frozen stocks were generated. Shortly, cells were harvested at 8DIV and resuspended in mFreSR™ (StemCell Technologies Inc., Cambridge, MA, USA), distributed in cryovials (one vial per harvested well of a 6-well plate) and placed at -80 °C overnight inside a Mr. Frosty™ Freezing Container (Thermo Fisher Scientific Inc., Waltham, MA, USA) filled with 100% isopropyl alcohol. Then, the cryovials were transferred to the cryopreservation tank (liquid nitrogen; -196 °C). Frozen 8DIV stocks of the 4 biological replicates of a cell line were thawed in parallel; for single-cell sorting, one tube of each biological replicate was thawed to two wells of a 6-well cell culture plate. All differentiations were performed in parallel to 17 DIV (instead of 16 DIV, giving cells an extra day to recover from the thawing process; Comella-Bolla et al., 2020b)

7. Massively parallel RNA single-cell sequencing (MARS-Seq)

7.1. Single-cell sorting

At 17 DIV we performed two rounds of cell harvesting and sorting. For each round, one well (6-well plate) of cells of each biological replicate was harvested and sorted to four 384-well plates (note that cells from all four biological replicates were sorted to each plate). Cells were harvested as described at 16 DIV of the *in vitro* ventral forebrain differentiation protocol (Comella-Bolla et al., 2020). After cell counting, the cell suspensions were centrifuged for three minutes at 1250 rcf and resuspended in cold filter sterilized sorting buffer [1x DPBS (-/-), 1 mM EDTA pH 8.0 (AM9261, Thermo Fisher Scientific Inc., Waltham, MA, USA), 25 mM HEPES (15630-056, Thermo Fisher Scientific Inc., Waltham, MA, USA)] + 1µM DAPI (D1306, Molecular Probes, Eugene, OR, USA) to 0.5 M total cells per ml and stored on ice. All cell suspensions were filtered using 100 µm pore size filters.

The 384 plates containing lysis buffer [0.2% Triton (Sigma-Aldrich, St. Louis, MO, USA); RNase inhibitor (Invitrogen, Waltham, MA, USA)] and reverse-transcription (RT) primers were thawed on ice from storage at -20 °C and centrifuged at 2250 rcf at 4 °C for 1 minute, then kept on ice until used. The RT primers contained single-cell barcodes and unique molecular identifiers (UMIs) for subsequent de-multiplexing and correction for amplification biases, respectively. Single DAPI negative cells were sorted to 384 well plates using the BD FACS Aria™ SORP (BD Biosciences, San Jose, CA, USA) at the Citomics core facility of the Institut d'Investigacions Biomèdiques August Pi i Sunyer (IDIBAPS) using stringent settings optimized for single-cell sorting. The plate holder of the cytometer was kept cold to keep the plate chilled during single-cell sorting. The cytometer was calibrated before each set of 4 plates using fluorescent beads and a 384 well plate to ensure cells were sorted to the center of each well. In between plates a quick calibration test was performed using an empty plate with a lid on and fluorescent beads. Each plate contained 95 cells from each biological replicate and 4 empty negative control wells. After sorting to a plate was complete the plate was centrifuged as above and flash-frozen on dry ice. Plates were then stored at -80 °C until shipping to the CNAG-CRG (Barcelona, Spain) on dry ice for processing.

7.2. Library preparation and MARS-Seq

For cDNA library construction, sequencing, and data processing we used the MARS-Seq (massively parallel single-cell RNA sequencing) protocol (Jaitin et al., 2014; Paul et al., 2015). Single-cell lysates were denatured and immediately placed on ice. The RT reaction mix, containing SuperScript III reverse transcriptase (Invitrogen, Waltham, MA, USA), was added to each sample. In the RT reaction, spike-in artificial transcripts (ERCC, Ambion, Austin, TX, USA) were included at a dilution of $1:16 \times 10^6$ per cell.

After RT, the complementary DNA (cDNA) was pooled using an automated pipeline (epMotion, Eppendorf, Hamburg, Germany). Unbound primers were eliminated by incubating the cDNA with exonuclease I (New England Biolabs, Ipswich, MA, USA). A second pooling was performed through cleanup with SPRI magnetic beads (Beckman Coulter, Brea, CA, USA). Subsequently, pooled cDNAs were converted into double-stranded DNA with the Second Strand Synthesis enzyme (New England Biolabs, Ipswich, MA, USA), followed by clean-up and linear amplification by T7 *in vitro* transcription overnight.

Afterward, the DNA template was removed by Turbo DNase I (Ambion, Austin, TX, USA) and the RNA was purified with SPRI beads. Amplified RNA was chemically fragmented with Zn^{2+} (Ambion, Austin, TX, USA), and then purified with SPRI beads. The fragmented RNA was ligated with ligation primers containing a pool barcode and partial Illumina Read1 sequencing adapter using T4 RNA ligase I (New England Biolabs, Ipswich, MA, USA).

Ligated products were reversed transcribed using the Affinity Script RT enzyme (Agilent Technologies) and a primer complementary to the ligated adapter, partial Read1. The cDNA was purified with SPRI beads. Libraries were completed through a polymerase chain reaction (PCR) step using the KAPA Hifi Hotstart ReadyMix (Kapa Biosystems, Wilmington, MA, USA) and a forward primer that contains Illumina P5-Read1 sequence and the reverse primer containing the P7-Read2 sequence. The final library was purified with SPRI beads to remove excess primers. Library concentration and molecular size were determined with High Sensitivity DNA Chip (Agilent Technologies, Santa Clara, CA, USA). The libraries consisted of 192 single-cell pools. Multiplexed pools (2) were run in one Illumina HiSeq 2500 Rapid two-lane flow cell following the manufacturer's protocol (Illumina, San Diego, CA, USA). Primary data

analysis was carried out with the standard Illumina pipeline (Illumina, San Diego, CA, USA).

All plates were processed to the second strand cDNA stage safe point (two pools per plate) at the CNAG-CRG. Two plates of each technical replicate of each cell line (four plates per cell line and 12 plates in total) were processed to produce final cDNA libraries. The remaining plates at the safe point were stored at –80 °C in case further sequencing was required in the future. The final cDNA libraries of selected pools of each technical replicate of each cell line were sequenced to one-third depth to verify library quality before full-depth sequencing. All the final cDNA libraries were then sequenced to full depth following library quality verification. cDNA library construction, sequencing and data processing were performed according to the MARS-Seq protocol (Jaitin et al., 2014).

7.3. Bioinformatics analysis of MARS-seq data

The MARS-seq data was processed using zUMIs (v2.9.2) (Parekh et al., 2018). We produced the STAR (v2.7.3a) (Dobin et al., 2013) index by setting the parameter "sjdbOverhang" to 51. Two FASTQ files were available for each sequence, with read 1 containing the transcript sequence and read 2 holding the cell and UMI barcodes only. The outcomes from each pair of files were then processed into a unique matrix and converted into a Seurat object for performing the downstream analysis of the complete dataset.

Downstream data analysis including integration, scaling, dimensionality reduction (UMAP), unsupervised clustering (resolutions of 0.05 and 0.1), differential gene expression analysis and visualization was performed using Seurat (4.1.2) (Stuart et al., 2019). Biological processes associated to differential transcriptomic profiles were investigated performing gene ontology (GO) functional enrichment analysis on the marker gene lists using EnrichR (v 4.2.0) (Kuleshov et al., 2016).

To measure the gene expression of a given marker, we calculated the $\log_2$ fold change of the average expression in its corresponding cluster compared to that of the other cluster. We performed enrichment analyses of positive cells for every gene of interest in each cluster or subcluster. To that end, we created a 2x2 contingency table for each analyzed gene, displaying the frequency of positive and negative cells for a given gene in each cluster or subcluster. Contingency tables were used to calculate the odds ratio (OR) to

measure the strength of association between the expression of a particular gene and its associated cell cluster or subcluster, i.e., to quantify marker specificity for its associated cluster or subcluster. An exact Fisher's test was used in each case to determine the statistical significance of the observed OR.

8. Bulk RNAseq

8.1. Cell lysis and RNA purification

Samples of each condition, sorting day and cell line underwent lysis at two different timepoints: two days and three weeks post-sorting. Cultures were lysed with TriReagent (TR-118, MRC, Cincinatti, OH, USA) according to the manufacturer´s protocol and the lysate was stored at -80ºC until RNA purification. Each well of a 24 well plate was lysed with 125µl of Trireagent. Each technical replicate corresponds to four to eight wells of a 24 well plate, which was pooled into a single 2 ml.

RNA was purified using the phenol-chloroform extraction protocol provided with Trireagent. In-house quantification of RNA concentration and purity was performed using a Nanodrop1000 spectrophotometer (Thermo Fisher Scientific Inc., Waltham, MA, USA). RNA quantification was performed at the Centre Nacional d'Anàlisi Genòmica-Centre for Genomic Regulation (CNAG-CRG, Barcelona, Spain) using the Qubit RNA BR Assay Kit (Thermo Fisher Scientific Inc., Waltham, MA, USA).

8.2. Stranded total RNAseq library preparation and sequencing

Stranded total RNAseq library preparation and sequencing was performed at the CNAG-CRG. The RNASeq libraries were prepared with Illumina® TruSeq® Stranded Total RNA Sample Preparation kit (Illumina Inc., San Diego, CA, USA) following the manufacturer´s recommendations with some modifications. Briefly, 500ng of total RNA was rRNA depleted using the RiboZero Magnetic Gold Kit (Illumina Inc., San Diego, CA, USA) and fragmented by divalent cations. The strand specificity was achieved during the second strand synthesis performed in the presence of dUTP. The cDNA was adenylated and ligated to Illumina platform compatible IDT adaptors with unique dual indexes with unique molecular identifiers or UMIs (Integrated DNA Technologies, Coralville, IA, USA) for paired end sequencing. The ligation products were enriched with 15 PCR cycles and the final library was validated on an Agilent 2100 Bioanalyzer with the DNA 7500 assay (Agilent Technologies, Santa Clara, CA, USA). The libraries were sequenced on HiSeq4000 (Illumina Inc., San Diego, CA, USA) following the

manufacturer's protocol for dual indexing. Image analysis, base calling and quality scoring of the run were processed using the manufacturer's software Real Time Analysis (RTA2.7.7) and followed by generation of FASTQ sequence files.

8.3. Bioinformatics analysis

For read mapping, gene quantification and quality control RNA-seq paired-end reads (76 bp x 2) were mapped against the human reference genome (GRCh38) with STAR/2.5.3a using the ENCODE parameters for long RNA. Genes were quantified with RSEM/1.3.0 and the GENCODE annotation v32. Quality control of the mapping and quantification steps was performed with 'gtfstats' from GEM-Tools 1.7.1. Sample similarities were inspected with a Principal Component Analysis (PCA), taking the top 500 most variable genes after regularized log transformation of the counts. Differential expression analysis was performed with DESeq2/1.18. For a change to be considered significant, we established a threshold of $p<0.05$ and a fold-change higher than 1.5. Heatmaps with the top 50 differentially expressed genes were performed with the R package 'pheatmap' and scaling by row. Functional enrichment analysis was performed using the g:Profiler webtool (https://biit.cs.ut.ee/gprofiler/gost)[39] with the default settings.

9. Immunocytochemistry (ICC)

Cultures during differentiation before and after cell sorting were fixed with 4% paraformaldehyde solution (FO090101.1221/50-00-0, Casa Alvarez, Madrid, Spain) and immunostained for key marker proteins as described previously (Comella-Bolla et al., 2020). Images were acquired with a Zeiss LSM 880 confocal microscope controlled with the Zeiss Zen 2.3 software (Oberkochen, Germany). Maximum intensity projections of Z-stacked images were obtained using the same software. Antibodies employed in ICC experiments can be found in Table 3. DAPI was used for counterstaining.

10. Flow cytometry (FC)-based screening of cell surface markers

Functional antibodies to be used for developing the cell labeling and cell sorting pipeline were identified based on the literature. We performed the FC-based marker screening by testing different primary monoclonal antibodies for potential cell surface markers, using hESC-derived 16 DIV forebrain progenitors obtained using the *in vitro* ventral forebrain differentiation protocol (Comella-Bolla et al., 2020). We tested different

concentrations of primary antibodies to establish the optimal conditions to identify the positive/negative (or high/low) populations for each marker. FC was performed as described below.

11. Cell sorting

11.1. FC and Fluorescence-Activated Cell Sorting (FACS)

Following *in vitro* differentiation as per the *in vitro* ventral forebrain differentiation protocol (Comella-Bolla et al., 2020), cell harvest and cell counting were performed according to what was previously described for 16 DIV (Comella-Bolla et al., 2020). Cells were centrifuged and resuspended in Staining Buffer [SB; DPBS (-/-), 1% BSA (A9647, Sigma-Aldrich, St. Louis, MO, USA)] to a concentration of 5 x 10^6 cells/ml and stained with the corresponding primary antibody (incubation for 20 minutes at 4 °C in the dark). Antibodies employed in FC and FACS experiments can be found in Table 3. The labeled cells were then washed with DPBS (-/-), centrifuged, and resuspended in cold sterile filtered FACS buffer [1x DPBS (-/-), 1 mM EDTA pH 8.0, 25 mM HEPES, 10% FBS (10270-106, Thermo Fisher Scientific Inc., Waltham, MA, USA)] +/- 1 µM DAPI as required. FC and cell sorting were performed using a BD FACSAria™ III (BD Biosciences, San Jose, CA, USA). For FACS we used a flow rate of 10 µl/min and a nozzle size of 100 µm, and samples were filtered using 100 µm pore size filters. Sorted cells were retrieved in Advanced DMEM/F-12 medium supplemented with penicillin/streptomycin and Glutamax. After separation, cells were seeded for further differentiation as described above according to the *in vitro* ventral forebrain differentiation protocol (Comella-Bolla et al., 2020). For each cell sorting experiment, FC was used as a quality control to evaluate cell viability and cell sorting efficiency in unsorted and sorted populations. After separation, cells were seeded for further differentiation as described above according to the *in vitro* ventral forebrain differentiation protocol (Comella-Bolla et al., 2020).

11.2. Magnetic-Activated Cell Sorting (MACS)

Following *in vitro* differentiation as per the *in vitro* ventral forebrain differentiation protocol (Comella-Bolla et al., 2020), cells were harvested, counted, and stained with designated primary antibodies or isotypes as described for FC and FACS, but using MACS buffer (MB) composed of 1x DPBS (-/-), 0.5% BSA, 2 mM EDTA and 25 mM HEPES for all the process. The appropriate volume of harvested cells was

centrifuged and resuspended in MB to a concentration of $1x10^7$ cells/mL. The cell suspension was distributed in aliquots of up to 2 x 10^7 cells. The CD200 antibody [mouse monoclonal PE anti-human CD200 (OX2), cat. number 329206, clone OX-104, Biolegend, San Diego, CA, USA] was added to the cell aliquots at a concentration of 1µg antibody/10^6 cells/100µl single cell suspension. The antibody was incubated with the cells for 20 minutes on ice in the dark. The cells were then washed with MB and the cell pellets were resuspended in 100 µl of MB per 10^7 cells. Following the wash of primary antibodies, $20x10^6$ single cells were incubated for 15 min at 4 ºC in 0.2 ml of a 1:5 dilution of designated anti-PE magnetic microbeads (130-048-801, Miltenyi Biotec, Bergisch Gladbach, Germany) in MB +/- 1 µM DAPI. Cells were washed with MB, centrifuged, and resuspended in 0.5ml MB. Magnetic separation of the positive and negative fractions was performed using MS MACS columns (130-042-201, Miltenyi Biotec, Bergisch Gladbach, Germany), as per the manufacturer´s instructions. MS columns were used for sorting up to $2x10^7$ cells per column, being placed in the magnetic field of a MiniMACS™ Separator (130-042-102, Miltenyi Biotech, Bergisch Gladbach, Germany). Columns were prepared by rinsing with MB. Cell suspensions were applied to the columns and the unlabeled cells that passed through were collected. The columns were washed three times with MB, and the total effluent (unlabeled or negative cell fraction) was collected. New buffer was only added once the column reservoir was empty. Columns were then removed from the separator and placed on a suitable collection tube. The labelled or positive cell fraction was then collected by pipetting 1mL of MB per column, and immediately flushing out the magnetically labeled cells by firmly pushing the plunger into the column.

After separation, cells were either analyzed by FC or seeded for further differentiation as described above according to the *in vitro* ventral forebrain differentiation protocol (Comella-Bolla et al., 2020). For each cell sorting experiment, FC was used as a quality control to evaluate cell viability and cell sorting efficiency in unsorted and sorted populations. Antibodies employed in MACS experiments can be found in Table 3.

11.3. Cell replating and terminal in vitro differentiation

Following cell sorting, cells were centrifuged and resuspended in Advanced DMEM/F-12 supplemented with GlutaMax supplement 100X, 100U/ml Penicillin-Streptomycin and serum-free B-27 supplement 50X to a concentration of 1 x 10^6 live cells/ml. Replating of the cells to coverslips at a density of 80,000 cells per coverslip was

performed as described in the LI differentiation protocol (Comella-Bolla et al., 2020). For each cell line, sorting timepoint and analysis timepoint, the following number of coverslips of each cell fraction were replated per experiment: four for ICC 1 hour after sorting, eight for bulk RNA sequencing 2 days post-sorting, eight for bulk RNA sequencing three weeks post-sorting, and four for *in situ* hybridization (ISH) three weeks post-sorting. Subsequent *in vitro* differentiation as described in the LI differentiation protocol (Comella-Bolla et al., 2020) was continued for three additional weeks, until 33DIV (sorting at 12DIV) or 37 DIV (sorting at 16 DIV), or alternatively until the corresponding analysis timepoint.

12. Unbiased neural progenitor cell counts

One hour after cell sorting of hPSC-derived neural progenitor populations at 12DIV and 16 DIV, cells were stained by ICC for relevant markers and quantified using a nonbiased CYTELL™ Cell Imaging System software (GE Healthcare Life Sciences, Chicago, IL, USA). Eleven random images, corresponding to the 3% of 12 mm diameter coverslip (1.2 cm^2), were taken using the automated epifluorescence CYTELL Cell Imaging System (GE Healthcare Life Sciences, Chicago, IL, USA).

13. Fluorescence RNA *in situ* hybridization (ISH)

13.1. Sample preparation

Cultures were fixed with 4% paraformaldehyde solution and dehydrated using increasing ethanol (1009832500, Merck, Rahway, NJ, USA) concentrations in MiliQ water. Samples were stored at –20 ºC until use. Upon thawing and before use, samples were rehydrated with decreasing ethanol concentrations. Fluorescence *in situ* hybridization (ISH) was performed using the RNAscope® Fluorescent Multiplex Reagent Kit (320850, ACDBio, Newark, CA, USA) according to the manufacturer´s protocol (RNAscope® Assay for Adherent Cells Cultured on Coverslips, technical note reference MK 50-012). We used the following RNAscope® Probes: (i) Hs-DRD1 -Homo sapiens dopamine receptor D1 (DRD1), mRNA (524991, ACDBio, Newark, CA, USA); (ii) Hs-BCL11B-C2 -Homo sapiens B-cell CLL/lymphoma 11B (zinc finger protein) (BCL11B; gene encoding for CTIP2) transcript variant 1 mRNA (425561-C2, ACDBio, Newark, CA, USA); and (iii) Hs-DRD2-C3 -Homo sapiens dopamine receptor D2 (DRD2) transcript variant 1 mRNA (553991-C3, ACDBio, Newark, CA, USA). DAPI (D1306, Molecular Probes, Eugene, OR, USA) was used for counterstaining. Images

were acquired with a Zeiss LSM 880 confocal microscope controlled with the Zeiss Zen 2.3 software (Zeiss, Oberkochen, Germany). Maximum intensity projections of Z-stacked images were obtained using the same software.

13.2. Image acquisition and unbiased quantification

Images were acquired with a Zeiss LSM 880 confocal microscope controlled with the Zeiss Zen 2.3 software. Maximum intensity projections of Z-stacked images were obtained using the same software. Images were quantified using the open-access CellProfiler 4.2.4 software (Broad Institute, Cambridge, MA, USA) (Stirling et al., 2021) to perform unbiased image analysis. Images were loaded in a customized pipeline with an initial nuclei detection by DAPI immunofluorescence in order to quantify the total number of cells, followed by mRNA spot detection in the second (green), third (red) and the fourth channels (far red) in order to determine the number of mRNA spots per nuclei for all mRNA transcripts of interest.

One to two spots per cell in ISH are considered background, and most housekeeping and cell marker genes are expressed at high levels (>10 spots per cell). Here, for the purpose of quantification, we considered individual cells with expression levels of more than three mRNA dots of a given transcript (i.e., *BCL11B*, *DRD1* or DRD2 mRNAs) to be positive for that particular marker. Furthermore, cells with simultaneous expression of three or more mRNA spots for BCL11B and DRD1 were considered dSPNs, while those with simultaneous expression of three or more mRNA spots for BCL11B and DRD2 were considered iSPNs.

14. Cell transplantation

Following MACS, unsorted and sorted cells were resuspended in DPBS (-/-) to a concentration of 50,000 cells/ml. Five-week-old mice were anesthetized by applying 3% isofluorane (IsoFlo, Esteve, Barcelona, Spain) for 1-2 minutes in an induction chamber and then maintained at 2% isofluorane mixed with oxygen. Two unilateral intra-striatal injections were performed using a stereotaxic apparatus (RWD Life Science, San Diego, CA, USA) coupled to a stereotaxic pump (World Precision Instruments Inc., Sarasota, FL, USA) setting the following coordinates (mm) relative to Bregma (anteroposterior and lateral) and dura (dorsoventral): AP: +0.80, +0.33; L: +1.80, +2.00; DV: −2.65, −2.65. Every animal received 100,000 cells divided into two deposits (1 µL/injection) using a 10

µL Hamilton syringe (33-gauge; Hamilton, Reno, NEV, USA) at an injection rate of 0,2 µL/min. After delivery, the syringe was left to achieve complete diffusion of the cell suspension in each depth for 3 min. Wounds were closed with silk sutures and mice were placed in individual cages on heating pads until recovery from anesthesia.

15. Immunosuppression regime

Mice received triple immunotherapy combining cyclosporine A (15 mg/kg, 30024, Sigma-Aldrich, St. Louis, MO, USA), azathioprine (10 mg/kg, A4638, Sigma-Aldrich, St. Louis, MO, USA), and prednisolone (20 mg/kg, P6004, Sigma-Aldrich, St. Louis, MO, USA). The immunosuppressive preparation was administered daily via i.p. injections, starting with a double dose on the day before surgery and continuing throughout the procedure.

16. Immunohistochemistry (IHC)

Mice were sacrificed on post-transplant day 7 (7d PST) and brains were removed and processed as previously described (Comella-Bolla et al., 2020). For cryosectioning, brains were embedded in a thin layer of Tissue-Tek optimal cutting temperature (OCT) compound (Sakura Finetek, Torrance, CA, USA). Serial coronal sections at a thickness of 14 µm were obtained using the cryostat Leica CM3050 S (Leica Biosystems, Deer Park, IL USA). IHC was performed on brain sections as previously described (Comella-Bolla et al., 2020) were mounted using DAPI Fluoromount-G (Thermo Fisher Scientific Inc., Waltham, MA, USA). Images were acquired with a Zeiss LSM 880 confocal microscope controlled with the Zeiss Zen 2.3 software. Maximum intensity projections of Z-stacked images were obtained using the same software. Antibodies employed for IHC can be found in Table 3.

17. Antibodies

A detailed list of the antibodies used for this study (for FC, FACS, MACS, ICC and IHC) can be found in Table 3.

18. Statistical analysis

Statistical analysis was carried out using GraphPad Prism version 9.4.0 (GraphPadSoftware Inc., San Diego, CA, USA). Data are presented as mean ± the standard error of the mean (SEM). Statistical analysis of continuous numerical data was performed using a two-tailed Student's t-test (for comparisons of two population groups)

or ordinary one-way ANOVA with correction for multiple comparisons using Tukey's statistical hypothesis testing (for pairwise comparisons of more than two population groups).

Alteration probability analysis was performed using a Kaplan–Meier survival analysis. The hPSCs which did not have an event occurrence (detection of the studied genomic alteration subtype) were censored. The hPSCs were divided into two different groups according to whether they had been adapted to standardized *in vitro* cell culture conditions under a Quality Management System (QMS). Adaptation was considered complete when at least 4 passages had been performed under these conditions. Passage number for both groups was normalized before analysis. Statistical significance for this analysis was determined by a log-rank (Mantel–Cox) test.

Differential gene expression analysis between cell types (NB vs NPC, NB direct vs NB indirect) was performed using the default mode in Seurat, consisting of a Wilcoxon Rank Sum test. This test was performed for those genes that were detected in at least 1% of cells in either of the two populations and for which the $\log_2$ fold change was greater than 0.25 in absolute value. All the computed p-values were adjusted for multiple hypothesis testing using the Bonferroni correction.

For all statistical analyses, *p* values were computed using the NEJM (New England Journal of Medicine) style. Differences were statistically significant at $p < 0.05$. One asterisk (*) summarizes *p* values less than 0.05 (significant), two asterisks (**) summarize *p* values less than 0.01 (very significant) and three asterisks (***) summarize *p* values less than 0.001 (extremely significant). *p* values above 0.05 (non-statistically significant) are either flagged with "ns" (Chapter I) or not flagged at all (Chapters II and III) in the corresponding Figures.

19. Quality Management System (QMS)

All procedures were conducted under UNE-EN-ISO9001:2015. All performed *in vitro* procedures comply with the Guidance Document on Good *In Vitro* Method Practices (GIVIMP; OECD, 2018)

Table 3. List of antibodies used for this study. Different concentrations at which each of these antibodies was used for different experiments and applications (FC/FACS/MACS or ICC/IHC) are indicated, with 1X being equivalent to the antibody concentration recommended by the manufacturer (in the case of FC/FACS/MACS). Ex/Em = Absorbance (excitation) and emission peak of a fluorophore

Marker	Fluorophore (Ex/Em)	Clone	Host	Company (location)	Reference	Concentration		
						FC	FACS / MACS	ICC / IHC
CD200	*PE (565/573nm)*	OX-104	Mouse	Biolegend (San Diego, CA, USA)	329206	2X, 1X, 0.5X, 0.2X, 0.1X, 0.05X, 0.01X	1X	1:100
NCAM1	*APC (651/660nm)*	HDC56	Mouse	Biolegend (San Diego, CA, USA)	318310	0.5X, 0.2X, 0.1X	NA	1:100
PSA-NCAM	*APC (651/660nm)*	2-2B	Mouse	Miltenyi Biotech (Bergisch Gladbach, Germany)	130-117-394	1X, 0.5X, 0.2X	NA	NA
NGFR	*FITC (491/516nm)*	ME20.4	Mouse	Biolegend (San Diego, CA, USA)	345104	2X, 1X, 0.5X, 0.2X, 0.1X	1X	1:200
PLP1	*AlexaFluor700 (696/719nm)*	plpc1	Mouse	Novus Biologicals (BioTechne; Littleton, CO, USA)	NB600-960AF700	1X, 0.5X, 0.1X	NA	NA
S1PR1	*PE (565/573nm)*	218713	Mouse	R&D Systems (BioTechne; Minneapolis, MN, USA)	FAB2016P	1X, 0.5X, 0.1X	NA	NA
S1PR1	*PE (565/573nm)*	MM0045-21L9	Mouse	Novus Biologicals (BioTechne; Littleton, CO, USA)	NB110-93513PE	2X, 1X, 0.5X, 0.1X	NA	NA
IFITM3	*AlexaFluor647 (650/671nm)*	EPR5242	Rabbit	Abcam (Cambridge, UK)	ab198573	1X, 0.5X, 0.1X	NA	NA
CD99	*FITC (491/516nm)*	TÜ12	Mouse	BD Pharmigen (BD Biosciences, San Diego, CA, USA)	555688	1X, 0.5X, 0.1X	NA	NA
CD99	*FITC (491/516nm)*	3B2/TA8	Mouse	Miltenyi Biotech (Bergisch Gladbach, Germany)	130-104-314	2X, 1X, 0.5X, 0.1X	NA	1:100
Ki-67	*NA*	SolA15	Rat	eBioscience, San Diego, CA, United States	14569882	NA	NA	1:100
Ki-67	*NA*	SP6	Rabbit	Abcam (Cambridge, UK)	ab16667	NA	NA	1:250
TUBB3 (β III Tubulin)	*NA*	NA	Rabbit	Sigma-Aldrich (St. Louis, MO, USA)	T2200	NA	NA	1:500
PanEBF	*NA*	C-8	Mouse	Santa Cruz Biotechnology (Dallas, TX, USA)	sc-137065	NA	NA	1:200
PanDLX	*NA*	NA	Rabbit	CHDI Foundation (New York, NY, USA)	PA5967	NA	NA	1:150
MAP2B	*NA*	18/MAP2B	Mouse	BD Transduction Laboratories (BD Biosciences, San Diego, CA, USA)	610460	NA	NA	1:500
MAP2B	*NA*	NA	Chicken	Abcam (Cambridge, UK)	ab92434	NA	NA	1:1000
GABA	*NA*	NA	Rabbit	Sigma-Aldrich (St. Louis, MO, USA)	A2052A2052	NA	NA	1:500
CTIP2	*NA*	25B6	Rat	Abcam (Cambridge, UK)	ab18465	NA	NA	1:300
FOXP1	*NA*	JC12	Mouse	Abcam (Cambridge, UK)	ab32010	NA	NA	1:500
STEM121	*NA*	NA	Mouse	Cellartis (TakaraBio; Gothenburg, Sweden)	Y40410	NA	NA	1:200
HNA	*NA*	NA	Mouse	Millipore-Sigma, Burlington, MA, USA	MAB1281	NA	NA	1:200
CC3 (Cleaved Caspase 3)	*NA*	Asp175	Rabbit	Cell Signalling (Danvers, MA, USA)	9661S	NA	NA	1:500
Rabbit IgG (H+L)	*AlexaFluor 488 (493/519nm)*	NA	Donkey	Jackson Immuno Research (West Grove, PA, USA)	711-545-152	NA	NA	1:500
Mouse IgG (H+L)	*Cy3 (555/569nm)*	NA	Donkey	Jackson Immuno Research (West Grove, PA, USA)	715-165-150	NA	NA	1:500
Rat IgG (H+L)	*AlexaFluor647 (650/671nm)*	NA	Goat	Invitrogen (Waltham, MA, USA)	A21247	NA	NA	1:500
Chicken IgY (H+L)	*NL557 (557/574nm)*	NA	Goat	R&D Systems (BioTechne; Minneapolis, MN, USA)	NL016	NA	NA	1:1000
Mouse IgG (H+L)	*AlexaFluor647 (650/671nm)*	NA	Goat	Invitrogen (Waltham, MA, USA)	A21236	NA	NA	1:500
Rat IgG (H+L)	*Cy3 (555/569nm)*	NA	Donkey	Jackson Immuno Research (West Grove, PA, USA)	712-165-150	NA	NA	1:500

RESULTS

Results

1. Chapter I: Analysis of the potential impact of standardized routine *in vitro* culture conditions in genomic stability of hPSCs

Clinical translation of striatal differentiation protocols in HD requires standardization of production procedures for reproducible the generation of a transplantable pure striatal cell population. While we have successfully transplanted hPSCs differentiated towards SPNs into mouse striatum, the transplanted cell population was mixed, containing a variety of phenotypes and degrees of maturity. We hypothesized that a first step towards refinement of our approach and optimization of the outcomes after transplantation would be to ensure the genomic stability of hPSCs used as starting material for *in vitro* striatal differentiation. Thus, in this section we investigated if the implementation of a Quality Management System (QMS) such as ISO9001:2015 for standardized cell culture conditions and frequent assessment of genomic stability via appropriate genomic screening strategies could impact the prevalence and types of genetic changes affecting hPSCs used for research applications.

To this aim, we carried out a retrospective analysis of data generated from conventional G-banding karyotype and array-based Comparative Genomic Hybridization (aCGH) analysis over a 5-year span (Jan 2017–Jan 2022) on hESC and hiPSC cultures maintained by our research group, before and after adaptation to standard conditions defined by appropriate Standard Operating Procedures (SOPs) under a QMS. This work shows that adaptation of hPSC lines to standardized cell culture conditions under a QMS leads to reduced genomic instability of hPSCs *in vitro*, as evidenced by a reduced probability of chromosomal aberrations and subchromosomal genomic alterations in hPSC lines.

1.1. The number of publications on hPSCs per year has experienced a large increase during the last 20 years

We first investigated the evolution of the scientific interest on hPSC over time, using the number of scientific publications on hPSCs per year as an indicator. To that aim, we performed a literature search worldwide to quantify the number of scientific publications on hPSCs during the last 32 years (January 1990–December 2021). Our sampling procedure yielded 44,464 records of scientific publications, whose distribution over the studied period was heterogeneous (Fig.9A). Briefly, we observed a 56-fold increase in the number of hPSC publications during the studied period. We found that while the

number of papers published per year on hPSCs initially remained stable, it started to increase regularly around 1998, when 134 papers were published. In fact, by 2007, published research works on hPSCs had increased more than 5-fold since 1998 (1187 publications). From then, the increase became steeper, and we observed an exponential rise in scientific works published per year on hPSCs, which has been maintained until the 4130 publications on hPSCs during 2021 (more than a 30-fold difference compared to 1998 and a 3.5-fold difference compared to 2007). We hypothesized that the inflection points observed in 1998 and 2007 could be explained by the fact that two of the most important breakthroughs in the hPSC field were reported in those years, namely the first derivation of an hESC line by Thomson et al. (Thomson et al., 1998) and the first generation of an hiPSC line by Yamanaka et al. (Takahashi et al., 2007), respectively.

To assess if differences existed among these hPSC types regarding the scientific interest that they have raised over time, we conducted two additional literature searches on the number of papers published per year during the same period on hESCs and hiPSCs separately. Our sampling procedure yielded 27,325 and 26,991 records of publications on hESCs and hiPSCs, respectively. We studied the distribution of these publications over time and discovered different trends depending on the hPSC type (Fig.9B). For instance, the number of papers published per year on hESCs rose from 1998 until reaching a maximum of 1,822 around 2014, where interest in hESC research seems to have declined; in turn, the rate of publication on hiPSC began to rise in 2007, sometime after that of hESCs, but this increase has been faster and uninterrupted until present. For instance, as of 2021, the number of publications on hiPSCs (3,436) more than doubled the number of papers on hESCs (1,148). Furthermore, from these results we identified 2013 as a third important inflection point regarding scientific interest on hPSC research. However, this turning point led to different trends depending on the analyzed hPSC type; while a decrease on published hESC research was observed, the number of publications per year on hiPSCs clearly increased. We hypothesized that this effect could be explained by the onset of the first clinical trial using autologous iPSC-derived cells in 2013 (Cyranoski, 2014).

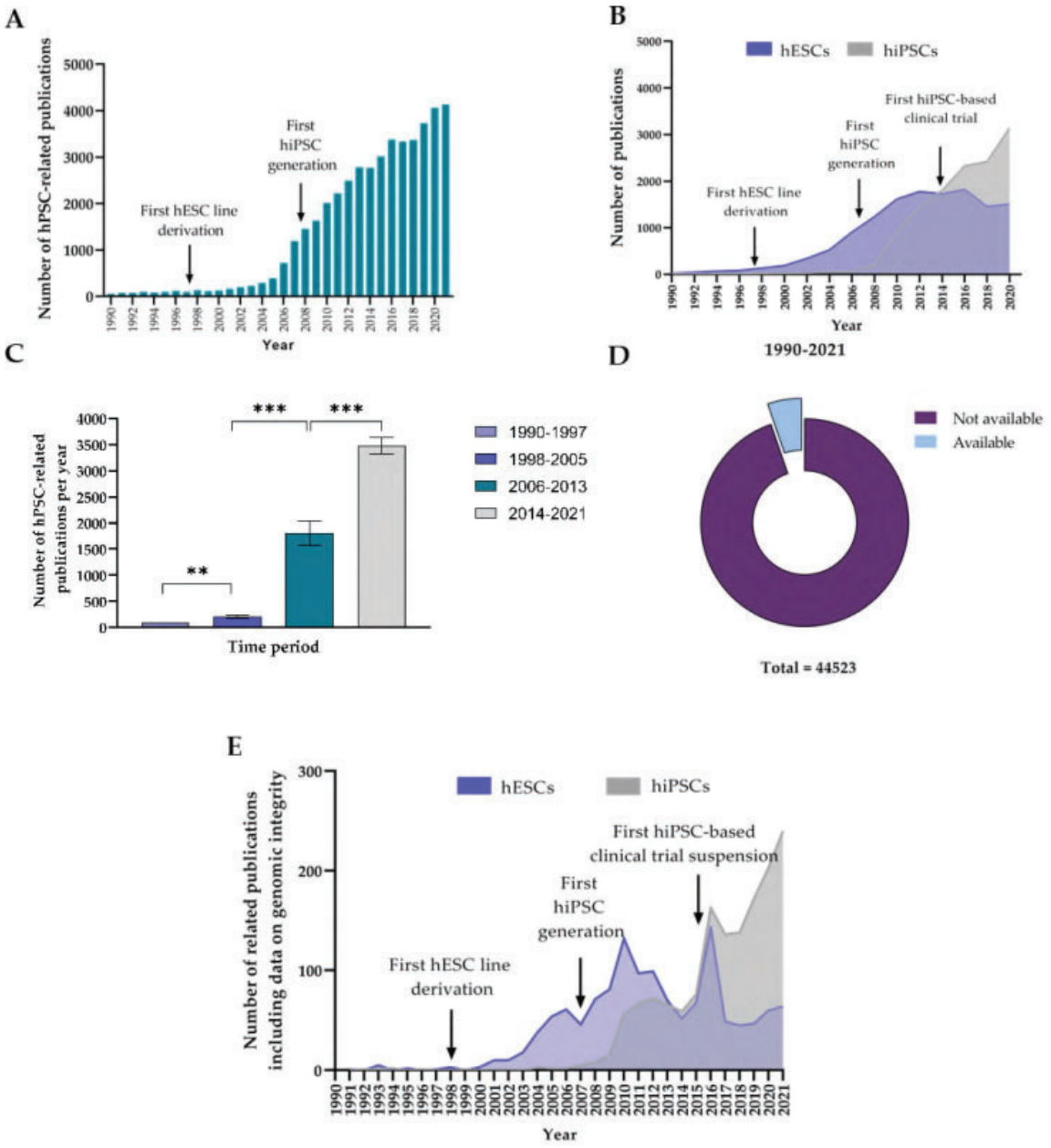

Figure 8. Analysis of the evolution in number of human pluripotent stem cell (hPSC)-related publications and level of reporting of hPSC genomic integrity monitoring.(A) Bar graph representing the number of publications on hPSCs per year; **(B)** compound line graph of trend of publications per year during on human embryonic stem cells (hESCs) and human induced pluripotent stem cells (hiPSCs). Notice the three inflection points relative to three major events in the PSC field: the first hESC line derivation by Thomson in 1998 (Thomson et al., 1998), the first hiPSC generation by Takahashi and Yamanaka in 2007 (Takahashi et al., 2007)cand the RIKEN first hiPSC-based clinical trial in 2013; **(C)** histogram of average number of publications per year in distinct temporal windows; **(D)** publications of hPSC research containing information on genomic integrity monitoring of hPSCs. Available segment indicates the percentage of articles with published data about genomic integrity of hPSCs, where the mean ± the standard error of the mean (SEM) is showed; **(E)** trend of publications per year on hESCs and hiPSCs reporting information on genomic integrity of cells used for the study: increasing interest about monitoring genomic integrity follows critical events about their usage.

To further confirm the significance of these results, we used the three milestones that we previously identified as inflection points (1998, 2007 and 2014) to define four different time segments (given the influence that they have on the trend of hPSC, hESC and hiPSC-related publications per year): (i) 1990–1997 (previous to the first hPSC derivation); (ii) 1998–2005 (between the first hESC derivation and the first hiPSC generation); (iii) 2006–2013 (between the first generation of a hiPSC line and the first hiPSC-based clinical trial); (iv) 2014–2021 (after the first application of hiPSC-derived cell products in humans. We compared the average number of publications per year for each of those segments (Fig.9C). As we expected, the average number of publications per time segment increased over time. Furthermore, the differences we found between adjacent time segments were heterogeneous, which indicates that each of the events leading to an inflection point had a variable effect on the analyzed parameter. For instance, the greatest increase that we observed was an 8-fold change from 1998–2005 to 2006–2013. Hence, we identified the creation of the first hiPSC lines as the most influential event in raising interest on hPSC research during the studied period. On the other hand, differences between the other time segments remained constant at approximately 2 to 3-fold difference.

1.2. Data on hPSC genomic integrity remains underreported despite the fast growth of hPSC research

Once we confirmed the fast-growing increase in interest of hPSC research since the first hPSC derivation in 1998, we investigated whether this increase in hPSC research had been accompanied by an appropriate reporting of data on genome integrity of the hPSCs being experimentally used. To that aim, we searched the number of publications on hPSC research which contained information on genomic integrity monitoring of hPSCs during the same period (January 1990–December 2021). This time, our sampling procedure yielded only 2,340 records, which represents only 5.26% of the total number of publications during that time (Fig.9D). We interpret this result as an indicator of a lack of appropriate reporting of genomic integrity of hPSC lines being used in research, despite the fast growth that the field is experiencing.

Furthermore, we repeated this search again to look at the evolution of this parameter for hESCs and hiPSCs individually (Fig.9D). For both groups, we observed an initial positive evolution starting when the first hESC or hiPSC line was derived. The number of papers including genomic integrity data of hESCs kept increasing until 2010, before

experiencing a decline which would result in having a similar number of publications containing genomic integrity information of both groups by 2014. From 2015 to 2016, we observed a steep 2-fold increase for both groups which matches the time period by when the RIKEN hiPSC clinical trial was halted (Garber, 2015). From that point and following the previously reported trends in hESC and hiPSC-related scientific publications during those 30 years, we observed a sudden decrease in hESC-related publications, whereas the number of hiPSC-related papers containing kept increasing steadily after a small decline.

1.3. Recurrent karyotypic aberrations in hPSCs are detected by G-banding with a low frequency after prolonged in vitro culture

We have performed routine hPSC *in vitro* maintenance and expansion for over 10 years in our laboratory, despite data on genomic stability of our hPSC lines being only available from 2017. This was achieved by adapting all our activities and processes to be performed according to high quality standards under compliance of ISO 9001:2015 rules and the Guidance Document on Good *In Vitro* Method Practices (GIVIMP; OECD) recommendations.

In order to assess whether the implementation of these standards and consequent development and use of SOPs could lead to improved cell culture conditions and genomic screening routines and a subsequent decrease in the number of recurrent genomic alterations of hPSCs, we performed a retrospective *post-hoc* analysis of data generated from routine genome integrity screening hESC and hiPSC cultures maintained by our research group over the 5-year span for which data were available (January 2017–January 2022). The composition and descriptive statistics of the analyzed dataset can be found in Figure 10. Briefly, we included a total of 19 different hPSC lines, from which 11 (57.89%) are hiPSCs whereas the remaining 8 (42.11%) are hESCs (Fig.10A). These cell lines were routinely cultured, and genome integrity data were obtained using two different methods which differ in resolution: karyotypic G-banding and aCGH. In total, data from more than 120 tests performed in hESC and hiPSC lines at different passage numbers was analyzed in this study (Fig.10B-C).

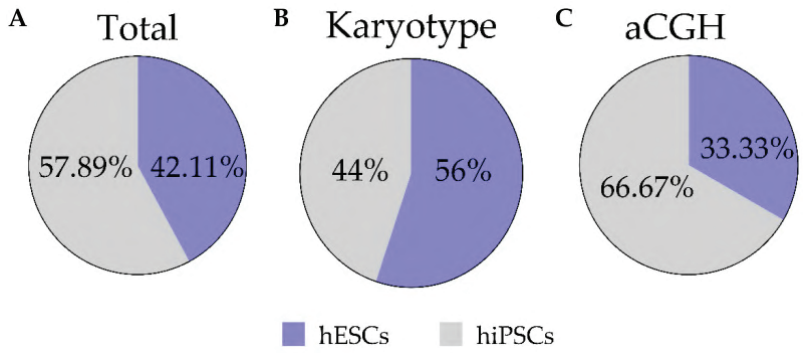

Figure 10. Descriptive statistics of the analyzed dataset. Pie charts showing the relative amount (%) of hESC and hiPSC lines used in this study (A), as well as the proportion of G-banding (B) and CGH array (aCGH) (C) which were performed in each of the hPSC types.

We started by investigating the types and prevalence of chromosomal abnormalities detected in our hPSCs by the classical karyotypic technique G-banding. After gathering data from 108 G-banding tests, we found that 24.1% of the hPSCs being analyzed showed genomic alteration which could be detected with the resolution of the used cytogenetic technique (that is, abnormalities above 5–10 Mb), whereas 75.9% of the hPSCs seemed to be unaltered. Furthermore, by distinguishing between pathogenic aberrations and frequent polymorphic variants, we noticed that 69.2% of the variants corresponded to the former; consequently, the pathogenic variants represented only 16.67% of all the analyzed hPSCs whereas frequent polymorphic alterations (FPAs) were discovered in 7.41% (Fig.11A).

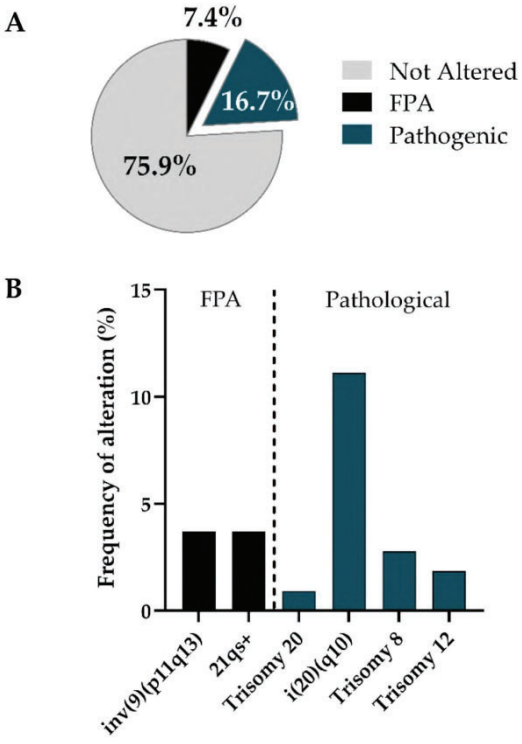

Figure 9. Recurrent karyotypic aberrations are detected in cultured hPSCs by G-banding. (A) Pie chart of fraction of genomic alterations detected with karyotype on the total of the cell lines analyzed; **(B)** histogram of chromosomal abnormalities found in hPSCs by using karyotype. Each bar represents the percentage of time that the alterations has been found in hPSCs. FPA: Frequent Polymorphic Alterations.

Then, we investigated the types of chromosomal abnormalities that were detected in hPSCs by using this approach (Fig.11B and Table 4). The most abundant alteration that we found was a recurrent gain in the long arm of chromosome 20, in the form of an isochromosome 20q [more specifically i(20)(q10)]. This alteration was present in 11.11% of the analyzed hPSCs. Interestingly, this was not the only gain involving chromosome 20, since we also observed trisomy of this chromosome in 0.92% of hPSCs, which means that chromosome 20 gains accounted for 50% of the total chromosomic alterations that we found (and 72.22% of all pathogenic alterations). We also detected other recurrent chromosomal gains in hPSCs, such as trisomies of chromosomes 8 (47, XX + 8) in 2.78% of hPSCs and 12 (47, XX + 12) in 1.85% of hPSCs. Interestingly, all detected gains were present in heterogeneous mosaic cultures in which the alteration was present in variable relative amounts, ranging from 10–20% for 47, XX,+8, 20% for i(20) (q10) or 25% for 47, XX, +20, to 40–50% of the cells for 47, XX,+12. Notably, all chromosomal aberrations were gains of whole chromosomes or chromosomal regions, which contrasts with the fact that chromosomal losses were not detected in any of the analyzed samples. Focusing on the non-pathogenic polymorphic variants, we found a pericentric inversion in one or both chromosomes 9 [46,XX,inv(9)(p11q13)] in 3.7% of hPSCs and the satellites in the distal region of the long arm of one of the 21 chromosomes (21qs+) in another 3.7% of hPSCs; both correspond, as reported above, with frequent polymorphic variants found in hPSCs *in vitro*.

Table 4. List of chromosomal alterations detected by G-banding in human embryonic stem cell (hESC) and human induced pluripotent stem cell (hiPSC) lines.

Alteration		% of Affected hPSCs	% of Affected hESCs	% of Affected hiPSCs
Chromosomal pathogenic alterations	47,XX+8	2.78	NA	6.12
	47,XX,+12	1.85	NA	4.08
	46,XX,i(20(q10)	11.11	10.17	12.24
Frequent Polymorphic Alterations (FPAs)	47,XX,+20	0.93	1.69	NA
	46,XX,inv(9)(p11q13)	3.70	1.69	6.12
	46,XX,21qs+	3.70	NA	8.16

1.4. hiPSCs cultured in vitro for a prolonged time show an increased propensity to acquire chromosomic aberrations

Next, we assessed differences in the propensity to acquire these chromosomal aberrations among different hPSC types. To that aim, we studied whether the probability of hESCs to acquire chromosomal alterations over time was significantly different than that of hiPSCs. We first normalized the passage number for both hPSC groups. We then used Kaplan–Meier curves to show the probability of hESCs and hiPSCs to acquire genomic alterations detectable by G-banding at a certain passage number (Fig.12A). The hESCs and hiPSCs were analyzed over a period of 42 passages *in vitro*. We found that chromosomal alterations in hESCs were significantly lower than in hiPSCs over the time ($p = 0.03$). In fact, this probability was around 2 times higher (~33% vs. ~15%) for hiPSCs by passage 42 compared to hESCs.

Furthermore, we also assessed the absolute frequency at which chromosomal alterations were observed in hESCs and hiPSCs using G-banding (Fig.12B). Once again, we observed an increased propensity of hiPSCs to acquire these mutations, being 2.7 times more likely than hESCs to acquire chromosomal alterations detected by G-banding (the observed frequency of altered karyotypes was 36.73% and 13.56% for hiPSC and hESC lines, respectively). By limiting the analysis to prevalence of pathogenic variants, we noticed a 1.9-fold increase in hiPSC lines (22.45%) compared to hESC lines (11.86%). Furthermore, hiPSCs showed to be also more likely to acquire frequent polymorphic alterations with no pathogenic effect, since we detected this kind of alteration in 14.29% of hiPSCs and only in 1.69% of hESCs (Fig.12B). We also investigated whether different hPSC types would have a proclivity for specific alterations detected by this technique (Fig.12C). Observations showed that the detected karyotypic alterations in hiPSCs tended to be distributed among chromosomes 8 (6.12%), 9 (6.12%), 12 (4.08%), 20 (12.25%) and 21 (8.16%), whereas 75.06% of all karyotypic alterations in hESCs were mostly limited to gains of the chromosome 20 or its long arm (detected in 11.86% of all analyzed hESCs). The frequent structural alteration (46,XX,inv(9)(p11q13)) was the only other aberration detected in hESCs, with a prevalence of 1.69%. Overall, these results highlight a tendency of hiPSC lines to acquire a wider range of numerical and structural chromosomal alterations, both pathogenic and polymorphic, in comparison to hESC lines.

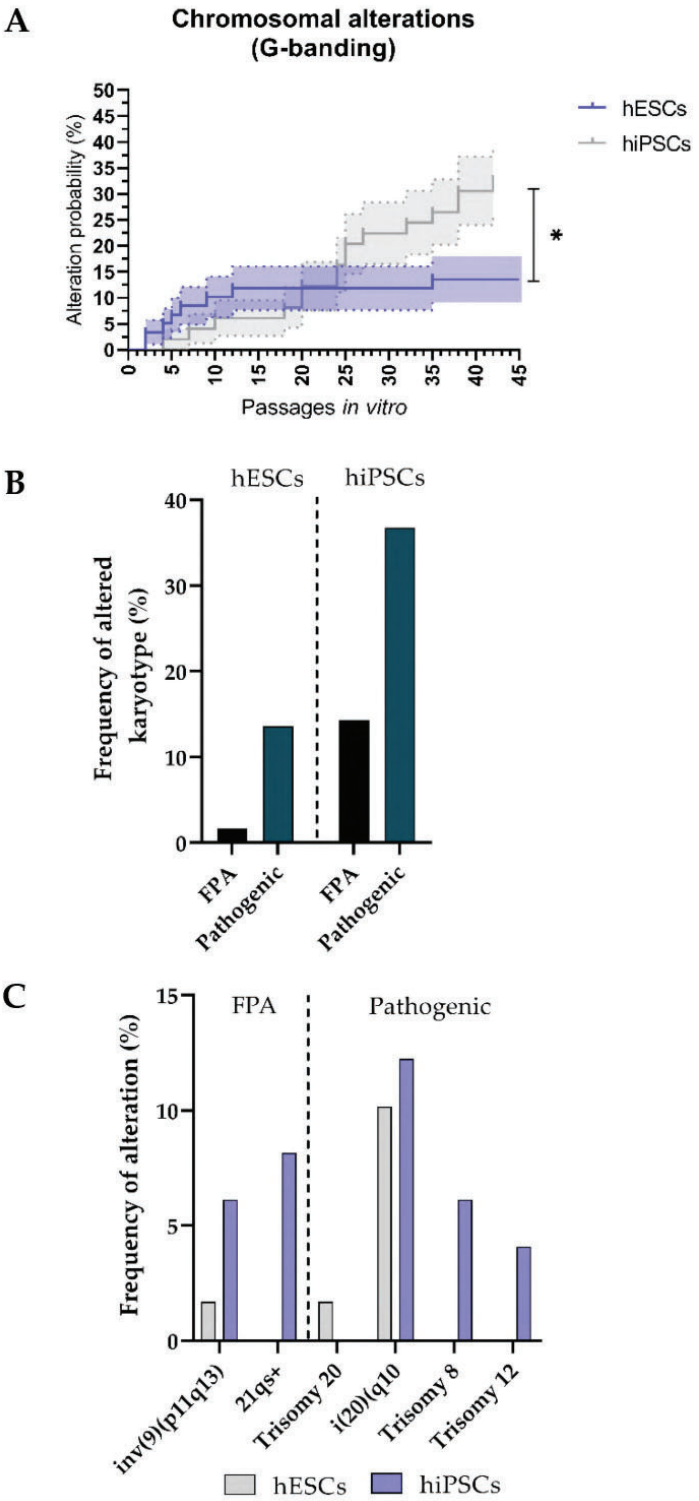

Figure 11. The hiPSCs lines show a higher prevalence of karyotype genomic aberrations detected by G-banding as compared to hESCs (A) Survival analysis (Kaplan–Meier curves) of the evolution of the probability (%) of hESCs and hiPSCs being affected by chromosomal genomic alterations detected by G-banding over time (passages in vitro). Error bars represent standard error of the mean (s.e.m.); **(B)** bar graph of percentage of frequency of all alterations found in hESCs compared with hiPSCs on a total number of 108 karyotypes performed; **(C)** histogram showing the frequency at which different types of FPAs and pathologic alterations are detected in hESCs and hiPSCs via karyotype. FPA: Frequent Polymorphic Alterations.

1.5. Comprehensive aCGH of hPSCs cultured in vitro reveals "hidden" recurrent Copy Number Variations (CNVs) and pathological Copy Number Alterations (CNAs)

Since aCGH analysis can detect DNA copy number changes (deletions or duplications) genome wide at a higher resolution than G-banding, we used this cytogenetic technique to refine our analysis. Briefly, we performed aCGH (with a resolution enabling detection of DNA gains or losses as small as 100–350 kb) to verify all previously-reported abnormalities found by G-banding, as well as to identify additional submicroscopic unbalanced rearrangements of genetic material which had remained hidden.

As expected, we noticed an increased prevalence of alterations in hPSCs by using this technique (Fig.13A). A total of 47 alterations were detected in 26 analyzed hPSC cultures, from which 34 did not correspond to reported polymorphic variants (which we will refer to as Copy Number Alterations or CNAs from this point), and 13 were considered polymorphic Copy Number Variations (CNVs) which are normal variants in the population. Since some of these alterations were simultaneously present in the same culture (i.e., some cultures presented both CNAs and CNVs), we decided to divide the analyzed hPSC cultures into three groups: (i) genomically stable cultures; (ii) cultures in which only one or more CNVs were detected, but not CNAs; and (iii) cultures which contained at least one CNA, regardless whether or not CNVs were simultaneously detected (that is, cultures containing any alteration with pathogenic potential). Only 7.6% of all analyzed hPSCs (n = 26) did not present any genomic alteration. Detection of polymorphic CNVs occurred in 11.5% of these cells, whereas likely pathogenic CNAs were found in 61.5% of hPSCs. A detailed list of detected CNVs and CNAs can be found in Table 5 and Table 6, respectively.

Table 5. List of Copy Number Variations (CNVs) detected by CGH array (aCGH) in hPSCs.

Alteration	Region	hESC/hiPSC	% Cells Affected	% of Total CNVs
Deletion	1p11.2	hiPSC	11.54	23.08
	3q26.1	hiPSC	11.54	23.08
	10q21.3	hiPSC	7.69	15.38
	22q11.21	hiPSC	.85	7.69
Insertion	4q35.2	hiPSC	7.69	15.38
	5p15.33	hiPSC	7.69	15.38

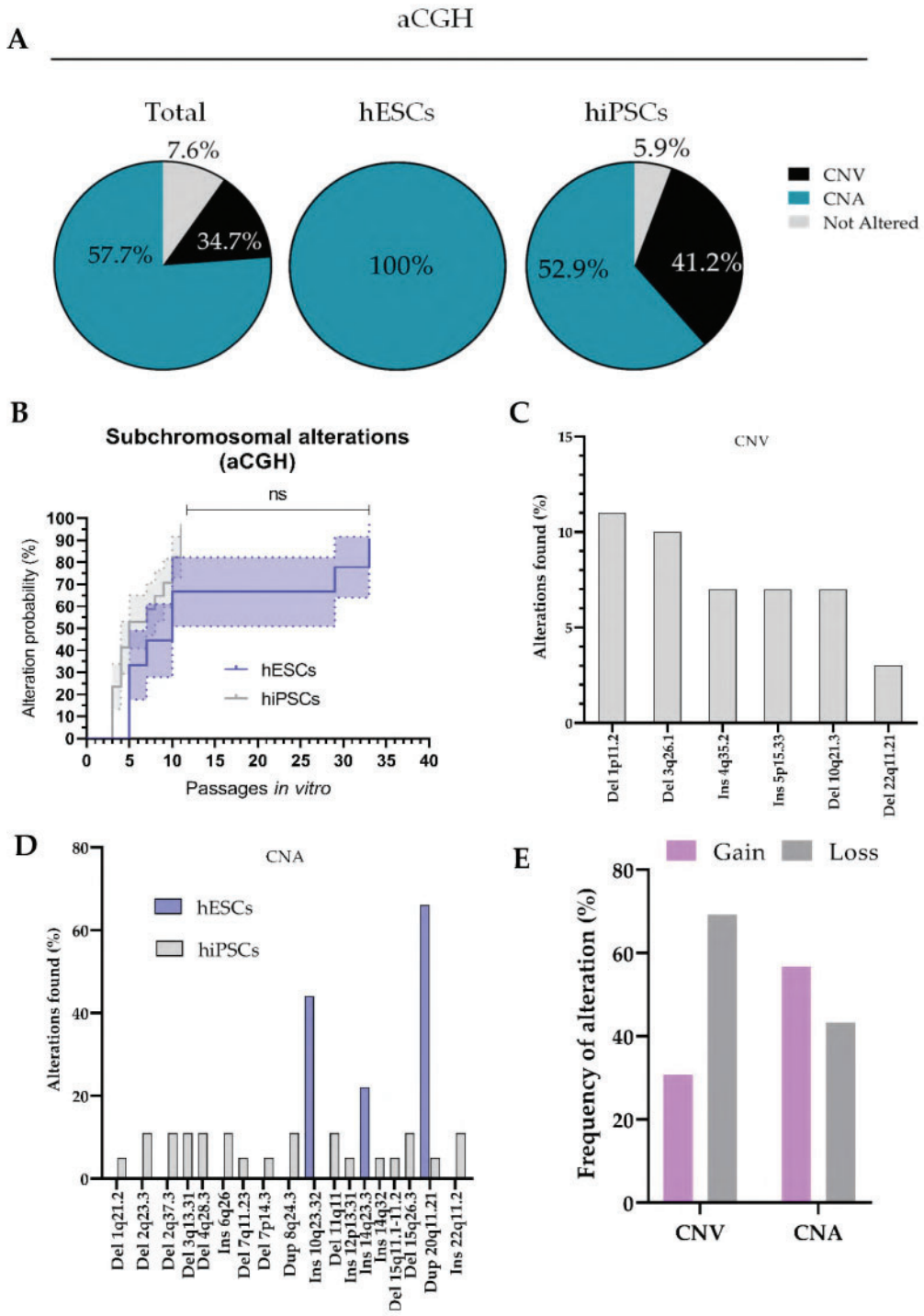

Figure 12. Recurrent subchromosomal Copy Number Variations (CNVs) and pathogenic Copy Number Alterations (CNAs) are detected in cultured hESC s and hiPSCs by Comparative Genomic Hybridization CGH array (aCGH) analysis. (A) Pie charts showing the percentage of cells harboring CNVs or CNAs, as well as cell lines for which no alteration were detected; **(B)** survival analysis (Kaplan–Meier curves) of the evolution of the probability (%) of hESCs and hiPSCs being affected by subchromosomal genomic alterations detected by aCGH over time (passages in vitro). Error bars represent standard error (SEM); **(C, D)** histograms showing the frequency at which different types of CNVs **(C)** and CNAs **(D)** are found in analyzed hESCs and hiPSCs; **(E)** bar graph showing the frequency at which DNA gains and losses are detected with aCGH for both CNV and CNA group.

1.6. In hPSCs cultured in vitro, polymorphic CNVs are more prevalent in hiPSCs than in hESCs, while potentially pathogenic CNAs are more frequent in hESCs

We then aimed to elucidate what was the contribution of each hPSC type to this frequency distribution. We observed that the relative amount of genomically stable cells was higher in hiPSC (5.88%) than in hESCs (for which surprisingly 100% of the analyzed cells were genomically unstable). While all the alterations found in hESCs were pathogenic, this was found to be the case for 64.86% of the alterations found in hiPSCs, whereas the rest were considered CNVs (35.14%). This shows an increased prevalence of CNVs in hiPSCs, whereas analyzed hESCs seem to have an increased likelihood of acquiring CNAs with potential pathogenic effects, as compared to hiPSCs (Fig.13A).

Next, we evaluated the differences in the propensity to acquire subchromosomal aberrations among different hPSC types. To that aim, we studied whether the probability of hESCs to acquire chromosomal alterations over time was significantly different than that of hiPSCs. We normalized the passage number for both hPSC groups and used Kaplan–Meier curves to show probability of hESCs and hiPSCs to acquire genomic alterations detectable by aCGH at a certain passage number (Fig.13B). The hESCs and hiPSCs were analyzed over a period of 33 and 11 passages *in vitro*, respectively. Our results showed no significant difference among hPSC groups ($p = 0.078$).

By studying the frequency, types and distribution of detected CNVs and CNAs in more detail we observed that, once again, polymorphic CNVs showed a tendency to be distributed throughout the whole genome (Fig.13C), since they were detected in chromosomes 1 (present in 11.54% of analyzed hiPSCs), 3 (11.54%), 4 (7.69%), 5 (7.69%), 10 (7.69%) and 22 (3.84%) (Table 5). Chromosomes 1 and 3 in hiPSC lines presented a special predisposition to acquire CNVs, having the highest frequencies of this type of alteration. Regarding the differential prevalence of CNAs among hESCs and hiPSCs, we found that hiPSCs also displayed a more varied set of alterations, which also showed to be more distributed throughout the genome (Fig.13D). In fact, and as shown in Table 6, CNAs in hiPSCs were detected in chromosomes 1 (which was altered in 5.88% of analyzed hiPSCs), 2 (23.52%), 3 (11.76%), 4 (11.76%) 6 (11.76%), 7 (5.88%), 8 (11.76%), 11 (11.76%), 12 (5.88%), 14 (5.88%), 15 (17.64%), 20 (5.88%) and 22 (11.76%), whereas hESCs alterations were limited to chromosomes 10 (where alterations were detected in 44.44% of hESCs), 14 (22.2%) and 20 (66.67%). These data indicate

that CNAs are more frequent in hESC lines than in hiPSCs lines, and that most CNAs affect chromosome 20, since 26.92% of all hPSCs (and 66.67% of hESCs) harbored CNAs in this chromosome (which represent around 16.67% of all detected CNAs; Fig.13D).

Table 6. List of Copy Number Alterations (CNAs) detected by aCGH in hESCs and hiPSCs.

Alteration	Region	hESC/hiPSC	% of Cells Affected		% of Total CNAs	
			All hPSCs	hPSC Type	All hPSCs	hPSC Type
Deletion	1q21.2	hiPSC	3.85	5.88	2.70	4
	2q23.3	hiPSC	7.69	11.76	5.41	8
	2q37.3	hiPSC	7.69	11.76	5.41	8
	3q13.31	hiPSC	7.69	11.76	5.41	8
	4q28.3	hiPSC	7.69	11.76	5.41	8
	7q11.23	hiPSC	3.85	5.88	2.70	4
	7p14.3	hiPSC	3.85	5.88	2.70	4
	11q11	hiPSC	7.69	11.76	5.41	8
	15q11.1–11.2	hiPSC	3.85	5.88	2.70	4
	15q26.3	hiPSC	7.69	11.76	5.41	8
Insertion	6q26	hiPSC	7.69	11.76	5.41	8
	10q23.32	hESC	15.38	44.44	10.81	16
	12p13.31	hiPSC	3.85	5.88	2.70	4
	14q23.3	hESC	7.69	22.22	5.41	8
	14q32	hiPSC	3.85	5.88	2.70	4
	22q11.2	hiPSC	7.69	11.76	2.70	8
Duplication	8q24.3	hiPSC	7.69	11.76	5.41	8
	20q11.21	hESC and hiPSC	26.92	66.67 (hESCs), 5.88 (hiPSCs)	16.22	24 (hESCs), 4 (hiPSCs)

We further characterized the genomic alterations found in hPSCs by analyzing the relative abundance of DNA gains and losses within each alteration type (CNVs and CNAs). We found that deletions represented 69.23% of all CNVs. On the other hand, only 30.77% of CNVs (more than 2 times less) corresponded to insertions (Fig.13E). Notably, we observed that gains of genetic material (insertions or duplications) accounted for 56.76% of all detected CNAs, while only the remaining 43.24% were deletions. Thus, these results show that insertions or duplications of genetic material are more likely to cause a potentially pathogenic CNA (frequency increased by 31% compared to deletions for this type of alterations), whereas deletions mostly give rise to CNVs (Fig.13E).

1.7. Standardization of culture conditions reduces the prevalence and types of de novo genomic alterations acquired by hPSCs in vitro

To investigate the effect of the introduction of cell culture SOPs under a QMS on the observed prevalence of CNVs and CNAs in hPSCs, only those alterations caused after adapting the hPSC lines to these conditions must be considered. We hypothesized that these alterations corresponded to *de novo* CNVs or CNAs, which had been acquired because of specific cell culture conditions, and hence must be distinguished from all those alterations which hPSCs already harbored either because they were already present in the embryo or as a consequence of suboptimal culture conditions or hiPSC generation (pre-existing alterations). To that aim, we divided the analyzed hPSCs into two groups: (i) hPSCs which had been adapted and cultured using standardized conditions for at least four passages (post-adaptation, or PoA); and (ii) hPSCs which had not been cultured under these conditions for at least four passages, being expanded using their original protocols (pre-adaptation, or PrA).

Briefly, we started by identifying all those alterations which had been detected in PrA hPSC lines, and classifying them as inherited variants (that is, alterations which had been originated before adaptation and hence were already harbored by the cells). After that, we studied the prevalence of pre-existing alterations, detected by conventional G-banding, in PrA hPSC lines. Pre-existing polymorphic chromosomal alterations were found to affect 11.76% of PrA hPSCs, while potentially pathogenic karyotypic aberrations were identified in 46.67% of these cells (Table 7).

Table 7. Prevalence of chromosomal and subchromosomal alterations detected by G-banding and aCGH, respectively, in pre- and post-adaptation hPSC lines. The reduction in the prevalence of each de novo alteration time in the post-adaptation (PoA) group compared to the pre-adaptation (PrA) group is showed, as well as the fold-change.

Culture Conditions	Chromosomal Alterations (G-banding)		Subchromosomal Alterations (aCGH)	
	FPA	Pathogenic	CNV	CNA
Pre-adaptation (PrA)	11.76%	46.67%	46.67%	80.00%
Post-adaptation (PoA)	5.49%	18.18%	18.18%	36.36%
Reduction $(-\frac{PoA-PrA}{PrA}*100)$	-53.31%	-61.05%	-61.05%	-53.31%
Fold-change $(-\frac{PrA}{PoA})$	**-2.14**	**-2.57**	**-2.57**	**-2.2**

To identify de novo alterations in PoA hPSCs, we identified all pre-existing alterations which had also been detected in PoA hPSCs. Then, these alterations were filtered out from the analysis, and the remaining genomic alterations were classified as *de novo* variants. The prevalence of these alterations in PoA hPSCs was then established (Table 7) and compared against that of pre-existing alterations in PrA hPSCs. By using this strategy, we were able to evaluate whether these conditions have a positive impact in preventing the acquisition of karyotypic alterations of hPSCs *in vitro*. The results showed that the prevalence of *de novo* polymorphic karyotypic variants in PoA hPSCs was 5.49%, while *de novo* karyotypic aberrations were only present in 18.18% of the cells (Table 7). This represents a reduction of 53.31% (2.14-fold) and 61.05% (2.57-fold) in the prevalence of polymorphic and pathogenic karyotypic alterations, respectively. These observations highlight that the development and use of hPSC culture SOPs results in a reduction in the frequency at which karyotypic polymorphic variants and aberrations are acquired, and hence improves genomic stability of these cells.

As expected, we also detected a higher prevalence of subchromosomal genomic alterations by aCGH in the analyzed PrA hPSCs, especially regarding potentially pathogenic alterations. More specifically, 46.67% and 80% of hPSCs presented CNV and CNA, respectively before adaptation (Table 7). On the other hand, once adaptation to the new conditions had been completed and under the new culture conditions, only 18.18% and 36.36% of hPSCs were found to be affected by *de novo* CNVs and CNAs, respectively (Table 7). Hence, in this case we observed a 2.2-fold reduction in the prevalence of *de novo* CNAs, and a 2.57-fold reduction in the prevalence of *de novo* CNVs. In addition, we observed that while PrA hPSCs displayed a wide range of different CNVs (6 different types) and CNAs (15 types), genomic alterations in PoA cells were limited to only two different CNVs and three different CNAs (Table 8).

These observations reveal that the application of SOPs to hPSCs maintenance under a QMS leads to more genomically stable cell products at a submicroscopic level. This strategy not only results in a reduction in the prevalence and types of polymorphic genomic variants, but also in a drastic decrease in the acquisition rate of potentially pathogenic karyotypic aberrations and subchromosomal CNAs.

Table 8. List of *de novo* chromosomal (FPAs and pathogenic alterations) and subchromosomal (CNVs and CNAs) detected by G-banding and aCGH, respectively, in post-adaptation hPSCs.

Alteration		Region	Size	% Affected hPSCs
Pathogenic chromosomal alterations	*Trisomy*	+8	NA	3.30
	Trisomy	+12	NA	2.20
	Isochromosome	i(20)(q10)	NA	3.30
Chromosomal FPAs	*Pericentric inversion*	inv(9)(p11q13)	NA	1.10
	Microsatellite	21qs+	NA	4.40
Subchromosomal CNVs	*Deletion*	3q26.21	62 kb	9.09
	Insertion	4q35.2	219 kb	9.09
Subchromosomal CNAs	*Insertion*	14q23.3	370 kb	18.18
	Insertion	14q32	136 kb	9.09
	Duplication	20q11.21	4.7 Mb	9.09

1.8. Standardization of culture conditions leads to a huge reduction in the probability of hPSCs acquiring de novo genomic alterations in vitro

Once we had observed that the absolute prevalence and types of both *de novo* chromosomic and subchromosomal alterations was reduced in hPSCs, which had been adapted to standardized *in vitro* cell culture conditions, we investigated whether the probability of hPSCs to become genomically altered over time was significantly lower during the PoA period compared to the PrA period. To that aim, we first normalized the passage number for both the PrA and PoA hPSC groups. In the first case, passage number 0 corresponds to the passage number at which each cell line arrived at our laboratory; however, for the post-adaptation group, passage number 0 equals the first passage number at which the adaptation to standardized conditions was completed (that is, the fourth passage number using our cell culture protocol).

Then, we studied the evolution of the probability of acquisition of genomic alterations in hPSCs over time in culture (passage number) for both the PrA and PoA periods. To that aim, we used Kaplan–Meier curves to show what the probability of a given analyzed hPSC acquiring a given type of *de novo* genomic alteration at a certain passage number for both groups. This analysis was performed for both chromosomal alterations detected

by G-banding karyotype (Fig.14A) and subchromosomal alterations detected by aCGH (Fig.14B).

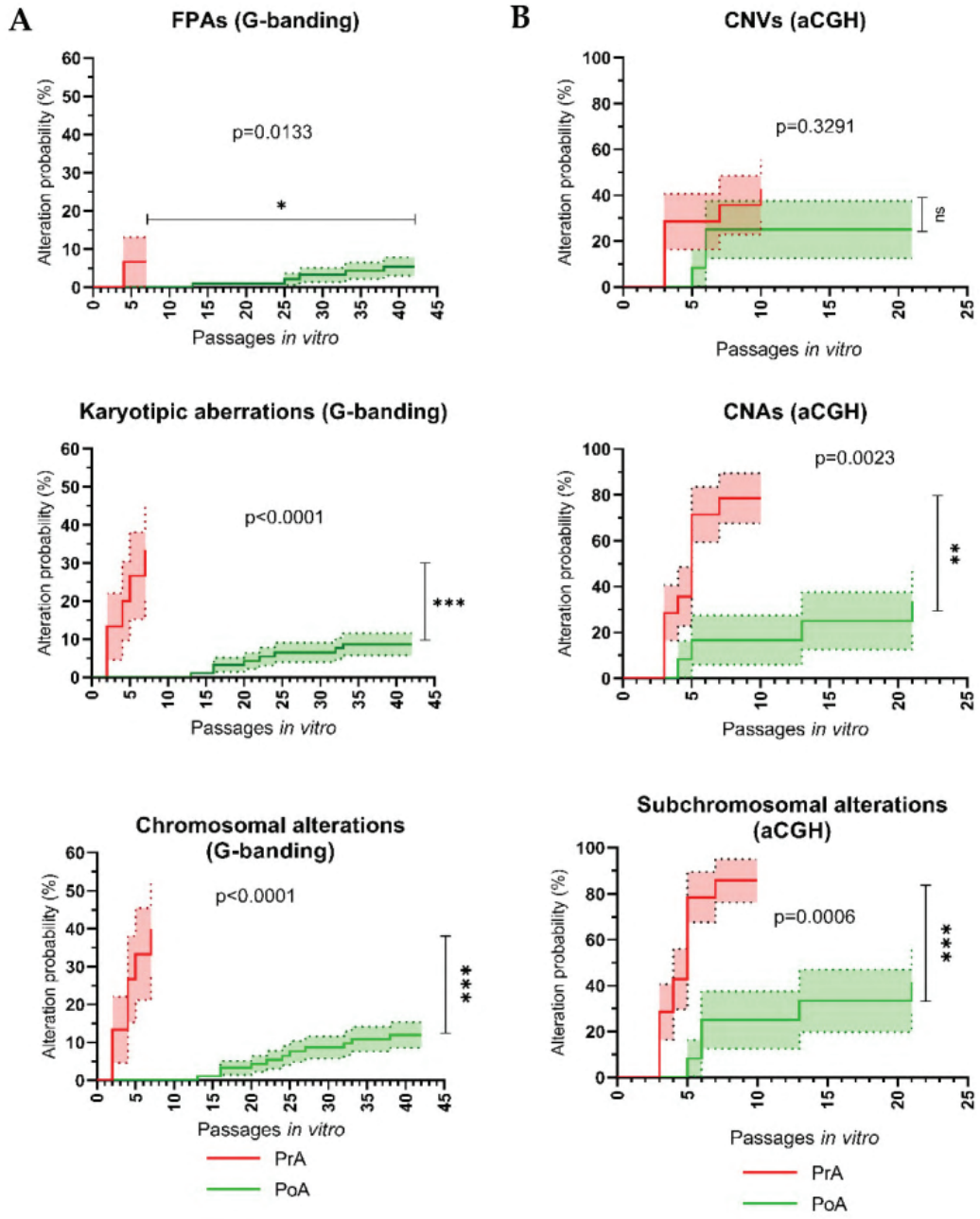

Figure 13. Adaptation to standardized cell culture conditions described by standard operating procedures (SOPs) under a Quality Management System (QMS) result in improved genomic stability of cultured hPSCs. Survival analysis (Kaplan–Meier curves) of the evolution of the probability (%) of hPSCs being affected by de novo genomic alterations over time (passages in vitro) before and after adaptation to standardized cell culture conditions, using G-banding karyotyping (A) and Comparative Genome Hybridization array (aCGH; B) as detection methods. For each panel, the top, middle and bottom plots show the probability of hPSCs acquiring polymorphic alterations, pathogenic alterations and total alterations, respectively. Pre-adaptation (PrA) and post-adaptation (PoA) refer to hPSCs analyzed before and after completing adaptation to the standard cell culture conditions used in our laboratory, respectively. Error bars represent standard error (S.E.M.). FPA: Frequent Polymorphic Alteration; CNV: Copy Number Variation; can: Copy Number Alteration.

For chromosomal alterations detected by G-banding, PrA and PoA hPSCs were analyzed over a period of 42 passages *in vitro* (Fig.14A). We found that the probability of *de novo* chromosomic alterations in PoA hPSCs was significantly lower than that of PrA hPSCs ($p < 0.0001$). In fact, this probability was around 4 times higher (~40% vs. ~10%) for PrA hPSCs at only passage 7 than PoA hPSCs which had been cultured under standardized conditions for around 6 times longer (i.e., passage 42). Interestingly, we observed that this difference was mainly due to karyotypic aberrations with pathogenic potential ($p < 0.0001$), for which the probability of being acquired by PrA hPSCs (~30% by passage 7) was around three times higher than that for PoA hPSCs cultured 6 times longer (i.e., ~10% by passage 42). Although this probability was found to be different for both groups when only considering chromosomal FPAs ($p = 0.0133$), this difference was not as striking (~6% for PrA hPSCs at passage 7 vs. ~5% for PoA hPSCs at passage 42). This highlights that the probability of hPSCs acquiring *de novo* pathogenic karyotypic aberrations during *in vitro* culture is hugely reduced (although not completely eliminated) by the adaptation of these cells to standardized conditions.

Finally, for subchromosomal alterations detected by aCGH, we analyzed data from PrA and PoA hPSCs over a more reduced period of time of 21 passages *in vitro* (Fig.14B). In this case, we also observed a significantly reduced probability ($p = 0.0006$) of acquiring subchromosomal alterations in the hPSCs of the PoA group (i.e., ~40% by passage 21) compared to hPSCs in the PrA group which had been cultured in our laboratory for about half the time (i.e., ~80% by passage 10). Once again, this difference was found to be mainly caused by pathogenic CNAs ($p = 0.0023$), since cells in the PrA group showed a 2-fold increase in the probability of acquiring CNAs compared to hPSCs in the PoA group which had been cultured *in vitro* by our group for two times longer (~80% by passage 10 vs. ~40% vs. passage 21). On the other hand, the probability of cells from both groups to acquire subchromosomal CNVs over time was not found to be significantly different ($p = 0.3291$). Hence, these data also underscore that the probability of hPSCs acquiring *de novo* CNAs during *in vitro* culture is hugely reduced (although not completely eliminated) by the adaptation of these cells to standardized conditions after SOP implementation, while the probability of acquisition of polymorphic CNVs is not altered.

2. Chapter II: Identification and validation of cell surface marker signatures for isolation of hPSC-derived striatal progenitors

One of the main challenges to be overcome to progress cell therapies to clinical application in HD (and other NDs) is the risk of teratoma formation and graft overgrowth after transplantation. While a potential solution could be to simply ensure that cell products are terminally differentiated neurons (e.g., mature SPNs in HD) with limited proliferative potential, it has been shown that these mature neuronal populations display reduced viability following transplantation into the striatum (Aubry et al., 2008). Thus, new strategies need to be implemented to ensure increased safety of cell products which can lead to clinical application.

One aspect which remains largely unknown is whether it is possible to produce homogeneous donor cells composed of purified target cells and depleted off-target cell types to ensure stable and predictable graft outcomes. To address this issue, cell sorting is anticipated to be an instrumental strategy. Along these lines significant attention has been focused on development standardization of hPSC-derived midbrain dopaminergic neural progenitors using cell sorting methods based on specific cell surface marker signatures (Aguila et al., 2014; Lehnen et al., 2017; Luzy et al., 2019; Samata et al., 2016). However, while these studies have made significant progress, they have demonstrated varying, and often suboptimal success, which underlines the need to develop improved strategies for the isolation of hPSC-derived neural cell types. Additionally, to our knowledge, no similar studies have been reported for hPSC-derived striatal progenitors.

Previously, we have successfully transplanted hPSCs differentiated towards SPNs into the mouse striatum (Comella-Bolla et al., 2020; Miguez et al., 2023). Nevertheless, the transplanted cell population was mixed, containing a variety of phenotypes and degrees of maturity. Here, to refine our approach, we investigated whether implementation of cell selection steps prior to transplantation could allow for isolation of hPSC-derived striatal progenitors, hypothesizing, to drive optimization of the outcomes *in vivo* (in terms of differentiation into SPNs) and reduce the risk of graft overgrowth.

To that aim, we first identified and validated a new cell surface marker (i.e., CD200) for hPSC-derived postmitotic striatal progenitors. Next, we used this marker to set up and optimize an immunomagnetic cell sorting pipeline and demonstrated that this approach can be used to generate highly purified cell compositions enriched in hPSC-derived

postmitotic striatal progenitors. Finally, we demonstrated that transplanted selected progenitors survive upon intra-striatal transplantation in adult mice with no evidence of graft overgrowth *in vivo* (Fig.15).

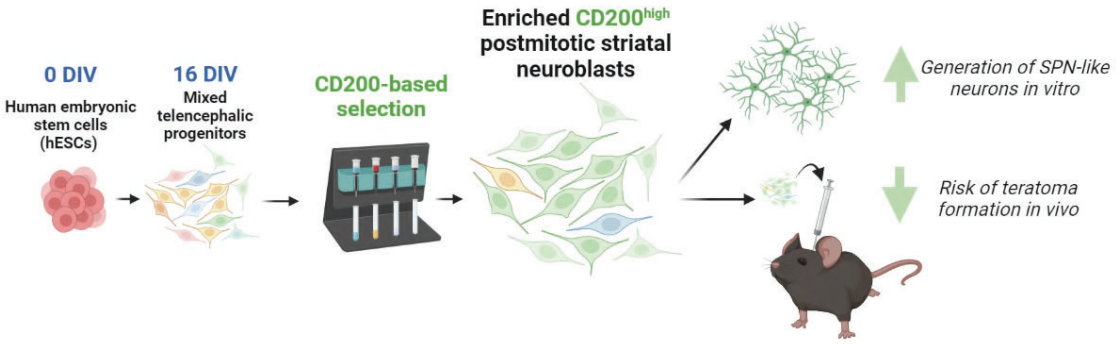

Figure 14. Graphical abstract of Chapter II. CD200 is a cell surface marker of hPSC-derived striatal neuroblasts (NBs). Cell sorting based on this marker allows for isolation of postmitotic striatal this progenitor subpopulation from mixed populations of hPSC-derived telencephalic progenitors, leading to increased generation of striatal projection neuron (SPN)-like neurons *in vitro* and reduction of the risk of teratoma formation *in vivo* upon intra-striatal transplantation in adult mice. DIV: Days *In Vitro.*

2.1. Neural Progenitor Cells (NPCs) and postmitotic neuroblasts (NBs) are the main progenitor subpopulations generated by hPSC in vitro striatal differentiation

To select a striatal progenitor population suitable for transplantation, we identified the main subpopulations of hPSC-derived neural progenitors generated by our ventral forebrain neuron differentiation protocol. We performed single-cell transcriptomic characterization (MARS-seq) of the mixed population of neural progenitors at 17 DIV using three hESC lines as a cell source. (i.e., GEN-019, H9 and RUES2) Clustering analysis of the 4,945 sequenced cells resulted in two main clusters of forebrain neural progenitors (Methods; Fig.16A). To establish cluster identity, we plotted the expression of the most significantly upregulated genes in each cluster (Fig.16B; Table 9). Top marker genes for cluster 1 corresponded to immature neural stem cell and proliferation markers, such as *VIM*, *TTYH1* or *FABP7*. Cluster 2 was characterized by upregulated expression of more mature postmitotic neuroblast (NB) or pan-neuronal markers such as *STMN2*, *MLTT11* or *MAP2*. Many cells from cluster 2 (NBs) were also characterized by the expression of GABAergic neuronal markers such as *GAD2*, and markers linked to striatal progenitor identity including *MEIS2*, *DLX5*, *RBP1* or *SIX3*.

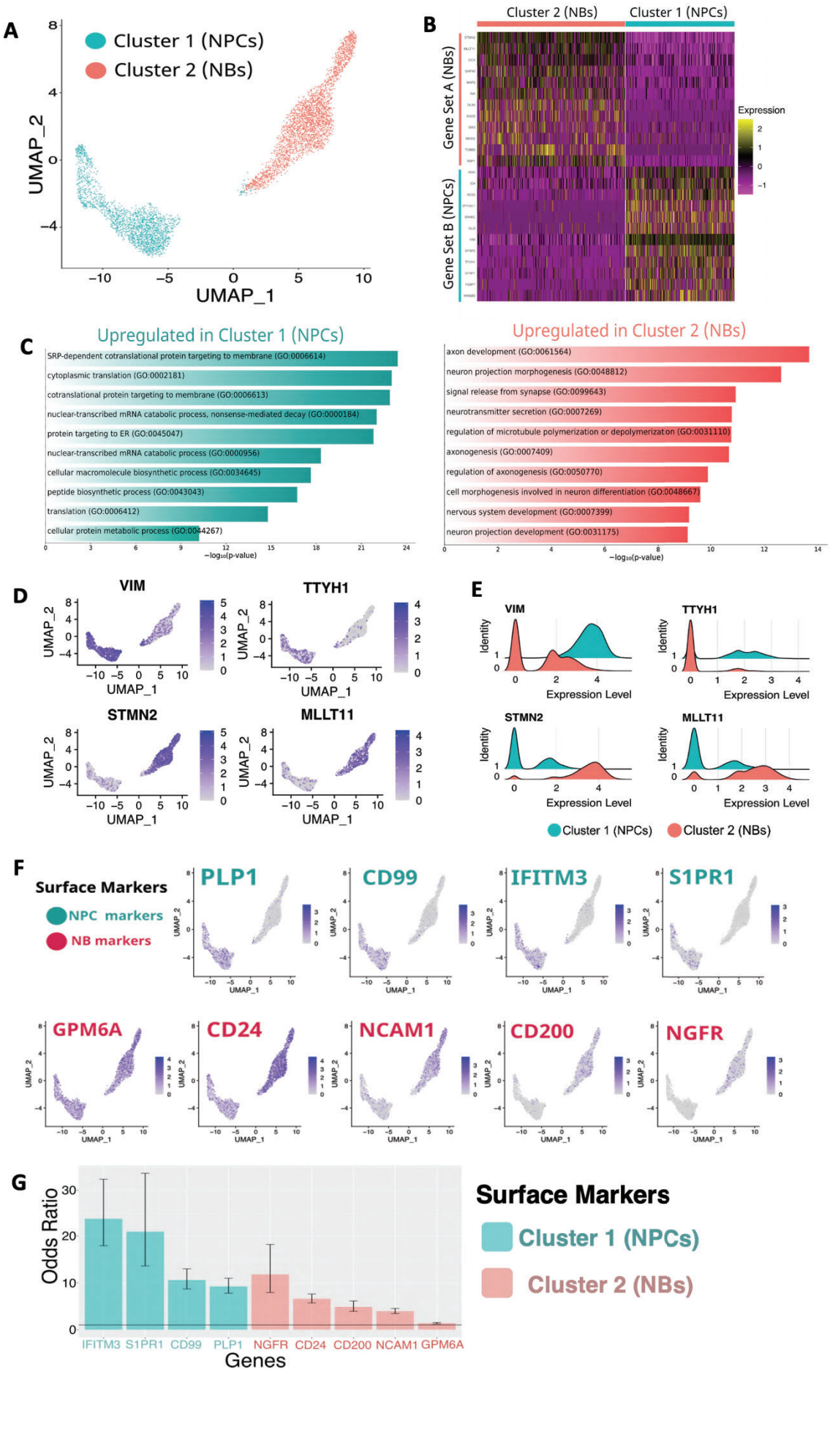
A
Cluster 1 (NPCs)
Cluster 2 (NBs)
UMAP_2
UMAP_1
B
Cluster 2 (NBs)
Cluster 1 (NPCs)
Gene Set A (NBs)
Gene Set B (NPCs)
Expression
C
Upregulated in Cluster 1 (NPCs)
SRP-dependent cotranslational protein targeting to membrane (GO:0006614)
cytoplasmic translation (GO:0002181)
cotranslational protein targeting to membrane (GO:0006613)
nuclear-transcribed mRNA catabolic process, nonsense-mediated decay (GO:0000184)
protein targeting to ER (GO:0045047)
nuclear-transcribed mRNA catabolic process (GO:0000956)
cellular macromolecule biosynthetic process (GO:0034645)
peptide biosynthetic process (GO:0043043)
translation (GO:0006412)
cellular protein metabolic process (GO:0044267)
−log10(p-value)
Upregulated in Cluster 2 (NBs)
axon development (GO:0061564)
neuron projection morphogenesis (GO:0048812)
signal release from synapse (GO:0099643)
neurotransmitter secretion (GO:0007269)
regulation of microtubule polymerization or depolymerization (GO:0031110)
axonogenesis (GO:0007409)
regulation of axonogenesis (GO:0050770)
cell morphogenesis involved in neuron differentiation (GO:0048667)
nervous system development (GO:0007399)
neuron projection development (GO:0031175)
−log10(p-value)
D
VIM
TTYH1
STMN2
MLLT11
UMAP_2
UMAP_1
E
VIM
TTYH1
STMN2
MLLT11
Identity
Expression Level
Cluster 1 (NPCs)
Cluster 2 (NBs)
F
Surface Markers
NPC markers
NB markers
PLP1
CD99
IFITM3
S1PR1
GPM6A
CD24
NCAM1
CD200
NGFR
UMAP_2
UMAP_1
G
Odds Ratio
IFITM3 S1PR1 CD99 PLP1 NGFR CD24 CD200 NCAM1 GPM6A
Genes
Surface Markers
Cluster 1 (NPCs)
Cluster 2 (NBs)

Figure 15. Distinct hPSC-derived forebrain progenitor subtypes of neural progenitor cells (NPCs) and postmitotic neuroblasts (NBs) are identified at 17 DIV (A) Uniform Manifold Approximation and Projection (UMAP) showing the unbiased clustering analysis of hPSC-derived 17 DIV populations of telencephalic progenitors, which identifies two progenitor subtypes: NPCs (Cluster 1, green) and NBs (Cluster 2, red); **(B)** Heatmap showing unbiased hierarchical clustering of the whole dataset based on the expression of selected differentially expressed genes among Cluster 1 and Cluster 2. Gene sets for each cluster include the top markers for each cluster identified by Seurat and selected, well-known markers for postmitotic NBs and neurons (Gen Set A) or classic neural stem cell markers (Gene Set B). Color code: purple = low expression; yellow = high expression; **(C)** Functional enrichment analysis of DEGs in Clusters 1 and 2 from the hierarchical analysis. The top ten Gene Ontology Biological Process (GO:BP) terms are shown for each cluster; **(D)** UMAP plots showing expression of some of the most relevant NPC (left) and NB (right) marker genes, from Gene Set A and B respectively. Color code: grey = low expression; purple = high expression; **(E)** Ridgeplots showing the distribution of the NPC (green) and NB (red) subpopulations according to expression levels of some of the most relevant NPC (left) and NB (right) marker genes; **(F)** UMAP plots showing expression of newly-identified potential cell surface markers of NPCs (upper plots) and NBs (lower plots). Color code: grey = low expression; purple = high expression; **(G)** Barplot showing the odds of each cell surface marker candidate being expressed in its corresponding cluster vs the odds of being expressed in the other cluster (odds ratio; OR). The black line at OR=1 represents the set threshold for a marker to be considered specific (OR>1).

Functional enrichment analysis revealed that cells from cluster 1 showed an upregulation of genes related to macromolecule biosynthesis and protein translation (GO:0034645, GO:0043043, GO:0006412, GO:0002181), metabolism (GO:0044267), RNA degradation (GO:0000184, GO:0000956) or protein transport (GO:0006614, GO:0045047, GO:0006613), all of which may be associated with increased cell proliferation of this population. In contrast, cells from cluster 2 were characterized by the expression of genes related to nervous system development (GO:0007399), axogenesis (GO:001564, GO:0099643, GO:0031175, GO:0007409, GO:0050770), neuron differentiation (GO:0048667), microtubule polymerization/depolymerization (GO:0031110), or synapse (GO:0007269, GO:0099643; Fig.16C). Altogether, these results suggested that cluster 1 corresponded to immature, stem cell-like proliferating Neural Progenitor Cells (NPCs), whereas cells in cluster 2 were postmitotic NBs with a more neuronal profile.

We confirmed cluster identity by mapping the expression of several marker genes of NPCs (*VIM* and *TTYH1*) and NBs (*STMN2* and *MLLT11*) onto the UMAP plot (Fig.16D). We also quantified the expression levels of these genes in the cells of each cluster (Fig.16E). We found that *VIM* was present in 98.9% of NPCs and 56.9% of NBs, and *TTYH1* expression was detected in 69.7% of NPCs and 13.9% of NBs. Regarding NB markers, 95% and 87.5% of NBs expressed *STMN2* and *MLLT1*, while these genes were

expressed in 41.6% and 34.5% of NPCs. *VIM* and *TTYH1* expression showed 5.54-fold and 3.84-fold increases in NPCs compared to NBs, whereas NBs showed 11.79-fold and 5.24-fold increases in *STMN2* and *MLLT11* expression compared to NPCs. Hence, we observed that these presented a higher and more prevalent expression among the cells of a particular cluster. We found that the rest of the top NPC and NB markers also followed a similar pattern.

Table 9. List of some examples of relevant marker genes differentially expressed in the Neuroblast (NB) and Neural Progenitor Cell (NPC) subpopulations at 16 DIV. For each marker, the cluster for which it is specifically expressed is indicated, as well as the average log2 fold change (Avg. log2 FC) and the percentage of NBs and NPCs expressing the marker. DIV: Days *In Vitro*

Cluster	Marker gene	Avg. log_2 FC	% Expression in:	
			NPCs	NBs
NPC (1)	*SFRP2*	2.56	72	12.4
	VIM	2.47	98.9	56.9
	ZFP36L1	2.06	49.2	5
	FABP7	1.98	59.6	11.7
	TTYH1	1.94	69.7	13.9
	SPARC	1.88	45.6	4.2
	HES5	1.8	67.8	15.3
	HMGB2	1.74	51.9	23
	GLI3	1.71	43.7	4.9
	SFRP1	1.67	67.9	21.3
	ID4	1.53	79.3	38.3
	MDK	1.32	81.5	38.5
NB (2)	*STMN2*	3.56	41.6	95
	RBP1	2.6	15.1	68.7
	GAP43	2.44	16.7	69.7
	MLLT11	2.39	34.5	87.5
	INA	2.36	14.4	66.7
	DLX5	2.3	8.7	48.9
	GAD2	2.04	6	42.4
	MAP2	1.6	69.2	33.5
	SIX3	1.48	18.6	42.1
	DCX	1.44	56.4	84.9
	TUBB3	1.31	3.3	30.3
	MEIS2	1.1	19.8	35.8

We also identified candidate cell surface markers for NPCs and NBs. We selected those genes encoding cell surface proteins which also showed the best potential to serve as a marker for any of the subpopulations. We shortlisted *PLP1*, *IFITM3*, *CD99* and *S1PR1* as potential NPC cell surface markers, and *CD24*, *NCAM1*, *CD200*, *NGFR* and *GPM6A* as candidate NB cell surface markers (Table 10). We mapped the expression of individual marker genes of NPCs and NBs (Fig.16F) onto the UMAP plot and quantified the odds ratio (OR) of expression of each of these genes in its corresponding cluster compared to the other cluster (Fig.16G). UMAP plots showed that the expression levels and the prevalence of expression of these markers in their corresponding subpopulation were generally lower than the classical marker genes discussed above. NPC marker candidates were expressed in only 41.4% (*PLP1*), 34.1% (*CD99*), 31.7% (*IFITM3*), and 14.6% (*S1PR1*) of NPCs. The expression prevalence of NB marker candidates in the NB cluster was generally higher, being expressed in 88% (*CD24*), 62.4% (*GPM6A*), 44.2% (*NCAM1*), 20.1% (*CD200*) and 13.3% (*NGFR*) of NBs. Regarding expression levels, average $\log_2$ fold change for NPC markers ranged from 1.75 (*PLP1*) to 0.83 (*S1PR1*), while for NB markers the levels ranged from 1.83 (*CD24*) to 0.51 (*GPM6A*). Nonetheless, we observed that all these marker candidates were highly specific, with all ORs being larger than 1 and some larger than 10, including *IFITM3* (23.89), *S1PR1* (20.92), *NGFR* (11.8), or *CD99* (10.6) (Fig.16G and Table 10).

Table 10. List of identified potential cell surface markers for the NPC and NB subpopulations at a transcriptional level. For each marker, the cluster for which it is specifically expressed is indicated, as well as the average $\log_2$ fold change (Avg. $\log_2$ FC), the percentage of NPCs and NBs expressing the marker, and the odds ratio (OR; the ratio between the probability of a gene being expressed in its associated cluster and the probability of that gene being expressed in the other cluster).

Cluster	Marker gene	Avg. $\log_2$ FC	% Expression in:		Odds Ratio (OR)	p-value
			NPCs	NBs		
NPC (1)	*PLP1*	1.75	41.1	7	9.24	5.26×10^{-188}
	IFITM3	1.4	31.7	1.9	23.89	1.35×10^{-206}
	CD99	1.28	34.1	4.6	10.6	1.84×10^{-168}
	S1PR1	0.83	14.6	0.8	20.92	2.28×10^{-90}
NB (2)	*CD24*	1.83	52.7	88	6.6	1.33×10^{-170}
	NCAM1	1.41	16.7	44.2	3.95	3.84×10^{-97}
	CD200	1.05	4.9	20.1	4.88	3.12×10^{-59}
	NGFR	0.74	1.3	13.3	11.8	1.49×10^{-63}
	GPM6A	0.51	54.6	62.4	1.38	$3.78\ 10^{-08}$

2.2. *NGFR and CD200 are two promising cell surface markers of hPSC-derived postmitotic NBs*

We next validated the selected markers at a protein level using a single hESC line (i.e., GEN-019) using flow cytometry (FC) and confirmed the specificity of CD99 and S1PR1 as NPC markers (Fig.17A) and NGFR and CD200 as NB markers (Fig.17B).

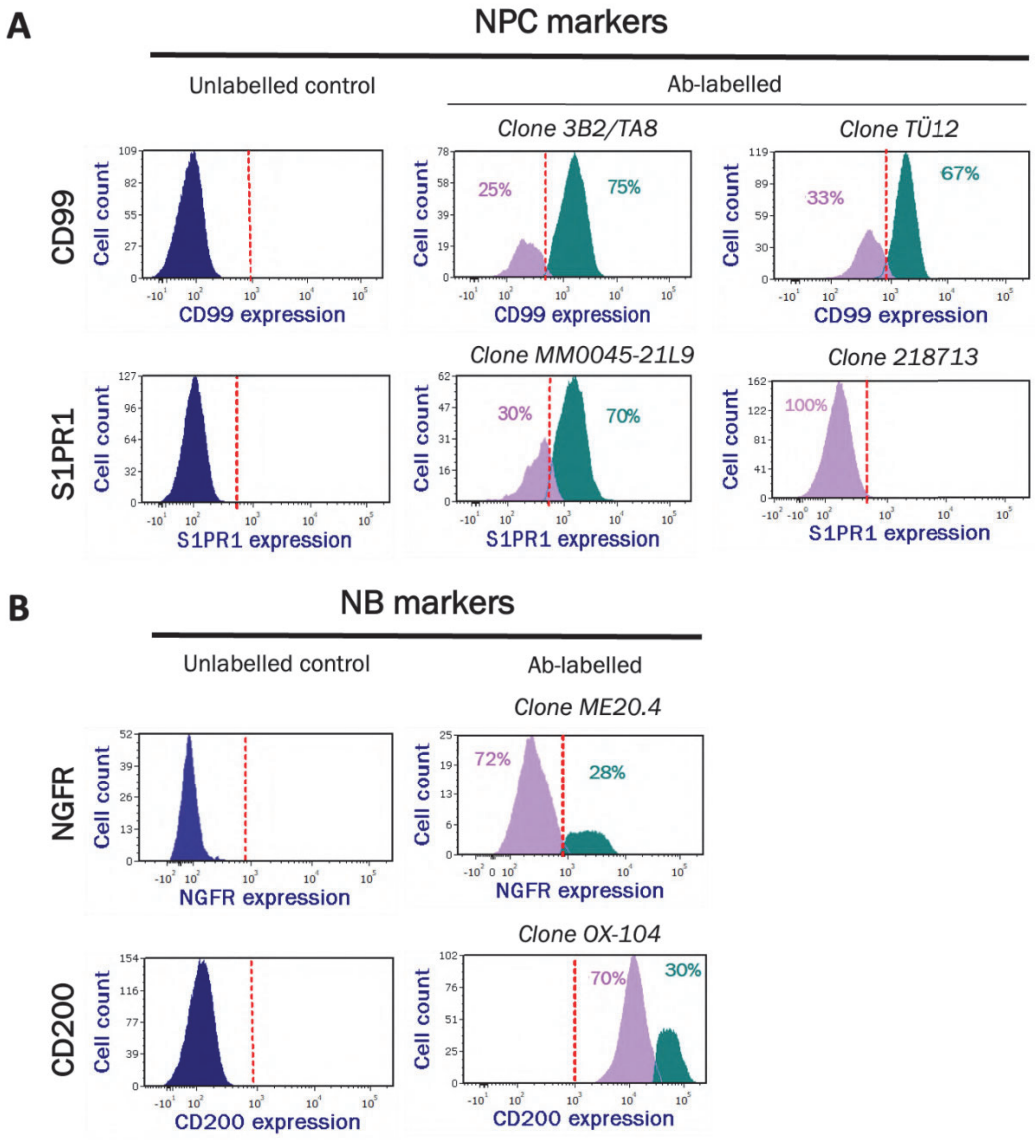

Figure 16. Validation by flow cytometry (FC) reveals promising cell surface markers to be used for the isolation of NPCs (CD99, S1PR1) and NBs (NGFR and CD200). Histograms showing FC characterization of 16 DIV hPSC-derived cell populations using the most promising NPC (A) and NB (B) cell surface markers identified by MARS-Seq (Table 10). The set threshold for positivity for each of the tested markers is indicated by a red dashed line. Color code: blue (unstained population), purple (low/negative population) and green (high/positive population)

We tested two different antibodies for CD99 which yielded similar results since they both led to the detection of a major population of $CD99^+$ NPCs (67% and 75% of the total progenitor population for clones TÜ12 and 3B2/TA8 respectively), and a less-abundant subpopulation of $CD99^-$ NBs (33% and 25% of total cells for clones TÜ12 and 3B2/TA8 respectively). On the other hand, only one of the two antibodies tested to label S1PR1 (clone MM0045-21L9) could be used to successfully detect a peak of $S1PR1^+$ cells of 70% of the total cell population (NPC subpopulation), while the remaining 30% of $S1PR1^-$ cells would correspond to NBs. However, the overlap between $S1PR1^-$ and $S1PR1^+$ peaks was greater compared to $CD99^-$ and $CD99^+$ peaks. The two additional prospective NPC markers that we tested (PLP1 and IFITM3) did not show subpopulation-specific differential expression at a protein level (Fig.18A).

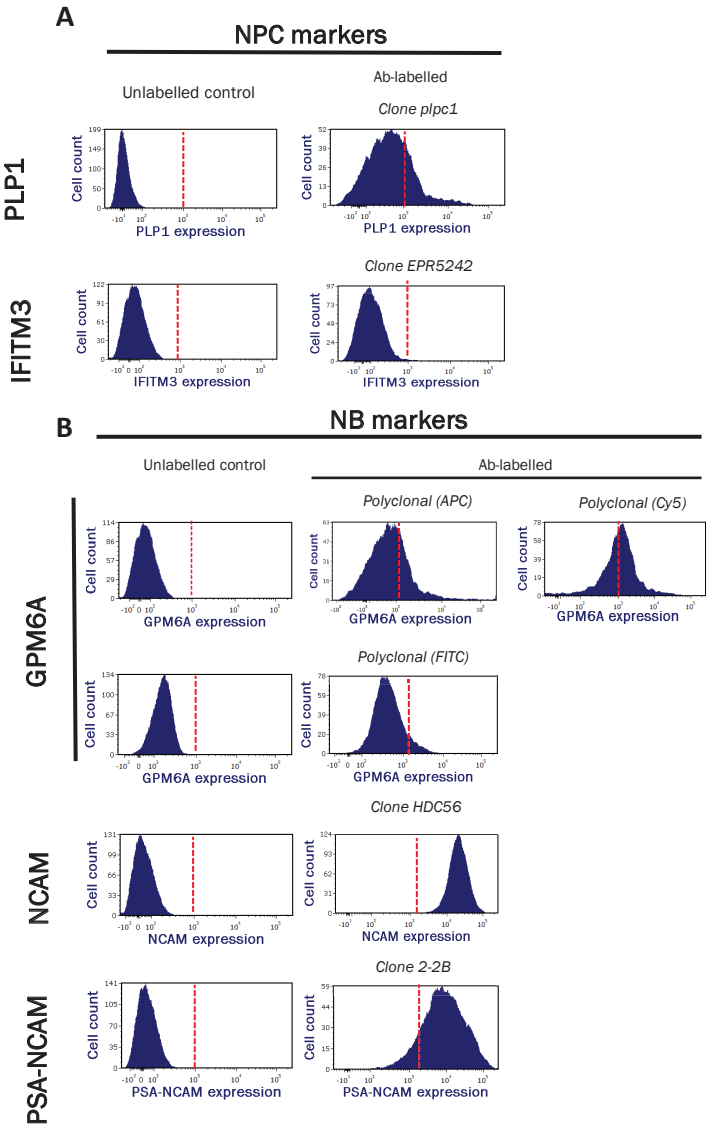

Figure 17. Validation by flow cytometry (FC) reveals that some of the most promising cell surface markers to be used for isolation of NPCs (PLP1, IFITM3) and NBs (GPM6A, NCAM, PSA-NCAM) are not specific at a protein level. (A, B) Histograms showing FC characterization of 16 DIV hESC-derived cell populations using the NPC (A) and NB (B) cell surface markers identified by MARS-seq (Table 10) whose specificity could not be validated at a protein level.

Cell labelling targeting NGFR (clone ME20.4 ;Fig.17B) resulted in a majority of $NGFR^-$ cells (72% of total cells; NPCs) and a scarcer population of $NGFR^+$ cells (28% of total cells; NBs). Interestingly, even if we detected 100% positive cells when labelling was performed targeting CD200 (clone OX-104; Fig.17B), the NB subpopulation consistently presented a higher expression of this marker compared to NPCs. For instance, we detected a $CD200^{low}$ NPC peak (70% of total cells) and a $CD200^{high}$ NB peak (30% of total cells). The remaining NB markers for which we tested specificity (CD24, GPM6A NCAM and PSA-NCAM) did not show subpopulation-specific differential expression at a protein level (Fig.18B).

Since CD200 was the most promising NB cell surface marker at a protein level, we performed additional ICCs to validate the identity of $CD200^{high}$ cells (Fig.19). $CD200^{high}$ cells were mostly found in NB-rich cell aggregates, did not express the proliferation marker Ki-67 and displayed a high expression of the premature neuronal marker TUBB3 (Fig.19B) Proliferating Ki-67^+ cells were mostly located in an NPC-rich monolayer in which cells presented $CD200^{low}$ expression (Fig.19C). CD200 and TUBB3 were expressed in both the cell body and projections, and we detected some TUBB3 high signal in the monolayer as the NBs in the aggregates projected their neurites through it. Besides these neurites, $TUBB3^{high}$ expression in the monolayer was found to be rare.

2.3. CD200 can be used to purify NBs via FACS with high purity and yield, but suboptimal cell viability

We selected CD200 and NGFR to be used to sort NPCs and NBs from the mixed population of forebrain progenitors via FACS using GEN-019. We compared two cell selection strategies, for which we assessed the relative abundance of different cell subpopulations: a single-marker selection based on differential CD200 expression (Fig.20A), and a double-marker selection based on differential expression of both CD200 and NGFR (Fig.20B). Consistent with previous observations, when single CD200 selection was performed we observed two different cell subpopulations based on CD200 expression in the unsorted fraction: a most prevalent $CD200^{low}$ subpopulation (NPCs) and a less frequent subpopulation of $CD200^{high}$ NBs. Following CD200 selection, successful purification of sorted fractions was confirmed, with NPC-like and NB-like sorted fractions almost exclusively containing $CD200^{low}$ and $CD200^{high}$ cells respectively (Fig.20A).

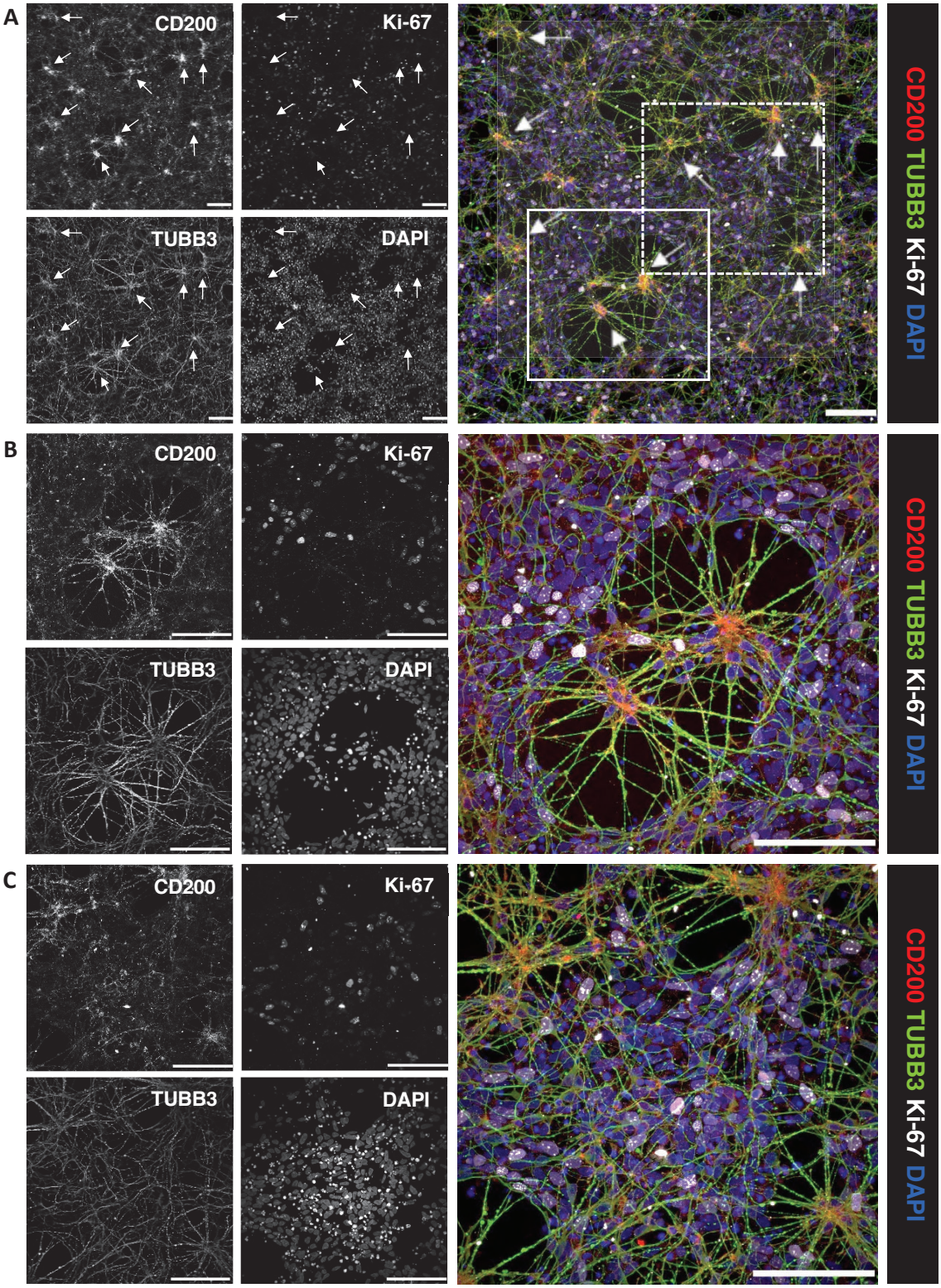

Figure 18. Validation of the NB cell surface marker CD200 via immunocytochemistry (ICC). (A-C) Confocal microscopy pictures of ICC of CD200 (NB marker), Ki-67 (proliferation marker), and TUBB3 (immature neuronal marker) in a 16 DIV culture of a control hPSC line (GEN-019). Panel A shows the distribution of the two cell subpopulations in the culture, where CD200 is highly expressed in NB-rich aggregates (white arrows), which also display a high TUBB3 expression and no Ki-67^{+} cells. The solid white box indicates one of the NB-rich aggregates (whose magnified pictures are shown in panel B), whereas the dashed white box contains a region of the cultures mostly composed of NPC-rich monolayer (magnified pictures shown in panel C). Scale bars = 100µm

When double CD200/NGFR selection was performed, we analyzed the NGFR expression profile in the unsorted fraction and found that most cells did not express NGFR, which was also consistent with previous observations. Analysis of CD200 expression profile in this fraction revealed that this population was mostly composed of $CD200^{low}$ cells. Following CD200/NGFR double selection, successful purification of sorted fractions was confirmed, with NPC-like and NB-like sorted fractions almost exclusively containing $CD200^{low}/NGFR^{-}$ and $CD200^{high}/NGFR^{+}$ cells respectively (Fig.20B). Notably, when CD200/NGFR double selection was performed we also detected the presence of $CD200^{high}/NGFR^{-}$ and $CD200^{low}/NGFR^{+}$ populations in the unsorted fraction that may have different properties compared to the sorted $CD200^{low}/NGFR^{-}$ and $CD200^{high}/NGFR^{+}$ populations (Fig.20C).

We quantified the relative abundance of NPCs ($CD200^{low}$ or $CD200^{low}/NGFR^{-}$) and NBs ($CD200^{high}$ or $CD200^{high}/NGFR^{+}$) in each fraction using different selection strategies (Fig.20D). We observed that the average percentage of NPC-like cells gated was 60.4 ± 11.18% of total cells for single CD200 selection and 60.36± 6.61% of total cells for CD200/NFGR double selection. Similarly, after selection, the purity of the NPC-like sorted fractions increased significantly ($p<0.001$) to 97.17 ± 2.45% and 97.53 ± 3.12% of total cells for CD200 single and CD200/NFGR double selection respectively (recovery of 1.61-fold in the sorted fraction compared to the unsorted fraction for both cases). Regarding the NB-like population, we found that $CD200^{high}/NFGR^{+}$ cells (9.43 ± 2.17% of total cells) were less abundant than $CD200^{high}$ cells (19.86 ± 5.24% of total cells). The purity of the NB-like sorted cells in the sorted fraction significantly increased ($p<0.001$) following cell selection, averaging 94.11 ± 4.78% (4.7-fold recovery with respect to the unsorted fraction) and 93 ± 5.11% (9.9-fold recovery with respect to the unsorted fraction) for CD200 single and CD200/NFGR double selection respectively. Even if the recovery was found to be better using the CD200/NFGR double selection strategy, both selection strategies showed a comparable ability to efficiently purify NPC-like and NB-like cells. Next, we compared both selection strategies by assessing the viability of the cells going through the sorter (Fig.20E). CD200/NGFR double selection resulted in a slightly increased viability (84.85 ± 3.73% of DAPI-negative cells in sorted fractions) compared to CD200-based FACS (77.36 ± 7.73% of DAPI-negative cells in sorted fractions), although this difference was not found significant ($p=0.07$).

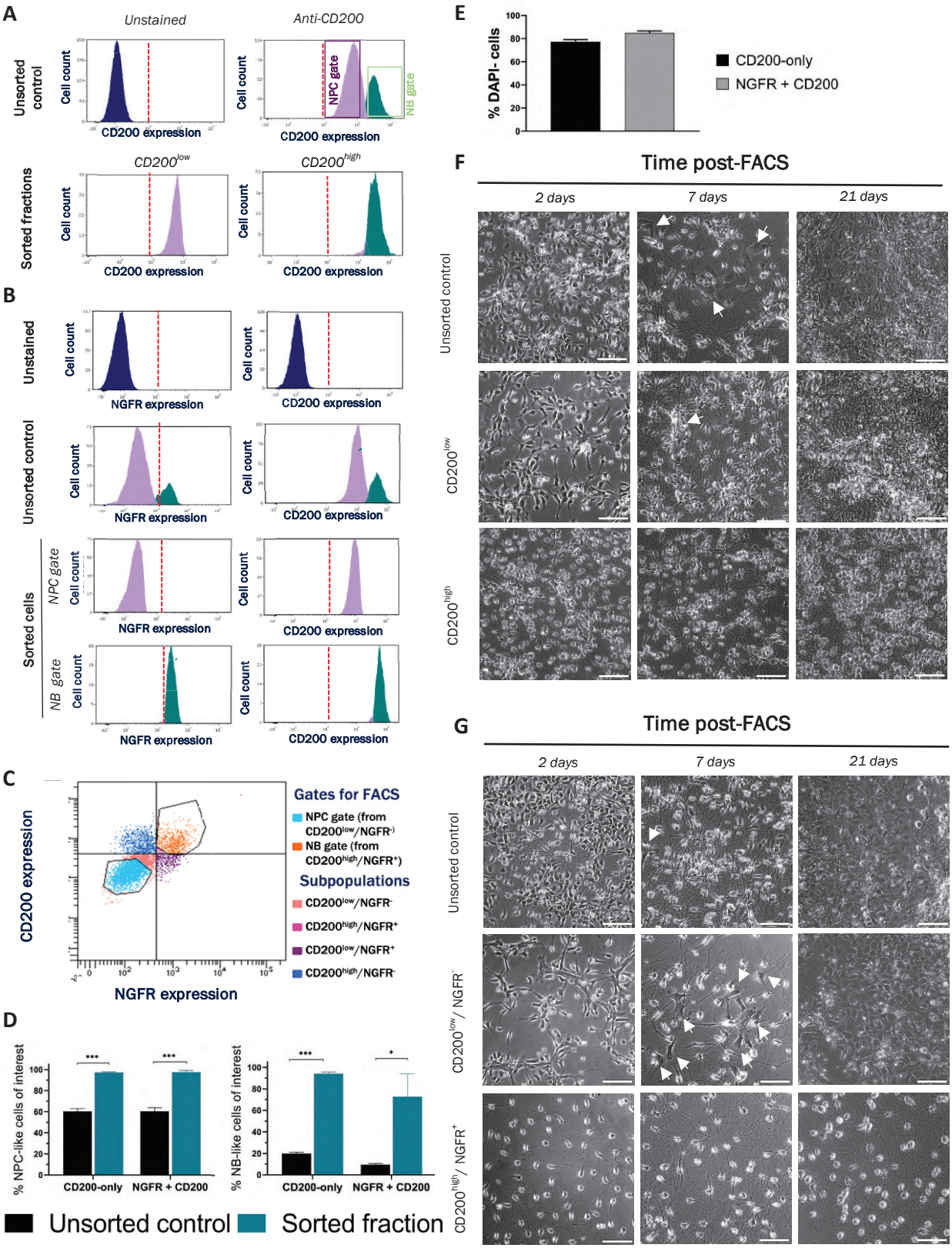
A
Unstained
Anti-CD200
Unsorted control
Cell count
CD200 expression
NPC gate
NB gate
Sorted fractions
CD200low
CD200high
B
Unstained
NGFR expression
Unsorted control
Sorted cells
NPC gate
NB gate
C
CD200 expression
NGFR expression
Gates for FACS
NPC gate (from CD200low/NGFR-)
NB gate (from CD200high/NGFR+)
Subpopulations
CD200low/NGFR-
CD200high/NGFR+
CD200low/NGFR+
CD200high/NGFR-
D
% NPC-like cells of interest
% NB-like cells of interest
CD200-only
NGFR + CD200
Unsorted control
Sorted fraction
E
% DAPI- cells
CD200-only
NGFR + CD200
F
Time post-FACS
2 days
7 days
21 days
Unsorted control
CD200low
CD200high
G
Time post-FACS
2 days
7 days
21 days
Unsorted control
CD200low/ NGFR-
CD200high/ NGFR+

Figure 19. CD200 can be used to sort highly-pure postmitotic NBs via Fluorescent-Activated Cell Sorting (FACS). **(A, B)** Histograms showing FC characterization (based on NGFR or CD200 expression) of sorted subpopulations obtained from 16 DIV cultures via FACS using CD200 (single CD200 selection; A) or NGFR in combination with CD200 (double CD200/NGFR selection; B) as selection marker(s). The set threshold for positivity for each of the tested markers is indicated by a red dashed line. Color code: blue (unstained population), purple (low/negative population), and green (high/positive population). Color boxes indicate the gating applied for sorting of $CD200^{low}$ (purple box) and $CD200^{high}$ (green box) subpopulations respectively. **(C)** Dot plot showing FC characterization of 16 DIV cultures before FACS using double CD200/NGFR selection. NGFR and CD200 expression are displayed on the x-axis and the y-axis respectively. Gates used for sorting NBs ($CD200^{high}$ /$NGFR^{+}$ cells) and NPCs ($CD200^{low}$ /$NGFR^{-}$ cells) are delimited by black boxes **(D)** Bar graphs showing the relative abundance (%) of NPC-like (left plot) and NB-like cells (right plot) in their corresponding cell subpopulations following CD200-only or double CD200/NGFR FACS. **(E)** Bar graphs showing the viability (% of DAPI- cells) of cells following single CD200 and double CD200/NGFR FACS. **(F, G)** Brightfield microscopy pictures showing the morphology of replated unsorted, NPC-like and NB-like subpopulations 2, 7, and 21 days after single CD200 selection (F) or double CD200/NGFR selection (G). Scale bars = 100µm.

The unsorted and sorted fractions were replated and further differentiated *in vitro*. After cell replating, the morphology of the different populations over time was tracked (Fig.20F-G). Two days after FACS at 16 DIV (18 DIV), we observed clear morphological differences between the NPC-like and NB-like populations for both selection methods (Fig19F-G). All cells of the NB-like populations (mostly composed of $CD200^{high}$/$NGFR^{+}$ or $CD200^{high}$ cells) displayed a more neuronal morphology and cell distribution that they maintained, with disaggregated cells exhibiting small somas and projections. On the other hand, the majority of NPC-like cells ($CD200^{low}$/ $NGFR^{-}$ or $CD200^{low}$) showed a polygonal and flat shape, lacked neurites and tended to be distributed in groups in contact with similar cells. The unsorted control contained a mix of both morphologies. Seven days after FACS (23 DIV), these morphological differences were diluted, with all fractions showing a more homogeneous neuronal morphology. Notably, even if most of the cells in the unsorted and NPC-like sorted subpopulation showed a neuronal morphology by then, a few polygonal cells remained visible in the cultures (Fig.20F-G, white arrows). We did not detect the presence of these polygonal cells in replated NB-like sorted subpopulations seven days post-FACS. We noticed that these polygonal cells began to proliferate and take over the cultures in the unsorted and NPC-like cultures, with proliferation being more obvious in the latter (Fig.20F-G). By 21 days post-FACS (37 DIV), we observed that the majority and a substantial part of the surface area of the NPC-like sorted and unsorted cultures respectively had been completely covered with a monolayer of these proliferative cells. This was not the case for the NB-like subpopulations, which successfully differentiated into cultures with neuronal morphology

that they maintained for the duration of the experiment without any signs of proliferation (Fig.20F-G).

2.4. CD200^{high} postmitotic NBs comprise two subpopulations of striatal progenitors

Next, we investigated whether the NB-like sorted populations had a striatal identity. We used the MARS-seq dataset to investigate the expression of different markers of SPN progenitors in hPSC-derived 17 DIV cultures derived from three different hESC lines (i.e., GEN-019, H9 and RUES2): *DLX1*, *DLX2*, *DLX5*, *DLX6*, *EBF1*, *FOXP2*, *SP8* and *SIX3*. We mapped the expression of these markers onto a UMAP plot of the NB subpopulation (Fig.21A). The expression of SPN progenitor markers showed a segregated distribution across NBs, with cells at the main body of the cluster expressing the DLX transcription factors, *SP8* and *SIX3* (type A NBs), while cells located at a tail in the upper part of the NB cluster expressed *EBF1* or *FOXP2* (type B NBs). The specificity of each of these markers for the corresponding NB subpopulation was confirmed by calculating the OR of expression in its corresponding NB cluster compared to the other NB cluster (Fig.21B). For Type A NBs, the highest ORs were for *DLX5* (OR=13.98), *SIX3* (OR=12.73) and *DLX2* (OR=12.68), while for Type B NBs the most specific markers were *FOXP2* (OR=7.78) and *EBF1* (OR=4.31).

To assess the relative abundance of each NB subpopulation in the unsorted and sorted cultures derived from GEN-019 following single CD200 selection at 16 DIV, we analyzed the expression of the Dlx family of transcription factors (type A NBs), and Ebf1 (type B NBs) in these populations at a protein level. We noticed that PanEBF and panDLX expression levels were increased in the CD200^{high} subpopulation compared to unsorted and CD200^{low} cells (Fig.21C). We also performed ICC quantification of cells expressing PanEBF and panDLX (Fig.21D). In the unsorted control, cells expressing PanEBF and panDLX were only 4.6 ± 0.2% and 4.7 ± 2.7% of total cells respectively. Following cell selection, the proportion of cells expressing panDLX in the sorted CD200^{low} cells was maintained (4.3 ± 1.4% of total cells) but panEBF-expressing cells were depleted from the cultures (0.04 ± 0.01% of total cells). On the other hand, we observed the enrichment of both panEBF-expressing cells and panDLX-expressing cells in the sorted NB population compared to the controls and the sorted NPC population.

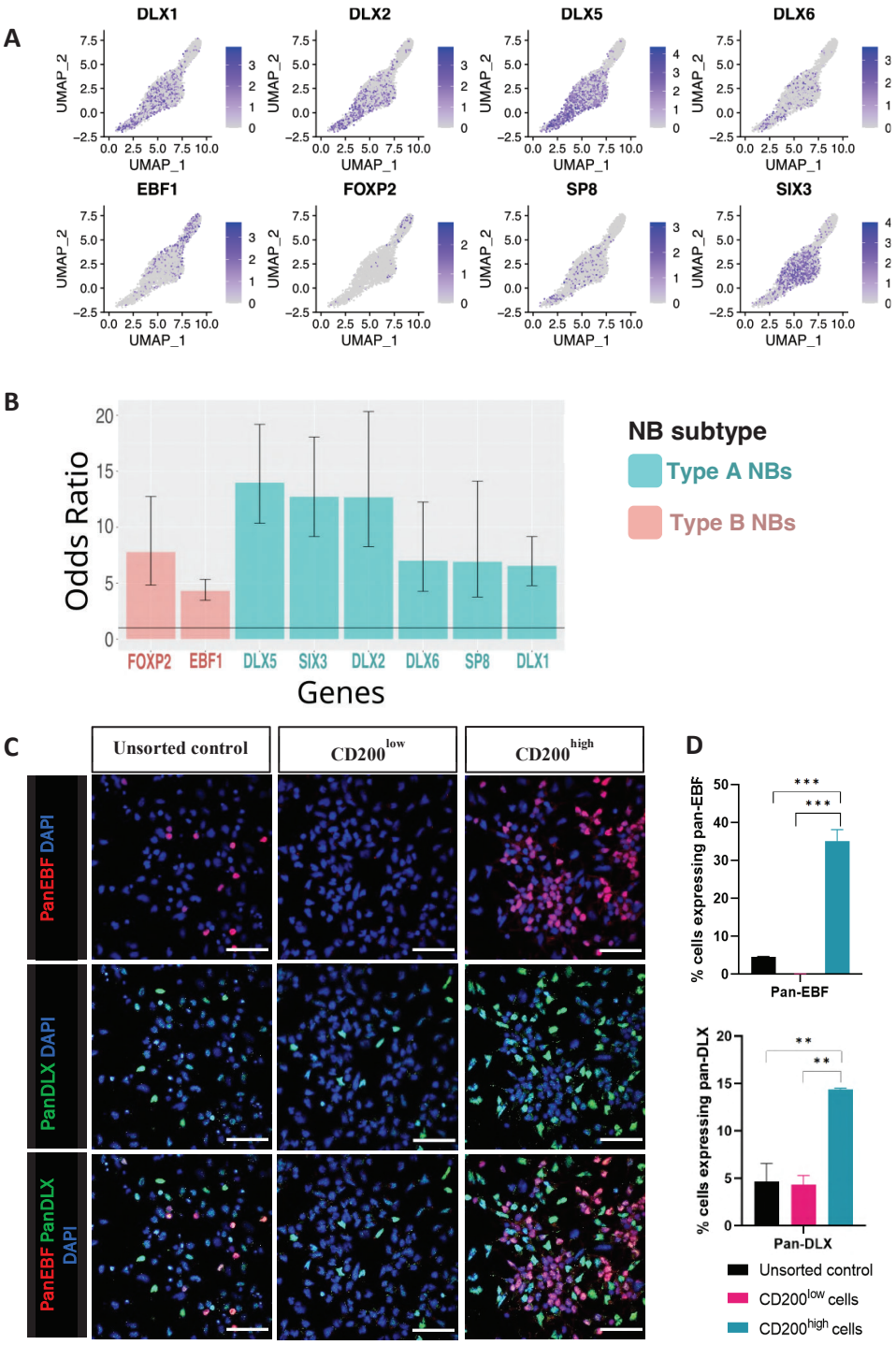

Figure 20. Selection of CD200^{high} cells via FACS results in an enrichment of postmitotic NBs expressing direct and indirect pathway markers. (A) UMAP plots of the postmitotic NB population at 17 DIV (MARS-Seq) showing RNA expression of relevant SPN progenitor markers. Color code: grey = low expression; purple = high expression. **(B)** Barplot showing the odds of each SPN progenitor marker to be expressed in its corresponding NB subcluster vs the odds of being expressed in the other NB subcluster (odds ratio; OR). The black line at OR=1 represents the set threshold for a marker to be considered specific (OR>1). **(C)**Confocal microscopy pictures ICC to detect pan-EBF and pan-DLX in unsorted and sorted (CD200^{low} and CD200^{high}) cells 1 hour after replating following FACS. Scale bars = 50µm. **(D)** Bar graphs representing unbiased automated counting of cells expressing pan-EBF (upper plot) and pan-DLX (lower plot) in unsorted and sorted cells after CD200-based FACS.

More specifically, we found that the largest (7.6-fold) and most significant ($p<0.001$) enrichment in the sorted NB fraction compared to the unsorted control was for panEBF-expressing cells, which constituted 35.2 ± 4.2% of the sorted NB population. To a lesser extent, the proportion of panDLX-expressing cells increased to 14.4 ± 0.2% of this fraction, which constituted a 3-fold enrichment ($p=0.02$) compared to the unsorted control. No co-expression of panEBF and panDLX was observed.

2.5. CD200^{high} striatal NBs can be efficiently and consistently enriched via Magnetic-Activated Cell Sorting (MACS)

Then, we set up and optimized a cell sorting pipeline for the enrichment of postmitotic striatal NBs derived from GEN-019 at 16 DIV using MACS for positive selection of CD200^{high} cells (Fig.22A-C). We compared two different MACS-based selection strategies: a single CD200^{high} positive selection (single CD200 selection) and two consecutive CD200^{high} positive selections (double CD200 selection). Both methods resulted in the obtention of a positive fraction highly enriched in CD200^{high} cells (Fig.22A). We observed that double CD200 selection resulted in isolation of an almost pure population of CD200^{high} cells comparable to selection by FACS, while the positive fraction obtained by single CD200 selection contained some remaining CD200^{low} cells (Fig.22A). However, despite the increased CD200^{high} cell enrichment, we noticed that double selection contributed to reduced cell yield since each round of selection increased cell loss.

We compared the relative abundance of CD200^{high} cells in the unsorted and sorted fractions resulting from single CD200 selection. We consistently observed a high-yield enrichment of striatal CD200^{high} NBs, with 84.85 ± 3.4%, of CD200^{high} cells in the positive fraction, which represented 3.22-fold and 8.77-fold enrichments ($p<0.001$) compared to the unsorted (26.32 ± 6.81%) and the negative (9.67 ± 4.9%) fractions (Fig.22B). By comparing the relative abundance of these cells of interest in the unsorted and negative fractions, we found a significant 2.72-fold reduction ($p=0.04$). To assess the potential impact of MACS on the viability of sorted cells, we also evaluated the percentage of alive cells in each fraction following single CD200 selection. We found that unsorted and sorted cell fractions following single CD200 selection showed high viability (92.98 ± 2.04%, 94.37 ± 1.19%, and 93.18 ± 1.79% of DAPI^{-} cells out of total

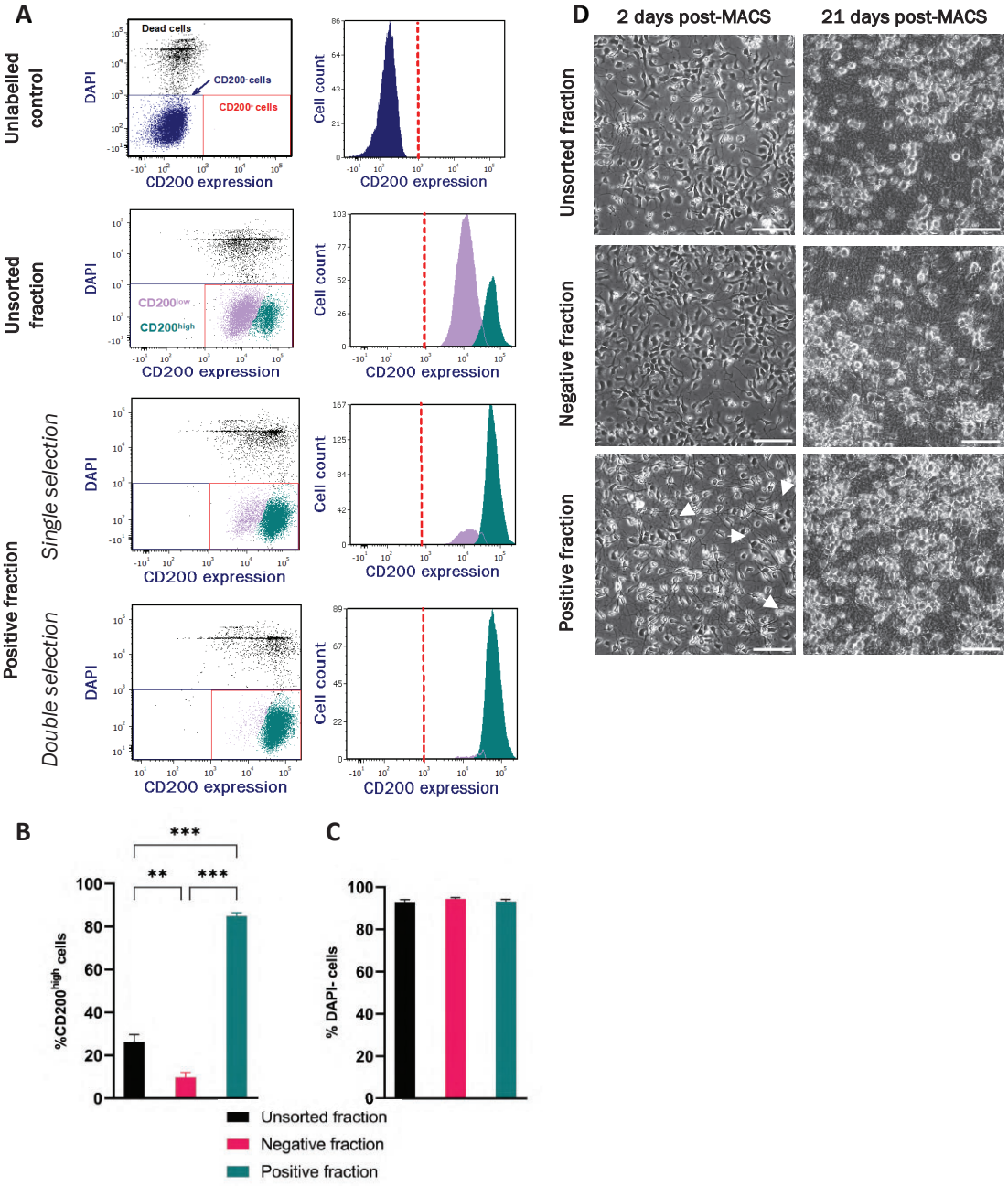

Figure 21. High-yield enrichment of striatal NBs using CD200-based Magnetic-Associated Cell Sorting (MACS). (A) Dot plots showing the expression of CD200 (x-axis) vs the intensity of DAPI staining (y-axis) (left) and histograms showing the expression of CD200 (x-axis) vs. the cell count (y-axis) (right) of cells sorted via CD200-based MACS for the unsorted (left plots) and positive fractions after a single MACS (middle plots) or two sequential MACS selection (right plots). Individual dots represent individual cells. **(B, C)** Bar graphs showing the relative amount of CD200^{high} cells (B) and viable (DAPI-negative) cells (C) in the unsorted, negative, and positive fractions after CD200-based MACS of hPSC-derived 16 DIV populations. Error bars represent SEM. **(D)** Brightfield images of the unsorted, negative, and positive fractions obtained via CD200-based MACS at 16 DIV (right), after replating and in vitro striatal differentiation for 2 days and 21 days.

cells for the unsorted, negative, and positive fractions respectively), with no significant differences found among fractions (Fig.22C).

Also, we replated the unsorted and sorted subpopulations following single CD200 selection and further differentiated them for 3 weeks *in vitro*. Following replating, the morphology of the different populations over time was tracked (Fig.22D). Two days after sorting at 16 DIV (18 DIV), most cells in the positive fraction showed a more neuronal morphology and distribution that they maintained over time (NB-like cells), while the majority of the negative fraction displayed a more polygonal and flat shape, lacked neurites and tended to be distributed in groups in contact with similar cells (NPC-like cells). The unsorted population contained a mix of both morphologies. These observations were consistent with what was reported previously for FACS-based experiments, although this time a noticeable number of colonies of NPC-like cells were observed in the positive fraction. Cell confluence for all fractions was similar to what is normally observed in these cultures at this stage of differentiation. Seven days after MACS (23 DIV), morphological differences were diluted, and the presence of NPC-like cells was not detected in any of the fractions. 21 days after sorting (37 DIV), all fractions showed a homogeneous neuronal morphology, with no evidence of proliferation (Fig.22D).

2.6. Striatal CD200^{high} NBs can be differentiated in vitro obtaining a high yield of neurons with an SPN phenotype

Next, we analyzed the identity of the neuronal populations resulting from each fraction at 37 DIV following MACS-based single CD200 selection at 16 DIV. Terminal *in vitro* striatal neuronal differentiation was confirmed by the expression of the neuronal marker MAP2B by almost 100% of hPSC-derived neurons (regardless of fraction; Fig.23 and Fig.24).

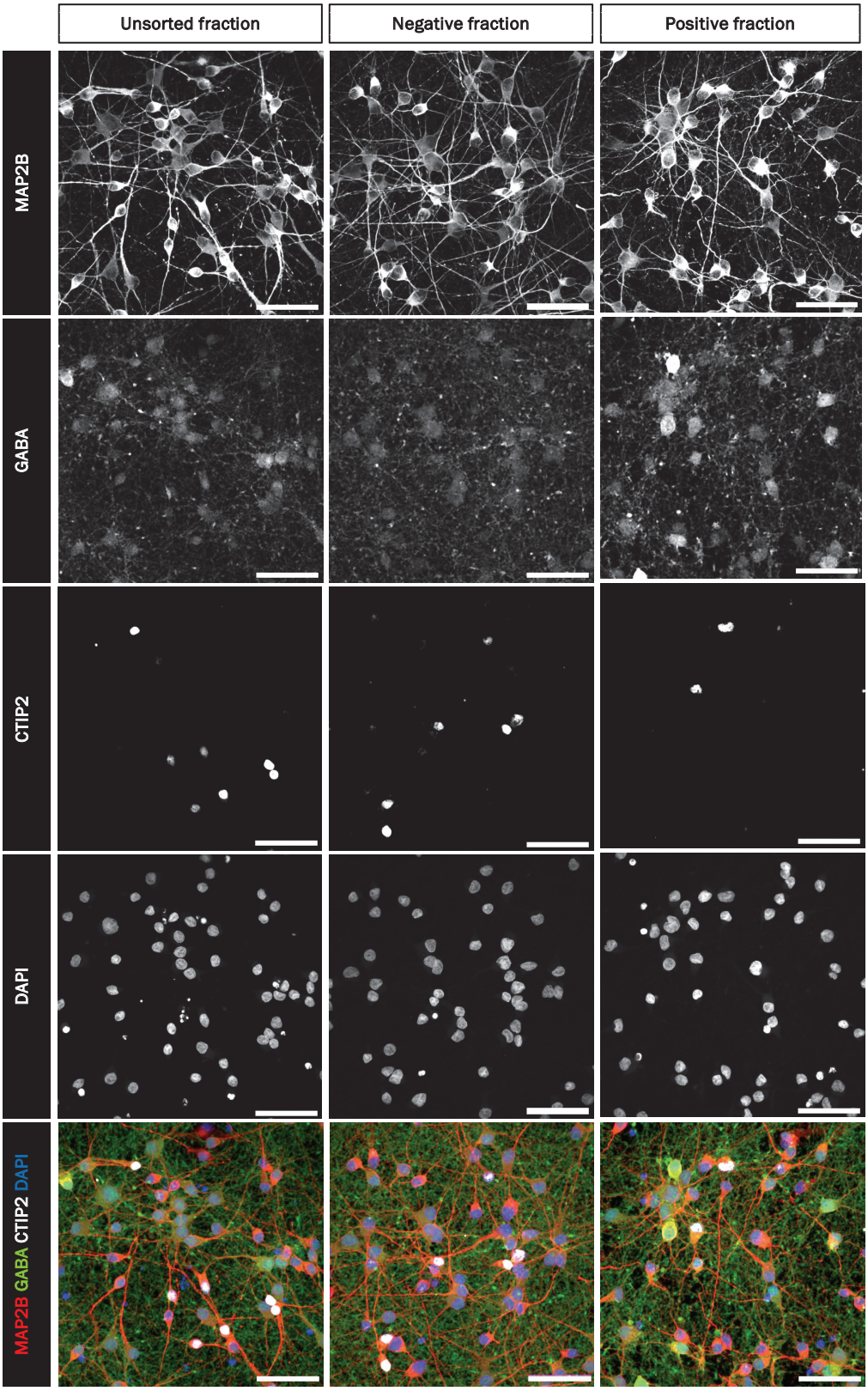

Figure 22. Sorted CD200^{high} cells can differentiate in vitro into neurons expressing SPN markers GABA and CTIP2. ICC images of control unsorted and sorted fractions replated following CD200-based MACS at 16 DIV and further differentiated for three weeks *in vitro*, taken using a confocal microscope. MAP2B (red, neuronal marker), GABA (green, marker of GABAergic neurons), CTIP2 (grey, SPN marker), and DAPI counterstaining (blue). Scale bars = 50µm

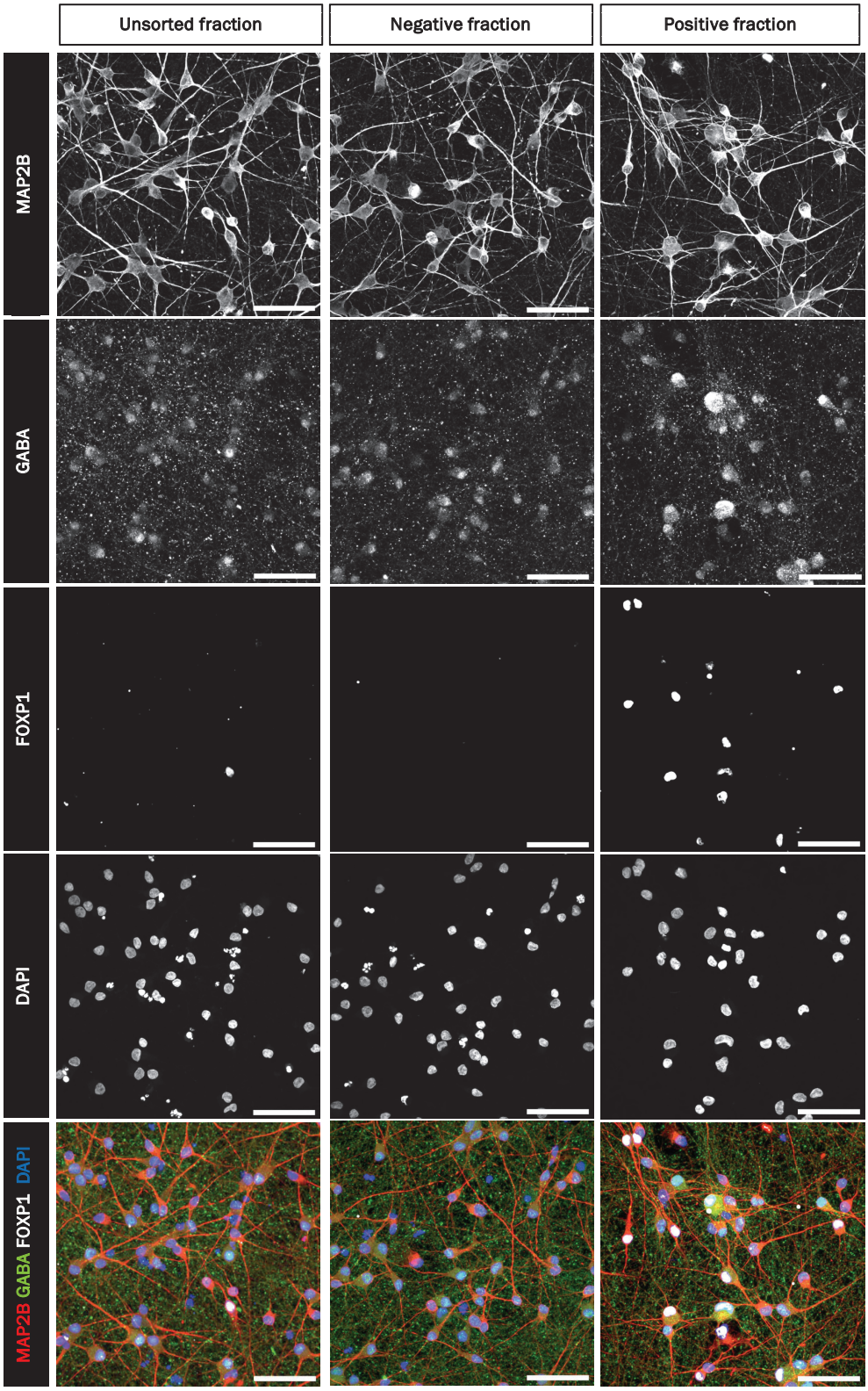

Figure 23. Sorted CD200^{high} cells can differentiate in vitro into neurons expressing SPN marker GABA and enriched in the early SPN marker FOXP1. ICC images of control unsorted and sorted fractions replated following CD200-based MACS at 16 DIV and further differentiated for three weeks in vitro, taken using a confocal microscope. MAP2B (red, neuronal marker), GABA (green, marker of GABAergic neurons), FOXP1 (grey, early SPN marker), and DAPI counterstaining (blue). Scale bars = 50µm

We identified striatal GABAergic SPNs by immunolabelling these neuronal cultures for GABA (GABAergic neuronal marker) and CTIP2 (SPN marker; Fig.23). In the unsorted fraction, even though we observed GABA expression, most of these $GABA^{+}$ cells displayed low expression levels ($GABA^{low}$), with only a minority of the total neuronal population showing intense GABA expression ($GABA^{high}$). We observed a decrease in the relative abundance of $GABA^{low}$ neurons and no $GABA^{high}$ neurons in the negative fraction with respect to the unsorted control. In turn, we observed an increased abundance of both $GABA^{low}$ and $GABA^{high}$ neurons in the positive fraction compared to the other fractions (Fig.23). Regarding CTIP2 expression, we detected a reduction of $CTIP2^{+}$ cells in the positive fraction compared to the unsorted and negative fractions (Fig.22). Interestingly, while most of the $CTIP2^{+}$ neurons in the unsorted and negative fractions did either not express GABA or were $GABA^{low}$ neurons, we found that the reduced $CTIP2^{+}$ expression in the positive fraction colocalized with both $GABA^{low}$ and $GABA^{high}$ neurons. We also analyzed the expression of the early SPN marker FOXP1 (Fig.24) and found that small subpopulations of $FOXP1^{+}$ cells were observed in the unsorted and negative fractions. However, we noticed a clear enrichment of $FOXP1^{+}$ neurons in the positive fraction, with all $FOXP1^{+}$ neurons colocalizing with either $GABA^{high}$ or $GABA^{low}$ expression (Fig.24)

We also investigated the presence of neurons with a dSPN or iSPN subtype identity by checking the co-expression (at an RNA level) of CTIP2 and DRD1 (dSPN marker; Fig.25) and CTIP2 and DRD2 (iSPN marker; Fig.26). We confirmed the presence of cells expressing these markers in the neuronal populations, with no observed differences across fractions. Interestingly, expression of BCL11B (gene encoding for CTIP2) was detected in only a subset of neurons (consistent with observations at the protein level). On the other hand, most cells across fractions showed expression of DRD1, DRD2, or both simultaneously; interestingly, the number of observed DRD2 transcripts was found to be highly increased compared to DRD1 transcripts for all neuronal populations.

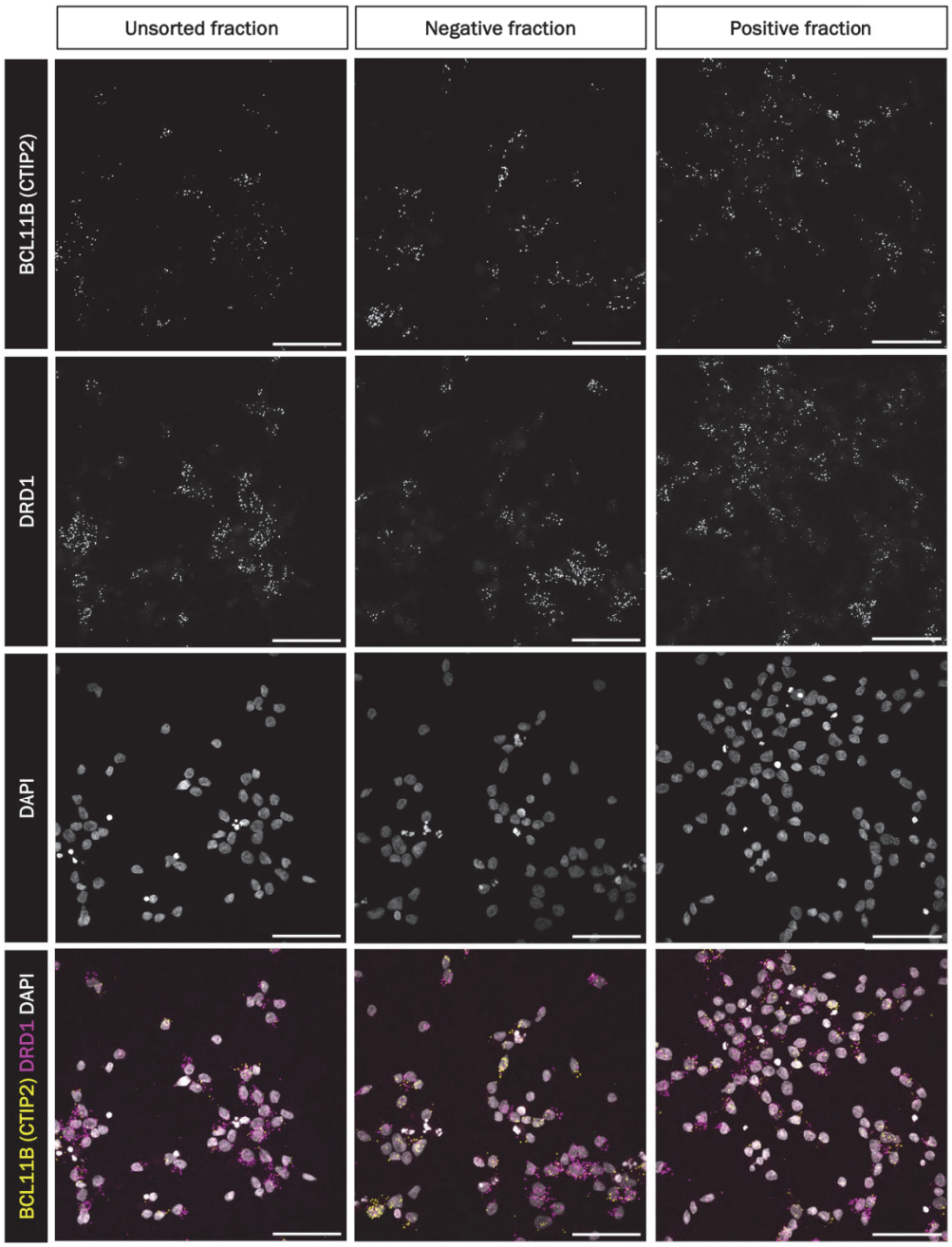

Figure 24. Sorted CD200^{high} cells can differentiate *in vitro* into neurons expressing RNA transcripts of direct pathway SPN markers BCL11B (CTIP2) and DRD1. Fluorescent RNA in situ hybridization (ISH) images of control unsorted and sorted fractions replated following CD200-based MACS at 16 DIV and further differentiated for three weeks *in vitro*, taken using a confocal microscope. Three different markers are shown as separate channels and merged: BCL11B (CTIP2; SPN marker, yellow in the merged imager), DRD1 (direct pathway SPN marker, purple in the merged image) and DAPI counterstaining (grey in the merged image). Scale bars = 50µm

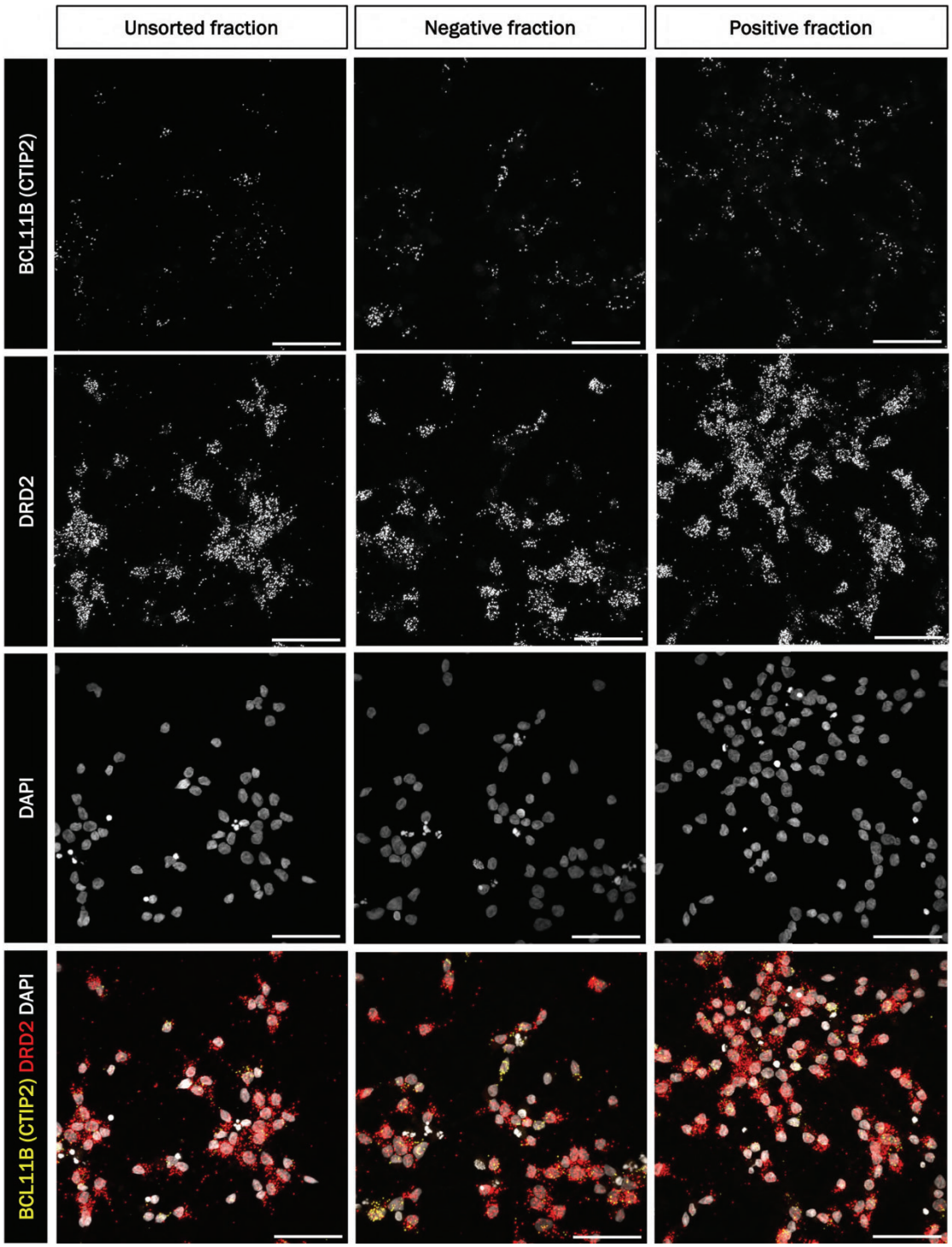

Figure 25. Sorted CD200^{high} cells can differentiate *in vitro* into neurons expressing RNA transcripts of indirect pathway SPN markers BCL11B (CTIP2) and DRD2. Fluorescent RNA in situ hybridization (ISH) images of control unsorted and sorted fractions replated following CD200-based MACS at 16 DIV and further differentiated for three weeks *in vitro*, taken using a confocal microscope. Three different markers are shown as separate channels and merged: BCL11B (CTIP2; SPN marker, yellow in the merged imager), DRD2 (direct pathway SPN marker, red in the merged image) and DAPI counterstaining (grey in the merged image). Scale bars = 50µm

2.7. hPSC-derived striatal NBs survive and integrate into the adult mouse striatum after transplant without evidence of tumor overgrowth.

Next, we assessed whether the sorted hPSC-derived $CD200^{high}$ striatal NBs could be used as a transplantable cell product. We first evaluated the survival and integration of these cells upon intra-striatal transplantation, by transplanting unsorted and sorted fractions (obtained following single CD200 MACS) into the striatum of immunosuppressed adult wild-type mice. The expression of relevant markers in the grafts was investigated seven days post-transplant (PST). We analyzed the expression of cleaved caspase 3 (CC3; apoptotic marker) and STEM121 (human marker; Fig.27A). We observed the presence of groups of $STEM121^{+}$ cells 7d PST in all cases, confirming the survival of grafts following transplantation into the striatum. Interestingly, we observed that transplantation of cells from the positive fraction gave rise to less compact and smaller grafts than those resulting from transplantation of the unsorted or negative fraction. We found no evidence of apoptosis in the analyzed grafts (no significant CC3 expression was detected). No differences were found regarding cell death among the different fractions being analyzed.

Then, we visualized the expression of Ki-67 (proliferation marker) and HNA (human marker; Fig.27B). We confirmed the presence of the grafts using HNA positivity and did not observe evidence of teratoma formation in any of them 7d PST. However, we noticed that Ki-67 expression was present in grafts of the unsorted and negative fractions while being absent from grafts of the positive fraction. Once again, these latter grafts showed a smaller size than those from the other two fractions.

Finally, we investigated the identity of the grafts by analyzing the expression of striatal NB markers panEBF (direct pathway striatal progenitors) and panDLX (indirect pathway striatal progenitors; Fig.27C). We observed widespread expression of panEBF and panDLX in grafts of all fractions at 7d PST, hence confirming the maintenance of the striatal identity of these grafts *in vivo*. No co-expression of panEBF and panDLX was observed for any graft, consistent with what was observed *in vitro*.

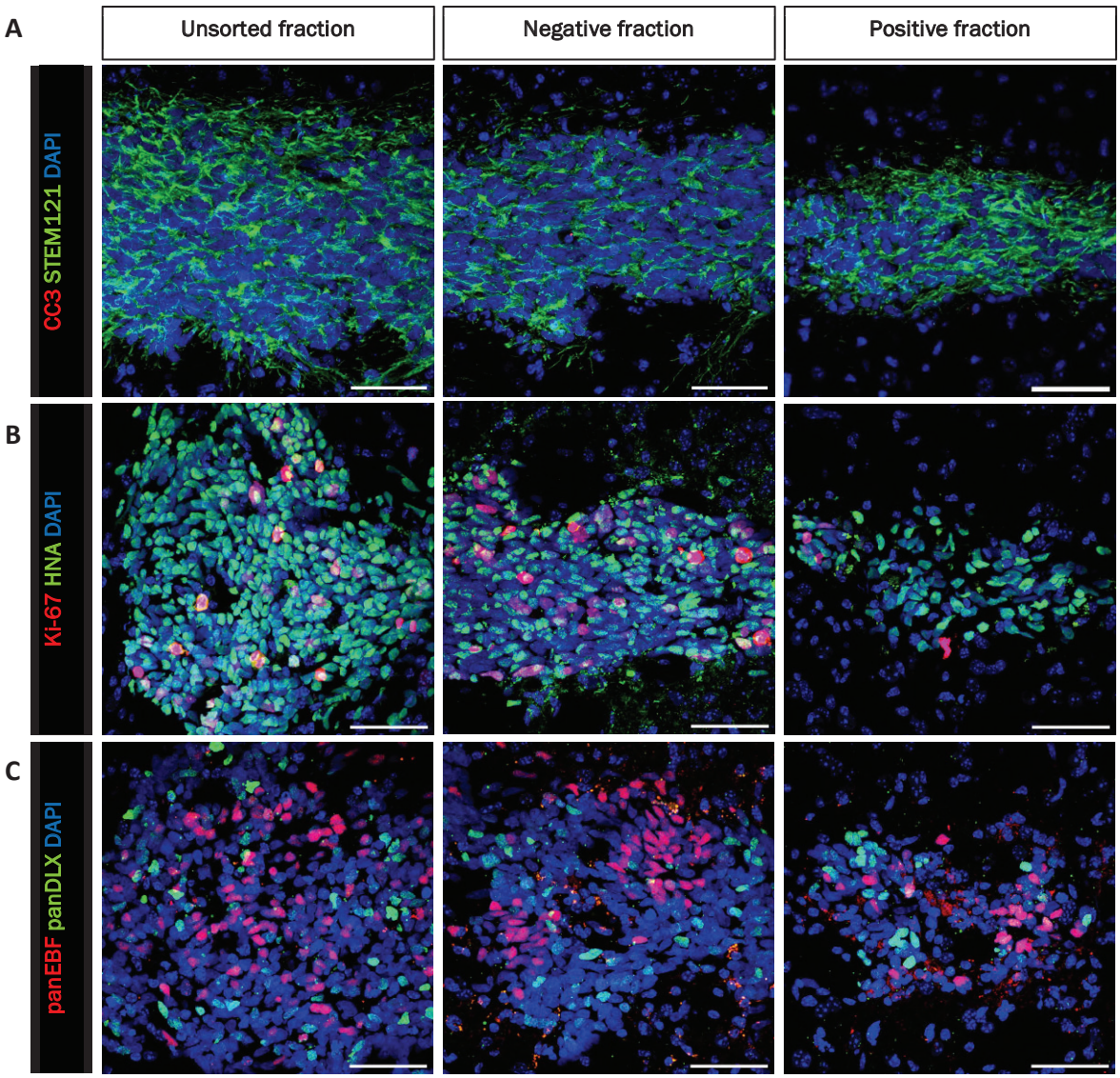

Figure 26. Sorted CD200^{high} postmitotic NBs can survive intra-striatal transplantation and integrate into the host brain without evidence of graft overgrowth. IHC images of control unsorted and sorted fractions transplanted at 16 DIV and analyzed 7 days post-transplant (7d PST), taken using a confocal microscope. The different panels show three sets of stainings: **(A)** STEM121 (green, marker of human cells), cleaved caspase 3 (CC3; red, cell death marker), and DAPI counterstaining (blue); **(B)** Human Nuclear Antigen (HNA; green, marker of human cells), Ki-67 (red, proliferation marker), and DAPI counterstaining (blue); **(C)** panEBF (red, direct pathway marker), panDLX (green, indirect pathway marker) and DAPI counterstaining (blue). Scale bars = 50µm.

3. Chapter III: Isolation of different subpopulations of hPSC-derived striatal progenitors using CD200 at different timepoints of *in vitro* differentiation

During striatal development dSPNs and iSPNs form two molecularly defined populations with distinct genetic fingerprints from early embryonic stages, which only progressively intersperse (Tinterri et al., 2018). Even if the precise timing of dSPN and iSPN specification remains largely to be characterized, birthdating experiments in mice have indicated that the majority of earliest-born SPN are dSPNs, while iSPNs are born later (Fishell & van der Kooy, 1991; Kelly et al., 2018; Tinterri et al., 2018). In the previous chapter, we have reported that following *in vitro* differentiation of hPSCs using our striatal differentiation protocol (Comella-Bolla et al., 2020), both dNBs and iNBs are identified at 16 DIV; however, the timing at which these two subpopulations are generated *in vitro* was not investigated.

One potential strategy for the selection of specific NB subpopulations that give rise to different neuronal subtypes such as dSPNs and iSPNs would entail the use of multiple antibodies targeting subtype-specific markers at the same time point. However, in the previous chapter we also demonstrated that CD200 is a marker of both dNBs and iNBs, which can be used to enrich these progenitor subpopulations in heterogenous cell mixtures, although this enrichment is not subtype-specific. Thus, in this chapter, we investigate whether cell sorting of different striatal progenitor subpopulations could be achieved by using a single marker (i.e., CD200) at several time points (i.e., 12 DIV, 16 DIV).

To that aim, we have investigated how hPSC-derived striatal dNB and iNB subpopulations are specified *in vitro* when using our striatal differentiation protocol (Comella-Bolla et al., 2020). Also, we have built ion our previous results and used CD200 to sort and characterize striatal NB subpopulations derived from control hPSCs at different timepoints of our striatal differentiation protocol. This approach has enabled us to demonstrate that CD200-based selection at different timepoints of *in vitro* differentiation leads to the obtention of cell compositions enriched in different subtypes of hPSC-derived postmitotic striatal progenitors (Fig.28).

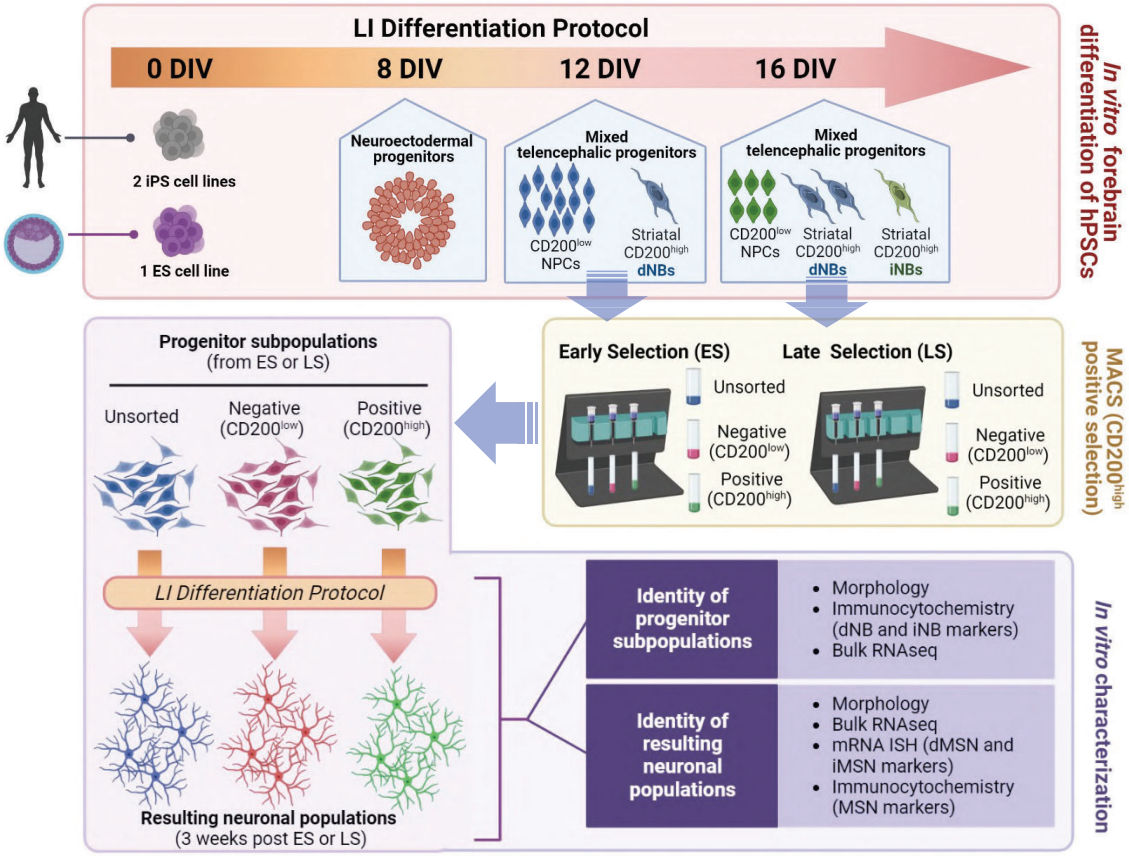

Figure 27. Graphical abstract of Chapter III. Striatal in vitro differentiation of hPSCs leads to generation different subpopulations of SPN progenitors mimicking endogenous neurodevelopment, with earlier specification of striatal dNBs, followed by production of striatal iNBs. Cell selection using CD200 as a single marker can be used to obtain cell compositions enriched in different subtypes of hPSC-derived postmitotic striatal progenitors

3. 1. hPSC striatal differentiation leads to earlier generation of dNBs compared to iNBs

To investigate how hPSC-derived striatal dNB and iNB subpopulations generated are specified *in vitro*, we performed bulk RNAseq analysis of the hPSC-derived populations at different time points of the protocol (8 DIV, 12 DIV, 16 DIV 23 DIV and 37 DIV), and studied the mean normalized expression over time of key striatal progenitors marker genes at different stages of development (Fig.29): NEP (*SOX2* and *NES*), NPCs (*VIM* and *CD99*), NBs (*STMN2*, *TUBB3* and *CD200*), dNBs (*EBF1*, *FOXP2*, and *ISL1*) and iNBs (*SP9*, *DLX2* and *DLX5*).

We observed that the NEP marker *SOX2* was progressively downregulated from 8 DIV to 23 DIV (Fig.29A). *NES* (another NEP marker) displayed a similar expression pattern, although with a slightly delayed downregulation (which started at 12 DIV). Regarding the NPC markers, we found that *VIM* and *CD99* followed similar patterns,

being upregulated from 8 DIV and showing expression peaks at 12/16 DIV, at which cell cultures are typically a mix of telencephalic progenitors mainly composed by NPCs (Comella-Bolla et al., 2020). From that point onwards, expression of these genes was downregulated as neurogenesis progressed (Fig.29A). Generic NB markers (*STMN2*, *TUBB3* and *CD200*), on the other hand, showed increasing expression from 12 DIV reaching an expression peak at 23 DIV (Fig.29B). These data suggest that NPCs start exiting the cell cycle to become postmitotic NBs around 12 DIV. It is not clear whether these newborn NBs correspond to dNBs, iNBs or both, since *STMN2*, *TUBB3* or *CD200* do not allow discrimination between NB subtypes. Furthermore, as differentiation progresses, the relative abundance of NBs increases (and so does the NB marker expression) whereas the NPC pool is gradually exhausted (as it can be inferred from the downregulation of NPC markers).

Next, we focused on markers specific to each of the two NB subtypes (Fig.29C and 29D). We observed that early dNB markers *EBF1* and *FOXP2* started being expressed around 12 DIV, reached an expression peak at 16 DIV and were then downregulated until 23 DIV. Furthermore, a late dNB marker (*ISL1*) started being strongly expressed around 23 DIV (and onwards to 37 DIV) once *EBF1* and *FOXP2* expression had dropped. This suggests that dNBs are born *in vitro* at 12 DIV and start showing signs of maturation at 23 DIV (postmitotic neurons). On the other hand, iNB markers *DLX2* and *DLX5* reached an expression peak at 23 DIV and started to be downregulated afterwards. In the case of *SP9*, its expression time window was found to be narrower: expression was only detected at 16 DIV (when the expression peak was reached). Altogether, these data indicate that dNBs are born *in vitro* at an earlier timepoint than iNBs.

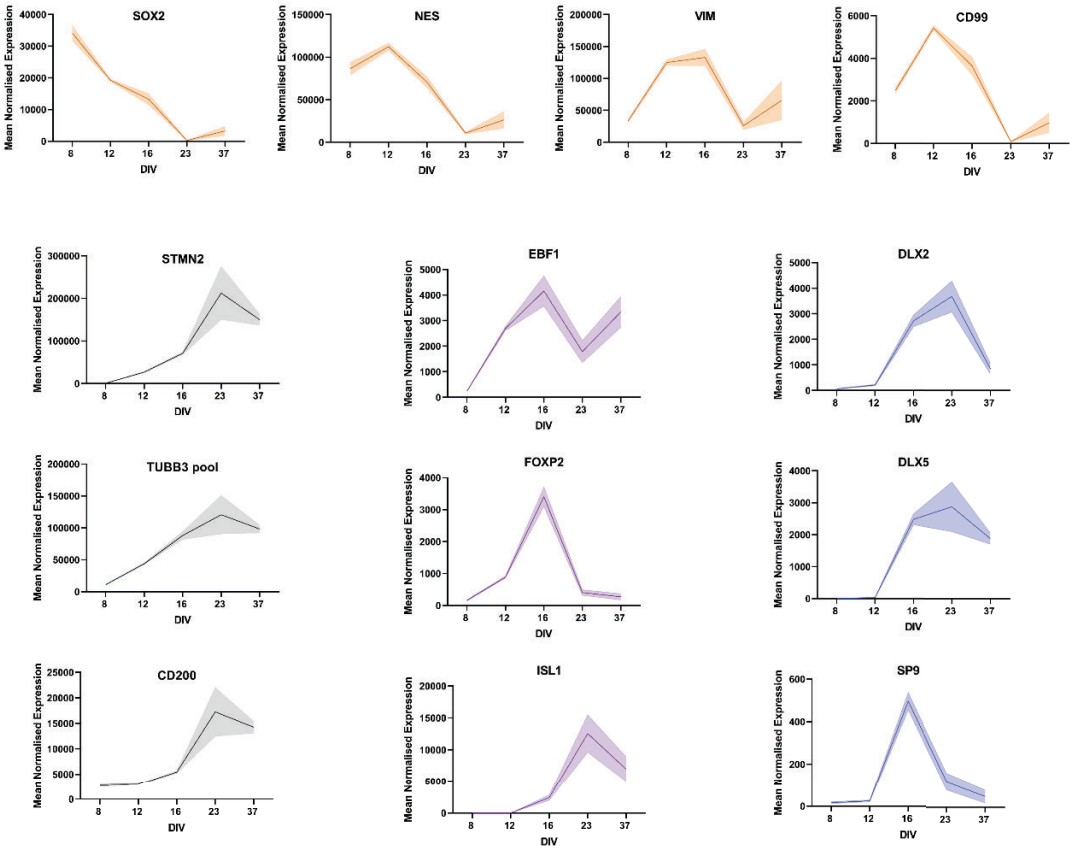

Figure 28. Striatal dNBs are generated earlier than iNBs *in vitro*. Line plots showing the mean normalized expression (bulk RNAseq) of key striatal progenitor marker genes in hPSC-derived cell populations at different time points of the LI forebrain differentiation protocol: Neuroectodermal Progenitor (NEP) and Neural Progenitor Cell (NPC) markers **(A)**; neuroblast (NB) markers **(B)**; direct pathway neuroblast (dNB) markers **(C)**; and indirect pathway neuroblast (iNB) markers **(D)**. Three replicates per cell line and timepoint were used. The shadowed areas represent standard error of the mean (SEM). DIV: Days In Vitro.

3.2. hPSC-derived striatal NBs can be efficiently selected using CD200 at different timepoints of in vitro differentiation

Next, we compared two different cell sorting timepoints (12 DIV and 16 DIV) and quantified the relative abundance of $CD200^{high}$ NBs in three different fractions: (i) unsorted fraction (control); (ii) negative fraction after $CD200^{high}$ positive selection; and (iii) positive fraction after $CD200^{high}$ positive selection (Fig.30A-B). The totality of cells in all fractions obtained at both timepoints showed CD200 protein expression (compared to the isotype control). Most cells in the unsorted fraction at 12 DIV were detected as $CD200^{low}$ NPCs, while only a minority of cells ($4.84 \pm 2.08\%$) were detected as $CD200^{high}$ cells. These $CD200^{high}$ NBs were displayed in FC histograms as a small tail of higher CD200 expression than the $CD200^{low}$ NPC peak. The low relative abundance of $CD200^{high}$ cells in the unsorted fraction at 12 DIV further confirmed that while $CD200^{high}$

dNBs had already started to be generated at this timepoint, the progenitor population was mostly composed of NPCs. As expected, the amount of $CD200^{high}$ cells in the unsorted fraction increased at the later timepoint 16 DIV, at which two overlapping peaks were detected: a large $CD200^{low}$ NPC peak and a smaller $CD200^{high}$ NB peak. At this timepoint, the $CD200^{high}$ NB population represented 35.44 ± 10.57% of all cells. which is consistent with the fact that at this timepoint a larger population of $CD200^{high}$ NBs (comprising both dNBs and iNBs) is known to be present in the culture.

Following cell sorting at 12 DIV, we found an average relative abundance of $CD200^{high}$ cells in the positive fraction of n55.78 ± 15.3%, which represented 11.5-fold ($p<0.001$) and 18-fold enrichments ($p<0.001$) compared to the unsorted and the negative (3.08 ± 1.69%) fractions. The slight decrease in the amount of $CD200^{high}$ NBs in the negative fraction compared to the unsorted fraction was also found to be significant ($p=0.03$). At 16 DIV, we consistently observed a high-yield enrichment of striatal $CD200^{high}$ NBs with an average relative abundance of $CD200^{high}$ cells in the positive fraction of 88.62 ± 3.71%, which represented 2.5-fold ($p<0.001$) and 5-fold enrichments ($p<0.001$) compared to the unsorted and the negative (17.79 ± 9.17%) fractions. By comparing the relative abundance of these cells of interest in the unsorted and negative fractions, we found that the observed reduction was also significant ($p<0.001$). At 12 DIV, even though $CD200^{high}$ enrichment in the positive fraction was found to be greater (11-fold change versus 2.5-fold increase at 16 DIV), sorting at 16 DIV yielded a purer positive fraction ($CD200^{high}$ cells represented 88.62 ± 3.71% of this fraction, versus 55.78 ± 15.3% at 12DIV). Furthermore, we found that following sorting, the batch-to-batch variability of the positive fraction at 12 DIV was increased.

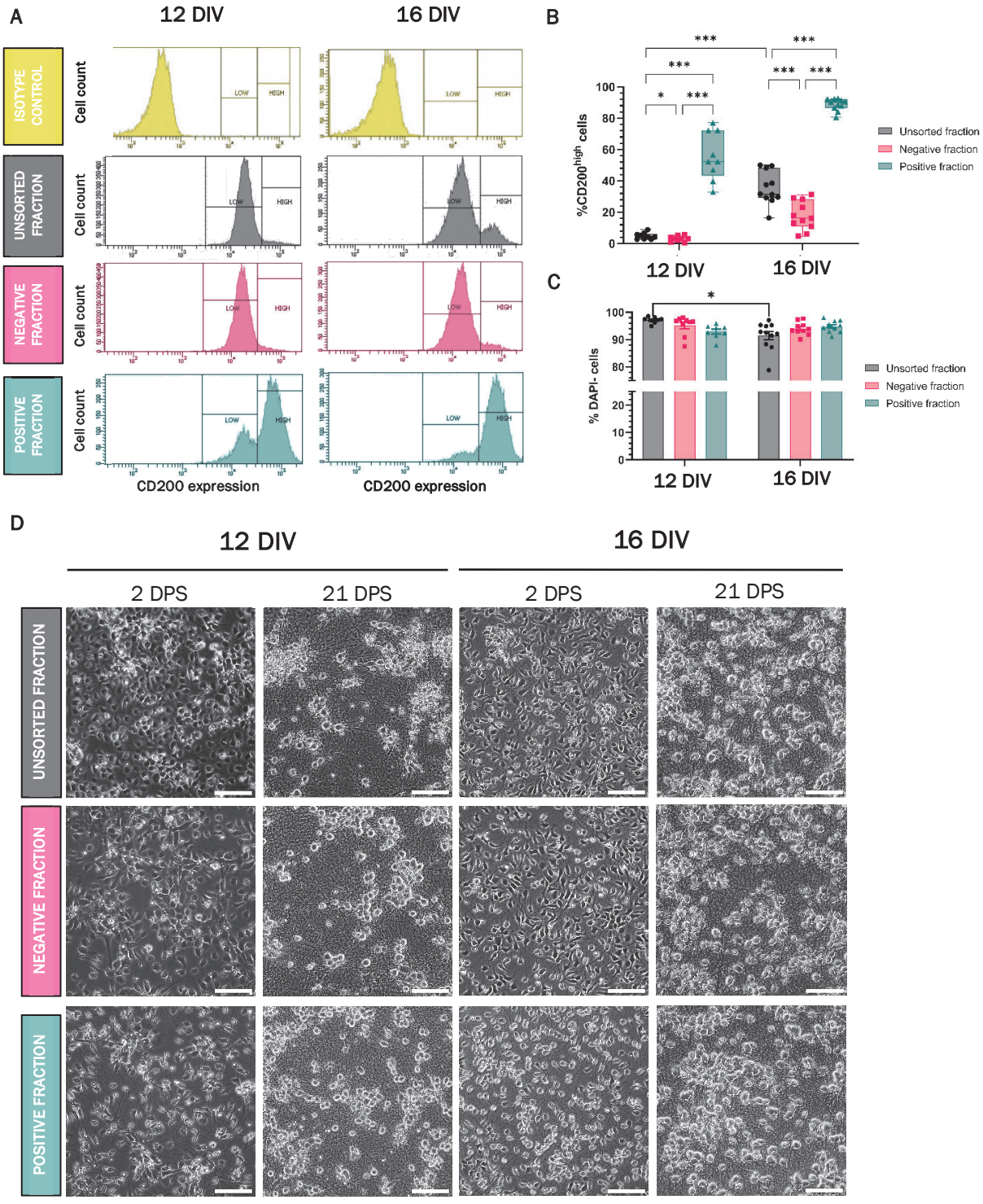

Figure 29. Striatal NBs can be efficiently selected using CD200 at different timepoints in a cell line-independent fashion. (A) Histograms showing the expression of CD200 (x-axis) vs. the cell count (y-axis) of cells sorted via CD200-based MACS at 12 DIV (left plots) or 16 DIV (right plots) for the resulting unsorted (grey), negative (pink) and positive (green) fractions, as well as for the isotype control (yellow). **(B)** Box and whiskers plots showing the relative amount of CD200high cells in each fraction after sorting at 12 or 16 DIV. **(C)** Bar graphs showing the relative amount of viable ($DAPI^-$ cells) in each fraction after sorting at 12 or 16 DIV. Error bars represent SEM. **(D)** Brightfield images of the unsorted, negative and positive fractions obtained via CD200-based MACS at 12 DIV (left plots) or 16 DIV (right plots), after replating and striatal differentiation for 2 days post sorting (DPS) and 21 DPS. Scale bar = 100µm.

To assess the potential impact of cell sorting in the viability of sorted cells at both timepoints, we also evaluated the relative number of alive cells in each fraction using DAPI as an indicator of cell viability via FC (Fig.30C). Our analysis found that unsorted and sorted cell fractions following CD200-based cell sorting at 12 DIV resulted in high viability (97.14 ± 1.74%, 95.14 ± 3.56% and 92.94 ± 2.51% for the unsorted, negative and positive fraction respectively), with no significant differences found among unsorted and negative fractions (p=0.73), unsorted and positive fractions (p=0.14), or negative and positive fractions (p=0.68). At 16 DIV, average cell viability was found to be 91.44 ± 5.15%, 94.04 ± 2.33% and 94.79 ± 2.17% for the unsorted, negative, and positive fraction respectively, and once again the differences among fractions were not significant (p=0.43 for unsorted fraction *vs.* negative fraction, p=0.2 for unsorted fraction *vs.* positive fraction and p>0.99 for negative fraction *vs*. positive fraction). Although not significant, the observed slight decrease in the average viability of the positive fraction compared to the unsorted and negative populations could be explained by the fact that selected $CD200^{high}$ cells correspond to more sensitive cells (postmitotic NBs).

To further characterize the sorted subpopulations using this strategy at different timepoints, we replated the unsorted (control) and sorted subpopulations (negative/$CD200^{low}$ and positive/$CD200^{high}$ cells) following sorting, and further differentiated them *in vitro* using our standard protocol. The morphology of the different subpopulations over time was tracked following replating (Fig.30D). 2 days post sorting (DPS) at 16 DIV, most of the cells sorted as positive fraction displayed a more neuronal morphology (NB-like cells) which included single-cell distribution, smaller somas and some projections, while the majority of the cells in the negative fraction showed a polygonal flat shape, lacked neurites and tended to be distributed in colony-like clusters composed by similar cells in contact with each other (NPC-like cells). The unsorted fraction contained a mix of both morphologies. Cell confluence for all fractions was found to be similar to what is normally observed in these cultures at this stage of differentiation. Regarding the fractions obtained following cell sorting at 12 DIV, we identified similar trends in terms of morphology of cells in each fraction, although with some remarks. For instance, we noticed a slight reduction in confluence in the positive fraction 2 DPS at 12 DIV. Furthermore, the NPCs observed in the unsorted and negative fractions 2 DPS at 12 DIV seemed to be bigger in size than those found in those fractions 2 DPS at 16 DIV. That was also the case with the NBs of positive fractions 2DPS at 12 DIV and 16 DIV:

even though both cell populations showed a neuronal phenotype, we noticed morphological differences among these fractions. At 7 DPS, morphological differences were diluted, and presence of NPC-like cells was not detected in any of the fractions of any sorting timepoint (not showed). Once striatal differentiation was completed (21 DPS) all fractions showed a homogeneous neuronal morphology, with no evidence of proliferation (Figure 28D). Interestingly, all fractions resulted from 12 DIV sorting showed a noticeable reduction in cell confluence at 21 DPS, compared to their counterparts at 21 DPS at 16 DIV.

3.3. Different subtypes of striatal NBs are selected at distinct cell sorting timepoints

Next, we investigated the identity of the progenitor subpopulations sorted at 12 and 16 DIV. To that aim, we examined the expression of EBF1and the DLX family of transcription factors (which are markers of the direct and indirect pathways respectively) by quantifying the relative abundance of cells expressing these transcription factors at a protein level in each fraction 1 hour after sorting at 12 DIV or 16 DIV (Fig.31).

Upon visualization, and in the case of 12 DIV sorting (Fig.31A), we observed a clear enrichment of panEBF$^+$ cells in the positive fraction compared to the unsorted control and the negative fraction (Fig. 31A). We did not observe enrichment of panDLX$^+$ cells at 12 DIV in either the positive or negative populations compared to the controls. These observations strongly suggest that dNBs can be enriched at 12 DIV using CD200. Regarding sorting at 16 DIV (Fig.31B), we observed enrichment of both panEBF$^+$ cells and panDLX$^+$ cells in the positive fraction compared to the unsorted and negative fractions. This suggests that both direct and indirect pathway NBs were enriched following sorting at this timepoint. We did not observe co-expression of panEBF and panDLX which is consistent with the specificity of these transcription factors for dNBs and iNBs respectively. These data validate previous results in a larger group of cell lines.

We performed ICC quantification of cells expressing panEBF and panDLX to confirm the enrichments observed by visual inspection (Fig.31C-D). In the 12 DIV unsorted fraction, the relative abundance of cells expressing panEBF and panDLX was found to be extremely low. For instance, only 1.76 ± 0.66% and 4.2 ± 1.01% of the cells in this fraction expressed panEBF and panDLX respectively before sorting at 12 DIV (Fig.31C). Following cell selection, the proportion of cells expressing panEBF and panDLX in the negative fraction was maintained (1.21 ± 0.4% and 5.43 ± 1.45% respectively; Fig.31C).

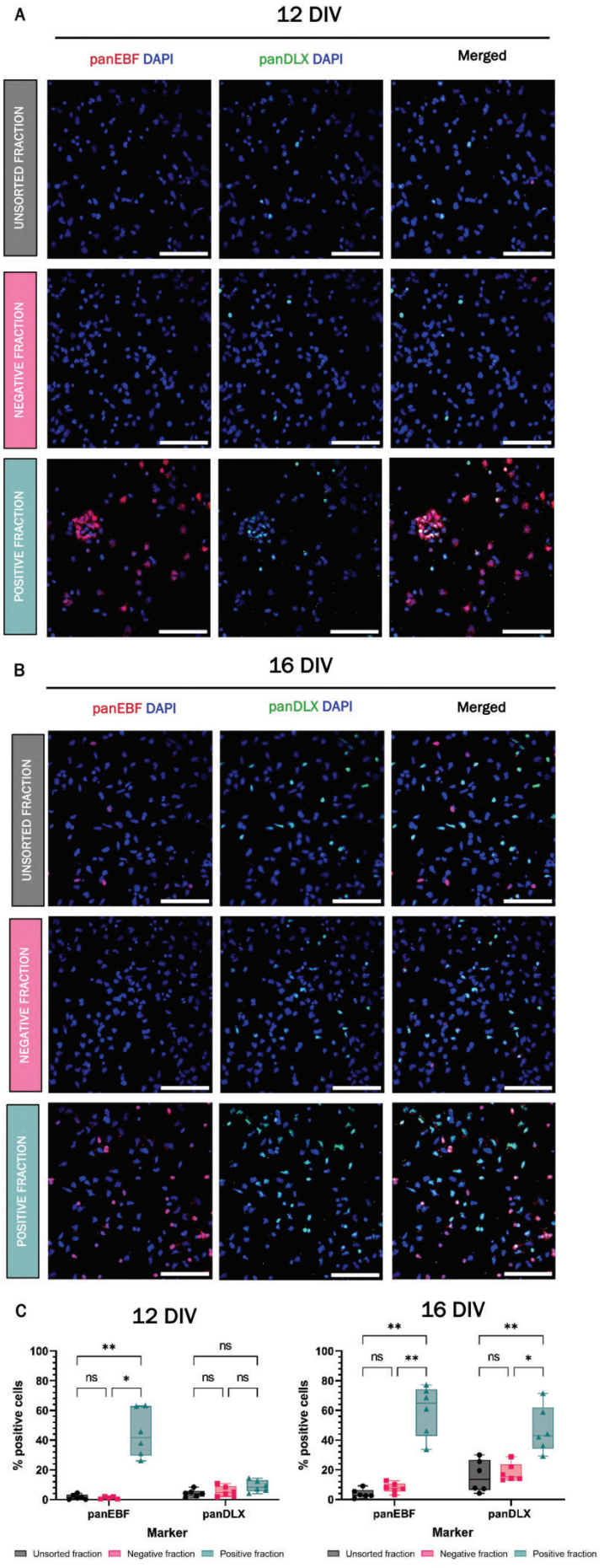

Figure 30. Different subtypes of striatal NBs are selected at distinct cell sorting timepoints. (A, B) Confocal microscopy pictures of samples after ICC were performed to detect pan-EBF (dNB marker) and pan-DLX (iNB marker) in unsorted (grey), negative (pink) and positive (green) fractions 1 hour after replating following MACS at 12 DIV (A) and 16 DIV (B). Scale bars = 50µm **(C, D)** Bar graphs representing unbiased automated counting of cells expressing pan-EBF and pan-DLX in unsorted and sorted cells after CD200-based MACS at 12 DIV (C) and 16 DIV (D). Error bars represent SEM.

However, we confirmed a 25-fold enrichment of panEBF$^+$ cells in the positive fraction at 12 DIV (p=0.006 compared to the unsorted fraction; Fig.31C), in which these cells accounted approximately for half of the cultures (44.37 ± 6.48% of total cells). Interestingly, this fraction also showed increased relative abundance (2-fold) in panDLX$^+$ cells compared to the unsorted and negative fractions, although this relative abundance was found to be very low (8.93± 1.58%), and the enrichment was not found to be significant (p=0.15 compared to the unsorted fraction). At 16 DIV, the relative abundance of cells in the unsorted fraction, expressing panEBF and panDLX was found to be low (3.88 ± 1.23% and 15.68 ± 4.4% of the cells were found to express panEBF and panDLX respectively), and even if it was measured to be 3 times higher than what was observed for the 12 DIV cultures, the increase was not significant (Fig.31D). The relative abundance of panEBF$^+$ and panDLX$^+$ cells in the negative fraction (7.87 ± 1.35% of panEBF$^+$ cells and 18.18 ± 2.5% of panDLX$^+$ cells) was found to be similar to those of the unsorted fraction (Fig.31D). On the other hand, we confirmed the enrichment of both panEBF$^+$ and panDLX$^+$ cells in the positive fraction following 16 DIV sorting compared to the unsorted and negative fractions. More specifically, we found that the largest (15.5-fold) and most significant (p=0.002) enrichment compared to the unsorted control happened for panEBF$^+$ cells, which accounted for 59.95 ± 6.88% of the positive fraction. To a lesser extent, the proportion of panDLX$^+$ cells increased to 46.92 ± 6.53%, which constituted a 3-fold enrichment (p=0.004) compared to the unsorted control (Fig.31D).

3.4. CD200^{high} NBs sorted at 16 DIV can be differentiated into neurons which express striatal dSPN and iSPN markers

Next, we aimed to characterize the neuronal populations resulting from *in vitro* striatal differentiation of hPSCs, and check whether CD200-based sorting could increase the relative abundance of SPNs in the final neuronal populations. To that aim, we focused on the investigation of the mRNA expression of SPN marker genes. We investigated the expression of relevant marker genes in the unsorted cell population over the course of *in vitro* striatal differentiation, to check whether (and when) hPSC-derived neurons using could acquire a dSPN and/or iSPN transcriptional profile. To that aim, we used the dataset from the bulk RNAseq analysis at different time points of the protocol (8 DIV, 12 DIV, 16 DIV 23 DIV and 37 DIV; Fig.29) and studied the mean normalized expression over time of key SPN markers (Fig.32A): general SPNs (*GAD2*, *BCL11B* and *ARPP21*), dSPNs (*DRD1*, *TAC1* and *PDYN*) and iSPNs (*DRD2*, *ADORA2A* and *PENK*). We

observed that expression of general SPN markers started to be detected by 16 DIV, and continued to increase until the end of differentiation at 37 DIV. When focusing specifically on dSPN markers, we noticed that even if expression was first detected later on in differentiation (around 23 DIV or even 37 DIV), these genes were robustly expressed by the end of the protocol. Expression of iSPN marker genes followed a similar trend; however, with the exception of *DRD2*, the expression of these markers was found to be generally low by the end of the protocol.

To establish the identity of the neuronal populations that differentiated from the sorted subpopulations at 12 DIV and 16 DIV, we performed fluorescent mRNA *in situ* hybridization (ISH) for the striatal neuron markers *DRD1*, *DRD2*, and *BCL11B* (CTIP2) on samples that were fixed three weeks after sorting at 12 DIV or 16 DIV (unsorted, negative and positive fractions) and which had been further differentiated during that time as per the LI differentiation protocol (Fig.32B). We then quantified both the total number of cells in each condition and the number of mRNA spots of transcripts of interest in each individual cell. Since SPNs simultaneously express *BCL11B* and *DRD1* (dSPNs) or *DRD2* (iSPNs), we focused on the analysis of $DRD1^{+}/BCL11B^{+}$ (dSPNs) and $DRD2^{+}/BCL11B^{+}$ (iSPNs) cells in unsorted and sorted cell subpopulations from both sorting timepoints (12 DIV and 16 DIV).

We compared the relative abundance of dSPNs (Fig.32C) and iSPNs (Fig.32D) in the unsorted fraction versus the sorted (negative and positive) fractions for each sorting timepoint, in order to investigate whether isolation of $CD200^{high}$ NBs resulted in a higher yield of striatal SPNs following *in vitro* differentiation. However, we did not observe any significant differences among fractions for any of the analyzed sorting timepoints, in terms of altered generation of either dSPNs or iSPNs. Interestingly, we observed that the most striking differences were found when comparing the fractions at 12 DIV with their counterparts at 16 DIV, even in the case of the unsorted controls. In fact, we observed that SPN subtypes were not efficiently generated from 12 DIV unsorted cells, since only 13.9 ± 11.5% and 7.3 ± 4.6% of neurons were identified as dSPNs and iSPNs respectively (Fig 30C-D). Terminal striatal differentiation of 16 DIV unsorted populations greatly increased the yield of SPN generation (Fig.32C-D), obtaining 40.4 ± 4.6% dSPNs (~3-fold increase compared to 12 DIV; $p<0.001$) and 54.9 ± 8.6% iSPNs (~7.5-fold increase compared to 12 DIV; $p<0.001$).

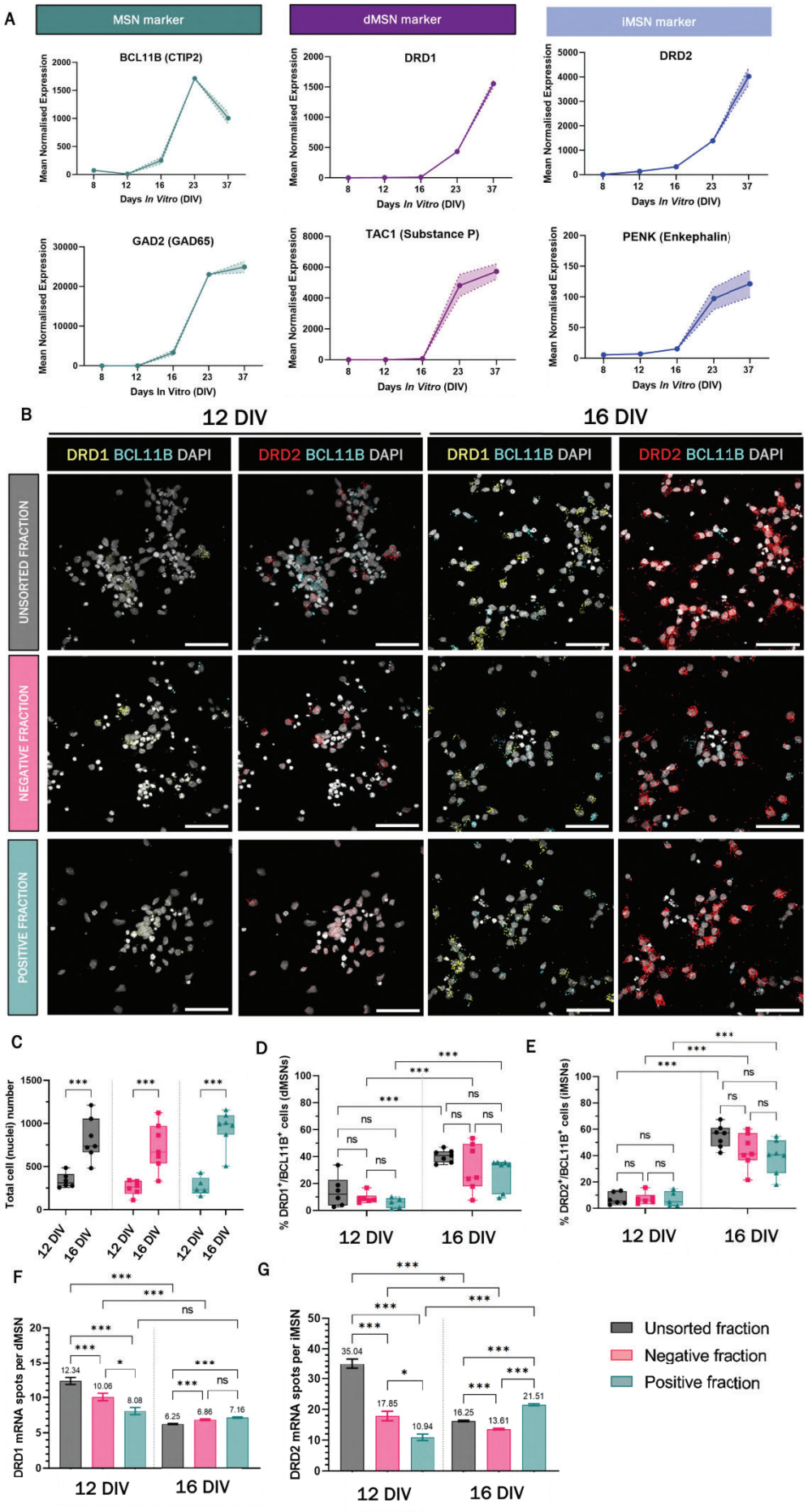
A
MSN marker
dMSN marker
iMSN marker
BCL11B (CTIP2)
DRD1
DRD2
GAD2 (GAD65)
TAC1 (Substance P)
PENK (Enkephalin)
Mean Normalised Expression
Days In Vitro (DIV)
B
12 DIV
16 DIV
DRD1 BCL11B DAPI
DRD2 BCL11B DAPI
UNSORTED FRACTION
NEGATIVE FRACTION
POSITIVE FRACTION
C
Total cell (nuclei) number
D
% DRD1+/BCL11B+ cells (dMSNs)
E
% DRD2+/BCL11B+ cells (iMSNs)
F
DRD1 mRNA spots per dMSN
G
DRD2 mRNA spots per iMSN
Unsorted fraction
Negative fraction
Positive fraction

Figure 31. CD200^{high} NBs sorted at 16 DIV can differentiate into neurons expressing dSPN and iSPN markers. **(A)** Line plots showing the mean normalised expression (bulk RNAseq) of key marker genes in hPSC-derived cell populations (three cell lines) at different time points of the LI forebrain differentiation protocol: general SPN markers (*GAD2*, *BCL11B* and *ARPP-21*), dSPN markers (*DRD1*, *TAC1*, *PDYN*) and iSPN markers (*DRD2*, *ADORA2A* and *PENK*). Three replicates per cell line and timepoint were used. The shadowed areas represent standard deviation (SD). **(B)** Visualization of gene expression by *in situ* hybridization (ISH) of striatal SPN markers *BCL11B* (CTIP2), *DRD1* or *DRD2* in the unsorted, (grey), negative (pink) and positive (green) fractions 21 Days Post-Sorting (DPS) at 12 DIV (left) and 16 DIV (right). Scale bars = 50 µm. **(C, D)** Automated ISH quantification of relative abundance (%) of CTIP2$^+$/DRD1$^+$ (dSPNs; C) and CTIP2$^+$/DRD2$^+$ (iSPNs; D) cells in unsorted and sorted fractions 21 DPS at 12 DIV and 16 DIV. **(E, F)** Automated ISH quantification of DRD1 mRNA spots per dSPN (E) and DRD2 mRNA spots per iSPNs (F) in unsorted and sorted fractions 21 DPS at 12 DIV and 16 DIV. DIV: Days *In Vitro*.

To further investigate whether CD200-based cell sorting led to an altered generation of SPN subtypes, we investigated changes in the expression levels of *DRD1* and *DRD2* in dSPNs and iSPNs respectively in each of the studied subpopulations. To that aim, we analyzed the average number of mRNA (*DRD1* or *DRD2*) spots detected only in those cells deemed as positive for a dSPN or iSPN identity respectively depending on the marker gene (Fig.32E-F). The dSPNs derived from the positive population at 12 DIV showed ~35% and ~20% reductions in *DRD1* expression (8.08 ± 0.50 *DRD1* mRNA spots/dSPN) compared to those in the unsorted control (12.34 ± 0.49 *DRD1* mRNA spots/dSPN; $p<0.001$) and negative fraction (10.06 ± 0.52 *DRD1* mRNA spots/dSPN; $p=0.02$) respectively. Sorting at 16 DIV resulted in a slight but significant increase of ~14% ($p<0.001$) in *DRD1* expression levels of dSPNs in the positive fraction (7.12 ± 0.10 *DRD1* mRNA spots/dSPN) compared to the unsorted fraction (6.25 ± 0.08 *DRD1* mRNA spots/dSPN), although no significant differences were found ($p=0.38$) when comparing dSPNs *DRD1* mRNA expression levels in the positive and negative (6.86 ± 0.11 *DRD1* mRNA spots/dSPN) fractions. Regarding the iSPN subtype in samples derived from fractions obtained at 12 DIV, our analysis revealed ~69% and ~39% reductions in *DRD2* mRNA spots per iSPN in the positive (10.94 ± 1.03 *DRD2* mRNA spots/iSPN) fraction compared to the unsorted (35.04 ± 1.64 DRD2 mRNA spots/iSPN; $p<0.001$) and negative (17.85 ± 1.56 *DRD2* mRNA spots/iSPN; $p=0.04$) fractions. On the other hand, in iSPNs derived from 16 DIV samples, *DRD2* mRNA expression in iSPNs of the positive fraction (21.51 ± 0.29 *DRD2* mRNA spots/iSPN) was found to be increased by ~32% and ~58% compared to that of iSPNs derived from the unsorted (16.25 ± 0.24 *DRD2* mRNA spots/iSPN; $p<0.001$) and negative (13.61 ± 0.23 *DRD2* mRNA spots/iSPN; $p<0.001$) fractions respectively.

3.5. CD200^{high} NBs display an enhanced neuronal transcriptional profile

To further enhance our understanding of the properties of different striatal progenitor subtypes, we analyzed the differential gene expression profiles of unsorted (control) and sorted subpopulations (NPC/CD200^{low} and NB/CD200^{high} cells) selected from 12 DIV and 16 DIV cultures, using bulk RNAseq. Following Principal Component Analysis (PCA) visualization, we identified developmental stage as the main source of variation (PC1; Fig.33A-B); in fact, developmental stage was observed to contribute to 64.16% of total variation of the dataset. Furthermore, sorting timepoint (i.e., 12 DIV or 16 DIV) was also identified as a main source of variation in the dataset (PC4, 4.08% total variation of the dataset). In a way, this factor is directly linked to PC1 above, since cells sorted at 12 DIV are in a more immature developmental stage than cells sorted at 16 DIV. Based on these two factors, samples formed three clusters. Interestingly, even though samples analyzed at 2 DPS were organized in two different clusters containing samples sorted at 12 DIV and 16 DIV respectively, in samples analyzed 21 DPS the separation based on developmental status (PC1) was not as clear, and the samples organize in a single cluster (Fig.33A). However, we did not observe any clear sample clustering based on sorting fraction identity (unsorted/control, NPC/CD200^{low} and NB/CD200^{high}; Fig.33B).

Next, we compared equivalent positive/CD200^{high} populations sorted at 12 DIV and 16 DIV to identify whether the differences observed in terminal differentiation of these populations was a result of differential gene expression profiles. In samples analyzed 2 DPS, we found 2,672 differentially expressed genes (DEGs) in the positive/CD200^{high} subpopulation selected at 16 DIV compared to its counterpart at 12 DIV (1,420 upregulated and 1,252 downregulated genes at 16 DIV vs 12 DIV; Fig.33C). At 21 DPS we observed a 2.04-fold decrease in the number of DEGs, which was found to be 1,308 (618 upregulated and 690 downregulated genes at 16 DIV vs 12 DIV; Fig.33D).

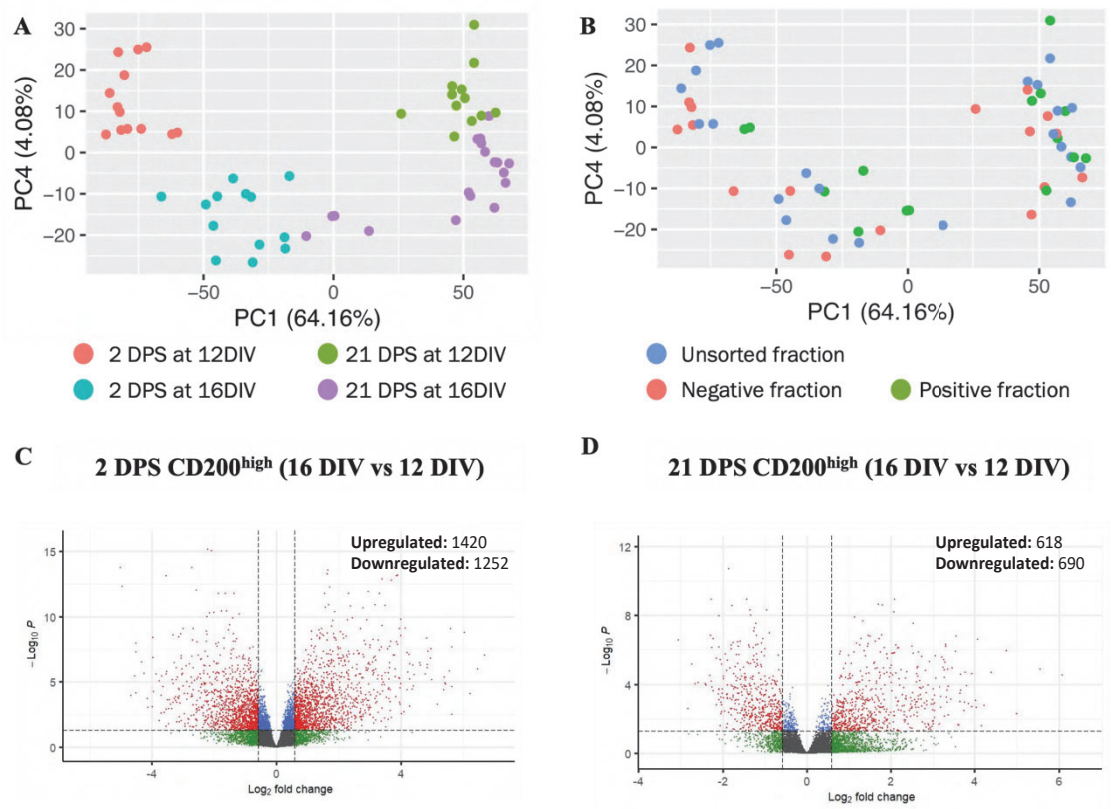

Figure 32. CD200^{high} NBs sorted at different timepoints display differential gene expression profiles. (A-B) Principal Component Analysis (PCA) of unsorted, negative and positive fractions 2 and 21 Days Post-Sorting (DPS) after cell selection at 12 DIV and 16 DIV. Principal component (PC) 1 splits the samples by developmental stage, while PC2 splits samples by sorting timepoint (12 DIV or 16 DIV). Samples are coloured in the plots either by analysis and sorting timepoint (A), or fraction (B). **(C-D)** Volcano plot of all differentially expressed genes (DEGs) between CD200^{high} NBs sorted at 16 DIV or 12 DIV at 2DPS (C) and 21 DPS (D). x-axis represents log2-fold-change (16 DIV vs 12 DIV), while y-axis represents -log10-adjusted-p-value. log2-fold-change threshold = 1, adjusted p-value threshold=0.05.

At 2 DPS, functional enrichment analysis revealed that CD200^{high} cells sorted at 16 DIV showed an upregulation of genes related to nervous system development, neurogenesis or synapsis (Fig.34A), while CD200^{high} cells sorted at 12 DIV were characterized by the expression of genes related to macromolecule biosynthesis or cytoplasmatic protein translation (Fig.34B). At 21 DPS, functional enrichment analysis also revealed increased expression of genes related to nervous system development and neurogenesis in CD200^{high} cells sorted at 16 DIV (Fig.35A); however, CD200^{high} cells sorted at 12 DIV showed increased expression of genes related to synapsis and cell signaling (Fig.35B)

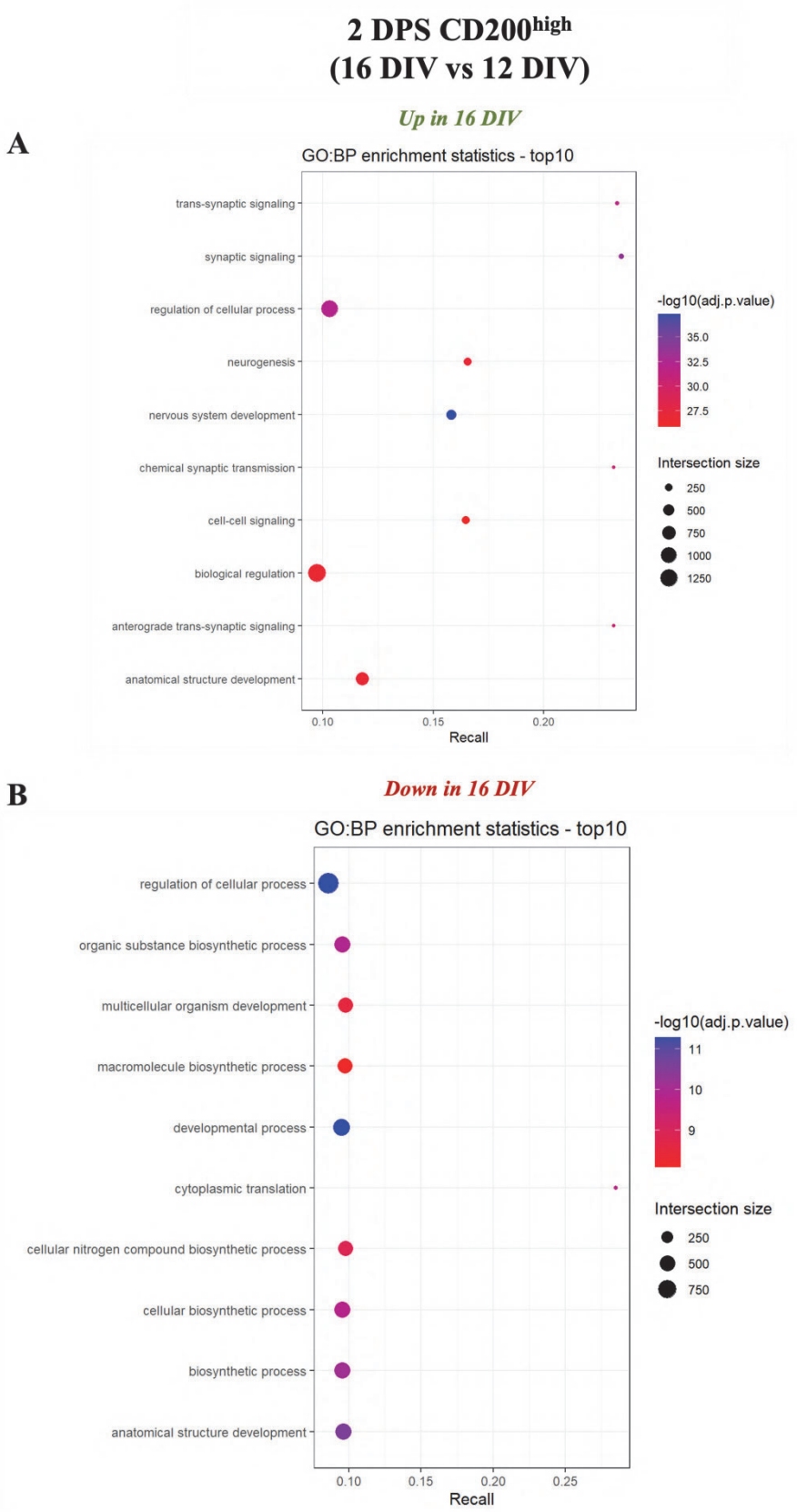

Figure 33. Functional enrichment analysis of CD200^{high} NBs sorted at 16 DIV and 12 DIV at 2 Days Post-Sorting (DPS). Dot plots of top 10 GO annotations of up-regulated (A) and down-regulated genes (B) in 16 DIV samples vs 12 DIV samples. The size of the dots represents the intersection size (i.e., number of significant genes associated with the GO term), and the color of the dots represent the *p*-value

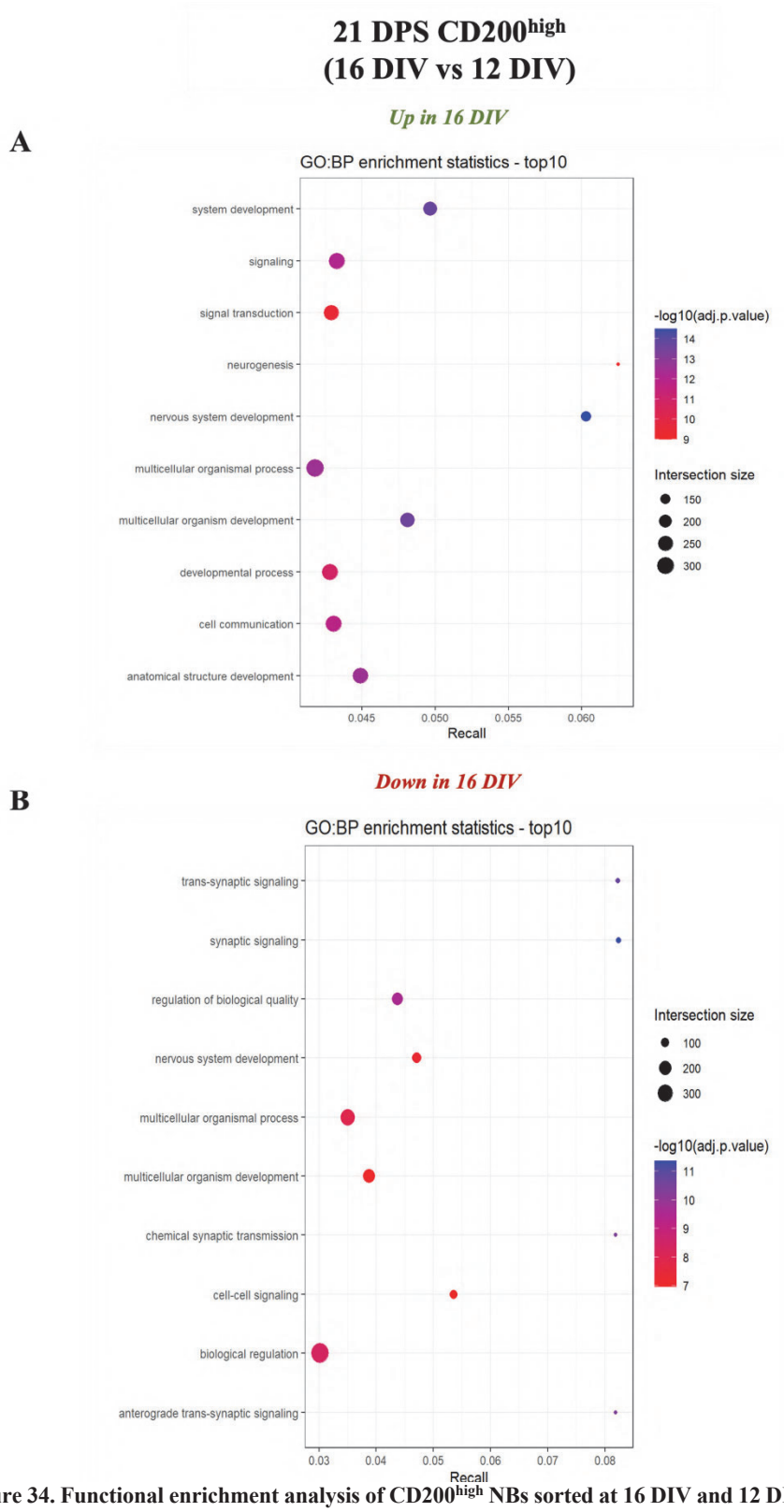

Figure 34. Functional enrichment analysis of CD200^{high} NBs sorted at 16 DIV and 12 DIV at 21 Days Post-Sorting (DPS). Dot plots of top 10 GO annotations of up-regulated (A) and down-regulated genes (B) in 16 DIV samples vs 12 DIV samples. The size of the dots represents the intersection size (i.e., number of significant genes associated with the GO term), and the color of the dots represent the *p*-value

Given that more subtle sources of variation in the dataset (i.e., $CD200^{low}$ vs $CD200^{high}$) may be masked by bigger, much larger sources of variation in the dataset (e.g., developmental status or sorting timepoint), we then compared NPC ($CD200^{low}$) and NB ($CD200^{high}$) populations sorted at each timepoint to further delineate differences among the NPC and the NB subpopulations present at 12 DIV and 16 DIV. In samples analyzed 2 DPS, we observed a total of 3,554 and 2,886 differentially expressed genes in $CD200^{low}$ cells compared to $CD200^{high}$ cells sorted at 12 DIV (1,710 upregulated and 1,844 downregulated genes in $CD200^{low}$ cells vs $CD200^{high}$ cells; Fig.36A) and 16 DIV (1,054 upregulated and 1,832 downregulated genes in $CD200^{low}$ cells vs $CD200^{high}$ cells; Fig.36B) respectively. At 21 DPS, we observed a 6.09-fold reduction in the number of differentially expressed genes in samples sorted at 12 DIV, which was found to be 584 (318 upregulated and 266 downregulated genes in $CD200^{low}$ cells vs $CD200^{high}$ cells; Fig.36C). This homogenization was found to be increased for 21 DPS samples sorted at 16 DIV. In fact, we observed a 41.83-fold reduction in the number of differentially expressed genes between 21 DPS $CD200^{low}$ and $CD200^{high}$ cells sorted at 16 DIV compared their 21 DPS counterparts sorted at 12 DIV, with only 69 differentially expressed genes (5 upregulated and 64 downregulated genes in $CD200^{low}$ cells vs $CD200^{high}$ cells; Fig.36D).

Functional enrichment analysis at 2 DPS revealed that NBs/$CD200^{high}$ showed an upregulation of genes related to cell signaling or synapsis, while NPCs/$CD200^{low}$ cells were characterized by expression of genes related to macromolecule biosynthesis or cytoplasmatic protein translation, for samples sorted both at 12 DIV (Fig.37) and at 16 DIV (Fig.38). In turn, functional enrichment analysis at 21 DPS cells sorted at 12 DIV, or 16 DIV did not yield any significant result, as expected given the low number of differentially expressed genes observed (data not shown).

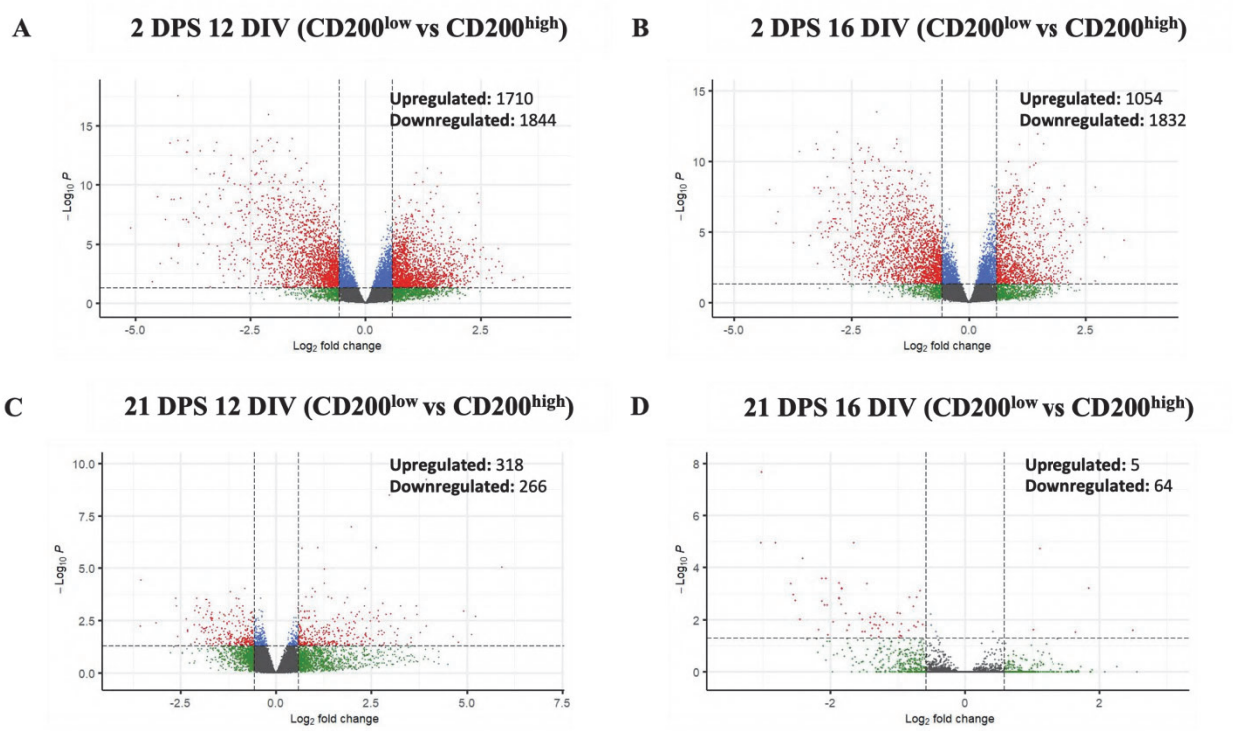

Figure 35. CD200^{high} NBs and CD200^{low} NPCs sorted at 12 DIV, or 16 DIV display different gene expression profiles, which are homogenized as in vitro striatal differentiation progresses (A-B) Volcano plot of all differentially expressed genes (DEGs) between 2PS CD200^{low} NPCs and CD200^{high} NBs sorted at 12 DIV (A) and 16 DIV (B). **(C-D)** Volcano plot of all DEGs between 21 DPS CD200^{low} NPCs and CD200^{high} NBs sorted at 12 DIV (C) and 16 DIV (D). x-axis represents log2-fold-change (CD200^{low} vs CD200^{high}), while y-axis represents -log10-adjusted-*p*-value. log2-fold-change threshold = 1, adjusted *p*-value threshold=0.05.

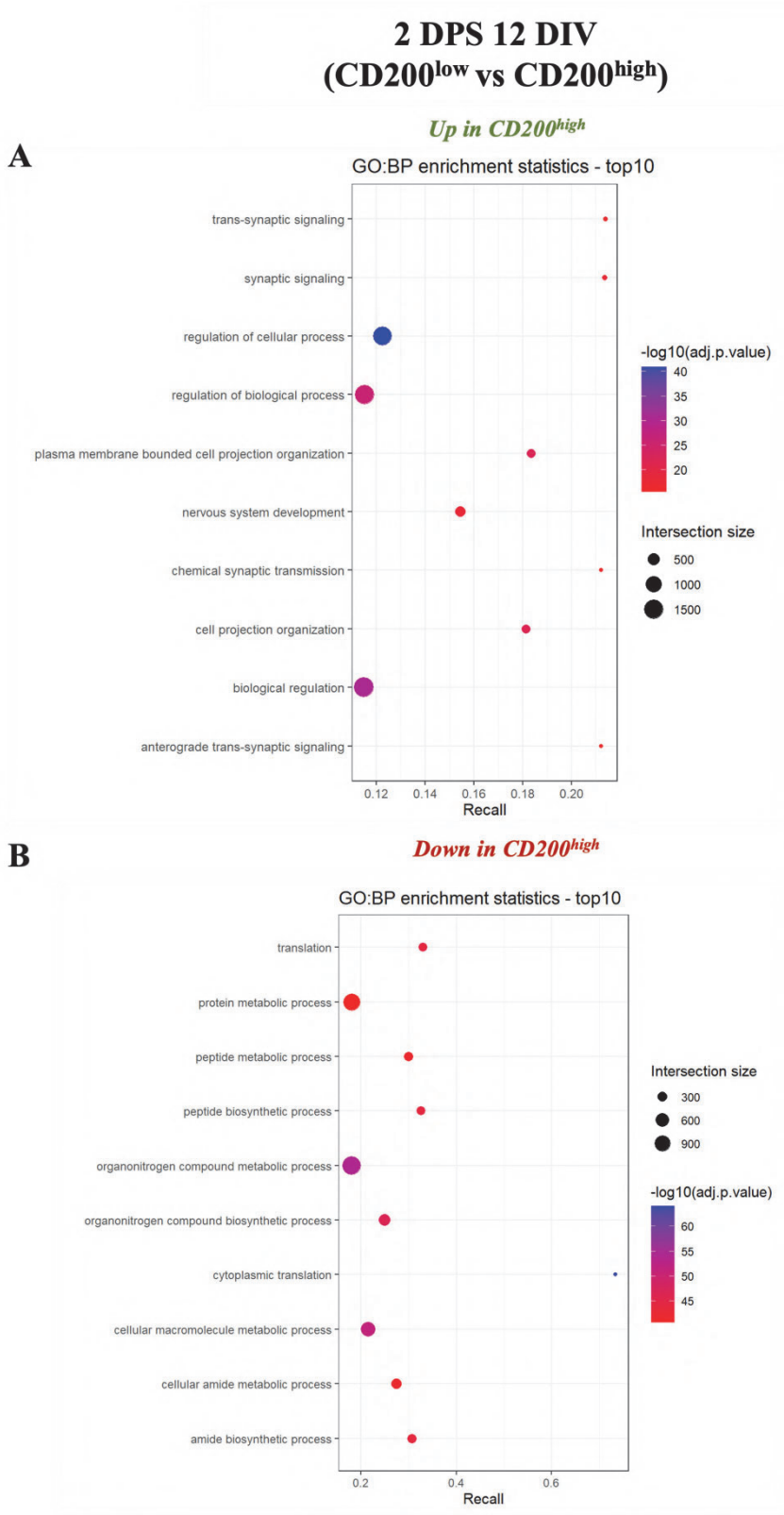

Figure 36. Functional enrichment analysis of CD200^{low} NPCs and CD200^{high} NBs sorted at 12 DIV, performed at 2 Days Post-Sorting (DPS). Dot plots of top 10 GO annotations of up-regulated (A) and down-regulated genes (B) in CD200^{low} samples vs CD200^{high} samples. The size of the dots represents the intersection size (i.e., number of significant genes associated with the GO term), and the color of the dots represent the *p*-value

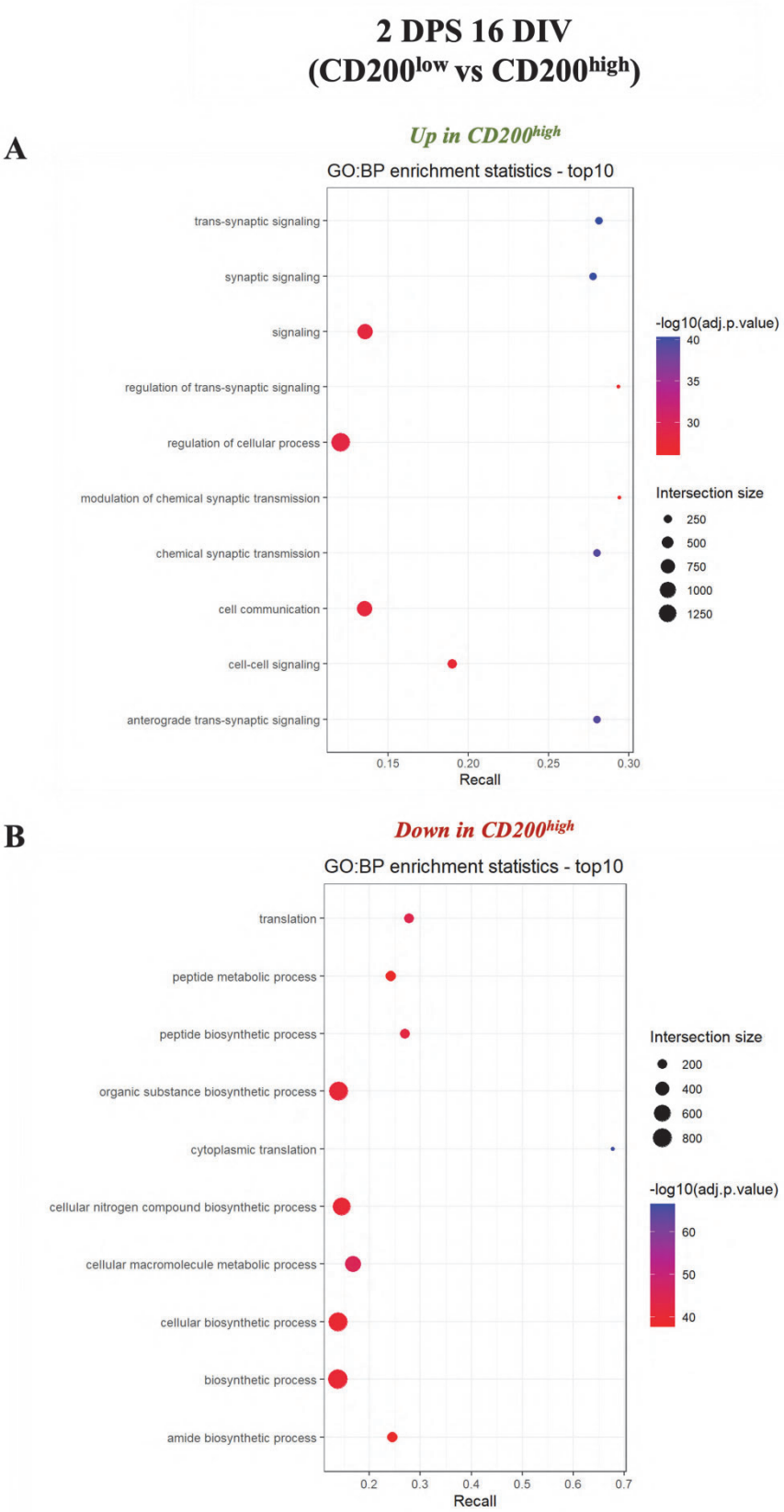

Figure 37. Functional enrichment analysis of CD200^{low} NPCs and CD200^{high} NBs sorted at 16 DIV, performed at 21 Days Post-Sorting (DPS). Dot plots of top 10 GO annotations of up-regulated (A) and down-regulated genes (B) in CD200^{low} samples vs CD200^{high} samples. The size of the dots represents the intersection size (i.e., number of significant genes associated with the GO term), and the color of the dots represent the *p*-value

DISCUSSION

Discussion

There is a considerable and growing body of preclinical evidence indicating that hPSC-based CRTs hold significant promise as a potential treatment for HD. In fact, pursuit of stem cell therapies for HD is not only important to meet the pressing need for therapeutics in this incurable condition, but also to provide a map for translation of cell therapies in other NDs. However, before these regenerative medicine approaches can be translated to the clinic and fulfill their full potential, several challenges need to be overcome. Here, to address some of those challenges, we have developed an innovative approach to generate safer and more homogeneous hPSC-derived products for CRT strategies in HD. This strategy has the potential to improve the outcomes and reduce the risk of graft overgrowth upon transplantation. To do so, we have combined standardization of hPSC *in vitro* culture conditions and cell sorting of postmitotic striatal NBs before transplantation using an appropriate cell surface marker of this population.

In conclusion, our findings serve as a proof of concept of the positive impact of a QMS in maintaining hPSC genomic integrity and underscore the critical need for implementing QMS in academic laboratories to enhance the consistency and safety of final hPSC-derived products. Additionally, our results highlight the potential of the dual approach of combining standardization of hPSC. Overall, implementation of this strategy will be key to overcome the current reproducibility crisis, hence ensuring a smooth translation of hPSC-based technologies such as cell therapies. Additionally, our results highlight the potential of the dual approach of combining standardization of hPSC culture conditions and CD200-based cell sorting of postmitotic striatal NBs before transplantation as a promising strategy to optimize the outcomes of hPSC-derived CRT products after transplantation. In fact, CD200-based cell selection not only leads to safer CRT products with reduced risk of graft overgrowth upon transplantation, but also allows for isolation of specific striatal NB subtypes. These strategies collectively advance the development and translation of safer, effective, and reproducible cell products to be used for clinical CRT applications in HD and potentially other NDs.

1. Impact of standardized culture conditions and genomic screening routines on hPSC genomic integrity

Genomic integrity of hPSCs is essential for research and clinical applications. However, one of the main concerns associated to hPSC-derived products is related to the presence of genomic mutations in the transplanted cells, since these could be associated with tumorigenicity. All of the available literature indicates that hPSCs are often genomically unstable with a growing body of research reporting a propensity for genomic instability during prolonged hPSC culture. This propensity to acquire genomic alterations *in vitro*, mainly due to suboptimal culture conditions and inappropriate routines to monitor genome integrity, poses a challenge to both the safety and the reliability of hPSC clinical applications. In this context, the standardization of the quality control of hPSCs is becoming increasingly important. To accelerate a safe clinical translation of stem cell therapies, there is a clear need to standardize culture conditions and genomic screening of starting hPSCs cultured *in vitro*. Prompted by this, in the first part of this work we hypothesized that the introduction of a QMS could improve the genomic stability of hPSCs. To evaluate our hypothesis, we carried out a retrospective analysis of data generated from conventional G-banding karyotype and aCGH analysis over a 5-year span on hPSCs maintained by our research group, before and after adaptation to standard conditions defined by appropriate SOPs under a QMS.

1.1. Sensitivity of routine hPSC genomic screening could be enhanced by integrating molecular and traditional techniques

Routine monitoring of hPSC cultures for the appearance of genomic alterations is essential, since some common variants can go from undetectable to compose the totality of the culture within five to ten passages (Olariu et al., 2010). Different screening methods have different advantages and limitations, which are linked to their ability to detect mosaic populations, resolution, the types of variants which are detectable, the cost, the speed and whether specialist facilities and expertise are required (Halliwell et al., 2020). Currently, there is a lack of consensus on a standard strategy for monitoring genomic integrity of hPSCs, which gives rise to different standards being applied in different laboratories. Consequently, clinical translational efforts are threatened, as data reproducibility is hampered. Along these lines, Rossi et al. have recently called for the international stem cell community to put forward clear guidelines on genome monitoring of hPSCs (Rossi et al., 2022).

Here, we selected a screening strategy that combines a classical cytogenetic technique (karyotypic G-banding) with the molecular technique aCGH. In principle, both karyotyping and arrays are genome-wide technologies which can be used to assess the presence of genomic alterations. The main difference between them is the resolution: while G-banding is only capable of detecting aberrations greater than 5Mb, aCGH can detect alterations down to 1 kb. The limited resolution of G-banding could have presented an issue for assessing the genetic status of hPSC cultures, as some of the most common changes in hPSCs are present at a subchromosomal level. On the other hand, it is a cost-effective, methodologically simple screening method for larger cytogenetic alterations and can detect numerical and structural aneuploidies as well as transpositions, deletions, duplications, and even inversions of chromosomal arms or larger chromosomal fragments (being the only convenient method to detect balanced genomic rearrangements; Steinemann et al., 2013). aCGH, in turn, enables high-resolution detection of submicroscopic unbalanced genomic alterations (Valli et al., 2011). Nonetheless, the frequent use of this technique is limited by its higher costs compared to conventional cytogenetic techniques.

All in all, by integrating molecular and traditional cytogenetics, this comprehensive approach (amenable to routine use) enabled identification of most chromosomal and subchromosomal genomic alterations which hPSCs could acquire during *in vitro* culture. Even so, we cannot exclude that mosaic alterations may have go unnoticed since this strategy is still limited by the low sensitivity of both approaches to low-grade mosaicism. In fact, all the chromosomal aberrations detected in this work were present in mosaic cultures at various degrees. Hence, although steps can be taken to minimize the appearance of variants within an hPSC culture, it is of paramount importance to find alternative genomic analysis which can detect low levels of mosaicism within a culture.

1.2. Increased frequency of chromosomal gains compared to losses in hPSCs cultured in vitro

Our results show that 24.07% of the hPSCs being analyzed display some aneuploidy which could be detected by G-banding. This data is consistent with the occurrence reported by separate large-scale studies, in which between 12.9% (Taapken et al., 2011) and 34% (Amps et al., 2011) of hPSC lines were found to acquire chromosome abnormalities over time (Amps et al., 2011; Taapken et al., 2011). As expected, the higher

resolution of aCGH led to detection of larger number of alterations in hPSCs (11.5% and 61.5% of hPSCs harboring polymorphic CNVs and potentially pathogenic CNAs respectively). Overall, gains of chromosome material are better tolerated by hPSCs than losses, and hence it is markedly more common in culture adaptation (Ben-David et al., 2014); this is also supported by observations in this study that all detected chromosomal aberrations corresponded to insertions or duplications. Interestingly, this does not seem to be the case for subchromosomal alterations, since only 56.76% of CNAs were found to be gains in our dataset.

1.3. Lower in vitro genomic stability of hiPSCs compared to hESCs

We observed a tendency of hiPSC lines to acquire wider range chromosomal alterations in comparison to hESC lines, which is in harmony with work from other groups demonstrating a lower genomic stability of hiPSCs due (at least partially) to low fidelity of DNA damage repair (Lu et al., 2013). Besides, cell reprogramming to generate hiPSC lines could also contribute to this phenomenon due to massive genome remodeling of hiPSCs (Hussein et al., 2011). In fact, more than one third (35.14%) of the subchromosomal alterations found in hiPSCs corresponded to polymorphic CNVs, whereas CNVs were not detected in any of the analyzed hESCs. Remarkably, CNVs tend to increase their prevalence with time in culture, since cultured hiPSCs have been shown to select rapidly against cells harboring them (Hussein et al., 2011). However, this observation does not imply that hiPSCs show more frequent pathogenic alterations, since our data suggests that CNAs are more prevalent in hESCs (for which CNAs were detected in all analyzed cells) than in hiPSCs (where only around ~60% of cells harbored some CNA).

1.4. Recurrent genomic alterations acquired by hPSCs in vitro are associated to increased proliferation, and are not completely eliminated by standardization of culture conditions under a QMS

The most common genomic alteration found in our hPSC cultures was a 20q11.21 amplification, a frequent gain of a small, variable region located near the centromere of chromosome arm 20q (Avery et al., 2013; Nguyen et al., 2014). In fact, this is a recurrent alteration, which was noted by single nucleotide polymorphism (SNP) array analysis in more than 20% of the cell lines in the ISCI study (Amps et al., 2011; Baker et al., 2016), and which results in overexpression of an isoform of the *BCL2L1* gene. Notably, this alteration confers a growth advantage due to reduced propensity for apoptosis (Avery et

al., 2013; Nguyen et al., 2014), reduced dependence on bFGF, delayed differentiation to neural lineages (Werbowetski-Ogilvie et al., 2009) and reduced efficiency of neuroectodermal lineage commitment (caused by perturbation of SMAD and TGFβ signaling; Markouli et al., 2019). As a result, acquisition of this particular alteration would limit the ability of hPSCs to be differentiated into SPNs, hence resulting in lower yields of SPNs in the final cell product following *in vitro* differentiation. In our study, we only detected this aberration in 11.11% of hPSCs by G-banding, which can be explained by the fact that this amplification is often below the resolution of current monitoring methods used in research laboratories, most often G-banding karyotyping (Halliwell et al., 2020). Conversely, by aCGH, we reported a much larger prevalence of this alteration in hPSCs (23.07%), closer to what was reported by the ISCI study (Amps et al., 2011).

Other examples of recurrent chromosomal aberrations found in our analysis were trisomies of chromosomes 8 and 12. The later alteration results in *NANOG* overexpression, increased proliferation rate and replication, and reduced propensity for spontaneous differentiation and apoptosis (Ben-David et al., 2014). Interestingly, we only detected this trisomy in hiPSCs (4.08%), a prevalence much lower than what has been reported for hESCs and hiPSCs (42.6% and 31.9% respectively; Taapken et al., 2011). Remarkably, most of these alterations have been associated with various cancers, notably the association of trisomy of chromosome 12 with embryonal carcinoma cells (Andrews, 2002) or testicular germ cell tumors (Atkin & Baker, 1982), or 20q11.21 amplification with colorectal cancer (Nguyen & Duong, 2018), cervical cancer (Scotto et al., 2008), and tumorigenic transformation (Beroukhim et al., 2010; Tabach et al., 2011). Regarding subchromosomal alterations besides gains in chromosome 20 and a small insertion in 14q23.3 (Riggs et al., 2021), none of the detected CNAs is, to our knowledge, associated with malignant transformation or impaired functional properties of cultured hPSCs.

Of note, we found that the most abundant *de novo* pathogenic alterations acquired by hPSCs under ISO9001-2015 were an insertion in 14q23.3 (which has been associated to a cancerous phenotype; Riggs et al., 2021), an insertion in 14q32 (linked to predisposition to early clonal hematopoiesis leading to myeloid neoplasms; Pegliasco et al., 2022), the 20q11.21 amplification and trisomies in chromosomes 8 and 12. Given that all of these alterations confer a selective advantage to variants which could lead to malignant phenotypes, it is clear that despite the improved genomic stability of hPSCs, genetic alterations which may potentially jeopardize the safety or impair the function of hPSCs

are not completely removed from cultured cells. We hypothesize that this may be a consequence of adapting hPSC lines to standard conditions well after they have been derived. It is still to be determined if implementation of a QMS since derivation will result in a greater improvement of hPSC genomic stability. In any case, the frequent genomic monitoring of hPSCs resulting from the application of a QMS enhances the ability of researchers to detect a larger number of genomic alterations earlier, before they hPSC variants take over the cultures.

1.5. The positive impact of a QMS in intrinsic hPSC genomic instability support its implementation in academic settings

Contrary to what is observed in clinical practice and R&D in the pharmaceutical industry, basic and preclinical biomedical academic laboratories often lack a structured QMS such as ISO9001-2015. The implementation of such systems in academia is challenging, mostly due to its immense documentation load and fears that it would limit creativity. However, this lack of QMSs, along with transparency are two reasons for the ongoing reproducibility crisis and subsequent translational roadblock crisis (Baker, 2016; Miyakawa, 2020; Tackett & Miller, 2019). This becomes especially relevant in the case of genomic alterations acquired by hPSCs *in vitro*, even by clinical grade lines (Thompson et al., 2020) which can ultimately confound experimental results and potentially jeopardize the outcome of clinical therapies.

Our results show that the adaptation of hPSC lines to maintenance conditions described by SOPs under ISO9001-2015 resulted in a striking improvement of genomic stability in hPSCs cultured *in vitro*. This approach resulted in a notable decrease in the prevalence and types of chromosomal and subchromosomal genomic alterations. In fact, we discovered a specially pronounced reduction of 70.11% in pathogenic chromosomal aberrations in hPSCs after they had been adapted to the new conditions, while similar yet less marked decreases were observed for FPAs (53.31%) and subchromosomal CNAs (54.55%) and CNVs (61.05%) post-adaptation. Our data also demonstrated a decreased probability to acquire pathogenic genomic alterations of hPSCs cultured under the new standardized conditions. In fact, the probability of pathogenic chromosomal alterations in hPSCs was found to be decreased by three times under these culture conditions, even when hPSCs had been cultured for an *in vitro* period 6 times longer compared to cells cultured under non-standard conditions. Similarly, the use of SOPs under ISO9001:2015 resulted in 2 times less probability of cells to acquire *de novo* pathogenic subchromosomal

CNAs even when time these cells had been maintained *in vitro* for twice as long as the controls. Our observations provide evidence of the positive impact of a QMS in the genomic stability of hPSCs maintained *in vitro*, and thus support the implementation of such systems to standardize culture conditions of hPSCs used as cell source for cell therapies, ultimately accelerating clinical translation.

2. Development of CD200-based cell selection to isolate post-mitotic striatal NBs

Another main challenge for clinical application of hPSC-derived products is associated to their heterogeneity. To date, hPSC differentiation protocols have not been able to synchronize the birth and development of cell populations to the extent seen in normal development, and consequently resulting cell products exhibit high batch-to-batch variability and broad cellular heterogeneity, which impedes their experimental and clinical utility. Furthermore, although all of the clinical applications require the cells to be differentiated, there is concern about residual undifferentiated cells in transplanted populations which carry the risk of teratoma formation upon transplantation due to their intrinsic pluripotency. In this context, selective depletion of undifferentiated hPSCs is key for the generation of a safe and more defined cell product that could then be safely transplanted with a significantly decreased risk of graft overgrowth. Hence, in the second part of this work we hypothesized that incorporation of selection steps prior to transplantation (to ensure the presence of a pure striatal cell population and the absence of unwanted overly proliferative cell types) could optimize the outcomes of CRTs for HD following transplantation, by reducing the risk of graft overgrowth.

Here, to generate more homogeneous cell products for transplantation in HD, we developed a novel strategy which combines *in vitro* striatal differentiation of hPSCs, and an appropriate cell selection methodology based on a cell surface marker which allows for enrichment of specified striatal progenitors. To that aim, we first identified the cell surface marker CD200 as a marker of hPSC-derived specified postmitotic striatal NBs and demonstrated that CD200-based cell selection leads to robust and reproducible enrichment of these progenitors. We showed that sorted $CD200^{high}$ cells display hallmark characteristics of SPN progenitors of the developing striatum and showed evidence of differentiation into neurons with the target SPN phenotype *in vitro*. We also demonstrated that these postmitotic SPN progenitors survive transplantation into the striatum of adult

mice and minimize the risk of teratoma formation *in vivo*. Finally, we demonstrated that CD200-based selection at different timepoints of *in vitro* differentiation leads to the obtention of cell compositions enriched in different subtypes of hPSC-derived postmitotic striatal progenitors.

2.1. Selection of a suitable cell surface marker for selection of post-mitotic striatal NBs: the most promising candidates identified at RNA level show low specificity at a protein level

We identified proliferating NPCs and postmitotic striatal NBs as the two main subtypes of hPSC-derived neural forebrain progenitors generated *in vitro* using our striatal differentiation protocol (Comella-Bolla et al., 2020). NBs are more amenable than NPCs to be used for transplantation purposes in the context of cell therapies for NDs, given their superior commitment to an SPN fate and their postmitotic status. Moreover, the NPC subpopulation was found to possess stem cell-like properties, which include proliferation or lack of differentiation and commitment to a particular neuronal fate. Thus, the inclusion of these NPCs in a cell product aimed at transplantation involves not only the obvious risk of teratoma formation due to the presence of proliferating cells but also a lack of certainty over the cell type composition of the final graft, which could severely hamper the efficacy of a strategy relying on transplantation of a single target cell type.

Development of cell selection strategies in the context of stem cell-based regenerative medicine requires the identification of compatible cell surface markers for this population of interest (i.e., post-mitotic striatal NBs specified towards a SPN fate, in the context of cell therapies for HD). Even though cell sorting has been explored to isolate dopaminergic progenitors as part of CRT strategies for PD (Doi et al., 2014; Fathi et al., 2018; Lehnen et al., 2017), cell surface markers which allow isolation of SPN progenitors have not been reported to our knowledge. Our cell surface marker screening has identified several known cell surface proteins as potential postmitotic striatal NB markers at a transcriptional level (CD24, NCAM1, CD200, NGFR, GPM6A). Some of these markers have been used in the past for cell selection strategies: CD24, for instance, has been used to select hPSC-derived NBs and neurons following *in vitro* differentiation (Pruszak et al., 2009), as well as committed excitatory and inhibitory neuronal lineages from dissected human fetal brains (Dan Liu et al., 2023). Another example is NCAM1, which is considered a marker of immature neuronal cells, and has been employed in sorting strategies to obtain homogeneous hPSC-derived neural grafts which showed no evidence

of graft overgrowth *in vivo* after 12 weeks (Kim et al., 2012). The lack of specificity showed by these and other markers at a protein level could be related to a lack of mRNA-protein correspondence, since many studies have shown notoriously poor correlation (~40%) between mRNA and protein expression levels (De Sousa Abreu et al., 2009; Maier et al., 2009; C. Vogel & Marcotte, 2012). Additionally, it is also possible that the epitope/antibody combinations tested in our FC-based screening are not compatible with cell sorting.

In this study, we identified CD200 as a useful cell surface marker of hPSC-derived striatal postmitotic NBs specified towards a SPN fate, which allows for superior discrimination of this subpopulation at a protein level compared to other promising cell surface marker candidates (e.g., NGFR). CD200 is a type I transmembrane glycoprotein mainly expressed by neurons and endothelial cells highly modulated during CNS development (Shrivastava et al., 2012), usually showing a diffuse distribution in the brain parenchyma and a higher intensity in grey matter compared to white matter areas, both in mice and humans (Koning et al., 2009; Shrivastava et al., 2012). Furthermore, neuronal CD200 is a well-known potent immunosuppressive and immunomodulatory molecule (Comella-Bolla et al., 2019; Heneka et al., 2014; Koning et al., 2009; Shrivastava et al., 2012) whose downregulation is a common feature of endangered neurons in the context of NDs, and which could trigger the innate immune response chronically activating microglia to stop disease progression (Heneka et al., 2014). In addition, a previous study by our group showed an increase in CD200 gene expression and protein levels in the neocortex, hippocampus, and striatum along with HD pathogenesis in a HD mouse model, which suggested a role of the extra CD200 ligand as a neurotrophic signal to sustain or extend neuronal function in the latest stages of HD as pro-survival mechanism (Comella-Bolla et al., 2019). Furthermore, we also identified NGFR as a postmitotic NB marker. Even if NGFR expression in SPNs is well known (Wehner et al., 2016), this marker has been also identified by previous studies as a marker of immature neural stem and precursor cells, being used to isolate a population of highly proliferative SVZ precursor cells (Young et al., 2007).

2.2. Selection of cell sorting technique for transplantation purposes: purity vs sorting efficiency and cell stress reduction

We also established proof-of-concept that CD200-based FACS could be used to define the exact final composition of a cell therapy product composed of purified

postmitotic striatal NBs. However, we found that the application of this method for the isolation of this low abundance, particularly sensitive cell subpopulation was associated with serious limitations which hamper the use of sorted cells in transplantation. It has been reported that MACS has comparable efficiency to FACS for isolation of hPSC-derived neuronal progenitor cells while reducing cell stress and improving viability, sorting yield and recovery time (Bowles et al., 2019). Other advantages of MACS over FACS include: speed as MACS is 4-6 times faster than FACS (Bowles et al., 2019; Sutermaster & Darling, 2019); scalability, allowing for vast increases in input cell numbers without appreciable increases in sorting time; and simplicity as it can be performed in a cell culture hood, reducing the risk of contamination from other facilities and mechanical fault. In this work, we have showed that CD200-based selection using MACS allows for high-yield reproducible isolation of low-abundance cell populations such as hPSC-derived $CD200^{high}$ postmitotic striatal progenitors. This approach did not affect cell viability, minimized sorting-associated cell stress, and did not result in abnormal proliferative phenotypes following differentiation.

2.3. While CD200-based selection results in enrichment of post-mitotic striatal NBs, selection at 16 DIV results in reduced batch-to-batch variability but increased mortality of sorted populations compared to selection at 12 DIV

We have proved that the use of CD200 for selection of post-mitotic striatal NBs constitutes a simple yet powerful method to control the composition of the final graft, obtaining homogeneous cell products amenable to be used for regenerative medicine applications. In fact, we demonstrated efficient and consistent enrichment of $CD200^{high}$ postmitotic striatal NBs in a cell line independent fashion from mixed populations of hPSC-derived telencephalic progenitors. We showed that this method leads to a reduction in the heterogeneity of the final cell product (by giving rise to a huge enrichment in $CD200^{high}$ striatal NBs), in a cell line independent fashion. This is important, since a general obstacle to the clinical translation of stem cell-derived therapeutic products is their limited purity, which results in heterogeneous cell compositions which ultimately causes variability in the quality and potency of the resulting cell products (Bachoud-Lévi et al., 2021; Stemberger et al., 2012). Consequently, current guidelines and recommendations from regulatory agencies such as the FDA and the European Medicines Agency (EMA), and independent organizations (ISCCR) on quality control and release criteria for investigational stem cell-derived ATMPs emphasize the need to define the composition of stem cell-based products as completely as possible, including at a

minimum the proportion of therapeutic target cells responsible for the bioactivity within the final cell product (EMA, 2011; FDA, 2008; ISCCR, 2021). To date, cell product impurity has hampered clinical translation of cell therapies for HD, due to variable yields of cells of an appropriate SPN phenotype (Bachoud-Lévi et al., 2021; Dunnett & Rosser, 2014). To make these promising treatments more effective and predictable, methods to ensure the enrichment of cell populations known to mediate clinical effects (i.e., striatal SPN progenitors) at the highest possible purity to generate well-defined cell preparations are required (Stemberger et al., 2012). For the translation of cell-based therapies to the clinical level, cell selection steps before transplantation to control cell populations, heterogeneity and yield will likely be required for reasons of reproducibility and to maximize therapeutic efficiency (Pruszak et al., 2007), which underlines the importance of the results of this study.

We also demonstrated the feasibility of performing CD200-based selection in mixed populations of hPSC-derived telencephalic progenitors at different timepoints of *in vitro* differentiation (i.e., 12 DIV and 16 DIV). As such, we showed that this cell sorting method leads to efficient selection of striatal NBs regardless of the sorting timepoint. Selection at 16 DIV consistently led to a reduction in the batch-to-batch variability of the final cell product, as evidenced by decreased standard deviation of the relative abundance of progenitors of interest in the sorted population compared to the unsorted population). However, we observed that the batch-to-batch variability of the positive fraction following CD200-based cell sorting at 12 DIV was increased, suggesting that application of NB selection at 12 DIV is less consistent than selection at 16 DIV. This could be related to the lower relative abundance of $CD200^{high}$ cells in 12 DIV cell populations (~5%) compared to 16 DIV cultures (30-35%) combined with the low discrimination power of MACS. Additionally, this sorting strategy does not have an impact on cell viability and does not result in abnormal proliferative phenotypes following differentiation regardless of the sorting timepoint. Interestingly, we found that cell viability in unsorted populations was significantly higher at 12 DIV than at 16 DIV. This observation is consistent with the higher amount (~7-fold) of $CD200^{high}$ post-mitotic NBs at 16 DIV, which are more fragile and prone to die as a consequence of cell harvest and cell sorting.

2.4. CD200^{high} NBs display a more mature neuronal phenotype compared to CD200^{low} NPCs, although differences are diluted as in vitro differentiation progresses

Furthermore, CD200^{high} NBs display hallmark characteristics of SPN progenitors of the developing striatum, as well as a more mature neuronal phenotype compared to CD200^{low} NPCs. In fact, CD200^{high} NBs display upregulation of genes related to cell signaling or synapsis, while CD200^{low} NPCs are characterized by expression of genes related to macromolecule biosynthesis or cytoplasmatic protein translation which are associated to proliferative cells. This constitutes an important advantage for transplantation purposes given their increased SPN specification.

However, upon *in vitro* striatal differentiation, these differences are diluted over time, with unsorted and sorted cultures ultimately displaying a homogeneous neuronal morphology and similar transcriptional profile. Further experiments are needed to investigate the cause of this results. However, a potential explanation for this outcome is that following cell sorting, the protocol we used terminal for *in vitro* striatal differentiation involves application of a small molecule cocktail (including γ-secretase inhibitors or CK4/6is) to induce forced cell cycle exit (Comella-Bolla et al., 2020; Telezhkin et al., 2016). This cocktail was originally optimized to be used in cell populations composed mainly of proliferating NPCs (in order to induce differentiation into post-mitotic NBs); as such, it is possible that the differentiation conditions and signaling factors need to be optimized for a correct neuronal differentiation of isolated post-mitotic CD200^{high} NBs.

2.5. *Sorted NBs survive transplantation in mice, but longer-term transplantation studies in HD models will be required to evaluate its potential for CRT applications*

Here, we have confirmed the sorted striatal NBs survive transplantation, which could be explained by the fact that they are early postmitotic progenitors which are not as sensitive as mature neurons. It is necessary to transplant SPN-committed progenitors, since mature SPNs cannot survive transplantation (Rosser et al., 2022). We have demonstrated that sorted CD200^{high} NBs displayed a more mature neuronal phenotype compared to the NPCs, which constitutes an important advantage for transplantation purposes given their increased SPN specification. However, at the same time, this also constituted a potential risk since NBs could prove to be more sensitive than these NPCs and die because of transplantation. This constitutes an insightful proof-of-concept to

explore longer-term transplantation of this cell subpopulation to assess its potential as a cell therapy product for HD.

We have also confirmed the increased value of CD200-based selection from a safety point of view *in vivo since* it greatly reduces the presence of proliferative cells and potential for tumorigenesis since remaining undifferentiated hPSCs pose a risk of teratoma formation after transplantation. We did not observe any evidence of teratomas after transplantation of these postmitotic progenitors; furthermore, our analysis not only revealed no cell overgrowth in the striatum but also an almost complete absence of proliferative cells in the positive fraction, which were indeed detected in the unsorted and negative fractions. The lack of graft overgrowth could stem from our transplantation of postmitotic SPN neuroblasts, more mature than unsorted populations normally used for transplantation purposes.

3. Isolation of distinct subpopulations of hPSC-derived post-mitotic striatal NBs

In the context of CRTs for NDs, targeting the right cell type with cell therapy is crucial for success. In addition to the aforementioned general benefits of the isolation of post-mitotic NBs for transplantation purposes, selection of specific NB subtypes can be used to tailor cell therapies to precisely replace the cells lost due to a specific condition.This focused approach offers a more promising avenue for effective and targeted treatment of NDs. For instance, isolation of iNBs in particular could be of great interest for potential CRT strategies in HD as a way to specifically address the source of the underlying imbalance present in the disease.

One potential strategy for the selection of specific NB subpopulations that give rise to different neuronal subtypes such as dSPNs and iSPNs would entail the use of multiple antibodies targeting subtype-specific markers at the same time point. In this work, we have established that CD200 is a marker of post-mitotic striatal NBs, which can be used to enrich these progenitor subpopulations in heterogenous cell mixtures. However, this enrichment is not subtype-specific with CD200 being a marker of both dNBs and iNBs. In the third part of this work, and to develop a simple method to isolate specific striatal NB subpopulations, we investigated whether cell sorting of different striatal progenitor subpopulations could be achieved by using a single marker (i.e., CD200) at several time points (i.e., 12 DIV, 16 DIV). . We hypothesized that such a strategy would be successful

if, similar to what has been described for endogenous striatal development, specification of SPN subtypes occurs at different timepoints (Tinterri et al., 2018).

To that aim, we investigated how hPSC-derived striatal dNB and iNB subpopulations are specified *in vitro* when using our striatal differentiation protocol (Comella-Bolla et al., 2020). Furthermore, we have built on our previous results and used CD200 to sort and characterize striatal NB subpopulations derived from hPSCs at different timepoints of our *in vitro* striatal differentiation protocol.

3.1. In vitro specification of hPSC-derived SPN subtypes recapitulates endogenous striatal development

In this work, transcriptional analysis of heterogeneous cell populations resulting from *in vitro* striatal differentiation of hPSCs revealed that the two main striatal NB subtypes (dNBs and iNBs) are generated *in vitro* at different timepoints. More specifically, we observed that dNBs were born earlier (12 DIV) than iNBs (16 DIV). Previous birthdating experiments in mice have shown that the majority of earliest-born SPNs are dSPNs and iSPNs are generated at later post-mitotic embryonic stages (Kelly et al., 2018). A recent study has also hinted at a potential earlier specification of dSPNs during development, showing that transcriptional networks involved in dSPN development are enriched with markers of early-born neurons compare to transcriptional networks involved in iSPN development. Additionally, this study also demonstrated that dSPNs have an extended period of gene expression dynamics and slower differentiation kinetics relative to iSPNs (Anderson et al., 2023). Taking all these results together, our findings suggest that *in vitro* specification of SPN subtypes mirroring what has been observed during endogenous striatal development (Tinterri et al., 2018).

3.2. CD200-based selection can be used to obtain cell products specifically enriched in dNBs, but isolation of iNBs is more challenging

This work sheds light on the feasibility of isolating specific striatal progenitor populations, paving the way for further development of CRT strategies for HD. For instance, strategies to allow isolation of iSPN progenitors would be of great interest, as they may provide a therapeutic advantage to counterbalance the preferential loss of this subpopulation observed in earlier stages of HD. We demonstrated CD200-based selection at different timepoints of *in vitro* differentiation (e.g., 12 DIV and 16 DIV) leads to the

obtention of cell compositions enriched in different subtypes of hPSC-derived postmitotic striatal NBs.

Our data indicated that CD200 identifies two different subpopulations of striatal NB subpopulations correctly specified towards an SPN fate, Type A and type B NBs. Interestingly, while both NB subpopulations are characterized by expression of ventral forebrain markers, we observed that type A NBs were defined by expression of markers of SPN progenitors (DLX1, DLX2, DLX,5 and DLX6; Long et al., 2009; Martín-Ibáñez et al., 2012) and markers involved in specification of iSPNs (SP8 and SIX3; Song et al., 2021; Xu et al., 2018), while type B NBs were defined by expression of markers involved in specification of dSPNs (FOXP2, and EBF1; Lobo et al., 2008). These results suggest that the identity of type A and type B NBs could correspond to indirect and direct pathway SPN progenitors, respectively.

Of note, cell selection at 12 DIV leads to enrichment of mostly dNBs. Hence, our strategy holds the potential to permit the obtention of cell products highly enriched in NBs specified towards a dSPN fate, which could potentially be further evaluated for multiple applications. For example, transplantation of these cell may provide a novel therapeutic strategy for NDs with underlying striatonigral degeneration. An example is the parkinsonian subtype of multiple system atrophy (MSA-P), characterized by degenerative changes in the SNpc and the putamen and for which transplantation of striatal grafts could provide a potential neuroprotective efficacy against striatal excitotoxicity (Wenning et al., 2000).

Notably, the approach described in this thesis does not allow for obtention of a defined cell product enriched in iNBs, since CD200-based cell sorting results in enrichment of both striatal NB subtypes (i.e., dNBs and iNBs) . Nevertheless, the ability to separate NPCs and NBs from each other at different timepoints may potentially allow to enrich for different neuronal types. For example, if the pool of $CD200^{low}$ NPCs present in 16 DIV cultures was sorted and further differentiated, it may eventually be enriched for iNBs given that our results suggest that 16 DIV NPCs are enriched for the indirect pathway subtype and primarily specify iNBs.

3.3.Accelerated differentiation NBs sorted at 16 DIV into SPNs-like neurons with increased FOXP1 and DRD2 expression, but decreased CTIP2 expression

We also demonstrated the capacity of striatal $CD200^{high}$ NBs sorted at 16 DIV to differentiate into neurons with the target SPN phenotype *in vitro*. Our results demonstrate an acceleration of $CD200^{high}$ NBs differentiation into SPN-like neurons compared to the $CD200^{low}$ NPCs, as indicated by a higher yield of $GABA^+/FOXP1^+$ cells. Surprisingly, we have also found that CD200-based selection leads to a reduced yield of CTIP2 expression at mRNA and protein levels following terminal *in vitro* striatal differentiation. Altogether, these observations could be explained by the different expression time windows of the SPN markers FOXP1 and CTIP2. Whereas FOXP1 is a marker of SPNs from an early progenitor stage right through to adulthood (Precious et al., 2016), CTIP2 is first expressed in immature SPNs but not in SPN progenitors (Arlotta et al., 2008). Hence, our findings could reflect the relative immaturity of the cells *in vitro*, which may be SPN progenitors not yet expressing CTIP2. Furthermore, CTIP2 is also a marker of neurons that reside in layer 5 of the cortex (Arlotta et al., 2005). Given that most of the $CTIP2^+$ neurons detected in unsorted and negative fractions present negative or low GABA expression, we hypothesize that the increased relative abundance of $CTIP2^+$ neurons in these fractions compared to the sorted populations may be attributable to a population of off-target cortical $CTIP2^+$ neurons in these fractions. Of note, we have previously reported generation of a small percentage of glutamatergic cortical neurons by our *in vitro* differentiation protocol (Comella-Bolla et al., 2020). However, given our observations, we hypothesize that cortical specification in our protocol could happen at a later timepoint than SPN specification. In this scenario, we propose that cortical progenitors could mainly be composed of proliferating NPCs at the time of sorting. This could provide a plausible explanation to the lack of enrichment of cortical progenitors following selection, considering the fact that CD200 is a marker of all post-mitotic NBs regardless of their specification.

Interestingly, we also observed ~58% increase in DRD2 mRNA expression in $CTIP2^+$ cells derived from sorted $CD200^{high}$ NBs compared to $CD200^{low}$ NPCs, which suggests that specification of $CD200^{high}$ NBs sorted at this timepoint could be biased towards an iSPN fate. This underscores the potential of these sorted NBs to be used for cell therapy in HD (considering the earlier vulnerability of iSPNs during this condition),

and future transplantation studies in animal models are warranted to confirm whether these observations are maintained *in vivo*.

3.4. 12 DIV populations display less efficient generation of SPN subtypes

On the other hand, we showed that terminal *in vitro* differentiation of 12 DIV cell populations leads to reduced viability and much less efficient generation of SPN subtypes compared to 16 DIV cell populations. This can be potentially explained by the fact that as part of our *in vitro* differentiation protocol, neuronal differentiation and maturation is not induced until 16 DIV; as such, early application of the cocktail of small molecules that stimulate cell cycle exit and neuronal maturation to less mature 12 DIV cultures may be the underlying cause of these inferior outcomes. This hypothesis is further supported by our observation that $CD200^{high}$ NBs sorted at 16 DIV showed an upregulation of genes related to nervous system development, neurogenesis or synapsis compared to $CD200^{high}$ NBs sorted at 12 DIV, which suggest a less mature neuronal phenotype an of the latter. Furthermore, this observation is maintained upon completion of *in vitro* differentiation, further underscoring the lower potential for neuronal differentiation of 12 DIV populations using our protocol.

CONCLUSIONS

Conclusions

I. Standardization of cell culture conditions via implementation of a Quality Management System (QMS) leads to a striking improvement of genomic stability in hPSC lines cultured *in vitro*.

II. High expression of the cell surface marker CD200 identifies hPSC-derived postmitotic striatal neuroblasts (NBs).

III. CD200-based selection can be used to generate highly purified cell compositions enriched in hPSC-derived postmitotic striatal NBs.

IV. hPSC-derived postmitotic striatal NBs survive transplantation into the striatum of adult mice and reduce the risk of teratoma formation *in vivo*.

V. Use of CD200- based selection at different timepoints results in obtention of cell compositions enriched in different subtypes of hPSC-derived postmitotic striatal NBs.

BIBLIOGRAPHY

Bibliography

Adil, M. M., Gaj, T., Rao, A. T., Kulkarni, R. U., Fuentes, C. M., Ramadoss, G. N., Ekman, F. K., Miller, E. W., & Schaffer, D. V. (2018). hPSC-Derived Striatal Cells Generated Using a Scalable 3D Hydrogel Promote Recovery in a Huntington Disease Mouse Model. *Stem Cell Reports*, *10*(5), 1481–1491. https://doi.org/10.1016/j.stemcr.2018.03.007

Agbas, A. (2018). Trends of Protein Aggregation in Neurodegenerative Diseases. *Neurochemical Basis of Brain Function and Dysfunction*. https://doi.org/10.5772/INTECHOPEN.81224

Aguila, J. C., Blak, A., van Arensbergen, J., Sousa, A., Vázquez, N., Aduriz, A., Gayosso, M., Lopez Mato, M. P., Lopez de Maturana, R., Hedlund, E., Sonntag, K.-C., & Sanchez-Pernaute, R. (2014). Selection Based on FOXA2 Expression Is Not Sufficient to Enrich for Dopamine Neurons From Human Pluripotent Stem Cells. *Stem Cells Translational Medicine*, *3*(9), 1032–1042. https://doi.org/10.5966/SCTM.2014-0011/-/DC1

Albin, R. L., Young, A. B., & Penney, J. B. (1989). The functional anatomy of basal ganglia disorders. *Trends in Neurosciences*, *12*(10), 366–375. https://doi.org/https://doi.org/10.1016/0166-2236(89)90074-X

Alexander, G. E., DeLong, M. R., & Strick, P. L. (2003). Parallel Organization of Functionally Segregated Circuits Linking Basal Ganglia and Cortex. *Https://Doi.Org/10.1146/Annurev.Ne.09.030186.002041*, *VOL. 9*, 357–381. https://doi.org/10.1146/ANNUREV.NE.09.030186.002041

Amps, K., Andrews, P. W., Anyfantis, G., Armstrong, L., Avery, S., Baharvand, H., Baker, J., Baker, D., Munoz, M. B., Beil, S., Benvenisty, N., Ben-Yosef, D., Biancotti, J. C., Bosman, A., Brena, R. M., Brison, D., Caisander, G., Camarasa, M. V., Chen, J., … Zhou, Q. (2011). Screening ethnically diverse human embryonic stem cells identifies a chromosome 20 minimal amplicon conferring growth advantage. *Nature Biotechnology 2011 29:12*, *29*(12), 1132–1144. https://doi.org/10.1038/nbt.2051

Anderson, A. G., Kulkarni, A., Harper, M., Correspondence, G. K., & Konopka, G. (2020). Single-cell analysis of Foxp1-driven mechanisms essential for striatal development. *Cell.ComAG Anderson, A Kulkarni, M Harper, G KonopkaCell Reports, 2020•cell.Com*. https://doi.org/10.1016/j.celrep.2020.02.030

Anderson, A. G., Kulkarni, A., & Konopka, G. (2023). A single-cell trajectory atlas of striatal development. *Scientific Reports 2023 13:1*, *13*(1), 1–11. https://doi.org/10.1038/s41598-023-36255-5

Anderson, S. A., Eisenstat, D. D., Shi, L., & Rubenstein, J. L. R. (1997). Interneuron migration from basal forebrain to neocortex: dependence on Dlx genes. *Science (New York, N.Y.)*, *278*(5337), 474–476. https://doi.org/10.1126/SCIENCE.278.5337.474

Andrews, P. W. (2002). From teratocarcinomas to embryonic stem cells. *Philosophical Transactions of the Royal Society of London. Series B, Biological Sciences*, *357*(1420), 405–417. https://doi.org/10.1098/rstb.2002.1058

Arber, C., Precious, S., Cambray, S., Risner-Janiczek, J., Chang, K.-H., Ungless, M. A., Rodriguez, T. A., Rosser, A., Dunnett, S., & Li, M. (2012). A novel strategy for generating transplantable DARPP32-positive striatal projection neurons from human pluripotent stem cells. *Nature Biotech.*, *submitted* .

Arlotta, P., Molyneaux, B. J., Chen, J., Inoue, J., Kominami, R., & MacKlis, J. D. (2005). Neuronal Subtype-Specific Genes that Control Corticospinal Motor Neuron Development In Vivo. *Neuron*, *45*(2), 207–221. https://doi.org/10.1016/J.NEURON.2004.12.036

Arlotta, P., Molyneaux, B. J., Jabaudon, D., Yoshida, Y., & Macklis, J. D. (2008). Ctip2 controls the differentiation of medium spiny neurons and the establishment of the cellular architecture of the striatum. *Journal of Neuroscience*, *28*(3), 622–632. https://doi.org/10.1523/JNEUROSCI.2986-07.2008

Aron Badin, R., Bugi, A., Williams, S., Vadori, M., Michael, M., Jan, C., Nassi, A., Lecourtois, S., Blancher, A., Cozzi, E., Hantraye, P., & Perrier, A. L. (2019). MHC matching fails to prevent long-term rejection of iPSC-derived neurons in non-human primates. *Nature Communications 2019 10:1*, *10*(1), 1–12. https://doi.org/10.1038/s41467-019-12324-0

Atkin, N. B., & Baker, M. C. (1982). Specific chromosome change, i(12p), in testicular tumours? *Lancet (London, England)*, *2*(8311), 1349. https://doi.org/10.1016/S0140-6736(82)91557-4

Aubry, L., Bugi, A., Lefort, N., Rousseau, F., Peschanski, M., & Perrier, A. L. (2008). Striatal progenitors derived from human ES cells mature into DARPP32 neurons in vitro and in quinolinic acid-lesioned rats. *Proceedings of the National Academy of Sciences of the United States of America*, *105*(43), 16707–16712. https://doi.org/10.1073/pnas.0808488105

Avery, S., Hirst, A. J., Baker, D., Lim, C. Y., Alagaratnam, S., Skotheim, R. I., Lothe, R. A., Pera, M. F., Colman, A., Robson, P., Andrews, P. W., & Knowles, B. B. (2013). BCL-XL mediates the strong selective advantage of a 20q11.21 amplification commonly found in human embryonic stem cell cultures. *Stem Cell Reports*, *1*(5), 379–386. https://doi.org/10.1016/j.stemcr.2013.10.005

Avior, Y., Sagi, I., & Benvenisty, N. (2016). Pluripotent stem cells in disease modelling and drug discovery. *Nature Reviews Molecular Cell Biology*, *17*(3), 170–182. https://doi.org/10.1038/nrm.2015.27

Bachoud-Levi, A. C., Remy, P., Nguyen, J. P., Brugieres L, P., Efaucheur, J. P., Bourdet, C., Baudic, S., Gaura, V., Maison, P., Haddad, B., & Boissé Grandmougin T. Jény R. Bar- tolomeo P. Dalla Barba G. Degos J. D. Lisovoski F. Ergis A. M. Pailhous E. Cesaro P. Hantraye P. and Peschanski M., M. F. (2000). Motor and cognitive improvements in patients with Huntington's disease after neural transplantation. *Lancet*, *356*, 1975–1979.

Bachoud-Lévi, A.-C. (2017). Chapter 10 - From open to large-scale randomized cell transplantation trials in Huntington's disease: Lessons from the multicentric intracerebral grafting in Huntington's disease trial (MIG-HD) and previous pilot studies. In S. B. Dunnett & A. B. T.-P. in B. R. Björklund (Eds.), *Functional Neural Transplantation IV* (Vol. 230, pp. 227–261). Elsevier. https://doi.org/https://doi.org/10.1016/bs.pbr.2016.12.011

Bachoud-Lévi, A.-C., Bourdet, C., Brugières, P., Nguyen, J.-P., Grandmougin, T., Haddad, B., Jény, R., Bartolomeo, P., Boissé, M.-F., Barba, G. D., Degos, J.-D., Ergis, A.-M., Lefaucheur, J.-P., Lisovoski, F., Pailhous, E., Rémy, P., Palfi, S., Defer, G. L., Cesaro, P., … Peschanski, M. (2000). Safety and Tolerability Assessment of Intrastriatal Neural Allografts in Five Patients with Huntington's Disease. *Experimental Neurology*, *161*(1), 194–202. https://doi.org/https://doi.org/10.1006/exnr.1999.7239

Bachoud-Lévi, A.-C., Gaura, V., Brugieres, P., Lefaucheur J. P., B. M. F. M. P. B. S. R. M. J. B. C. R. P. C. P. H. P., & Peschanski, M. (2006). Effect of fetal neural transplants in patients with Huntington's disease 6 years after surgery: a long-term follow-up study. *Lancet Neurol*, *5*, 303–309.

Bachoud-Lévi, A.-C., Hantraye, P., & Peschanski, M. (2002). Fetal neural grafts for Huntington's disease: A prospective view. *Movement Disorders*, *17*(3), 439–444. https://doi.org/10.1002/mds.10117

Bachoud-Lévi, A.-C., Massart, R., & Rosser, A. (2021). Cell therapy in Huntington's disease: Taking stock of past studies to move the field forward. *STEM CELLS*, *39*(2), 144–155. https://doi.org/https://doi.org/10.1002/stem.3300

Baker, D. E. C., Harrison, N. J., Maltby, E., Smith, K., Moore, H. D., Shaw, P. J., Heath, P. R., Holden, H., & Andrews, P. W. (2007). Adaptation to culture of human embryonic stem cells and oncogenesis in vivo. *Nature Biotechnology*, *25*(2), 207–215. https://doi.org/10.1038/nbt1285

Baker, D., Hirst, A. J., Gokhale, P. J., Juarez, M. A., Williams, S., Wheeler, M., Bean, K., Allison, T. F., Moore, H. D., Andrews, P. W., & Barbaric, I. (2016). Detecting Genetic Mosaicism in Cultures of Human Pluripotent Stem Cells. *Stem Cell Reports*, *7*(5), 998–1012. https://doi.org/https://doi.org/10.1016/j.stemcr.2016.10.003

Baker, M. (2016). IS THERE A REPRODUCIBILITY CRISIS? *Nature*, *533*, 452–454.

Barboza, L. A., & Ghisi, N. C. (2018). Evaluating the current state of the art of Huntington disease research: a scientometric analysis . In *Brazilian Journal of Medical and Biological Research* (Vol. 51). scielo .

Barker, R. A., Mason, S. L., Harrower, T. P., Swain, R. A., Ho, A. K., Sahakian, B. J., Mathur, R., Elneil, S., Thornton, S., Hurrelbrink, C., Armstrong, R. J., Tyers, P., Smith, E., Carpenter, A., Piccini, P., Tai, Y. F., Brooks, D. J., Pavese, N., Watts, C., … Dunnett, S. B. (2013). The long-term safety and efficacy of bilateral transplantation of human fetal striatal tissue in patients with mild to moderate Huntington's disease. *Journal of Neurology, Neurosurgery and Psychiatry*, *84*(6), 657–665. https://doi.org/10.1136/jnnp-2012-302441

Barker, R. A., Parmar, M., Studer, L., & Takahashi, J. (2017). Human Trials of Stem Cell-Derived Dopamine Neurons for Parkinson's Disease: Dawn of a New Era. In *Cell Stem Cell* (Vol. 21, Issue 5, pp. 569–573). Cell Press. https://doi.org/10.1016/j.stem.2017.09.014

Bartus, R. T., & Johnson, E. M. (2017). Clinical tests of neurotrophic factors for human neurodegenerative diseases, part 1: Where have we been and what have we learned? *Neurobiology of Disease*, *97*, 156–168. https://doi.org/https://doi.org/10.1016/j.nbd.2016.03.027

Bates, G. P., Dorsey, R., Gusella, J. F., Hayden, M. R., Kay, C., Leavitt, B. R., Nance, M., Ross, C. A., Scahill, R. I., Wetzel, R., Wild, E. J., & Tabrizi, S. J. (2015). Huntington disease. *Nature Reviews Disease Primers*, *1*, 15005.

Baydyuk, M., & Xu, B. (2012). BDNF in Huntington's Disease: Role in Pathogenesis and Treatment. *Huntington's Disease - Core Concepts and Current Advances*. https://doi.org/10.5772/31359

Ben-David, U., Arad, G., Weissbein, U., Mandefro, B., Maimon, A., Golan-Lev, T., Narwani, K., Clark, A. T., Andrews, P. W., Benvenisty, N., & Carlos Biancotti, J. (2014). Aneuploidy induces profound changes in gene expression, proliferation and tumorigenicity of human pluripotent stem cells. *Nature Communications*, *5*, 4825. https://doi.org/10.1038/ncomms5825

Ben-David, U., Benvenisty, N., & Mayshar, Y. (2010). Genetic instability in human induced pluripotent stem cells: Classification of causes and possible safeguards. *Cell Cycle*, *9*(23), 4603–4604. https://doi.org/10.4161/cc.9.23.14094

Beroukhim, R., Mermel, C. H., Porter, D., Wei, G., Raychaudhuri, S., Donovan, J., Barretina, J., Boehm, J. S., Dobson, J., Urashima, M., Mc Henry, K. T., Pinchback, R. M., Ligon, A. H., Cho, Y.-J., Haery, L., Greulich, H., Reich, M., Winckler, W., Lawrence, M. S., … Meyerson, M. (2010). The landscape of somatic copy-number alteration across human cancers. *Nature*, *463*(7283), 899–905. https://doi.org/10.1038/nature08822

Besusso, D., Schellino, R., Boido, M., Belloli, S., Parolisi, R., Conforti, P., Faedo, A., Cernigoj, M., Campus, I., Laporta, A., Bocchi, V. D., Murtaj, V., Parmar, M., Spaiardi, P., Talpo, F., Maniezzi, C., Toselli, M. G., Biella, G., Moresco, R. M., … Cattaneo, E. (2020). Stem Cell-Derived Human Striatal Progenitors Innervate Striatal Targets and Alleviate Sensorimotor Deficit in a Rat Model of Huntington Disease. *Stem Cell Reports*, *14*(5), 876–891. https://doi.org/10.1016/J.STEMCR.2020.03.018/ATTACHMENT/D54B5F19-EA91-40C7-B083-58EF420CAE7C/MMC1.PDF

Bolam, J. P., Hanley, J. J., Booth, P. A., & Bevan, M. D. (2000). Synaptic organisation of the basal ganglia. *Journal of Anatomy*, *196 (Pt 4*(Pt 4), 527–542. https://doi.org/10.1046/j.1469-7580.2000.19640527.x

Bowles, K. R., Julia, T. C. W., Qian, L., Jadow, B. M., & Goate, A. M. (2019). Reduced variability of neural progenitor cells and improved purity of neuronal cultures using

magnetic activated cell sorting. *PLoS ONE*, *14*(3). https://doi.org/10.1371/JOURNAL.PONE.0213374

Bradley, C. K., Scott, H. A., Chami, O., Peura, T. T., Dumevska, B., Schmidt, U., & Stojanov, T. (2011). Derivation of Huntington's disease-affected human embryonic stem cell lines. *Stem Cells and Development*, *20*(3), 495–502. https://doi.org/10.1089/scd.2010.0120

Brimblecombe, K. R., & Cragg, S. J. (2017). The Striosome and Matrix Compartments of the Striatum: A Path through the Labyrinth from Neurochemistry toward Function. *ACS Chemical Neuroscience*, *8*(2), 235–242. https://doi.org/10.1021/acschemneuro.6b00333

Canals, J. M., Pineda, J. R., Torres-Peraza, J. F., Bosch, M., Martín-Ibañez, R., & Alberch, J. (2004). Brain-Derived Neurotrophic Factor Regulates the Onset and Severity of Motor Dysfunction Associated with Enkephalinergic Neuronal Degeneration in Huntington's Disease. *Journal of Neuroscience*, *24*(35), 7727–7739. https://doi.org/10.1523/JNEUROSCI.1197-04.2004

Capetian, P., Knoth, R., Maciaczyk, J., Pantazis, G., Ditter, M., Bokla, L., Landwehrmeyer, G. B., Volk, B., & Nikkhah, G. (2009). Histological findings on fetal striatal grafts in a Huntington's disease patient early after transplantation. *Neuroscience*, *160*(3), 661–675. https://doi.org/https://doi.org/10.1016/j.neuroscience.2009.02.035

Carroll, J. B., Warby, S. C., Southwell, A. L., Doty, C. N., Greenlee, S., Skotte, N., Hung, G., Bennett, C. F., Freier, S. M., & Hayden, M. R. (2011). Potent and selective antisense oligonucleotides targeting single-nucleotide polymorphisms in the huntington disease gene / allele-specific silencing of mutant huntingtin. *Molecular Therapy*, *19*(12), 2178–2185. https://doi.org/10.1038/mt.2011.201

Cattaneo, E., Zuccato, C., & Tartari, M. (2005). Normal huntingtin function: an alternative approach to Huntington's disease. *Nature Reviews Neuroscience*, *6*(12), 919–930. https://doi.org/10.1038/nrn1806

Chen, S. Y., Lu, K. M., Ko, H. A., Huang, T. H., Hao, J. H. J., Yan, Y. T., Chang, S. L. Y., Evans, S. M., & Liu, F. C. (2020). Parcellation of the striatal complex into dorsal and ventral districts. *Proceedings of the National Academy of Sciences of the United States of America*, *117*(13), 7418–7429. https://doi.org/10.1073/PNAS.1921007117/SUPPL_FILE/PNAS.1921007117.SAPP.PDF

Chen, Y. J. J., Friedman, B. A., Ha, C., Durinck, S., Liu, J., Rubenstein, J. L., Seshagiri, S., & Modrusan, Z. (2017). Single-cell RNA sequencing identifies distinct mouse medial ganglionic eminence cell types. *Scientific Reports*, *7*. https://doi.org/10.1038/SREP45656

Chevalier, G., Vacher, S., Deniau, J. M., & Desban, M. (1985). Disinhibition as a basic process in the expression of striatal functions. I. The striato-nigral influence on tecto-spinal/tecto-diencephalic neurons. *Brain Research*, *334*(2), 215–226. https://doi.org/https://doi.org/10.1016/0006-8993(85)90213-6

Choompoo, N., Bartley, O. J. M., Precious, S. V., Vinh, N. nga, Schnell, C., Garcia, A., Roberton, V. H., Williams, N. M., Kemp, P. J., Kelly, C. M., & Rosser, A. E. (2021). Induced pluripotent stem cells derived from the developing striatum as a potential donor source for cell replacement therapy for Huntington disease. *Cytotherapy*, *23*(2), 111–118. https://doi.org/10.1016/J.JCYT.2020.06.001/ATTACHMENT/462A6D5F-9B4C-40E0-A36C-0184179E7A1C/MMC1.DOCX

Cicchetti, F., Prensa, L., Wu, Y., & Parent, A. (2000). Chemical anatomy of striatal interneurons in normal individuals and in patients with Huntington's disease. *Brain Research Reviews*, *34*(1–2), 80–101. https://doi.org/10.1016/S0165-0173(00)00039-4

Cisbani, G., Freeman, T. B., Soulet, D., Saint-Pierre, M., Gagnon, D., Parent, M., Hauser, R. A., Barker, R. A., & Cicchetti, F. (n.d.). Striatal allografts in patients with Huntington's disease: impact of diminished astrocytes and vascularization on graft viability. *A JOURNAL OF NEUROLOGY*. https://doi.org/10.1093/brain/aws359

Comella-Bolla, A., Orlandi, J. G., Miguez, A., Straccia, M., García-Bravo, M., Bombau, G., Galofré, M., Sanders, P., Carrere, J., Segovia, J. C., Blasi, J., Allen, N. D., Alberch, J., Soriano, J., & Canals, J. M. (2020). Human Pluripotent Stem Cell-Derived Neurons Are Functionally Mature In Vitro and Integrate into the Mouse Striatum Following Transplantation. *Molecular Neurobiology*, 1–33. https://doi.org/10.1007/s12035-020-01907-4

Comella-Bolla, A., Valente, T., Miguez, A., Brito, V., Gines, S., Solà, C., Straccia, M., & Canals, J. M. (2019). CD200 is up-regulated in R6/1 transgenic mouse model of Huntington's disease. *PLOS ONE*, *14*(12), e0224901. https://doi.org/10.1371/JOURNAL.PONE.0224901

Corbin, J. G., Nery, S., & Fishell, G. (2001). Telencephalic cells take a tangent: non-radial migration in the mammalian forebrain. *Nature Neuroscience 2001 4:11*, *4*(11), 1177–1182. https://doi.org/10.1038/nn749

Crittenden, J. R., & Graybiel, A. M. (2011). Basal ganglia disorders associated with imbalances in the striatal striosome and matrix compartments. *Frontiers in Neuroanatomy*, *5*(SEP), 12277. https://doi.org/10.3389/FNANA.2011.00059/BIBTEX

Crittenden, J. R., Tillberg, P. W., Riad, M. H., Shima, Y., Gerfen, C. R., Curry, J., Housman, D. E., Nelson, S. B., Boyden, E. S., & Graybiel, A. M. (2016). Striosome-dendron bouquets highlight a unique striatonigral circuit targeting dopamine-containing neurons. *Proceedings of the National Academy of Sciences of the United States of America*, *113*(40), 11318–11323. https://doi.org/10.1073/PNAS.1613337113/SUPPL_FILE/PNAS.1613337113.SM01.AVI

Cui, G., Jun, S. B., Jin, X., Pham, M. D., Vogel, S. S., Lovinger, D. M., & Costa, R. M. (2013). Concurrent activation of striatal direct and indirect pathways during action

initiation. *Nature 2013 494:7436*, *494*(7436), 238–242. https://doi.org/10.1038/nature11846

Cyranoski, D. (2014). Japanese woman is first recipient of next-generation stem cells. In *Nature*. https://doi.org/10.1038/nature.2014.15915

da Cruz, L., Fynes, K., Georgiadis, O., Kerby, J., Luo, Y. H., Ahmado, A., Vernon, A., Daniels, J. T., Nommiste, B., Hasan, S. M., Gooljar, S. B., Carr, A.-J. F., Vugler, A., Ramsden, C. M., Bictash, M., Fenster, M., Steer, J., Harbinson, T., Wilbrey, A., … Coffey, P. J. (2018). Phase 1 clinical study of an embryonic stem cell-derived retinal pigment epithelium patch in age-related macular degeneration. *Nature Biotechnology*, *36*(4), 328–337. https://doi.org/10.1038/nbt.4114

Dan Liu, D., He, J. Q., Sinha, R., Eastman, A. E., Toland, A. M., Morri, M., Neff, N. F., Vogel, H., Uchida, N., & Weissman, I. L. (2023). *Purification and characterization of human neural stem and progenitor cells Graphical abstract*. https://doi.org/10.1016/j.cell.2023.02.017

De Sousa Abreu, R., Penalva, L. O., Marcotte, E. M., & Vogel, C. (2009). Global signatures of protein and mRNA expression levels. *Molecular BioSystems*, *5*(12), 1512–1526. https://doi.org/10.1039/B908315D

Deacon, T. W., Pakzaban, P., & Isacson, O. (1994). The lateral ganglionic eminence is the origin of cells committed to striatal phenotypes: neural transplantation and developmental evidence. *Brain Research*, *668*(1), 211–219. https://doi.org/https://doi.org/10.1016/0006-8993(94)90526-6

Delli Carri, A., Onorati, M., Castiglioni, V., Faedo, A., Camnasio, S., Toselli, M., Biella, G., & Cattaneo, E. (2013). Human Pluripotent Stem Cell Differentiation into Authentic Striatal Projection Neurons. *Stem Cell Reviews and Reports*, *9*(4), 461–474. https://doi.org/10.1007/s12015-013-9441-8

DeLong, M. R. (1990). Primate models of movement disorders of basal ganglia origin. *Trends in Neurosciences*, *13*(7), 281–285. https://doi.org/https://doi.org/10.1016/0166-2236(90)90110-V

DeLong, M., & Wichmann, T. (2010). Changing views of basal ganglia circuits and circuit disorders. In *Clinical EEG and Neuroscience* (Vol. 41, Issue 2, pp. 61–67). EEG and Clinical Neuroscience Society (ECNS). https://doi.org/10.1177/155005941004100204

Deng, Y. P., Xie, J. P., Wang, H. B., Lei, W. L., Chen, Q., & Reiner, A. (2007). Differential Localization of the GluR1 and GluR2 Subunits of the AMPA-type Glutamate Receptor Among Striatal Neuron Types in Rats. *Journal of Chemical Neuroanatomy*, *33*(4), 167. https://doi.org/10.1016/J.JCHEMNEU.2007.02.008

Di Maio, L., Squitieri, F., Napolitano, G., Campanella, G., Trofatter, J. A., & Conneally, P. M. (1993). Suicide risk in Huntington's disease. *Journal of Medical Genetics*, *30*(4), 293 LP – 295. https://doi.org/10.1136/jmg.30.4.293

DiFiglia, M., Sapp, E., Chase, K., Schwarz, C., Meloni, A., Young, C., Martin, E., Vonsattel, J.-P., Carraway, R., Reeves, S. A., Boyce, F. M., & Aronin, N. (1995).

Huntingtin is a cytoplasmic protein associated with vesicles in human and rat brain neurons. *Neuron*, *14*(5), 1075–1081. https://doi.org/https://doi.org/10.1016/0896-6273(95)90346-1

Divino, V., DeKoven, M., Warner, J. H., Giuliano, J., Anderson, K. E., Langbehn, D., & Lee, W. C. (2013). The direct medical costs of Huntington's disease by stage. A retrospective commercial and Medicaid claims data analysis. *Journal of Medical Economics*, *16*(8), 1043–1050. https://doi.org/10.3111/13696998.2013.818545

Dobin, A., Davis, C. A., Schlesinger, F., Drenkow, J., Zaleski, C., Jha, S., Batut, P., Chaisson, M., & Gingeras, T. R. (2013). STAR: ultrafast universal RNA-seq aligner. *Bioinformatics*, *29*(1), 15. https://doi.org/10.1093/BIOINFORMATICS/BTS635

Döbrössy, M. D., & Dunnett, S. B. (2003). Motor training effects on recovery of function after striatal lesions and striatal grafts. *Experimental Neurology*, *184*(1), 274–284. https://doi.org/https://doi.org/10.1016/S0014-4886(03)00028-1

Doi, D., Samata, B., Katsukawa, M., Kikuchi, T., Morizane, A., Ono, Y., Sekiguchi, K., Nakagawa, M., Parmar, M., & Takahashi, J. (2014). Isolation of Human Induced Pluripotent Stem Cell-Derived Dopaminergic Progenitors by Cell Sorting for Successful Transplantation. *Stem Cell Reports*, *2*(3), 337. https://doi.org/10.1016/J.STEMCR.2014.01.013

Douaud, G., Gaura, V., Ribeiro, M.-J., Lethimonnier, F., Maroy, R., Verny, C., Krystkowiak, P., Damier, P., Bachoud-Levi, A.-C., Hantraye, P., & Remy, P. (2006). Distribution of grey matter atrophy in Huntington's disease patients: A combined ROI-based and voxel-based morphometric study. *NeuroImage*, *32*(4), 1562–1575. https://doi.org/https://doi.org/10.1016/j.neuroimage.2006.05.057

Drago, D., Cossetti, C., Iraci, N., Gaude, E., Musco, G., Bachi, A., & Pluchino, S. (2013). The stem cell secretome and its role in brain repair. *Biochimie*, *95*(12), 2271–2285. https://doi.org/10.1016/j.biochi.2013.06.020

Draper, J. S., Smith, K., Gokhale, P., Moore, H. D., Maltby, E., Johnson, J., Meisner, L., Zwaka, T. P., Thomson, J. A., & Andrews, P. W. (2004). Recurrent gain of chromosomes 17q and 12 in cultured human embryonic stem cells. *Nature Biotechnology*, *22*(1), 53–54. https://doi.org/10.1038/nbt922

Dunnett, S. B., & Björklund, A. (2017). Mechanisms and use of neural transplants for brain repair. In *Progress in Brain Research* (Vol. 230, pp. 1–51). Elsevier B.V. https://doi.org/10.1016/bs.pbr.2016.11.002

Dunnett, S. B., & Rosser, A. E. (2011a). Cell-Based Treatments for Huntington's Disease. In J. Brotchie, E. Bezard, & P. B. T.-I. R. of N. Jenner (Eds.), *Pathophysiology, Pharmacology, and Biochemistry of Dyskinesia* (Vol. 98, pp. 483–508). Academic Press. https://doi.org/https://doi.org/10.1016/B978-0-12-381328-2.00017-1

Dunnett, S. B., & Rosser, A. E. (2011b). Clinical translation of cell transplantation in the brain. *Current Opinion in Organ Transplantation*, *16*(6).

Dunnett, S. B., & Rosser, A. E. (2014). Challenges for taking primary and stem cells into clinical neurotransplantation trials for neurodegenerative disease. *Neurobiology of Disease*, *61*, 79–89. https://doi.org/https://doi.org/10.1016/j.nbd.2013.05.004

Duyao, M., Ambrose, C., Myers, R., Novelletto, A., Persichetti, F., Frontali, M., Folstein, S., Ross, C., Franz, M., Abbott, M., Gray, J., Conneally, P., Young, A., Penney, J., Hollingsworth, Z., Shoulson, I., Lazzarini, A., Falek, A., Koroshetz, W., … MacDonald, M. (1993). Trinucleotide repeat length instability and age of onset in Huntington's disease. *Nature Genetics*, *4*(4), 387–392. https://doi.org/10.1038/ng0893-387

Ehrlich, M. E. (2012). Huntington's Disease and the Striatal Medium Spiny Neuron: Cell-Autonomous and Non-Cell-Autonomous Mechanisms of Disease. *Neurotherapeutics*, *9*(2), 270–284. https://doi.org/10.1007/s13311-012-0112-2

Elliotson, J. (1832). CLINICAL LECTURE. *The Lancet*, *18*(464), 486–491. https://doi.org/10.1016/S0140-6736(02)94771-9

EMA. (2011). *Reflection paper on stem cell-based medicinal products (EMA/CAT/571134/2009)*. www.ema.europa.eu

Evans, A. E., Kelly, C. M., Precious, S. V, & Rosser, A. E. (2012). Molecular regulation of striatal development: a review. *Anatomy Research International*, *2012*, 106529. https://doi.org/10.1155/2012/106529

Evans, M. J., & Kaufman, M. H. (1981). Establishment in culture of pluripotential cells from mouse embryos. *Nature*, *292*, 154. http://dx.doi.org/10.1038/292154a0

Evans, S. J. W., Douglas, I., Rawlins, M. D., Wexler, N. S., Tabrizi, S. J., & Smeeth, L. (2013). Prevalence of adult Huntington's disease in the UK based on diagnoses recorded in general practice records. *Journal of Neurology, Neurosurgery &Amp; Psychiatry*, *84*(10), 1156 LP – 1160. https://doi.org/10.1136/jnnp-2012-304636

Fathi, A., Mirzaei, M., Dolatyar, B., Sharifitabar, M., Bayat, M., Shahbazi, E., Lee, J., Javan, M., Zhang, S. C., Gupta, V., Lee, B., Haynes, P. A., Baharvand, H., & Salekdeh, G. H. (2018). Discovery of Novel Cell Surface Markers for Purification of Embryonic Dopamine Progenitors for Transplantation in Parkinson's Disease Animal Models. *Molecular & Cellular Proteomics*, *17*(9), 1670–1684. https://doi.org/10.1074/MCP.RA118.000809

FDA. (2008). *Content and Review of Chemistry, Manufacturing, and Control (CMC) Information for Human Somatic Cell Therapy Investigational New Drug Applications (INDs)*. https://www.fda.gov/regulatory-information/search-fda-guidance-documents/content-and-review-chemistry-manufacturing-and-control-cmc-information-human-somatic-cell-therapy

Figueredo-Cardenas, G., Morello, M., Sancesario, G., Bernardi, G., & Reiner, A. (1996). Colocalization of somatostatin, neuropeptide Y, neuronal nitric oxide synthase and NADPH-diaphorase in striatal interneurons in rats. *Brain Research*, *735*(2), 317–324. https://doi.org/10.1016/0006-8993(96)00801-3

Fishell, G., & van der Kooy, D. (1991). Pattern formation in the striatum: Neurons with early projections to the substantia nigra survive the cell death period. *Journal of Comparative Neurology*, *312*(1), 33–42. https://doi.org/10.1002/CNE.903120104

Fisher, E. R., & Hayden, M. R. (2014). Multisource ascertainment of Huntington disease in Canada: Prevalence and population at risk. *Movement Disorders*, *29*(1), 105–114. https://doi.org/10.1002/mds.25717

Forsyth, N. R., Musio, A., Vezzoni, P., Simpson, A. H. R. W., Noble, B. S., & McWhir, J. (2006). Physiologic oxygen enhances human embryonic stem cell clonal recovery and reduces chromosomal abnormalities. *Cloning and Stem Cells*, *8*(1), 16–23. https://doi.org/10.1089/clo.2006.8.16

Freeze, B. S., Kravitz, A. V., Hammack, N., Berke, J. D., & Kreitzer, A. C. (2013). Control of basal ganglia output by direct and indirect pathway projection neurons. *The Journal of Neuroscience : The Official Journal of the Society for Neuroscience*, *33*(47), 18531–18539. https://doi.org/10.1523/JNEUROSCI.1278-13.2013

Furtado, S., Sossi, V., Hauser, R. A., Samii, A., Schulzer, M., Murphy, C. B., Freeman, T. B., & Stoessl, A. J. (2005). Positron emission tomography after fetal transplantation in Huntington's disease. *Annals of Neurology*, *58*(2), 331–337. https://doi.org/10.1002/ana.20564

Gallina, P., Paganini, M., Biggeri, A., Marini, M., Romoli, A., Sarchielli, E., Berti, V., Ghelli, E., Guido, C., Lombardini, L., Mazzanti, B., Simonelli, P., Peri, A., Maggi, M., Porfirio, B., Di Lorenzo, N., & Vannelli, G. B. (2014). Human Striatum Remodelling after Neurotransplantation in Huntington's Disease. *Stereotactic and Functional Neurosurgery*, *92*(4), 211–217. https://doi.org/10.1159/000360583

Gallina, P., Paganini, M., Di Rita, A., Lombardini, L., Moretti, M., Vannelli, G., & Di Lorenzo, N. (2008). Human fetal striatal transplantation in Huntington's disease: A refinement of the stereotactic procedure. *Stereotactic and Functional Neurosurgery*, *86*(5), 308–313. https://doi.org/10.1159/000155233

Gallina, P., Paganini, M., Lombardini, L., Mascalchi, M., Porfirio, B., Gadda, D., Marini, M., Pinzani, P., Salvianti, F., Crescioli, C., Bucciantini, S., Mechi, C., Sarchielli, E., Romoli, A., Bertini, E., Urbani, S., Bartolozzi, B., De Cristofaro, M., Piacentini, S., … Di Lorenzo, N. (2010). Human striatal neuroblasts develop and build a striatal-like structure into the brain of Huntington's disease patients after transplantation. *Experimental Neurology*, *222*(1), 30–41. https://doi.org/https://doi.org/10.1016/j.expneurol.2009.12.005

Gangarossa, G., Espallergues, J., Mailly, P., De Bundel, D., de Kerchove d'Exaerde, A., Hervé, D., Girault, J. A., Valjent, E., & Krieger, P. (2013). Spatial distribution of D1R- and D2R-expressing medium-sized spiny neurons differs along the rostro-caudal axis of the mouse dorsal striatum. *Frontiers in Neural Circuits*, *7*(JUL). https://doi.org/10.3389/FNCIR.2013.00124

Garber, K. (2015). RIKEN suspends first clinical trial involving induced pluripotent stem cells. *Nature Biotechnology*, *33*(9), 890–891. https://doi.org/10.1038/nbt0915-890

Garcia Jareño, P., Bartley, O. J. M., Precious, S. V., Rosser, A. E., & Lelos, M. J. (2022). Challenges in progressing cell therapies to the clinic for Huntington's disease: A review of the progress made with pluripotent stem cell derived medium spiny neurons. *International Review of Neurobiology*, *166*, 1–48. https://doi.org/10.1016/BS.IRN.2022.09.003

Garitaonandia, I., Amir, H., Boscolo, F. S., Wambua, G. K., Schultheisz, H. L., Sabatini, K., Morey, R., Waltz, S., Wang, Y.-C., Tran, H., Leonardo, T. R., Nazor, K., Slavin, I., Lynch, C., Li, Y., Coleman, R., Gallego Romero, I., Altun, G., Reynolds, D., … Laurent, L. C. (2015). Increased risk of genetic and epigenetic instability in human embryonic stem cells associated with specific culture conditions. *PloS One*, *10*(2), e0118307–e0118307. https://doi.org/10.1371/journal.pone.0118307

Gaura, V., Bachoud-Lévi, A., Ribeiro, M., Nguyen, J., Frouin, V., Baudic, S., Brugières, P., Mangin, J., Boissé, M., Palfi, S., Cesaro, P., Samson, Y., Hantraye, P., Peschanski, M., & Remy, P. (2004). Striatal neural grafting improves cortical metabolism in Huntington's disease patients. *Brain*, *127*(1), 65–72. https://doi.org/10.1093/brain/awh003

Gauthier, L. R., Charrin, B. C., Borrell-Pagès, M., Dompierre, J. P., Rangone, H., Cordelières, F. P., De Mey, J., MacDonald, M. E., Leßmann, V., Humbert, S., & Saudou, F. (2004). Huntingtin Controls Neurotrophic Support and Survival of Neurons by Enhancing BDNF Vesicular Transport along Microtubules. *Cell*, *118*(1), 127–138. https://doi.org/https://doi.org/10.1016/j.cell.2004.06.018

Gerfen, C. R. (1984). The neostriatal mosaic: compartmentalization of corticostriatal input and striatonigral output systems. *Nature*, *311*(5985), 461–464. https://doi.org/10.1038/311461A0

Ghosh, R., & Tabrizi, S. J. (2018). *Clinical Features of Huntington's Disease BT - Polyglutamine Disorders* (C. Nóbrega & L. Pereira de Almeida, Eds.; pp. 1–28). Springer International Publishing. https://doi.org/10.1007/978-3-319-71779-1_1

Goldberg, Y. P., Nicholson, D. W., Rasper, D. M., Kalchman, M. A., Koide, H. B., Graham, R. K., Bromm, M., Kazemi-Esfarjani, P., Thornberry, N. A., Vaillancourt, J. P., & Hayden, M. R. (1996). Cleavage of huntingtin by apopain, a proapoptotic cysteine protease, is modulated by the polyglutamine tract. *Nature Genetics*, *13*(4), 442–449. https://doi.org/10.1038/ng0896-442

Grabel, L. B., Germain, N. D., Hartman, N. W., Cai, C., Becker, S., & Naegele, J. R. (2012). Teratocarcinoma Formation in Embryonic Stem Cell-Derived Neural Progenitor Hippocampal Transplants. *Cell Transplantation*, *21*, 1603–1611. https://doi.org/10.3727/096368912X647243

Graybiel, A. M., Liu, F. C., & Dunnett, S. B. (1989). Intrastriatal grafts derived from fetal striatal primordia. I. Phenotypy and modular organization. *The Journal of Neuroscience*, *9*(9), 3250 LP – 3271. https://doi.org/10.1523/JNEUROSCI.09-09-03250.1989

Gribkoff, V. K., & Kaczmarek, L. K. (2017). The need for new approaches in CNS drug discovery: Why drugs have failed, and what can be done to improve outcomes.

Neuropharmacology, *120*, 11–19. https://doi.org/https://doi.org/10.1016/j.neuropharm.2016.03.021

Grossberg, S. (2003). How Does the Cerebral Cortex Work? Development, Learning, Attention, and 3-D Vision by Laminar Circuits of Visual Cortex. *Https://Doi.Org/10.1177/1534582303002001003*, *2*(1), 47–76. https://doi.org/10.1177/1534582303002001003

Grueter, B. A., Rothwell, P. E., & Malenka, R. C. (2012). Integrating synaptic plasticity and striatal circuit function in addiction. *Current Opinion in Neurobiology*, *22*(3), 545–551. https://doi.org/10.1016/J.CONB.2011.09.009

Gusella, J. F., Wexler, N. S., Conneally, P. M., Naylor, S. L., Anderson, M. A., Tanzi, R. E., Watkins, P. C., Ottina, K., Wallace, M. R., Sakaguchi, A. Y., Young, A. B., Shoulson, I., Bonilla, E., & Martin, J. B. (1983). A polymorphic DNA marker genetically linked to Huntington's disease. *Nature*, *306*(5940), 234–238. https://doi.org/10.1038/306234a0

Gustavsson, A., Svensson, M., Jacobi, F., Allgulander, C., Alonso, J., Beghi, E., Dodel, R., Ekman, M., Faravelli, C., Fratiglioni, L., Gannon, B., Jones, D. H., Jennum, P., Jordanova, A., Jönsson, L., Karampampa, K., Knapp, M., Kobelt, G., Kurth, T., … Olesen, J. (2011). Cost of disorders of the brain in Europe 2010. *European Neuropsychopharmacology : The Journal of the European College of Neuropsychopharmacology*, *21*(10), 718–779. https://doi.org/10.1016/J.EURONEURO.2011.08.008

Haber, S. N. (2022). Corticostriatal circuitry. *Https://Doi.Org/10.31887/DCNS.2016.18.1/Shaber*, *18*(1), 7–21. https://doi.org/10.31887/DCNS.2016.18.1/SHABER

Hagimoto, K., Takami, S., Murakami, F., & Tanabe, Y. (2017). Distinct migratory behaviors of striosome and matrix cells underlying the mosaic formation in the developing striatum. *Journal of Comparative Neurology*, *525*(4), 794–817. https://doi.org/10.1002/CNE.24096

Halliday, A. L., & Cepko, C. L. (1992). Generation and migration of cells in the developing striatum. *Neuron*, *9*(1), 15–26. https://doi.org/10.1016/0896-6273(92)90216-Z

Halliwell, J., Barbaric, I., & Andrews, P. W. (2020). Acquired genetic changes in human pluripotent stem cells: origins and consequences. *Nature Reviews Molecular Cell Biology*, *21*(12), 715–728. https://doi.org/10.1038/s41580-020-00292-z

Hamasaki, T., Goto, S., Nishikawa, S., & Ushio, Y. (2003). Neuronal cell migration for the developmental formation of the mammalian striatum. *Brain Research Reviews*, *41*(1), 1–12. https://doi.org/10.1016/S0165-0173(02)00216-3

Harper, P. S. (2002). Huntington's disease: a historical background. In G. Bates, P. Harper, & L. Jones (Eds.), *Huntington's Disease*.

Hauser, R. A., Sandberg, P. R., Freeman, T. B., & Stoessl, A. J. (2002). Bilateral human fetal striatal transplantation in Huntington's disease. *Neurology*, *58*(11), 1704 LP – 1704. https://doi.org/10.1212/WNL.58.11.1704

HD iPSC Consortium. (2012). Induced pluripotent stem cells from patients with Huntington's disease show CAG-repeat-expansion-associated phenotypes. *Cell Stem Cell*, *11*(2), 264–278. https://doi.org/10.1016/j.stem.2012.04.027

HD iPSC Consortium. (2017). Developmental alterations in Huntington's disease neural cells and pharmacological rescue in cells and mice. *Nature Neuroscience*, *20*(5), 648–660. https://doi.org/10.1038/nn.4532

Helder, D. I., Kaptein, A. A., van Kempen, G. M., van Houwelingen, J. C., & Roos, R. A. (2001). Impact of Huntington's disease on quality of life. *Movement Disorders : Official Journal of the Movement Disorder Society*, *16*(2), 325–330.

Heneka, M. T., Kummer, M. P., & Latz, E. (2014). Innate immune activation in neurodegenerative disease. *Nature Reviews Immunology 2014 14:7*, *14*(7), 463–477. https://doi.org/10.1038/nri3705

Hentze, H., Soong, P. L., Wang, S. T., Phillips, B. W., Putti, T. C., & Dunn, N. R. (2009). Teratoma formation by human embryonic stem cells: evaluation of essential parameters for future safety studies. *Stem Cell Research*, *2*(3), 198–210. https://doi.org/10.1016/J.SCR.2009.02.002

Hoffner, G., Kahlem, P., & Djian, P. (2002). Perinuclear localization of huntingtin as a consequence of its binding to microtubules through an interaction with β-tubulin: relevance to Huntington's disease. *Journal of Cell Science*, *115*(5), 941 LP – 948.

Hunnicutt, B. J., Jongbloets, B. C., Birdsong, W. T., Gertz, K. J., Zhong, H., & Mao, T. (2016). A comprehensive excitatory input map of the striatum reveals novel functional organization. *ELife*, *5*(November2016). https://doi.org/10.7554/ELIFE.19103

Huntington, G. (n.d.). *On Chorea*.

Hussain, R., Zubair, H., Pursell, S., & Shahab, M. (2018). Neurodegenerative Diseases: Regenerative Mechanisms and Novel Therapeutic Approaches. *Brain Sciences*, *8*(9). https://doi.org/10.3390/BRAINSCI8090177

Hussein, S. M., Batada, N. N., Vuoristo, S., Ching, R. W., Autio, R., Närvä, E., Ng, S., Sourour, M., Hämäläinen, R., Olsson, C., Lundin, K., Mikkola, M., Trokovic, R., Peitz, M., Brüstle, O., Bazett-Jones, D. P., Alitalo, K., Lahesmaa, R., Nagy, A., & Otonkoski, T. (2011). Copy number variation and selection during reprogramming to pluripotency. *Nature*, *471*(7336), 58–62. https://doi.org/10.1038/nature09871

ISCCR. (2021). *Guidelines — International Society for Stem Cell Research*. https://www.isscr.org/guidelines

Jacobs, K., Zambelli, F., Mertzanidou, A., Smolders, I., Geens, M., Nguyen, H. T., Barbé, L., Sermon, K., & Spits, C. (2016). Higher-Density Culture in Human Embryonic

Stem Cells Results in DNA Damage and Genome Instability. *Stem Cell Reports*, *6*(3), 330–341. https://doi.org/10.1016/j.stemcr.2016.01.015

Jaitin, D. A., Kenigsberg, E., Keren-Shaul, H., Elefant, N., Paul, F., Zaretsky, I., Mildner, A., Cohen, N., Jung, S., Tanay, A., & Amit, I. (2014). Massively parallel single-cell RNA-seq for marker-free decomposition of tissues into cell types. *Science*, *343*(6172), 776–779. https://doi.org/10.1126/SCIENCE.1247651/SUPPL_FILE/TABLE_S6.XLS

Jeon, I., Choi, C., Lee, N., Im, W., Kim, M., Oh, S. H., Park, I. H., Kim, H. S., & Song, J. (2014). In vivo roles of a patient-derived induced pluripotent stem cell line (HD72-iPSC) in the YAC128 model of huntington's disease. *International Journal of Stem Cells*, *7*(1), 43–47. https://doi.org/10.15283/ijsc.2014.7.1.43

Jeon, I., Lee, N., Li, J.-Y. Y., Park, I.-H. H., Park, K. S., Moon, J., Shim, S. H., Choi, C., Chang, D.-J. J., Kwon, J., Oh, S.-H. H., Shin, D. A., Kim, H. S., Do, J. T., Lee, D. R., Kim, M., Kang, K.-S. S., Daley, G. Q., Brundin, P., & Song, J. (2012). Neuronal Properties, In Vivo Effects, and Pathology of a Huntington's Disease Patient-Derived Induced Pluripotent Stem Cells. *STEM CELLS*, *30*(9), 2054–2062. https://doi.org/10.1002/stem.1135

Jones, C., Busse, M., Quinn, L., Dawes, H., Drew, C., Kelson, M., Hood, K., Rosser, A., & Edwards, R. T. (2016). The societal cost of Huntington's disease: are we underestimating the burden? *European Journal of Neurology*, *23*(10), 1588–1590. https://doi.org/10.1111/ene.13107

Kawaguchi, Y., Wilson, C. J., Augood, S. J., & Emson, P. C. (1995). Striatal interneurones: chemical, physiological and morphological characterization. *Trends in Neurosciences*, *18*(12), 527–535. https://doi.org/10.1016/0166-2236(95)98374-8

Kay, C., Hayden, M. R., & Leavitt, B. R. (2017). Chapter 3 - Epidemiology of Huntington disease. In A. S. Feigin & K. E. B. T.-H. of C. N. Anderson (Eds.), *Huntington Disease* (Vol. 144, pp. 31–46). Elsevier. https://doi.org/https://doi.org/10.1016/B978-0-12-801893-4.00003-1

Keene, C. D., Chang, R. C., Leverenz, J. B., Kopyov, O., Perlman, S., Hevner, R. F., Born, D. E., Bird, T. D., & Montine, T. J. (2009). A patient with Huntington's disease and long-surviving fetal neural transplants that developed mass lesions. *Acta Neuropathologica*, *117*(3), 329–338. https://doi.org/10.1007/s00401-008-0465-0

Keene, C. D., Sonnen, J. A., Swanson, P. D., Kopyov, O., Leverenz, J. B., Bird, T. D., & Montine, T. J. (2007). Neural transplantation in Huntington disease: Long-term grafts in two patients. *Neurology*, *68*(24), 2093 LP – 2098. https://doi.org/10.1212/01.wnl.0000264504.14301.f5

Keller, A., & Spits, C. (2021). The Impact of Acquired Genetic Abnormalities on the Clinical Translation of Human Pluripotent Stem Cells. *Cells*, *10*(11), 3246. https://doi.org/10.3390/cells10113246

Kelly, S. M., Raudales, R., He, M., Lee, J. H., Kim, Y., Gibb, L. G., Wu, P., Matho, K., Osten, P., Graybiel, A. M., & Huang, Z. J. (2018). Radial Glial Lineage Progression

and Differential Intermediate Progenitor Amplification Underlie Striatal Compartments and Circuit Organization. *Neuron*, *99*(2), 345-361.e4. https://doi.org/10.1016/j.neuron.2018.06.021

Kendall, A. L., Rayment, F. D., Torres, E. M., Baker, H. F., Ridley, R. M., & Dunnett, S. B. (1998). Functional integration of striatal allografts in a primate model of Huntington's disease. *Nature Medicine*, *4*(6), 727–729. https://doi.org/10.1038/nm0698-727

Kim, D. S., Lee, D. R., Kim, H. S., Yoo, J. E., Jung, S. J., Lim, B. Y., Jang, J., Kang, H. C., You, S., Hwang, D. Y., Leem, J. W., Nam, T. S., Cho, S. R., & Kim, D. W. (2012). Highly Pure and Expandable PSA-NCAM-Positive Neural Precursors from Human ESC and iPSC-Derived Neural Rosettes. *PLoS ONE*, *7*(7). https://doi.org/10.1371/JOURNAL.PONE.0039715

Klöppel, S., Henley, S. M., Hobbs, N. Z., Wolf, R. C., Kassubek, J., Tabrizi, S. J., & Frackowiak, R. S. J. (2009). Magnetic resonance imaging of Huntington's disease: preparing for clinical trials. *Neuroscience*, *164*(1), 205–219. https://doi.org/10.1016/J.NEUROSCIENCE.2009.01.045

Knowles, R., Dehorter, N., & Ellender, T. (2021). From Progenitors to Progeny: Shaping Striatal Circuit Development and Function. *Journal of Neuroscience*, *41*(46), 9483–9502. https://doi.org/10.1523/JNEUROSCI.0620-21.2021

Koning, N., Swaab, D. F., Hoek, R. M., & Huitinga, I. (2009). Distribution of the Immune Inhibitory Molecules CD200 and CD200R in the Normal Central Nervous System and Multiple Sclerosis Lesions Suggests Neuron-Glia and Glia-Glia Interactions. *Journal of Neuropathology & Experimental Neurology*, *68*(2), 159–167. https://doi.org/10.1097/NEN.0B013E3181964113

Koós, T., & Tepper, J. M. (1999). Inhibitory control of neostriatal projection neurons by GABAergic interneurons. *Nature Neuroscience*, *2*(5), 467–472. https://doi.org/10.1038/8138

Kopyov, O. V, Jacques, S., Lieberman, A., Duma, C. M., & Eagle, K. S. (1998). Safety of Intrastriatal Neurotransplantation for Huntington's Disease Patients. *Experimental Neurology*, *149*(1), 97–108. https://doi.org/https://doi.org/10.1006/exnr.1997.6685

Kordower, J. H., Freeman, T. B., Snow, B. J., Vingerhoets, F. J. G., Mufson, E. J., Sanberg, P. R., Hauser, R. A., Smith, D. A., Nauert, G. M., Perl, D. P., & Olanow, C. W. (1995). Neuropathological evidence of graft survival and striatal reinnervation after the transplantation of fetal mesencephalic tissue in a patient with parkinson's disease. *New England Journal of Medicine*, *332*(17), 1118–1124. https://doi.org/10.1056/NEJM199504273321702

Kovacs, G. G. (2014). Neuropathology of Neurodegenerative Diseases: A Practical Guide. *Neuropathology of Neurodegenerative Diseases: A Practical Guide*, 1–309. https://doi.org/10.1017/CBO9781107588660

Kravitz, A. V, Freeze, B. S., Parker, P. R. L., Kay, K., Thwin, M. T., Deisseroth, K., & Kreitzer, A. C. (2010). Regulation of parkinsonian motor behaviours by optogenetic control of basal ganglia circuitry. *Nature*, *466*(7306), 622–626. https://doi.org/10.1038/nature09159

Kravitz, A. V., Tye, L. D., & Kreitzer, A. C. (2012). Distinct roles for direct and indirect pathway striatal neurons in reinforcement. *Nature Neuroscience*, *15*(6), 816–818. https://doi.org/10.1038/NN.3100

Kreitzer, A. C., & Malenka, R. C. (2008). Striatal Plasticity and Basal Ganglia Circuit Function. *Neuron*, *60*(4), 543–554. https://doi.org/10.1016/j.neuron.2008.11.005

Krystkowiak, P., Gaura, V., Labalette, M., Rialland, A., Remy, P., Peschanski, M., & Bachoud-Lévi, A.-C. (2007). Alloimmunisation to Donor Antigens and Immune Rejection Following Foetal Neural Grafts to the Brain in Patients with Huntington's Disease. *PLOS ONE*, *2*(1), e166–e166. https://doi.org/10.1371/journal.pone.0000166

Kuleshov, M. V., Jones, M. R., Rouillard, A. D., Fernandez, N. F., Duan, Q., Wang, Z., Koplev, S., Jenkins, S. L., Jagodnik, K. M., Lachmann, A., McDermott, M. G., Monteiro, C. D., Gundersen, G. W., & Maayan, A. (2016). Enrichr: a comprehensive gene set enrichment analysis web server 2016 update. *Nucleic Acids Research*, *44*(Web Server issue), W90. https://doi.org/10.1093/NAR/GKW377

Lahiri, A. K., & Bevan, M. D. (2020). Dopaminergic Transmission Rapidly and Persistently Enhances Excitability of D1 Receptor-Expressing Striatal Projection Neurons. *Neuron*, *106*(2), 277-290.e6. https://doi.org/10.1016/j.neuron.2020.01.028

Lanciego, J. L., Luquin, N., & Obeso, J. A. (2012). Functional neuroanatomy of the basal ganglia. *Cold Spring Harbor Perspectives in Medicine*, *2*(12). https://doi.org/10.1101/CSHPERSPECT.A009621

Lane, R. M., Smith, A., Baumann, T., Gleichmann, M., Norris, D., Bennett, C. F., & Kordasiewicz, H. (2018). Translating antisense technology into a treatment for Huntington's disease. In *Methods in Molecular Biology* (Vol. 1780, pp. 497–523). Humana Press Inc. https://doi.org/10.1007/978-1-4939-7825-0_23

Lanska, D. J., Lanska, M. J., Lavine, L., & Schoenberg, B. S. (1988). Conditions Associated With Huntington's Disease at Death: A Case-Control Study. *Archives of Neurology*, *45*(8), 878–880. https://doi.org/10.1001/archneur.1988.00520320068017

Laurent, L., Wong, E., Li, G., Huynh, T., Tsirigos, A., Ong, C. T., Low, H. M., Sung, K. W. K., Rigoutsos, I., Loring, J., & Wei, C. L. (2010). Dynamic changes in the human methylome during differentiation. *Genome Research*, *20*(3), 320–331. https://doi.org/10.1101/GR.101907.109

Leavitt, B. R., & Tabrizi, S. J. (2020). Antisense oligonucleotides for neurodegeneration. *Science*, *367*(6485), 1428–1429. https://doi.org/10.1126/science.aba4624

Lebouc, M., Richard, Q., Garret, M., & Baufreton, J. (2020). Striatal circuit development and its alterations in Huntington's disease. *Neurobiology of Disease*, *145*, 105076. https://doi.org/10.1016/J.NBD.2020.105076

Leegwater-Kim, J., & Cha, J.-H. J. (2004). The paradigm of Huntington's disease: Therapeutic opportunities in neurodegeneration. *NeuroRX*, *1*(1), 128–138. https://doi.org/10.1602/neurorx.1.1.128

Lehnen, D., Barral, S., Cardoso, T., Grealish, S., Heuer, A., Smiyakin, A., Kirkeby, A., Kollet, J., Cremer, H., Parmar, M., Bosio, A., & Knöbel, S. (2017). IAP-Based Cell Sorting Results in Homogeneous Transplantable Dopaminergic Precursor Cells Derived from Human Pluripotent Stem Cells. *Stem Cell Reports*, *9*(4), 1207. https://doi.org/10.1016/J.STEMCR.2017.08.016

Leisman, G., Melillo, R., & R., F. (2013). Clinical Motor and Cognitive Neurobehavioral Relationships in the Basal Ganglia. In *Basal Ganglia - An Integrative View*. InTech. https://doi.org/10.5772/55227

Li, M., & Rosser, A. E. (2017). Pluripotent stem cell-derived neurons for transplantation in Huntington's disease. *Progress in Brain Research*, *230*, 263–281. https://doi.org/10.1016/BS.PBR.2017.02.009

Lindvall, O., & Wahlberg, L. U. (2008). Encapsulated cell biodelivery of GDNF: A novel clinical strategy for neuroprotection and neuroregeneration in Parkinson's disease? *Experimental Neurology*, *209*(1), 82–88. https://doi.org/10.1016/j.expneurol.2007.08.019

Lobo, M. K., Karsten, S. L., Gray, M., Geschwind, D. H., & Yang, X. W. (2006). FACS-array profiling of striatal projection neuron subtypes in juvenile and adult mouse brains. *Nature Neuroscience 2006 9:3*, *9*(3), 443–452. https://doi.org/10.1038/nn1654

Lobo, M. K., Yeh, C., & Yang, X. W. (2008). Pivotal role of early B-cell factor 1 in development of striatonigral medium spiny neurons in the matrix compartment. *Journal of Neuroscience Research*, *86*(10), 2134–2146. https://doi.org/10.1002/JNR.21666

Long, J. E., Swan, C., Liang, W. S., Cobos, I., Potter, G. B., & Rubenstein, J. L. R. (2009). Dlx1&2 and Mash1 Transcription Factors Control Striatal Patterning and Differentiation Through Parallel and Overlapping Pathways. *The Journal of Comparative Neurology*, *512*(4), 556. https://doi.org/10.1002/CNE.21854

Lu, J., Liu, H., Huang, C. T.-L., Chen, H., Du, Z., Liu, Y., Sherafat, M. A., & Zhang, S.-C. (2013). Generation of integration-free and region-specific neural progenitors from primate fibroblasts. *Cell Reports*, *3*(5), 1580–1591. https://doi.org/10.1016/j.celrep.2013.04.004

Lu, X. H., & Yang, X. W. (2012). " Huntingtin Holiday" : Progress toward an Antisense Therapy for Huntington's Disease. In *Neuron* (Vol. 74, Issue 6, pp. 964–966). NIH Public Access. https://doi.org/10.1016/j.neuron.2012.06.001

Lund, R. J., Närvä, E., & Lahesmaa, R. (2012). Genetic and epigenetic stability of human pluripotent stem cells. *Nature Reviews. Genetics*, *13*(10), 732–744. https://doi.org/10.1038/nrg3271

Luzy, I. R. D., Niclis, J. C., Gantner, C. W., Kauhausen, J. A., Hunt, C. P. J., Ermine, C., Pouton, C. W., Thompson, L. H., & Parish, C. L. (2019). Isolation of LMX1a Ventral Midbrain Progenitors Improves the Safety and Predictability of Human Pluripotent Stem Cell-Derived Neural Transplants in Parkinsonian Disease. *The Journal of Neuroscience*, *39*(48), 9521. https://doi.org/10.1523/JNEUROSCI.1160-19.2019

Ma, L., Hu, B., Liu, Y., Vermilyea, S. C., Liu, H., Gao, L., Sun, Y., Zhang, X., & Zhang, S.-C. (2012). Human embryonic stem cell-derived GABA neurons correct locomotion deficits in quinolinic acid-lesioned mice. *Cell Stem Cell*, *10*(4), 455–464. https://doi.org/10.1016/j.stem.2012.01.021

MacDonald, M. E., Ambrose, C. M., Duyao, M. P., Myers, R. H., Lin, C., Srinidhi, L., Barnes, G., Taylor, S. A., James, M., Groot, N., MacFarlane, H., Jenkins, B., Anderson, M. A., Wexler, N. S., Gusella, J. F., Bates, G. P., Baxendale, S., Hummerich, H., Kirby, S., … Harper, P. S. (1993). A novel gene containing a trinucleotide repeat that is expanded and unstable on Huntington's disease chromosomes. *Cell*, *72*(6), 971–983. https://doi.org/10.1016/0092-8674(93)90585-E

Maier, T., Güell, M., & Serrano, L. (2009). Correlation of mRNA and protein in complex biological samples. *FEBS Letters*, *583*(24), 3966–3973. https://doi.org/https://doi.org/10.1016/j.febslet.2009.10.036

Mandai, M., Kurimoto, Y., & Takahashi, M. (2017). Autologous Induced Stem-Cell-Derived Retinal Cells for Macular Degeneration. In *The New England journal of medicine* (Vol. 377, Issue 8, pp. 792–793). https://doi.org/10.1056/NEJMc1706274

Marin, O., Anderson, S. A., & Rubenstein, J. L. (2000). Origin and molecular specification of striatal interneurons. *The Journal of Neuroscience : The Official Journal of the Society for Neuroscience*, *20*(16), 6063–6076.

Markouli, C., Couvreu De Deckersberg, E., Regin, M., Nguyen, H. T., Zambelli, F., Keller, A., Dziedzicka, D., De Kock, J., Tilleman, L., Van Nieuwerburgh, F., Franceschini, L., Sermon, K., Geens, M., & Spits, C. (2019). Gain of 20q11.21 in Human Pluripotent Stem Cells Impairs TGF-β-Dependent Neuroectodermal Commitment. *Stem Cell Reports*, *13*(1), 163–176. https://doi.org/10.1016/j.stemcr.2019.05.005

Martín-Ibáñez, R., Crespo, E., Esgleas, M., Urban, N., Wang, B., Waclaw, R., Georgopoulos, K., Martínez, S., Campbell, K., Vicario-Abejón, C., Alberch, J., Chan, S., Kastner, P., Rubenstein, J. L., & Canals, J. M. (2012). Helios Transcription Factor Expression Depends on Gsx2 and Dlx1&2 Function in Developing Striatal Matrix Neurons. *Stem Cells and Development*, *21*(12), 2239. https://doi.org/10.1089/SCD.2011.0607

Martins-Taylor, K., & Xu, R.-H. (2012). Concise review: Genomic stability of human induced pluripotent stem cells. *Stem Cells (Dayton, Ohio)*, *30*(1), 22–27. https://doi.org/10.1002/stem.705

Mascalchi, M., Diciotti, S., Paganini, M., Bianchi, A., Ginestroni, A., Lombardini, L., Porfirio, B., Conti, R., Di Lorenzo, N., Vannelli, G. B., & Gallina, P. (2014). Large-sized Fetal Striatal Grafts in Huntington's Disease Do Stop Growing: Long-term Monitoring in the Florence Experience. *PLoS Currents*, *6*, ecurrents.hd.c0ad575f12106c38f9f5717a8a7d05ae. https://doi.org/10.1371/currents.hd.c0ad575f12106c38f9f5717a8a7d05ae

Mason, S. L., & Barker, R. A. (2016). Advancing pharmacotherapy for treating Huntington's disease: a review of the existing literature. *Expert Opinion on Pharmacotherapy*, *17*(1), 41–52. https://doi.org/10.1517/14656566.2016.1109630

Maxan, A., Mason, S., Saint-Pierre, M., Smith, E., Ho, A., Harrower, T., Watts, C., Tai, Y., Pavese, N., Savage, J. C., Tremblay, M. È., Gould, P., Rosser, A. E., Dunnett, S. B., Piccini, P., Barker, R. A., & Cicchetti, F. (2018). Outcome of cell suspension allografts in a patient with Huntington's disease. *Annals of Neurology*, *84*(6), 950–956. https://doi.org/10.1002/ana.25354

Mayer, C., Hafemeister, C., Bandler, R. C., Machold, R., Batista Brito, R., Jaglin, X., Allaway, K., Butler, A., Fishell, G., & Satija, R. (2018). Developmental diversification of cortical inhibitory interneurons. *Nature*, *555*(7697), 457. https://doi.org/10.1038/NATURE25999

Mazzocchi-Jones, D., Döbrössy, M., & Dunnett, S. B. (2009). Embryonic striatal grafts restore bi-directional synaptic plasticity in a rodent model of Huntington's disease. *European Journal of Neuroscience*, *30*(11), 2134–2142. https://doi.org/10.1111/j.1460-9568.2009.07006.x

McColgan, P., Gregory, S., Seunarine, K. K., Razi, A., Papoutsi, M., Johnson, E., Durr, A., Roos, R. A. C., Leavitt, B. R., Holmans, P., Scahill, R. I., Clark, C. A., Rees, G., Tabrizi, S. J., Coleman, A., Decolongon, J., Fan, M., Petkau, T., Jauffret, C., … Crawfurd, D. (2018). Brain Regions Showing White Matter Loss in Huntington’s Disease Are Enriched for Synaptic and Metabolic Genes. *Biological Psychiatry*, *83*(5), 456–465. https://doi.org/10.1016/j.biopsych.2017.10.019

McLeod, M. C., Kobayashi, N. R., Sen, A., Baghbaderani, B. A., Sadi, D., Ulalia, R., Behie, L. A., & Mendez, I. (2013). Transplantation of GABAergic Cells Derived from Bioreactor-Expanded Human Neural Precursor Cells Restores Motor and Cognitive Behavioral Deficits in a Rodent Model of Huntington's Disease. *Cell Transplantation*, *22*(12), 2237–2256. https://doi.org/10.3727/096368912X658809

Mehler, V. J., Burns, C. J., Stauss, H., Francis, R. J., & Moore, M. L. (2020). Human iPSC-Derived Neural Crest Stem Cells Exhibit Low Immunogenicity. *Molecular Therapy. Methods & Clinical Development*, *16*, 161. https://doi.org/10.1016/J.OMTM.2019.12.015

Meiser, I., Majer, J., Katsen-Globa, A., Schulz, A., Schmidt, K., Stracke, F., Koutsouraki, E., Witt, G., Keminer, O., Pless, O., Gardner, J., Claussen, C., Gribbon, P., Neubauer, J. C., & Zimmermann, H. (2021). Droplet-based vitrification of adherent human induced pluripotent stem cells on alginate microcarrier influenced by adhesion time and matrix elasticity. *Cryobiology*, *103*, 57–69. https://doi.org/https://doi.org/10.1016/j.cryobiol.2021.09.010

Middleton, F. A., & Strick, P. L. (2000). Basal ganglia and cerebellar loops: motor and cognitive circuits. *Brain Research Reviews*, *31*(2–3), 236–250. https://doi.org/10.1016/S0165-0173(99)00040-5

Miguez, A., Gomis, C., Vila, C., Monguió-Tortajada, M., Fernández-García, S., Bombau, G., Galofré, M., García-Bravo, M., Sanders, P., Fernández-Medina, H., Poquet, B., Salado-Manzano, C., Roura, S., Alberch, J., Segovia, J. C., Allen, N. D., Borràs, F. E., & Canals, J. M. (2023). Soluble mutant huntingtin drives early human pathogenesis in Huntington's disease. *Cellular and Molecular Life Sciences*, *80*(8), 238. https://doi.org/10.1007/S00018-023-04882-W

Miyakawa, T. (2020). No raw data, no science: another possible source of the reproducibility crisis. In *Molecular brain* (Vol. 13, Issue 1, p. 24). https://doi.org/10.1186/s13041-020-0552-2

Miyamoto, Y., Katayama, S., Shigematsu, N., Nishi, A., & Fukuda, T. (2018). Striosome-based map of the mouse striatum that is conformable to both cortical afferent topography and uneven distributions of dopamine D1 and D2 receptor-expressing cells. *Brain Structure & Function*, *223*(9), 4275–4291. https://doi.org/10.1007/S00429-018-1749-3

Morigaki, R., & Goto, S. (2017). Striatal Vulnerability in Huntington's Disease: Neuroprotection Versus Neurotoxicity. *Brain Sciences*, *7*(6), 63. https://doi.org/10.3390/brainsci7060063

Moumné, L., Betuing, S., & Caboche, J. (2013). Multiple Aspects of Gene Dysregulation in Huntington's Disease. *Frontiers in Neurology*, *4*(October), 1–10. https://doi.org/10.3389/fneur.2013.00127

Myers, R. H. (2004). Huntington's disease genetics. *NeuroRx : The Journal of the American Society for Experimental NeuroTherapeutics*, *1*(2), 255–262. https://doi.org/10.1602/neurorx.1.2.255

Nery, S., Fishell, G., & Corbin, J. G. (2002). The caudal ganglionic eminence is a source of distinct cortical and subcortical cell populations. *Nature Neuroscience*, *5*(12), 1279–1287. https://doi.org/10.1038/NN971

Nguyen, H. T., Geens, M., Mertzanidou, A., Jacobs, K., Heirman, C., Breckpot, K., & Spits, C. (2014). Gain of 20q11.21 in human embryonic stem cells improves cell survival by increased expression of Bcl-xL. *Molecular Human Reproduction*, *20*(2), 168–177. https://doi.org/10.1093/molehr/gat077

Nguyen Thi, H., & Duong, H. (2018). The molecular characteristics of colorectal cancer: Implications for diagnosis and therapy (Review). *Oncol Lett*, *16*(1), 9–18. https://doi.org/10.3892/ol.2018.8679

Nicoleau, C., Viegas, P., Peschanski, M., & Perrier, A. L. (2011). Human Pluripotent Stem Cell Therapy for Huntington's Disease: Technical, Immunological, and Safety Challenges. *Neurotherapeutics*, *8*(4), 562–576. https://doi.org/10.1007/s13311-011-0079-4

Novak, M. J. U., & Tabrizi, S. J. (2010). Huntington's disease. *BMJ*, *340*, c3109. https://doi.org/10.1136/bmj.c3109

OECD. (2018). *Guidance Document on Good In Vitro Method Practices (GIVIMP)*. OECD. https://doi.org/10.1787/9789264304796-en

Olariu, V., Harrison, N. J., Coca, D., Gokhale, P. J., Baker, D., Billings, S., Kadirkamanathan, V., & Andrews, P. W. (2010). Modeling the evolution of culture-adapted human embryonic stem cells. *Stem Cell Research*, *4*(1), 50–56. https://doi.org/10.1016/j.scr.2009.09.001

Oldenburg, I. A., & Ding, J. B. (2011). Cholinergic modulation of synaptic integration and dendritic excitability in the striatum. *Current Opinion in Neurobiology*, *21*(3), 425. https://doi.org/10.1016/J.CONB.2011.04.004

Olesen, J., Gustavsson, A., Svensson, M., Wittchen, H. U., & Jönsson, B. (2012). The economic cost of brain disorders in Europe. *European Journal of Neurology*, *19*(1), 155–162. https://doi.org/10.1111/J.1468-1331.2011.03590.X

Olsson, M., Björklund, A., & Campbell, K. (1998). Early specification of striatal projection neurons and interneuronal subtypes in the lateral and medial ganglionic eminence. *Neuroscience*, *84*(3), 867–876. https://doi.org/https://doi.org/10.1016/S0306-4522(97)00532-0

Olsson, M., Campbell, K., Wictorin, K., & Björklund, A. (1995). Projection neurons in fetal striatal transplants are predominantly derived from the lateral ganglionic eminence. *Neuroscience*, *69*(4), 1169–1182. https://doi.org/https://doi.org/10.1016/0306-4522(95)00325-D

Ooi, J., Langley, S. R., Xu, X., Utami, K. H., Sim, B., Huang, Y., Harmston, N. P., Tay, Y. L., Ziaei, A., Zeng, R., Low, D., Aminkeng, F., Sobota, R. M., Ginhoux, F., Petretto, E., & Pouladi, M. A. (2019). Unbiased Profiling of Isogenic Huntington Disease hPSC-Derived CNS and Peripheral Cells Reveals Strong Cell-Type Specificity of CAG Length Effects. *Cell Reports*, *26*(9), 2494-2508.e7. https://doi.org/https://doi.org/10.1016/j.celrep.2019.02.008

Osafune, K., Caron, L., Borowiak, M., Martinez, R. J., Fitz-Gerald, C. S., Sato, Y., Cowan, C. A., Chien, K. R., & Melton, D. A. (2008). Marked differences in differentiation propensity among human embryonic stem cell lines. *Nature Biotechnology*, *26*(3), 313–315. https://doi.org/10.1038/nbt1383

Ouimet, C. C., Miller, P. E., Hemmings, H. C., Ivar Walaas, S., & Greengard, P. (1984). DARPP-32, a dopamine- and adenosine 3':5'-monophosphate-regulated

phosphoprotein enriched in dopamine-innervated brain regions. III. Immunocytochemical localization. *The Journal of Neuroscience : The Official Journal of the Society for Neuroscience*, *4*(1), 111–124. https://doi.org/10.1523/JNEUROSCI.04-01-00111.1984

Paganini, M., Biggeri, A., Romoli, A. M., Mechi, C., Ghelli, E., Berti, V., Pradella, S., Bucciantini, S., Catelan, D., Saccardi, R., Lombardini, L., Mascalchi, M., Massacesi, L., Porfirio, B., Di Lorenzo, N., Vannelli, G. B., & Gallina, P. (2014). Fetal striatal grafting slows motor and cognitive decline of Huntington's disease. *Journal of Neurology, Neurosurgery & Psychiatry*, *85*(9), 974–981. https://doi.org/10.1136/JNNP-2013-306533

Parekh, S., Ziegenhain, C., Vieth, B., Enard, W., & Hellmann, I. (2018). zUMIs - A fast and flexible pipeline to process RNA sequencing data with UMIs. *GigaScience*, *7*(6). https://doi.org/10.1093/GIGASCIENCE/GIY059

Parent, A., Fortin, M., Côté, P.-Y., & Cicchetti, F. (1996). Calcium-binding proteins in primate basal ganglia. *Neuroscience Research*, *25*(4), 309–334. https://doi.org/10.1016/0168-0102(96)01065-6

Parent, A., & Hazrati, L. N. (1995). Functional anatomy of the basal ganglia. I. The cortico-basal ganglia-thalamo-cortical loop. In *Brain Research Reviews* (Vol. 20, Issue 1, pp. 91–127). https://doi.org/10.1016/0165-0173(94)00007-C

Paul, F., Arkin, Y., Giladi, A., Jaitin, D. A., Kenigsberg, E., Keren-Shaul, H., Winter, D., Lara-Astiaso, D., Gury, M., Weiner, A., David, E., Cohen, N., Lauridsen, F. K. B., Haas, S., Schlitzer, A., Mildner, A., Ginhoux, F., Jung, S., Trumpp, A., … Amit, I. (2015). Transcriptional Heterogeneity and Lineage Commitment in Myeloid Progenitors. *Cell*, *163*(7), 1663–1677. https://doi.org/10.1016/j.cell.2015.11.013

Paulsen, J. S., Langbehn, D. R., Stout, J. C., Aylward, E., Ross, C. A., Nance, M., Guttman, M., Johnson, S., MacDonald, M., Beglinger, L. J., Duff, K., Kayson, E., Biglan, K., Shoulson, I., Oakes, D., & Hayden, M. (2008). Detection of Huntington's disease decades before diagnosis: the Predict-HD study. *Journal of Neurology, Neurosurgery &Amp; Psychiatry*, *79*(8), 874 LP – 880. https://doi.org/10.1136/jnnp.2007.128728

Paulsen, J. S., Ready, R. E., Hamilton, J. M., Mega, M. S., & Cummings, J. L. (2001). Neuropsychiatric aspects of Huntington's disease. *Journal of Neurology, Neurosurgery, and Psychiatry*, *71*(3), 310–314. https://doi.org/10.1136/jnnp.71.3.310

Pauly, M.-C., Piroth, T., Döbrössy, M., & Nikkhah, G. (2012). Restoration of the striatal circuitry: from developmental aspects toward clinical applications. In *Frontiers in Cellular Neuroscience* (Vol. 6, p. 16). https://www.frontiersin.org/article/10.3389/fncel.2012.00016

Pegliasco, J., Hirsch, P., Marzac, C., Isnard, F., Meniane, J.-C., Deswarte, C., Pellet, P., Lemaitre, C., Leroy, G., Rabadan Moraes, G., Guermouche, H., Schmaltz-Panneau, B., Pasquier, F., Colas, C., Benusiglio, P. R., Bera, O., Bourhis, J.-H., Brissot, E., Caron, O., … Bellanné-Chantelot, C. (2022). Germline ATG2B/GSKIP-containing

14q32 duplication predisposes to early clonal hematopoiesis leading to myeloid neoplasms. *Leukemia*, *36*(1), 126–137. https://doi.org/10.1038/s41375-021-01319-w

Peterson, S. E., Westra, J. W., Rehen, S. K., Young, H., Bushman, D. M., Paczkowski, C. M., Yung, Y. C., Lynch, C. L., Tran, H. T., Nickey, K. S., Wang, Y.-C., Laurent, L. C., Loring, J. F., Carpenter, M. K., & Chun, J. (2011). Normal human pluripotent stem cell lines exhibit pervasive mosaic aneuploidy. *PloS One*, *6*(8), e23018–e23018. https://doi.org/10.1371/journal.pone.0023018

Philpott, L. M., Kopyov, O. V, Lee, A. J., Jacques, S., Duma, C. M., Caine, S., Yang, M., & Eagle, K. S. (1997). Neuropsychological functioning following fetal striatal transplantation in Huntington's chorea: Three case presentations. *Cell Transplantation*, *6*(3), 203–212. https://doi.org/10.1016/S0963-6897(97)00028-6

Pidgeon, C., & Rickards, H. (2013). The Pathophysiology and Pharmacological Treatment of Huntington Disease. *Behavioural Neurology*, *26*(4), 245–253. https://doi.org/10.3233/BEN-2012-120267

Pilz, G. A., Shitamukai, A., Reillo, I., Pacary, E., Schwausch, J., Stahl, R., Ninkovic, J., Snippert, H. J., Clevers, H., Godinho, L., Guillemot, F., Borrell, V., Matsuzaki, F., & Götz, M. (2013). Amplification of progenitors in the mammalian telencephalon includes a new radial glial cell type. *Nature Communications 2013 4:1*, *4*(1), 1–11. https://doi.org/10.1038/ncomms3125

Piquet, A. L., Venkiteswaran, K., Marupudi, N. I., Berk, M., & Subramanian, T. (2012). The immunological challenges of cell transplantation for the treatment of Parkinson's disease. *Brain Research Bulletin*, *88*(4), 320–331. https://doi.org/10.1016/j.brainresbull.2012.03.001

Ponsi, G., Scattolin, M., Villa, R., & Aglioti, S. M. (2021). Human moral decision-making through the lens of Parkinson's disease. *Npj Parkinson's Disease 2021 7:1*, *7*(1), 1–7. https://doi.org/10.1038/s41531-021-00167-w

Porfirio, B., Paganini, M., Mazzanti, B., Bagnoli, S., Bucciantini, S., Ghelli, E., Nacmias, B., Putignano, A. L., Rombolà, G., Saccardi, R., Lombardini, L., Di Lorenzo, N., Vannelli, G. B., & Gallina, P. (2015). Donor-Specific Anti-HLA Antibodies in Huntington's Disease Recipients of Human Fetal Striatal Grafts. *Cell Transplantation*, *24*(5), 811–817. https://doi.org/10.3727/096368913X676222

Potkin, K. T., & Potkin, S. G. (2018). New directions in therapeutics for Huntington disease. *Future Neurology*, *13*(2), 101–121. https://doi.org/10.2217/fnl-2017-0035

Precious, S. V. (2017). Transplantation in HD: Are We Transplanting the Right Cells? In C. M. K. E.-N. E. Tunalı (Ed.), *Huntington's Disease* (p. Ch. 6-Ch. 6). IntechOpen. https://doi.org/10.5772/66490

Precious, S. V., Kelly, C. M., Reddington, A. E., Vinh, N. N., Stickland, R. C., Pekarik, V., Scherf, C., Jeyasingham, R., Glasbey, J., Holeiter, M., Jones, L., Taylor, M. V., & Rosser, A. E. (2016). FoxP1 marks medium spiny neurons from precursors to

maturity and is required for their differentiation. *Experimental Neurology*, *282*, 9. https://doi.org/10.1016/J.EXPNEUROL.2016.05.002

Pringsheim, T., Wiltshire, K., Day, L., Dykeman, J., Steeves, T., & Jette, N. (2012). The incidence and prevalence of Huntington's disease: A systematic review and meta-analysis. *Movement Disorders*, *27*(9), 1083–1091. https://doi.org/10.1002/mds.25075

Pruszak, J., Ludwig, W., Blak, A., Alavian, K., & Isacson, O. (2009). CD15, CD24, and CD29 Define a Surface Biomarker Code for Neural Lineage Differentiation of Stem Cells EMBRYONIC STEM CELLS/INDUCED PLURIPOTENT STEM CELLS CD15, CD24, and CD29 Define a Surface Biomarker Code for Neural Lineage Differentiation of Stem Cells. *STEM CELLS*, *27*, 2928–2940. https://doi.org/10.1002/stem.211

Pruszak, J., Sonntag, K.-C., Aung, M. H., Sanchez-Pernaute, R., & Isacson, O. (2007). Markers and Methods for Cell Sorting of Human Embryonic Stem Cell-Derived Neural Cell Populations. *Stem Cells (Dayton, Ohio)*, *25*(9), 2257. https://doi.org/10.1634/STEMCELLS.2006-0744

Pundt, L. L., Kondoh, T., Conrad, J. A., & Low, W. C. (1996). Transplantation of human fetal striatum into a rodent model of Huntington's disease ameliorates locomotor deficits. *Neuroscience Research*, *24*(4), 415–420. https://doi.org/10.1016/0168-0102(95)01009-2

Rawlins, M. D., Wexler, N. S., Wexler, A. R., Tabrizi, S. J., Douglas, I., Evans, S. J. W., & Smeeth, L. (2016). The Prevalence of Huntington's Disease. *Neuroepidemiology*, *46*(2), 144–153. https://doi.org/10.1159/000443738

Reidling, J. C., Relaño-Ginés, A., Holley, S. M., Ochaba, J., Moore, C., Fury, B., Lau, A., Tran, A. H., Yeung, S., Salamati, D., Zhu, C., Hatami, A., Cepeda, C., Barry, J. A., Kamdjou, T., King, A., Coleal-Bergum, D., Franich, N. R., LaFerla, F. M., … Thompson, L. M. (2018). Human Neural Stem Cell Transplantation Rescues Functional Deficits in R6/2 and Q140 Huntington's Disease Mice. *Stem Cell Reports*, *10*(1), 58–72. https://doi.org/10.1016/j.stemcr.2017.11.005

Reiner, A., Dragatsis, I., Zeitlin, S., & Goldowitz, D. (2003). Wild-type huntingtin plays a role in brain development and neuronal survival. *Molecular Neurobiology*, *28*(3), 259–275. https://doi.org/10.1385/MN:28:3:259

Reuter, I., Tai, Y. F., Pavese, N., Chaudhuri, K. R., Mason, S., Polkey, C. E., Clough, C., Brooks, D. J., Barker, R. A., & Piccini, P. (2008). Long-term clinical and positron emission tomography outcome of fetal striatal transplantation in Huntington's disease. *Journal of Neurology, Neurosurgery &Amp; Psychiatry*, *79*(8), 948 LP – 951. https://doi.org/10.1136/jnnp.2007.142380

Reza-Zaldivar, E. E., Hernández-Sapiéns, M. A., Gutiérrez-Mercado, Y. K., Sandoval-Ávila, S., Gomez-Pinedo, U., Márquez-Aguirre, A. L., Vázquez-Méndez, E., Padilla-Camberos, E., & Canales-Aguirre, A. A. (2019). Mesenchymal stem cell-derived exosomes promote neurogenesis and cognitive function recovery in a mouse

model of Alzheimer's disease. *Neural Regeneration Research*, *14*(9), 1626–1634. https://doi.org/10.4103/1673-5374.255978

Riggs, M. J., Sheridan, S. D., & Rao, R. R. (2021). ARHGDIA Confers Selective Advantage to Dissociated Human Pluripotent Stem Cells. *Stem Cells and Development*, *30*(14), 705–713. https://doi.org/10.1089/scd.2021.0079

Ronen, D., & Benvenisty, N. (2012). Genomic stability in reprogramming. *Current Opinion in Genetics & Development*, *22*(5), 444–449. https://doi.org/10.1016/j.gde.2012.09.003

Ross, B. D., Hoang, T. Q., Blüml, S., Dubowitz, D., Kopyov, O. V, Jacques, D. B., Lin, A., Seymour, K., & Tan, J. (1999). In vivo magnetic resonance spectroscopy of human fetal neural transplants. *NMR in Biomedicine*, *12*(4), 221–236. https://doi.org/10.1002/(SICI)1099-1492(199906)12:4<221::AID-NBM582>3.0.CO;2-Q

Ross, C. A., Aylward, E. H., Wild, E. J., Langbehn, D. R., Long, J. D., Warner, J. H., Scahill, R. I., Leavitt, B. R., Stout, J. C., Paulsen, J. S., Reilmann, R., Unschuld, P. G., Wexler, A., Margolis, R. L., & Tabrizi, S. J. (2014). Huntington disease: natural history, biomarkers and prospects for therapeutics. *Nature Reviews Neurology*, *10*(4), 204–216. https://doi.org/10.1038/nrneurol.2014.24

Ross, C. A., & Poirier, M. A. (2004). Protein aggregation and neurodegenerative disease. *Nature Medicine*, *10 Suppl*(7), S10. https://doi.org/10.1038/NM1066

Ross, C. A., & Tabrizi, S. J. (2011). Huntington's disease: from molecular pathogenesis to clinical treatment. *The Lancet Neurology*, *10*(1), 83–98. https://doi.org/10.1016/S1474-4422(10)70245-3

Rosser, A. E., Barker, R. A., Harrower, T., Watts, C., Farrington, M., Ho, A. K., Burnstein, R. M., Menon, D. K., Gillard, J. H., Pickard, J., & Dunnett, S. B. (2002). Unilateral transplantation of human primary fetal tissue in four patients with Huntington's disease: NEST-UK safety report ISRCTN no 36485475. *Journal of Neurology, Neurosurgery &Amp; Psychiatry*, *73*(6), 678 LP – 685. https://doi.org/10.1136/jnnp.73.6.678

Rosser, A. E., Busse, M. E., Gray, W. P., Aron Badin, R., Perrier, A. L., Wheelock, V., Cozzi, E., Perpiña Martin, U., Salado-Manzano, C., Mills, L. J., Drew, C., & Goldman, S. A. (n.d.). *Translating cell therapies for neurodegenerative diseases: Huntington's disease as a model disorder*. https://doi.org/10.1093/brain/awac086

Rosser, A. E., Busse, M. E., Gray, W. P., Badin, R. A., Perrier, A. L., Wheelock, V., Cozzi, E., Martin, U. P., Salado-Manzano, C., Mills, L. J., Drew, C., Goldman, S. A., Canals, J. M., & Thompson, L. M. (2022). Translating cell therapies for neurodegenerative diseases: Huntington's disease as a model disorder. *Brain : A Journal of Neurology*, *145*(5), 1584–1597. https://doi.org/10.1093/BRAIN/AWAC086

Rossi, A., Lickfett, S., Martins, S., & Prigione, A. (2022). A call for consensus guidelines on monitoring the integrity of nuclear and mitochondrial genomes in human

pluripotent stem cells. *Stem Cell Reports*. https://doi.org/https://doi.org/10.1016/j.stemcr.2022.01.019

Rouhani, F. J., Nik-Zainal, S., Wuster, A., Li, Y., Conte, N., Koike-Yusa, H., Kumasaka, N., Vallier, L., Yusa, K., & Bradley, A. (2016). Mutational History of a Human Cell Lineage from Somatic to Induced Pluripotent Stem Cells. *PLoS Genetics*, *12*(4), e1005932–e1005932. https://doi.org/10.1371/journal.pgen.1005932

Russo, S. J., Dietz, D. M., Dumitriu, D., Morrison, J. H., Malenka, R. C., & Nestler, E. J. (2010). The addicted synapse: Mechanisms of synaptic and structural plasticity in nucleus accumbens. *Trends in Neurosciences*, *33*(6), 267–276. https://doi.org/10.1016/j.tins.2010.02.002

Salado-Manzano, C., Perpiña, U., Straccia, M., Molina-Ruiz, F. J., Cozzi, E., Rosser, A. E., & Canals, J. M. (2020). Is the Immunological Response a Bottleneck for Cell Therapy in Neurodegenerative Diseases? *Frontiers in Cellular Neuroscience*, *14*, 250. https://doi.org/10.3389/fncel.2020.00250

Salgado, A. J., Sousa, J. C., Costa, B. M., Pires, A. O., Mateus-Pinheiro, A., Teixeira, F. G., Pinto, L., & Sousa, N. (2015). Mesenchymal stem cells secretome as a modulator of the neurogenic niche: Basic insights and therapeutic opportunities. *Frontiers in Cellular Neuroscience*, *9*(JULY), 1–18. https://doi.org/10.3389/fncel.2015.00249

Samata, B., Doi, D., Nishimura, K., Kikuchi, T., Watanabe, A., Sakamoto, Y., Kakuta, J., Ono, Y., & Takahashi, J. (2016). Purification of functional human ES and iPSC-derived midbrain dopaminergic progenitors using LRTM1. *Nature Communications*, *7*. https://doi.org/10.1038/NCOMMS13097

Sato, Y., Bando, H., Di Piazza, M., Gowing, G., Herberts, C., Jackman, S., Leoni, G., Libertini, S., MacLachlan, T., McBlane, J. W., Pereira Mouriès, L., Sharpe, M., Shingleton, W., Surmacz-Cordle, B., Yamamoto, K., & van der Laan, J. W. (2019). Tumorigenicity assessment of cell therapy products: The need for global consensus and points to consider. *Cytotherapy*, *21*(11), 1095–1111. https://doi.org/10.1016/j.jcyt.2019.10.001

Saudou, F., & Humbert, S. (2016). The Biology of Huntingtin. *Neuron*, *89*(5), 910–926. https://doi.org/10.1016/j.neuron.2016.02.003

Schackel, S., Pauly, M. C., Piroth, T., Nikkhah, G., & Döbrössy, M. D. (2013). Donor age dependent graft development and recovery in a rat model of Huntington's disease: Histological and behavioral analysis. *Behavioural Brain Research*, *256*, 56–63. https://doi.org/10.1016/J.BBR.2013.07.053

Scheiner, Z. S., Talib, S., & Feigal, E. G. (2014). The Potential for Immunogenicity of Autologous Induced Pluripotent Stem Cell-derived Therapies. *The Journal of Biological Chemistry*, *289*(8), 4571. https://doi.org/10.1074/JBC.R113.509588

Schuurmans, C., & Guillemot, F. (2002). Molecular mechanisms underlying cell fate specification in the developing telencephalon. *Current Opinion in Neurobiology*, *12*(1), 26–34. https://doi.org/10.1016/S0959-4388(02)00286-6

Schwartz, S. D., Hubschman, J.-P., Heilwell, G., Franco-Cardenas, V., Pan, C. K., Ostrick, R. M., Mickunas, E., Gay, R., Klimanskaya, I., & Lanza, R. (2012). Embryonic stem cell trials for macular degeneration: a preliminary report. *Lancet (London, England)*, *379*(9817), 713–720. https://doi.org/10.1016/S0140-6736(12)60028-2

Schwartz, S. D., Regillo, C. D., Lam, B. L., Eliott, D., Rosenfeld, P. J., Gregori, N. Z., Hubschman, J.-P., Davis, J. L., Heilwell, G., Spirn, M., Maguire, J., Gay, R., Bateman, J., Ostrick, R. M., Morris, D., Vincent, M., Anglade, E., Del Priore, L. V, & Lanza, R. (2015). Human embryonic stem cell-derived retinal pigment epithelium in patients with age-related macular degeneration and Stargardt's macular dystrophy: follow-up of two open-label phase 1/2 studies. *Lancet (London, England)*, *385*(9967), 509–516. https://doi.org/10.1016/S0140-6736(14)61376-3

Schweitzer, J. S., Song, B., Herrington, T. M., Park, T.-Y., Lee, N., Ko, S., Jeon, J., Cha, Y., Kim, K., Li, Q., Henchcliffe, C., Kaplitt, M., Neff, C., Rapalino, O., Seo, H., Lee, I.-H., Kim, J., Kim, T., Petsko, G. A., … Kim, K.-S. (2020). Personalized iPSC-Derived Dopamine Progenitor Cells for Parkinson's Disease. *Https://Doi.Org/10.1056/NEJMoa1915872*. https://doi.org/10.1056/NEJMOA1915872

Scotto, L., Narayan, G., Nandula, S. V, Arias-Pulido, H., Subramaniyam, S., Schneider, A., Kaufmann, A. M., Wright, J. D., Pothuri, B., Mansukhani, M., & Murty, V. V. (2008). Identification of copy number gain and overexpressed genes on chromosome arm 20q by an integrative genomic approach in cervical cancer: potential role in progression. *Genes, Chromosomes & Cancer*, *47*(9), 755–765. https://doi.org/10.1002/gcc.20577

Shrivastava, K., Gonzalez, P., & Acarin, L. (2012). The immune inhibitory complex CD200/CD200R is developmentally regulated in the mouse brain. *Journal of Comparative Neurology*, *520*(12), 2657–2675. https://doi.org/10.1002/CNE.23062

Silberberg, G., & Bolam, J. P. (2015). Local and afferent synaptic pathways in the striatal microcircuitry. In *Current Opinion in Neurobiology* (Vol. 33, pp. 182–187). Elsevier Ltd. https://doi.org/10.1016/j.conb.2015.05.002

Smith, Y., Bevan, M. D., Shink, E., & Bolam, J. P. (1998). Microcircuitry of the direct and indirect pathways of the basal ganglia. In *Neuroscience* (Vol. 86, Issue 2, pp. 353–387). Elsevier Ltd. https://doi.org/10.1016/S0306-4522(98)00004-9

Song, D. D., & Harlan, R. E. (1994). Genesis and migration patterns of neurons forming the patch and matrix compartments of the rat striatum. *Brain Research. Developmental Brain Research*, *83*(2), 233–245. https://doi.org/10.1016/0165-3806(94)00144-8

Song, W. K., Park, K.-M., Kim, H.-J., Lee, J. H., Choi, J., Chong, S. Y., Shim, S. H., Del Priore, L. V., & Lanza, R. (2015). Treatment of Macular Degeneration Using Embryonic Stem Cell-Derived Retinal Pigment Epithelium: Preliminary Results in Asian Patients. *Stem Cell Reports*, *4*(5), 860–872. https://doi.org/https://doi.org/10.1016/j.stemcr.2015.04.005

Song, X., Chen, H., Shang, Z., Du, H., Li, Z., Wen, Y., Liu, G., Qi, D., You, Y., Yang, Z., Zhang, Z., & Xu, Z. (2021). Homeobox Gene Six3 is Required for the Differentiation of D2-Type Medium Spiny Neurons. *Neuroscience Bulletin*, *37*(7), 985. https://doi.org/10.1007/S12264-021-00698-5

Soto, C., & Pritzkow, S. (2018). Protein misfolding, aggregation, and conformational strains in neurodegenerative diseases. *Nature Neuroscience*, *21*(10), 1332. https://doi.org/10.1038/S41593-018-0235-9

Sousa, V. H., & Fishell, G. (2010). Sonic hedgehog functions through dynamic changes in temporal competence in the developing forebrain. *Current Opinion in Genetics & Development*, *20*(4), 391–399. https://doi.org/10.1016/J.GDE.2010.04.008

Squitieri, F., Andrew, S. E., Goldberg, Y. P., Kremer, B., Spence, N., Zelsler, J., Nichol, K., Theilmann, J., Greenberg, J., Goto, J., Kanazawa, I., Vesa, J., Peltonen, L., Almqvist, E., Anvret, M., Telenius, H., Lin, B., Napolitano, G., Morgan, K., & Hayden, M. R. (1994). DNA haplotype analysis of Huntington disease reveals clues to the origins and mechanisms of CAG expansion and reasons for geographic variations of prevalence. *Human Molecular Genetics*, *3*(12), 2103–2114. https://doi.org/10.1093/hmg/3.12.2103

Steinemann, D., Göhring, G., & Schlegelberger, B. (2013). Genetic instability of modified stem cells-a first step towards malignant transformation? *American Journal of Stem Cells*, *2*(1), 39.

Stemberger, C., Dreher, S., Tschulik, C., Piossek, C., Bet, J., Yamamoto, T. N., Schiemann, M., Neuenhahn, M., Martin, K., Schlapschy, M., Skerra, A., Schmidt, T., Edinger, M., Riddell, S. R., Germeroth, L., & Busch, D. H. (2012). Novel Serial Positive Enrichment Technology Enables Clinical Multiparameter Cell Sorting. *PLOS ONE*, *7*(4), e35798. https://doi.org/10.1371/JOURNAL.PONE.0035798

Stenman, J., Toresson, H., & Campbell, K. (2003). Identification of Two Distinct Progenitor Populations in the Lateral Ganglionic Eminence: Implications for Striatal and Olfactory Bulb Neurogenesis. *Journal of Neuroscience*, *23*(1), 167–174. https://doi.org/10.1523/JNEUROSCI.23-01-00167.2003

Stiles, J., & Jernigan, T. L. (2010). The Basics of Brain Development. *Neuropsychology Review*, *20*(4), 327. https://doi.org/10.1007/S11065-010-9148-4

Stirling, D. R., Swain-Bowden, M. J., Lucas, A. M., Carpenter, A. E., Cimini, B. A., & Goodman, A. (2021). CellProfiler 4: improvements in speed, utility and usability. *BMC Bioinformatics*, *22*(1), 1–11. https://doi.org/10.1186/S12859-021-04344-9/FIGURES/6

Straccia, M., Carrere, J., Rosser, A. E., & Canals, J. M. (2016). Human t-DARPP is induced during striatal development. *Neuroscience*, *333*, 320–330. https://doi.org/https://doi.org/10.1016/j.neuroscience.2016.07.022

Stuart, T., Butler, A., Hoffman, P., Hafemeister, C., Papalexi, E., Mauck, W. M., Hao, Y., Stoeckius, M., Smibert, P., & Satija, R. (2019). Comprehensive Integration of

Single-Cell Data. *Cell*, *177*(7), 1888-1902.e21. https://doi.org/10.1016/J.CELL.2019.05.031

Sur, M., & Rubenstein, J. L. R. (2005). Patterning and Plasticity of the Cerebral Cortex. *Science*, *310*(5749), 805–810. https://doi.org/10.1126/SCIENCE.1112070

Sutermaster, B. A., & Darling, E. M. (2019). Considerations for high-yield, high-throughput cell enrichment: fluorescence versus magnetic sorting. *Scientific Reports 2019 9:1*, *9*(1), 1–9. https://doi.org/10.1038/s41598-018-36698-1

Taapken, S. M., Nisler, B. S., Newton, M. A., Sampsell-Barron, T. L., Leonhard, K. A., McIntire, E. M., & Montgomery, K. D. (2011). Karotypic abnormalities in human induced pluripotent stem cells and embryonic stem cells. In *Nature biotechnology* (Vol. 29, Issue 4, pp. 313–314). https://doi.org/10.1038/nbt.1835

Tabach, Y., Kogan-Sakin, I., Buganim, Y., Solomon, H., Goldfinger, N., Hovland, R., Ke, X.-S., Oyan, A. M., Kalland, K.-H., Rotter, V., & Domany, E. (2011). Amplification of the 20q Chromosomal Arm Occurs Early in Tumorigenic Transformation and May Initiate Cancer. *PLOS ONE*, *6*(1), e14632.

Tabrizi, S. J., Leavitt, B. R., Landwehrmeyer, G. B., Wild, E. J., Saft, C., Barker, R. A., Blair, N. F., Craufurd, D., Priller, J., Rickards, H., Rosser, A., Kordasiewicz, H. B., Czech, C., Swayze, E. E., Norris, D. A., Baumann, T., Gerlach, I., Schobel, S. A., Paz, E., … Lane, R. M. (2019). Targeting Huntingtin Expression in Patients with Huntington's Disease. *New England Journal of Medicine*, *380*(24), 2307–2316. https://doi.org/10.1056/NEJMoa1900907

Tabrizi, S. J., Reilmann, R., Roos, R. A. C., Durr, A., Leavitt, B., Owen, G., Jones, R., Johnson, H., Craufurd, D., Hicks, S. L., Kennard, C., Landwehrmeyer, B., Stout, J. C., Borowsky, B., Scahill, R. I., Frost, C., & Langbehn, D. R. (2012). Potential endpoints for clinical trials in premanifest and early Huntington's disease in the TRACK-HD study: Analysis of 24 month observational data. *The Lancet Neurology*, *11*(1), 42–53. https://doi.org/10.1016/S1474-4422(11)70263-0

Tabrizi, S. J., Scahill, R. I., Owen, G., Durr, A., Leavitt, B. R., Roos, R. A., Borowsky, B., Landwehrmeyer, B., Frost, C., Johnson, H., Craufurd, D., Reilmann, R., Stout, J. C., & Langbehn, D. R. (2013). Predictors of phenotypic progression and disease onset in premanifest and early-stage Huntington's disease in the TRACK-HD study: analysis of 36-month observational data. *The Lancet Neurology*, *12*(7), 637–649. https://doi.org/10.1016/S1474-4422(13)70088-7

Tackett, J. L., & Miller, J. D. (2019). Introduction to the special section on increasing replicability, transparency, and openness in clinical psychology. In *Journal of abnormal psychology* (Vol. 128, Issue 6, pp. 487–492). https://doi.org/10.1037/abn0000455

Takahashi, K., Tanabe, K., Ohnuki, M., Narita, M., Ichisaka, T., Tomoda, K., & Yamanaka, S. (2007). Induction of Pluripotent Stem Cells from Adult Human Fibroblasts by Defined Factors. *Cell*, *131*(5), 861–872. https://doi.org/https://doi.org/10.1016/j.cell.2007.11.019

Takahashi, K., & Yamanaka, S. (2006). Induction of Pluripotent Stem Cells from Mouse Embryonic and Adult Fibroblast Cultures by Defined Factors. *Cell*, *126*(4), 663–676. https://doi.org/10.1016/j.cell.2006.07.024

Tanimura, A., Pancani, T., Lim, S. A. O., Tubert, C., Melendez, A. E., Shen, W., & Surmeier, D. J. (2018). Striatal cholinergic interneurons and Parkinson's disease. *European Journal of Neuroscience*, *47*(10), 1148–1158. https://doi.org/10.1111/EJN.13638

Tartaglione, A. M., Popoli, P., & Calamandrei, G. (2017). Regenerative medicine in Huntington's disease: Strengths and weaknesses of preclinical studies. *Neuroscience & Biobehavioral Reviews*, *77*, 32–47. https://doi.org/https://doi.org/10.1016/j.neubiorev.2017.02.017

Telezhkin, V., Schnell, C., Yarova, P., Yung, S., Cope, E., Hughes, A., Thompson, B. A., Sanders, P., Geater, C., Hancock, J. M., Joy, S., Badder, L., Connor-Robson, N., Comella, A., Straccia, M., Bombau, G., Brown, J. T., Canals, J. M., Randall, A. D., … Kemp, P. J. (2015). Forced cell cycle exit and modulation of GABAA, CREB, and GSK3β signaling promote functional maturation of induced pluripotent stem cell-derived neurons. *American Journal of Physiology-Cell Physiology*, *310*(7), C520–C541. https://doi.org/10.1152/ajpcell.00166.2015

Telezhkin, V., Schnell, C., Yarova, P., Yung, S., Cope, E., Hughes, A., Thompson, B. A., Sanders, P., Geater, C., Hancock, J. M., Joy, S., Badder, L., Connor-Robson, N., Comella, A., Straccia, M., Bombau, G., Brown, J. T., Canals, J. M., Randall, A. D., … Kemp, P. J. (2016). Forced cell cycle exit and modulation of GABAA, CREB, and GSK3β signaling promote functional maturation of induced pluripotent stem cell-derived neurons. *American Journal of Physiology - Cell Physiology*, *310*(7), C520–C541. https://doi.org/10.1152/AJPCELL.00166.2015/ASSET/IMAGES/LARGE/ZH00061678900012.JPEG

Tepper, J. M., Koós, T., & Wilson, C. J. (2004). GABAergic microcircuits in the neostriatum. *Trends in Neurosciences*, *27*(11), 662–669. https://doi.org/10.1016/J.TINS.2004.08.007

Thompson, O., von Meyenn, F., Hewitt, Z., Alexander, J., Wood, A., Weightman, R., Gregory, S., Krueger, F., Andrews, S., Barbaric, I., Gokhale, P. J., Moore, H. D., Reik, W., Milo, M., Nik-Zainal, S., Yusa, K., & Andrews, P. W. (2020). Low rates of mutation in clinical grade human pluripotent stem cells under different culture conditions. *Nature Communications*, *11*(1), 1528. https://doi.org/10.1038/s41467-020-15271-3

Thomson, J. A., Itskovitz-Eldor, J., Shapiro, S. S., Waknitz, M. A., Swiergiel, J. J., Marshall, V. S., & Jones, J. M. (1998). Embryonic Stem Cell Lines Derived from Human Blastocysts. *Science*, *282*(5391), 1145 LP – 1147. http://science.sciencemag.org/content/282/5391/1145.abstract

Tinterri, A., Menardy, F., Diana, M. A., Lokmane, L., Keita, M., Coulpier, F., Lemoine, S., Mailhes, C., Mathieu, B., Merchan-Sala, P., Campbell, K., Gyory, I., Grosschedl,

R., Popa, D., & Garel, S. (2018). Active intermixing of indirect and direct neurons builds the striatal mosaic. *Nature Communications*, *9*(1), 4725. https://doi.org/10.1038/s41467-018-07171-4

Trottier, Y., Lutz, Y., Stevanin, G., Imbert, G., Devys, D., Cancel, G., Saudou, F., Weber, C., David, G., Tora, L., Agid, Y., Brice, A., & Mandel, J.-L. (1995). Polyglutamine expansion as a pathological epitope in Huntington's disease and four dominant cerebellar ataxias. *Nature*, *378*(6555), 403–406. https://doi.org/10.1038/378403a0

Turrero García, M., & Harwell, C. C. (2017). Radial glia in the ventral telencephalon. *FEBS Letters*, *591*(24), 3942–3959. https://doi.org/10.1002/1873-3468.12829

Valli, R., Marletta, C., Pressato, B., Montalbano, G., Lo Curto, F., Pasquali, F., & Maserati, E. (2011). Comparative genomic hybridization on microarray (a-CGH) in constitutional and acquired mosaicism may detect as low as 8% abnormal cells. *Molecular Cytogenetics*, *4*, 13. https://doi.org/10.1186/1755-8166-4-13

Van Vugt, J. P. P., & Roos, R. A. C. (2012). Huntington's Disease. *CNS Drugs 1999 11:2*, *11*(2), 105–123. https://doi.org/10.2165/00023210-199911020-00003

Velier, J., Kim, M., Schwarz, C., Kim, T. W., Sapp, E., Chase, K., Aronin, N., & DiFiglia, M. (1998). Wild-Type and Mutant Huntingtins Function in Vesicle Trafficking in the Secretory and Endocytic Pathways. *Experimental Neurology*, *152*(1), 34–40. https://doi.org/https://doi.org/10.1006/exnr.1998.6832

Vicente, A. M., Galvão-Ferreira, P., Tecuapetla, F., & Costa, R. M. (2016). Direct and indirect dorsolateral striatum pathways reinforce different action strategies. *Current Biology : CB*, *26*(7), R267–R269. https://doi.org/10.1016/J.CUB.2016.02.036

Vogel, A., Upadhya, R., & Shetty, A. K. (2018). Neural stem cell derived extracellular vesicles: Attributes and prospects for treating neurodegenerative disorders. *EBioMedicine*, *38*, 273–282. https://doi.org/10.1016/j.ebiom.2018.11.026

Vogel, C., & Marcotte, E. M. (2012). Insights into the regulation of protein abundance from proteomic and transcriptomic analyses. *Nature Reviews Genetics 2012 13:4*, *13*(4), 227–232. https://doi.org/10.1038/nrg3185

Vonsattel, J. P. G., & Difiglia, M. (1998). Huntington Disease. *Journal of Neuropathology & Experimental Neurology*, *57*(5), 369–384. https://doi.org/10.1097/00005072-199805000-00001

Vonsattel, J. P., Myers, R. H., Stevens, T. J., Ferrante, R. J., Bird, E. D., & Richardson, E. P. (1985). Neuropathological classification of huntington's disease. *Journal of Neuropathology and Experimental Neurology*, *44*(6), 559–577. https://doi.org/10.1097/00005072-198511000-00003

Vonsattel, J.-P., Myers, R. H., Stevens, T. J., Ferrante, R. J., Bird, E. D., & Richardson Jr., E. P. (1985). Neuropathological Classification of Huntington's Disease. *Journal of Neuropathology & Experimental Neurology*, *44*(6), 559–577. https://doi.org/10.1097/00005072-198511000-00003

Warmflash, A., Sorre, B., Etoc, F., Siggia, E. D., & Brivanlou, A. H. (2014). A method to recapitulate early embryonic spatial patterning in human embryonic stem cells. *Nature Methods*, *11*(8), 847–854. https://doi.org/10.1038/nmeth.3016

Watt, D. (1990). Huntington's Disease: A Disorder of Families. By S. E. Folstein. (Pp. 251; £25.00.) Johns Hopkins University Press: Baltimore. 1989. *Psychological Medicine*, *20*(3), 728–731. https://doi.org/10.1017/s0033291700017281

Wehner, A. B., Milen, A. M., Albin, R. L., & Pierchala, B. A. (2016). THE p75 NEUROTROPHIN RECEPTOR AUGMENTS SURVIVAL SIGNALING IN THE STRIATUM OF PRE-SYMPTOMATIC Q175WT/HD MICE. *Neuroscience*, *324*, 297. https://doi.org/10.1016/J.NEUROSCIENCE.2016.02.069

Wenning, G. K., Tison, F., Scherfler, C., Puschban, Z., Waldner, R., Granata, R., Ghorayeb, I., & Poewe, W. (2000). Towards neurotransplantation in multiple system atrophy: clinical rationale, pathophysiological basis, and preliminary experimental evidence. *Cell Transplantation*, *9*(2), 279–288. https://doi.org/10.1177/096368970000900213

Werbowetski-Ogilvie, T. E., Bossé, M., Stewart, M., Schnerch, A., Ramos-Mejia, V., Rouleau, A., Wynder, T., Smith, M.-J., Dingwall, S., Carter, T., Williams, C., Harris, C., Dolling, J., Wynder, C., Boreham, D., & Bhatia, M. (2009). Characterization of human embryonic stem cells with features of neoplastic progression. *Nature Biotechnology*, *27*(1), 91–97. https://doi.org/10.1038/nbt.1516

Wexler, N. S. (2004). Venezuelan kindreds reveal that genetic and environmental factors modulate Huntington's disease age of onset. *Proceedings of the National Academy of Sciences of the United States of America*, *101*(10), 3498 LP – 3503. https://doi.org/10.1073/pnas.0308679101

Wichterle, H., Garcia-Verdugo, J. M., Herrera, D. G., & Alvarez-Buylla, A. (1999). Young neurons from medial ganglionic eminence disperse in adult and embryonic brain. *Nature Neuroscience*, *2*(5), 461–466. https://doi.org/10.1038/8131

Wichterle, H., Turnbull, D. H., Nery, S., Fishell, G., & Alvarez-Buylla, A. (2001). In utero fate mapping reveals distinct migratory pathways and fates of neurons born in the mammalian basal forebrain. *Development (Cambridge, England)*, *128*(19), 3759–3771. https://doi.org/10.1242/DEV.128.19.3759

Wild, E. J. (2016). Huntington's Disease: The Most Curable Incurable Brain Disorder? *EBioMedicine*, *8*, 3–4. https://doi.org/10.1016/j.ebiom.2016.05.023

Wild, E. J., & Tabrizi, S. J. (2014). Targets for future clinical trials in Huntington's disease: What's in the pipeline? *Movement Disorders*, *29*(11), 1434–1445. https://doi.org/10.1002/mds.26007

Wild, E. J., & Tabrizi, S. J. (2017). Therapies targeting DNA and RNA in Huntington ' s disease. *The Lancet Neurology*, *16*(10), 837–847. https://doi.org/10.1016/S1474-4422(17)30280-6

Williams, A. (2002). Defining neurodegenerative diseases : Disorders will be named after responsible rogue proteins and their solutions. *BMJ : British Medical Journal*, *324*(7352), 1465. https://doi.org/10.1136/BMJ.324.7352.1465

Wu, M., Zhang, D., Bi, C., Mi, T., Zhu, W., Xia, L., Teng, Z., Hu, B., & Wu, Y. (2018). A Chemical Recipe for Generation of Clinical-Grade Striatal Neurons from hESCs. *Stem Cell Reports*, *11*(3), 635. https://doi.org/10.1016/J.STEMCR.2018.08.005

Xu, Z., Liang, Q., Song, X., Zhang, Z., Lindtner, S., Li, Z., Wen, Y., Liu, G., Guo, T., Qi, D., Wang, M., Wang, C., Li, H., You, Y., Wang, X., Chen, B., Feng, H., Rubenstein, J. L., & Yang, Z. (2018). SP8 and SP9 coordinately promote D2-type medium spiny neuron production by activating Six3 expression. *Development (Cambridge, England)*, *145*(14). https://doi.org/10.1242/DEV.165456

Yacoubian, T. A. (2017). Neurodegenerative Disorders: Why Do We Need New Therapies? *Drug Discovery Approaches for the Treatment of Neurodegenerative Disorders: Alzheimer's Disease*, 1–16. https://doi.org/10.1016/B978-0-12-802810-0.00001-5

Yamanaka, S. (2020). Pluripotent Stem Cell-Based Cell Therapy-Promise and Challenges. *Cell Stem Cell*, *27*(4), 523–531. https://doi.org/10.1016/j.stem.2020.09.014

Yasuda, S., Kusakawa, S., Kuroda, T., Miura, T., Tano, K., Takada, N., Matsuyama, S., Matsuyama, A., Nasu, M., Umezawa, A., Hayakawa, T., Tsutsumi, H., & Sato, Y. (2018). Tumorigenicity-associated characteristics of human iPS cell lines. *PloS One*, *13*(10), e0205022–e0205022. https://doi.org/10.1371/journal.pone.0205022

Yhnell, E., Dunnett, S. B., & Brooks, S. P. (2016). A Longitudinal Operant Assessment of Cognitive and Behavioural Changes in the HdhQ111 Mouse Model of Huntington's Disease. *PLOS ONE*, *11*(10), e0164072. https://doi.org/10.1371/JOURNAL.PONE.0164072

Young, K. M., Merson, T. D., Sotthibundhu, A., Coulson, E. J., & Bartlett, P. F. (2007). p75 Neurotrophin Receptor Expression Defines a Population of BDNF-Responsive Neurogenic Precursor Cells. *The Journal of Neuroscience*, *27*(19), 5146. https://doi.org/10.1523/JNEUROSCI.0654-07.2007

Yung, K. K. L., & Bolam, J. P. (2000). Localization of Dopamine D1 and D2 Receptors in the Rat Neostriatum: Synaptic Interaction With Glutamate-and GABA-Containing Axonal Terminals. *Synapse*, *38*, 413–420. https://doi.org/10.1002/1098-2396(20001215)38:4

Zhang, Q., Zhang, Y., Wang, C., Xu, Z., Liang, Q., An, L., Li, J., Liu, Z., You, Y., He, M., Mao, Y., Chen, B., Xiong, Z. Q., Rubenstein, J. L., & Yang, Z. (2016). The Zinc Finger Transcription Factor Sp9 Is Required for the Development of Striatopallidal Projection Neurons. *Cell Reports*, *16*(5), 1431–1444. https://doi.org/10.1016/J.CELREP.2016.06.090

Zheng, J. C., & Chen, S. (2022). Translational Neurodegeneration in the era of fast growing international brain research. *Translational Neurodegeneration*, *11*(1), 1–2. https://doi.org/10.1186/S40035-021-00276-9/METRICS

Zhu, Z., & Huangfu, D. (2013). Human pluripotent stem cells: an emerging model in developmental biology. *Development (Cambridge, England)*, *140*(4), 705–717. https://doi.org/10.1242/dev.086165

Zuccato, C., & Cattaneo, E. (2007). Role of brain-derived neurotrophic factor in Huntington's disease. *Progress in Neurobiology*, *81*(5–6), 294–330. https://doi.org/10.1016/j.pneurobio.2007.01.003

Zuccato, C., Valenza, M., & Cattaneo, E. (2010). Molecular Mechanisms and Potential Therapeutical Targets in Huntington's Disease. *Physiological Reviews*, *90*(3), 905–981. https://doi.org/10.1152/physrev.00041.2009

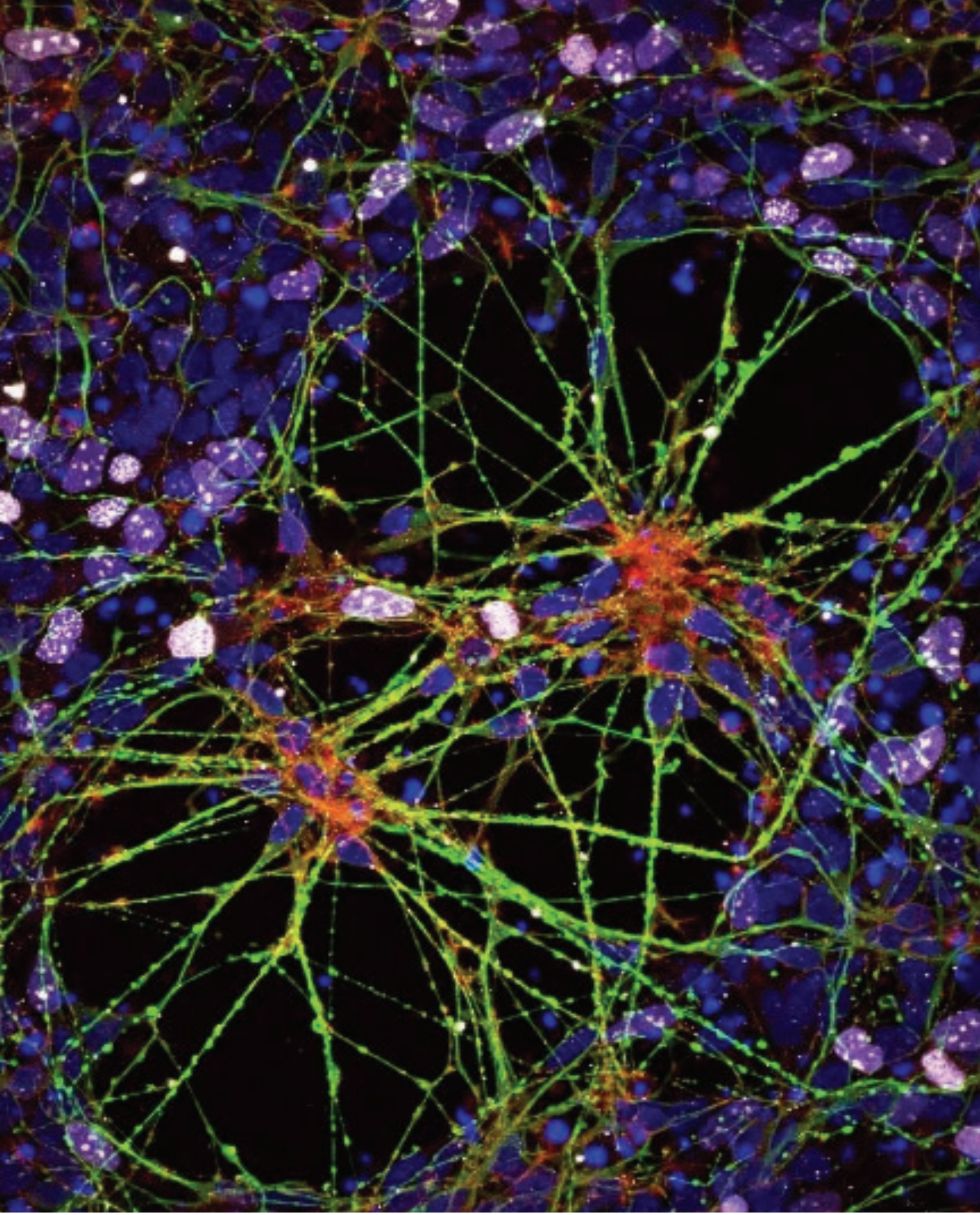

UNIVERSITAT DE BARCELONA

Creatio

Production and validation
center of advanced therapies
UNIVERSITAT DE BARCELONA

ASCTN
TRAINING